University of Nevada, Reno

Delineating the putative protein O-fucosyltransferase family in *Arabidopsis thaliana*

A dissertation submitted in partial fulfillment of the requirements for the degree of

Doctor of Philosophy

by

Devin Kathryn Smith

Dr. Ian S. Wallace/ Dissertation Advisor

August 2021

THE GRADUATE SCHOOL

We recommend that the dissertation
prepared under our supervision by

Devin Kathryn Smith

entitled

Delineating the putative protein O-fucosyltransferase family in Arabidopsis thaliana

be accepted in partial fulfillment of the
requirements for the degree of

Doctor of Philosophy

Dr. Ian Wallace
Advisor

Dr. Jeffrey Harper
Committee Member

Dr. Dylan Kosma
Committee Member

Dr. Won-Gyu Choi
Committee Member

Dr. Matthew Tucker
Graduate School Representative

David W. Zeh, Ph.D., Dean
Graduate School

August, 2021

Abstract:
Terrestrial plant genomes are widely expanded in genes that encode glycosyltransferases, which facilitate the attachment of sugar moieties onto proteins, lipids, or function in the biosynthesis of polysaccharides. Specifically, in *Arabidopsis thaliana,* 39 genes are predicted to encode protein O-fucosyltransferases (POFTs). In contrast to POFTs in metazoan systems, very little is known about these enzymes in plants, and biochemical evidence for POFT activity for even one of these Arabidopsis genes remains elusive. Nonetheless, this family of enzymes play fundamental roles in essential plant processes, including angiosperm sexual reproduction, termed double fertilization. Importantly, this process is responsible for the production of the majority of our food crops. During double fertilization, the male gametophyte (pollen) germinates to produce a sperm cell trafficking structure called the pollen tube that physically penetrates through the pistil tissues to deliver its gametes to a distant ovule located deep within the ovary. Whereas the process of pollen tube penetration through the pistil has been anatomically well-described, the genetic regulation remains poorly understood. In this dissertation, we identify one novel member of the Arabidopsis putative POFT family, *O-FUCOSYL TRANSFERASE 1* (*AtOFT1*), which plays a key role in pollen tube penetration through the stigma−style interface. *oft1* mutant pollen tubes have a reduced ability to elongate past the style, leading to a nearly 2000-fold decrease in *oft1* pollen transmission efficiency and as much as a 10-fold reduction in seed set. We demonstrate that AtOFT1 is localized to the Golgi apparatus, indicating its potential role in cellular glycosylation events. Furthermore, we show *AtOFT1* and other similar Arabidopsis genes represent a novel clade of sequences related to metazoan POFTs, and that mutation of residues that

are important for O-fucosyltransferase activity compromise AtOFT1 function *in vivo*. Finally, we catalytically assess two other putative POFT family members and show that they utilize the metazoan POFT substrate, GDP-fucose. The results of this study elucidate a physiological function for AtOFT1 in pollen tube penetration during double fertilization, expands our biochemical knowledge of this hypothesized gene family in Arabidopsis, and highlights the potential significance of protein O-glycosylation events in plant systems.

Dedication:

I would like to dedicate the entire body of my graduate research efforts that are partially detailed in this dissertation to my beloved and intensely missed friend and lab mate, Bret Edward Hart. Bret was an exceptionally special human that infectiously motivated me as well as many others to be better in all areas of our lives, especially as scientists. This was especially true in the lab as his work ethic and dedication to his research could not be matched. Although Bret took his life on November 1, 2019, his compassion, unsurpassed sense of humor, and intelligence has left a profound imprint on the hearts of so many individuals, which was truly extraordinary and will never be forgotten.

~ Bret,

> If somehow out in the multiverse you stumble across this document, I would like you to know that it is now clear to me what your purpose in my life was and continues to be. Throughout my day, the thought of our friendship seems to never slip my mind as you continue to inspire and push me to journey beyond the boundaries of my comfort zone and force myself to keep growing and going…even on the hard days. Thank you for the brief but meaningful time we shared, and may you finally be at peace, “One-T.”

Acknowledgments:

Many people have supported me during my time in graduate school. The first and most profound person I would like to sincerely thank is my PI and mentor Dr. Ian Wallace. He has not only been my main supporter even before entering graduate school, but he was fundamental in reorienting my degree path to scientific research early in my undergraduate degree. Dr. Wallace has guided me through very high and low periods I e experienced throughout my time working for him and pushed me to achieve things that I never believed I was capable of attaining. I will truly miss being a member of his research team, and there are no words in the English dictionary to express how appreciative, thankful, and grateful I am to have worked for him.

I would also like to thank Dr. Jeffrey Harper, who was not only acted as one of my graduate committee members but was further instrumental in helping me learn key skills necessary to generate the data in this dissertation. Additionally, Dr. Harper's excitement for science is infectious and some of my most enjoyable interactions with him took place in committee meeting and journal club, as he would propose such novel ideas related and unrelated to my research that expanded the way I generally think about science. I would further like to extend my gratitude to my other committee members, including Dr. Dylan Kosma, Dr. Won-Gyu Choi, and Dr. Matthew Tucker, which have been instrumental in further aiding me in my investigatory efforts, broadening my science centric mindset, and supported my development as a scientist.

I am additionally grateful to my lab mates, specifically Dr. José Villalobos, Edward Cruz, Celeste Rodriguez, and Bret Hart, which ended up being some of my closest friends that made my years as a graduate student fun and extremely entertaining.

My fellow peers Dr. John Baggett and Julia Wright further supported me during my studies and continue to brighten my day on a regular basis. Lastly, I would like to thank my friends and family, although mostly unsure of what I was really doing in the lab for all of these years, were continuously supportive as I worked to achieve my academic dreams.

Table of Contents

List of Figures and Tables

Chapter 1: Introduction

Chapter 2: Materials and Methods

Chapter 3: Results

Chapter 1: Introduction

I. Angiosperms: The evolution of flowering plants

Green land plants are approximately 500 billion years old and are believed to have originated from evolutionarily developed algae that acquired the ability to live on land (Dresselhaus and Franklin-Tong, 2013; Morris *et al.,* 2018). This landfall of green algae is considered to be the most significant evolutionary event on Earth and is responsible for the evolution of the plant kingdom (Leebens-Mack *et al.,* 2019; Morris *et al.,* 2018). The significance of this evolutionary outcome is underscored by the consequences of how it shaped our planet as we now see and exist on it. As land plants began to invade and adapt to terrestrial life on Earth, it remodeled its entire surface, creating different habitats that facilitated the evolution of other life forms, which speciated as the photosynthetic biproducts of land plant energy metabolism drastically increased the atmospheric oxygen most forms of life either depend on directly or indirectly (Boyce and Lee, 2017). Today, the plantae kingdom is estimated to encompasses approximately 500,000 different species that range from small mosses to giant sequoia trees (Leebens-Mack *et al.,* 2019). Angiosperms, otherwise known as flowering plants, are the largest clade of green land plants, which represent approximately 90% of all land plants and encompass more than 370,000 different species (Sauquet *et al.,* 2017; Leebens-Mack *et al.,* 2019). Flowering plants originated from the evolution of green land plants approximately 140-250 million years ago and represent the largest and most diverse group in the plantae kingdom (Friis *et al.,* 2011; Dresselhaus and Franklin-Tong, 2013; Sauquet *et al.,* 2017). Angiosperms main defining feature from other members of this kingdom is their mechanism of reproduction, called double

fertilization, which is facilitated by its unique reproductive structure, the flower (Friis *et al.,* 2011).

II. Double fertilization

a. Floral anatomy and development

Angiosperms are specifically characterized by their unique mechanism of sexual reproduction termed double fertilization (Qu *et al.,* 2015; Palanivelu and Tsukamoto, 2011). The characteristic flower of angiosperms is not only credited with being the source of a major evolutionary innovation responsible for the explosive diversification of angiosperms and other life forms, but the flower is additionally the site where double fertilization takes place (Endress, 2011). The vast array of floral characteristics displayed by angiosperms today exemplifies this sweeping evolutionary event that has allowed this clade to dominate Earth's terrestrial environments (Becker *et al.,* 2011).

The flower arises from the shoot apical meristem (SAM) (Bowman and Eshed, 2000). Upon shoot bolting, the SAM transitions into the primary inflorescence shoot apical meristem (IM), which further develops lateral meristems that can produce flowers or grow secondary floral branches (Alvarez-Buylla *et al.,* 2010) . Additionally, the SAM is subdivided into three distinct tissue zones that exhibit discrete cell types and rates of cell division: the central zone (CZ), the peripheral zone (PZ) that encompasses the CZ, and the rib zone (RZ) localized to the underside of the CZ (Alvarez-Buylla *et al.,* 2010) . Floral development originates from founder cells in the PZ of the IM, and initiation of floral organ biogenesis is controlled by cell expansion and division that is specifically and discretely regulated by different mechanisms throughout floral development (Jenik and Irish, 2000).

The development of the floral organs in the Brassicaceae family can be assessed by 20 distinct developmental stages, but floral anthesis is achieved at stage 13, and although floral structure differs considerably between angiosperm species, 4 main organs remain mostly conserved: sepals, petals, stamens, and carpels (Smyth *et al.,* 1990; Becker *et al.,* 2011; Alvarez-Buylla *et al.,* 2010). Stage 1 and 2 define the emergence of the floral primordia from the IM, and by Stage 3, sepal primordia begin to develop. Furthermore, Stage 4 is defined by the elongation of the peduncle, Stage 5 gives rise to the petal and stamen primordia, Stage 6 initiates gynoecium (pistil) development and is characterized by the sepals having enlarged to completely encapsulate and protect the immature floral bud. Stage 7 is characterized by the growth of the stamen filaments, while Stage 8 is defined by stamen development as anther primordia appear as well as petal development, which continues to rapidly elongate in Stage 9 and 10. Stages 10 through 11 are defined by the appearance of the apical most structure of the pistil, the stigmatic papillae. Stage 12 marks the differentiation of the stigmatic papillae from the style of the pistil and by the end of this stage the sepals open. Finally, by Stage 13, the flower is sexually mature, and the filaments of the stamen rapidly extend past the length of the pistil in this stage, resulting in self-pollination in self-compatible angiosperm species (Alvarez-Buylla *et al.,* 2010).

b. <u>The process of angiosperm double fertilization</u>

By the end of Stage 13, the floral organs as well as male and female gametes are fully mature (Figure 1.1A; Alvarez-Buylla *et al.,* 2010), and double fertilization may commence. At the sexually mature flower, the process of double fertilization is initiated in compatible species upon pollen grain dehiscence from the anther and deposition on the

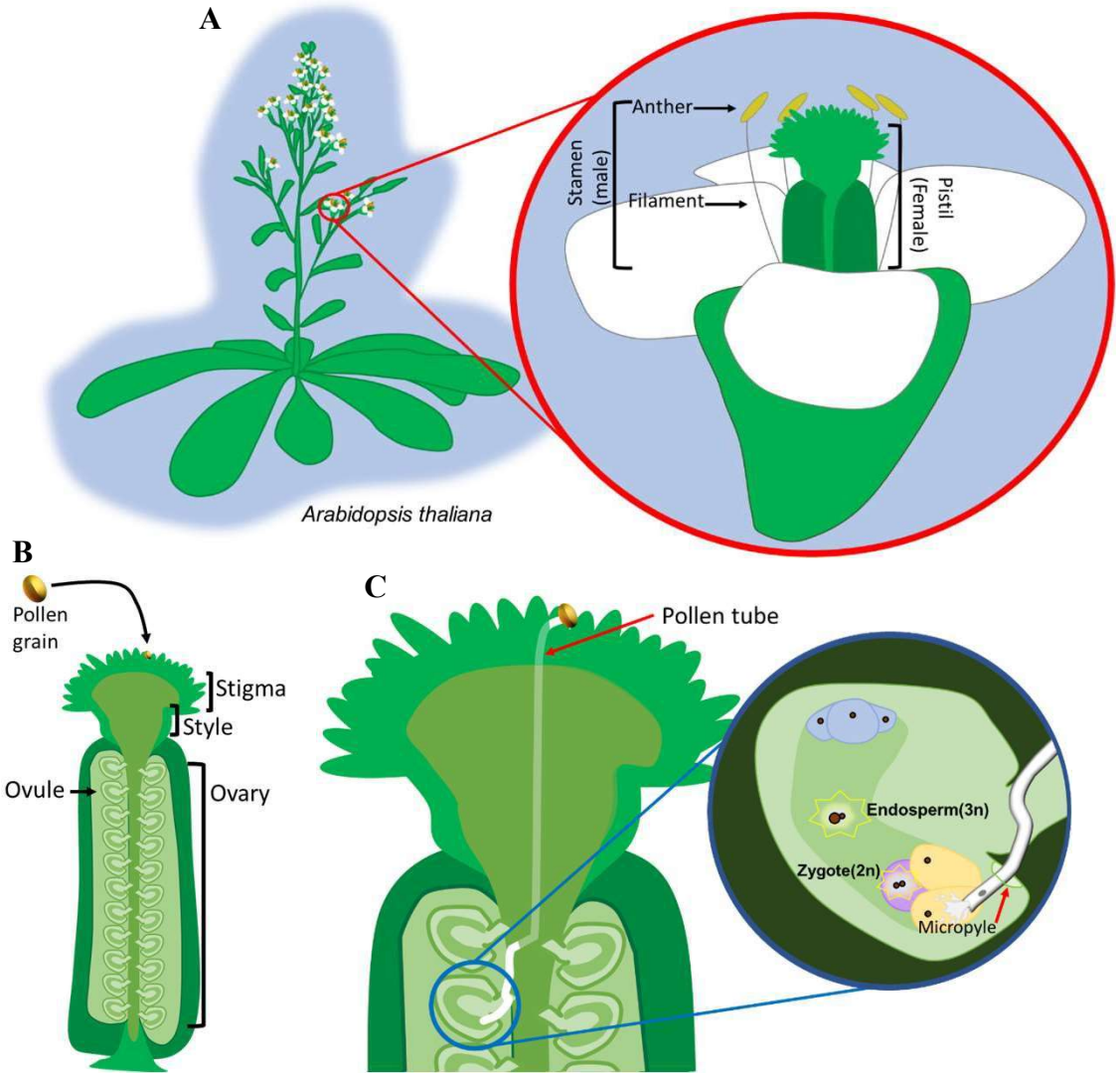

Figure 1.1: Diagram of the process of double fertilization in *Arabidopsis thaliana.* A, The model organism used throughout these investigations is *A. thaliana.* The process of angiosperm double fertilization takes place at the floral organ, which is enlarged (right) to allow for the gender specific structures to be visualized. The stamen is composed of the filament, which holds up the anther that contains the male gamete (pollen). The pistil represents both the female reproductive tissues as well as houses the female gametes (ovules). B, Closeup cross section of the female pistil depicting the essential structures that the pollen tube must penetratively traverse to reach the ovary where the unfertilized ovules are housed. A pollen grain is deposited on the most apical stigmatic surface of thepistil by gravity, wind, or animal transfer. C, Once deposited on the stigma, the pollen grain hydratesand develops a pollen tube that functions to traffic its two sperm nuclei through the stigma, through the stylar transmitting tract (TT), and into the ovary where it is able to sense an unfertilized ovule. Atthe ovule (right enlarged illustration), the pollen tube enters though a pore called the micropyle and interacts with one of two synergid cells (yellow), which signals the pollen tube to burst, resulting in the release of its two sperm nuclei. The two sperm nuclei independently migrate to the egg cell and the central cell and undergo fusion events, giving rise to the zygote and endosperm of the fertilized seed, respectively.

apical-most surface of the pistil, the stigmatic papillae (Figure 1.1B; Zheng *et al.,* 2018). The pollen grain adheres to the finger-shaped papillae cells of the stigma and adhesion is initially mediated by the extracellular matrix of the pollen grain, which is covered in hydrophobic lipids and proteins (Johnson and Preuss, 2002; Cascallares *et al.,* 2020). The stigmatic papillae of both wet and dry stigmas also contribute to pollen grain adherence, as wet stigmas randomly capture pollen through their secretions, while dry stigmas, such as stigmas of *Arabidopsis thaliana*, promote grain adherence through a waxy layer on the surface of their papillae cells (Zheng *et al.,* 2018; Johnson and Preuss, 2002).

Following adhesion, the pollen grain hydrates by absorbing water provided by the female tissues, resulting in the initiation of pollen grain metabolism (Mollet *et al.,* 2013; Zheng *et al.,* 2018; Palanivelu and Tsukamoto, 2011; Johnson and Preuss, 2002). The hydrated pollen grain undergoes cytoplasmic and cytoskeletal reorganization that transforms the pollen intine into a polarized cell (Zheng *et al.,* 2018). Through focused secretion of vesicles targeted to a specific location on the plasma membrane, the pollen intine protrudes from the pollen grain though a pore usually adjacent to the site of pollen adhesion to stigmatic papillae surface, forming a tubular structure called the pollen tube (PT) (Figure 1.1C; Johnson and Preuss, 2002). Unlike animal gametes, plant sperm are non-motile, therefore, requiring a mechanism to transport its two sperm nuclei to an ovule located deep within the pistil tissues (Sprunck, 2020). The PT functions as a sperm cell trafficking structure that rapidly elongates through the pistil tissues to deliver its gametes to the distant ovule (Mollet *et al.,* 2013).

The polarized apex of the PT first penetrates into the stigmatic papillae cell and directionally elongates down through the dense cell wall matrix of the stigma and style

(Figure 1.1C; Johnson and Preuss, 2002). Passage through the stigma and style represents a critical checkpoint for the PT, as it primes the PT to perceive the necessary chemical guidance signals from the pistil tissues that focus growth toward the ovary and drastically alters the PT gene expression profile (Palanivelu and Tsukamoto, 2011). The importance of growth through these female tissues is exemplified by an increase in PT ovule targeting efficiency following exiting the style (Qin *et al.,* 2009; Boavida *et al.,* 2011).

After passing through the style, the PT merges onto a highway of specialized tissue called the transmitting tract (TT) that extends from the style into the ovary (Qu *et al.,* 2015; Cascallares *et al.,* 2020). In the TT, PTs grow between cells in the extracellular matrix (ECM), where they are provided female-supplemented nutrients, proteins, and unique small molecules that critically support the PT's trajectory to fertilize the distant ovule, as they facilitate rapid PT growth, adhesion, and guidance cues to the ovary (Figure 1.2; Zheng *et al.,* 2018; Cascallares *et al.,* 2020; Palanivelu and Tsukamoto, 2011). Arabinogalactan proteins (AGPs), which control signaling and trafficking processes in this specialized tissue have been shown to be endocytosed by the PT and deglycosylated (Cheung and Wu, 1999). Furthermore, injection of AGP-specific precipitating agents, such as phenyl glycosides into the TT inhibit PT growth (Palanivelu and Tsukamoto, 2011). In Arabidopsis, loss-of-function mutants in the gene encoding *no transmitting tract (ntt)*, a C2H2/C2HC zinc finger transcription factor, display a decreased PT growth rate and premature growth arrest that results in a reduced seed set localized to the apical-most region of ovules (Crawford *et al.,* 2007; Palanivelu and

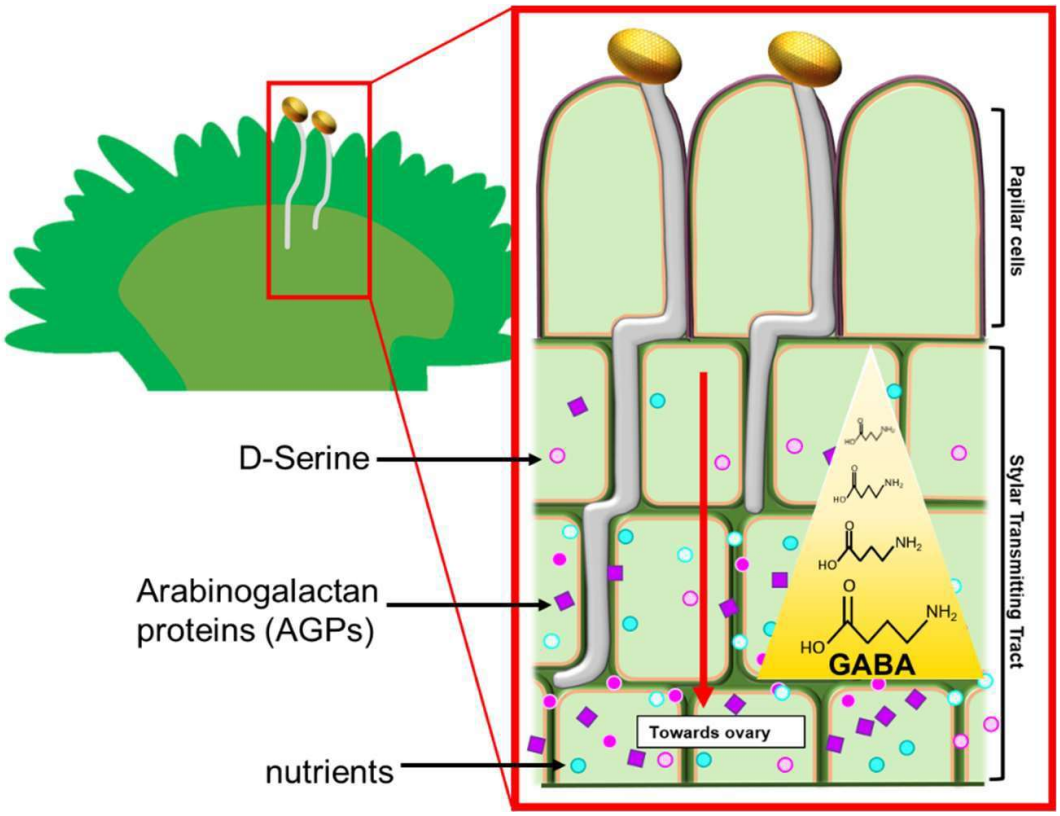

Figure 1.2: Pollen-pistil interactions during the process of double fertilization. The pistil actively participates in the process of double fertilization from start to finish and can prevent incompatible fertilization events as early as blocking pollen grain hydration at the stigmatic surface. In compatible pollen-pistil interactions, the process of double fertilization proceeds as described in Figure 1.1. As the pollen tube (PT) penetrates through the pistil tissues, it interactswith a variety of different cell types, making this an ideal and rare system to study single cell- cell interactions. The pistil's participation in the process of double fertilization is essential and the molecules it provides from beginning to end for the PT directly facilitates successful fertilization events. The unique pistil cell types that the PT penetrates past supply chemoattractants, small molecules, neurotransmitter gradients, and nutrients that are exocytosedinto the surrounding pistil extracellular matrix. The PT will integrate the provided signals as positional guidance cues that direct it toward the ovary as well as uptake the nutrients to sustainits rapid elongation. In the ovary, other specific small molecule peptides inform the PT which ovules are fertilized and unfertilized, and even the PT's last interaction with one of the two ovule synergid cells within the ovule mediates the release of its two sperm nuclei, completing the function of the PT and its role in the process of double fertilization.

Tsukamoto, 2011). Furthermore, the double mutant line in two TT-localized AGPs from *Nicotiana tabacum* (tobacco), *transmitting tract-specific 1 and 2 (tts1/ tts2)*, are completely sterile, and these proteins natively exhibit a gradient of increasing glycosylation moieties that was directionally correlated with the trajectory of proper PT growth in the TT (Palanivelu and Tsukamoto, 2011). Other molecular players in the TT include directional gradients of gamma-aminobutyric acid (GABA), D-serine, as well as auxin (Cascallares *et al.,* 2020; Palanivelu and Tsukamoto, 2011; Palanivelu *et al.*, 2003; Renault *et al.,* 2011; Michard *et al.,* 2011). Additionally, many vital TT-specific genetic players have been identified through genetic analysis and are well documented by Zheng and colleagues, 2018.

The PT continues to traverse the TT tissues into the ovary and then ceases penetrative growth following recognition of ovary-specific guidance cues, and emerges from the TT onto the septum, potentially by localized degradation of the apical cuticle layer (Palanivelu and Tsukamoto, 2011). The septum is a structure that symmetrically subdivides the ovary and functions as the scaffold to which the ovules are anchored by a tether called the funiculus (Palanivelu and Tsukamoto, 2011). The PT elongates on the surface of the septum until perceiving chemoattractants emanating from an unfertilized ovule, such as LURE peptides and the AGP AMOR (Figure 1.1C; Mizukami *et al.,* 2016; Zheng *et al.,* 2018). Upon recognition of these signals, the PT grows with toward the ovule in a tightly controlled manner to the funiculus of the unfertilized ovule, and with a precisely choreographed migration, arrives in the ovule through the micropyle (Figure 1.1C; Palanivelu and Tsukamoto, 2011; Qu *et al.,* 2015; Sprunk, 2020). The functional importance of each genetic and molecular player in this process is demonstrated by

simultaneous mutation in the receptor-like kinases *LOST IN POLLEN TUBE GUIDANCE1 and 2 (LIP1/LIP2),* which results in defective PT guidance into the micropyle as well as significantly reduces the ability of *lip1/lip2* mutant PTs perception of the key ovular guidance cue LURE1 in Arabidopsis (Liu *et al.,* 2013; Zheng *et al.,* 2018).

Most angiosperms develop a seven-celled ovule with eight nuclei, including three haploid antipodal cells positioned farthest from the micropyle, a homodiploid central cell positioned behind the haploid egg cell, and two synergid cells localized closest to the micropylar opening (Sprunk, 2020; Qu *et al.,* 2015; Johnson and Preuss, 2002). Upon arriving in the ovule, the PT comes in direct contact with one of two synergid cells, and the PT-synergid cell interaction mediates PT growth arrest at the synergid cell and rupture, facilitating the release of the PT's cytoplasm containing the two sperm cells into the embryo sac (Figure 1.1C; Johnson and Preuss, 2002). Multiple genes in Arabidopsis have been identified that mediate PT growth arrest and release in the synergid cell (Palanivelu and Tsukamoto, 2011). For example, the serine/threonine receptor-like kinase, *FERONIA/SIRENE (FER/SER)*, is required for PT growth arrest as exemplified in pistils of *fer/ser* double mutants in which the PT continues to grow in the ovule and fails to burst (Rotman *et al.,* 2003; Escobar-Restrepo *et al.,* 2007; Huck *et al.,* 2003).

Finally, in a spatiotemporal fashion, one of the released sperm cells migrates and fuses with the egg cell, which develops into the zygote, while the other sperm cell fuses with the central cell, giving rise to the endosperm (Johnson and Preuss, 2002). This fusion event of two male gametes (sperm cells) with the two female gametes (egg cell and central cell) marks the end of this rigidly controlled process and is the respective

origin of the term “double fertilization” for this mode of plant sexual reproduction (Palanivelu and Tsukamoto, 2011; Johnson and Preuss, 2002)

III. Protein O-Fucosylation: An important post-translational modification

a. Enzymes, substrates, and mechanism

Protein O-fucosylation is an important post-translational modification that was first identified in 1975 in amino acid fucosides isolated from human urine, and subsequently, 15 years later, the first protein reported to contain this modification was human urinary-type plasminogen activator (uPA) (Hallgren *et al.,* 1975; Kentzer *et al.,* 1990). Protein O-fucosylation is defined as the attachment of the monosaccharide L-fucose (6-deoxy-L-galactose) onto the hydroxyl moiety of serine or threonine residues within a protein, and although this modification is rare, it is essential for optimal organismal health in eukaryotic organisms (Lira-Navarette *et al.,* 2011; Liu *et al.,* 2019).

Protein O-fucosylation is catalyzed by enzymes called protein O-fucosyltransferases (POFT(s)), and in most reports across different species, this modification is catalyzed by only two proteins, POFUT1 and POFUT2 (Lira-Navarette *et al.,* 2011; Holdener and Haltiwanger, 2019). POFTs utilize the sugar-nucleotide GDP-β-L-fucose (guanosine 5'-[3-(6-deoxy-L-galactopyranosyl) dihydrogen diphosphate]) to α-fucosylate a specific set of non-overlapping protein targets containing a conserved cystine-rich protein domain, and this modification broadly functions to mediate protein-protein interactions as well as functions as a chaperone protein assisting in the proper folding of other proteins (Figure 1.3A; Holdener and Haltiwanger, 2019; Lira-Navarette *et al.,* 2011). POFUT1 enzymes recognize properly folded cystine-rich epidermal growth factor (EGF) repeat domains on protein substrates, and O-fucosylates serine or threonine

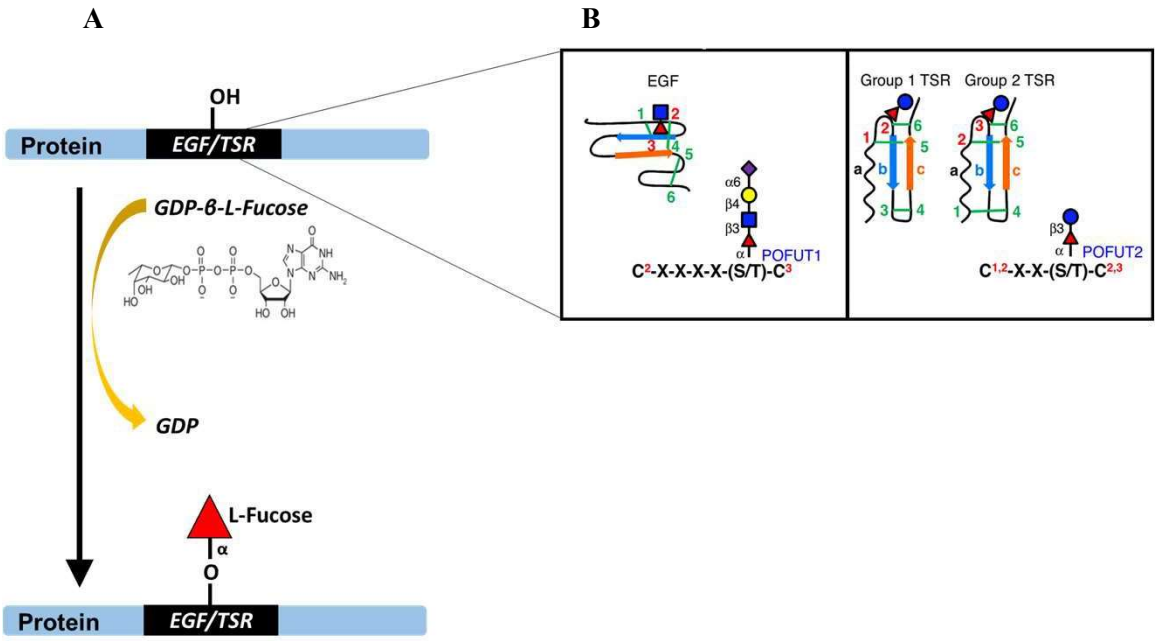

Figure 1.3: Mechanism of protein O-fucosylation. A, Protein O-fucosyltransferases (POFTs; denoted in figure as POFUT1 or POFUT2 and referenced here and throughout this dissertationas POFT1 or POFT2, respectively) utilize GDP-β-L-fucose to α-fucosylate serine or threoninehydroxyl groups within target proteins. B, These modifications occur within properly folded cystine-rich epidermal growth factor (EGF) or thrombospondin type I (TSR) repeat domains within the target protein that display a defined amino acid consensus sequence for each POFT.Fucose is depicted as a red triangle in A and B. O-fucosylation can act as a priming sugar to allows for further elaboration of the glycan by other glycosyltransferases (depicted as a blue square, yellow and blue circles, and a purple diamond). Figure adapted from Holdener and Haltiwanger, 2019.

residues within the consensus sequence C^2-X_1-X_2-X_3-X_4-[S/T]-C^3, where C^2 and C^3 respectively represent the second and third conserved cystine residues within the domain and X denoting any amino acid (Figure 1.3B; Holdener and Haltiwanger, 2019; Chen *et al.,* 2012). Similarly, POFUT2 enzymes recognize and catalyze O-fucosylation of within cystine-rich thrombospondin type 1 (TSR) repeat domains exhibiting the consensus sequences C^1-X_1-X_2-(S/T)-C^2 or C^2-X_1-X_2-(S/T)-C^3, depending upon the disulfide bonding pattern of the specific TSR domain (Figure 1.3B; Holdener and Haltiwanger, 2019).

Glycosyltransferases are classified into families based on their known function as well as amino acid sequence similarity in the continuously updated Carbohydrate-Active enZYme Database (cazy.org, CAZy; Hansen *et al.,* 2010). For example, the GlycosylTransferase 65 (GT65) family are defined as GDP-fucose protein O-α-fucosyltransferases that are distantly related to the GT68, GT23, and GT11 glycosyltransferase families, and are only represented by a handful of solved proteins structures of POFUT1 enzymes from 3 metazoan organisms: *Caenorhabditis elegans (C. elegans)*, *Homo sapiens (*human*, H. sapiens), and Mus musculus (*mouse, *M. musculus)* (Coutinho *et al.,* 2003; Campbell *et al.,* 1997; Lombard *et al.,* 2014). Two POFUT2 structures have been delineated and represent the GT68 family, including one generated from *H. sapiens* and the other from *C. elegans*, and this family shares an equal annotation of function in CAZy as GT65 enzymes as well as a distant relationship with the GT65 family and the other fucosyltransferase families, GT23 and GT11 (cazy.org; Lombard *et al.,* 2014; Lairson *et al.,* 2008). Moreover, sugar-nucleotide-dependent glycosyltransferase, such as POFTs conform to 3 general types of tertiary fold

architectures: 1) GlycosylTransferase-A (GT-A), 2) GlycosylTransferase-B (GT-B), or 3) GlycosylTransferase-C (GT-C) three-dimensional (3-D) structural topology, which further relates to their mechanism of catalysis and indicates an evolutionary divergence between glycosyltransferases displaying these different folds (Lombard *et al.,* 2014; Lairson *et al.,* 2008). GT65 and GT68 enzymes exhibit a GT-B fold topology with two distinct β/α/β Rossmann domains that face each other and are subdivided by a flexible linker (Lairson *et al.,* 2008; Lombard *et al.,* 2014). GT-A folds are fairly homologous to GT-B topology with the exception of the two β/α/β Rossmann domains being tightly linked, creating one continuous β-sheet, while the rare GT-C fold containing glycosyltransferases are represented by large, hydrophobic integral membrane proteins that function in the endoplasmic reticulum (ER) or plasma membrane (PM) and possess 8-13 transmembrane helices with an active site localized to a long loop domain (Lairson *et al.,* 2008). Aside from GT family and type of fold, glycosyltransferases are further grouped by the stereochemistry of the novel glycosidic linkage they impart with respect to the anomeric reaction center of the donor sugar, which can either result in net retention or net inversion of the transferred sugar moiety (Lairson *et al.,* 2008). Both POFUT1 and POFUT2 (*henceforth denoted as "POFT1" and "POFT2" in this study)* and their respective families are characterized as inverting glycosyltransferases that utilize GDP-β-L-fucose to α-L-fucosylate protein targets (Lombard *et al.,* 2014; Lairson *et al.,* 2008; Lira-Navarette *et al.,* 2011; McMillan *et al.,* 2017; Li *et al.,* 2017; Chen *et al.,* 2012; Valero-Gonzalez *et al.,* 2016).

Inverting glycosyltransferases are reported to perform their enzymatic function through an S_N2-like reaction mechanism, in which a residue within the active site serves

as a base catalyst that functions to deprotonate the nucleophile of the acceptor substrate, facilitating cleavage and displacement of the substituted nucleoside diphosphate (Liarson *et al.,* 2008). However, defining the base catalyst for inverting GT-B enzymes remains the key inquiry surrounding characterizing the mechanism of catalysis, as these glycosyltransferases display a high degree of variability in their method of catalysis between as well as within a given GT family in comparison to the straightforward reactions of inverting GT-A fold glycosyltransferases, which follow an S_N2-like reaction mechanism with a defined catalytic base (Lairson *et al.,* 2008; Li *et al.,* 2017). This variability in inverting GT-B catalysis has been postulated to be attributed with the greater diversity in reactions catalyzed by this class of glycosyltransferases as well as with the physical distance separating the two distinct domains of inverting GT-B glycosyltransferases (Lairson *et al.,* 2008). Interestingly, reports indicate that POFT1 and POFT2 do not share a conserved mechanism of catalysis, as POFT1s lack a typical catalytic base and seem to adopt an S_N1-like mechanism, whereas *C. elegans* and *H. sapiens* POFT2 possess a glutamic acid residue in their active sites at amino acid 52 and 54, respectively, that functions as the catalytic base and follows a typical S_N2-like reaction mechanism (Li *et al.,* 2017; Lira-Navarette *et al.,* 2011; McMillan *et al.,* 2017; Chen *et al.,* 2012; Valero-Gonzalez *et al.,* 2016).

Unconventionally, reports on *C. elegans, H. sapiens, and M. musculus* POFT1 suggest this family of inverting GTs carries out an S_N1-like reaction mechanism that is facilitated by only a few highly conserved key catalytic residues positioned in the active site that also forms an extensive network of hydrogen bonds (H-bonds) that confer stability as well as functions to correctly position substrates during the reaction (Lira-

Navarette *et al.,* 2011; Li *et al.,* 2017; McMillan *et al.,* 2017). POFT1 catalysis has been proposed to begin with cleavage of the glycosidic bond between GDP and fucose and is initiated by a highly conserved arginine residue in the C-terminal domain of these enzymes (Lira-Navarette *et al.,* 2011; Li *et al.,* 2017; McMillan *et al.,* 2017). In *C. elegans* POFT1 (CePOFT1), Asn43 in the N-term then coordinates with the critical arginine residue (Arg260) in the C-term of this enzyme to position the incoming hydroxyl group of the acceptor protein substrate in close proximity to both a single water molecule and the oxygen atom of the β-phosphate of GDP, which is additionally considered the catalytic base, resulting in the formation of an oxocarbenium-phosphate ion pair transition state (Lira-Navarette *et al.,* 2011). These residues are highly conserved in model metazoan POFT1s and the proximity of these molecules has been proposed to function as a proton shuttle with the water molecule, providing efficient proton transfer from the acceptor protein hydroxyl to the leaving group β-phosphate (Li *et al.,* 2017). Furthermore, positively charged residues positioned in the catalytic cleft of POFT1s promote the departure of GDP following protonation, while the water molecule further functions to stabilize the oxocarbenium ion-like transition state though H-bonding. The reaction is completed following nucleophilic attack by the charged oxygen atom of the acceptor substrate to the anomeric carbon of fucose (Lira-Navarette *et al.,* 2011; Li *et al.,* 2017; McMillan *et al.,* 2017; Lairson *et al.,* 2008).

b. <u>The Notch Signaling Pathway</u>

Interestingly, in humans, POFUT1 and POFUT2 share only 21% sequence identity, which is a common but unique feature of POFTs, and reports as well as querying these fucosylation domains in PROSITE (prosite.expasy.org) demonstrate a limited

number of proteins exhibit α-O-fucosylation, with approximately 200 proteins possessing O-fucosylated EGF domains and ~50 proteins with fucosylated TSR domains (prosite.expasy.org; Sigrist *et al.,* 2013; Schneider *et al.,* 2017; Chen *et al.,* 2012; Li *et al.,* 2017). Surprisingly, loss-of-function of POFT1 or POFT2 in mice is embryonic lethal, but no metazoan disorders have been directly associated with loss-of-function or dysregulation of POFT2, which functions primarily in optimal secretion of proteins (Chen *et al.,* 2012; Benz *et al.,* 2016; Holdener and Haltiwanger, 2019). Inversely, loss-of-function and/or mutations to POFT1 is highly associated with multiple human developmental syndromes as well as adult-onset diseases, including many forms of cancer originating from diverse organs (Ge and Stanley, 2008; Schneider *et al.,* 2017; Kopan and Ilagan, 2009; Stahl *et al.,* 2008; Li *et al.,* 2013; Penton *et al.,* 2012; Lasky and Wu, 2005; McMillan *et al.,* 2017). In fact, overexpression of POFT1 is used as an indicator of disease prognosis and has been proposed as a target for therapeutic development (Schneider *et al.,* 2017; Deschuyter *et al.,* 2020).

The necessity of a properly functioning POFT1 enzyme in maintaining organismal health is due in part, to its critical role in the evolutionarily conserved metazoan Notch signaling pathway, which is a direct cell-cell interaction pathway that is broadly responsible for regulating numerous biologically important processes underlying metazoan growth and developmental throughout the lifecycle of the organisms, including cell proliferation, differentiation, and death (Kopan, 2012; Penton *et al.,* 2012; Lasky and Wu, 2005; Deschuyter *et al.,* 2020; Wang, 2011). The 4 NOTCH proteins themselves are type II integral membrane cell surface receptors localized to the PM and contain distinct extra- and intracellular protein domains that functions to transmit short-distance signals

through direct binding with one of its cognate ligands, DELTA or SERRATE/JAGGED, displayed on the surfaces of neighboring cells (Kopan, 2012; Stahl *et al.,* 2008; Wang, 2011). Notch receptors contain up to 36 EGF repeat domains, and O-fucosylation by POFT1 in the ER, especially EGF8 and 12, are critical for ligand binding, as these sugar moieties directly form hydrogen bonds and salt bridges with the cognate ligand backbone, facilitating their interaction (Luca *et al.,* 2017). The curved extracellular domain of Notch is sequentially activated by a catch-bond mechanism , which is initiated by ligand binding, followed by mechanical tension on the receptor-ligand complex that is induced by receptor or ligand endocytosis. Furthermore, the amount of tensile force required to activate the Notch receptor by each of its ligands is specific and additionally facilitates conformational changes to both the ligand and Notch receptor, resulting in the exposure of Notch's intracellular proteolytic cleavage site (Luca *et al.,* 2017). The formerly protected Notch intracellular domain is then proteolytically cleaved and translocates to the nucleus where it binds to DNA-binding CSL transcriptional repressor proteins, leading to activation of a myriad of CSL-regulated downstream genes (Figure 1.4; Kopan, 2012; Stahl *et al.,* 2008; Kopan and Ilagan, 2009). Moreover, POFT1 not only functions in the Notch signaling pathway to mono-O-fucosylate EGF domains on the extracellular region of Notch receptors, but these single fucosylation events are further required for proper receptor folding and for further N-glycosylation of the fucose residue by FRINGE N-acetylglucosaminyltransferases in the Golgi-apparatus (Figure 1.4; Penton *et al.,*2012; Stahl *et al.,* 2008; Kopan and Ilagan, 2009).

Notch receptor fucosylation by POFT1 as well as other post-translational modification events, specifically glycosylation and ubiquitination, directly influence

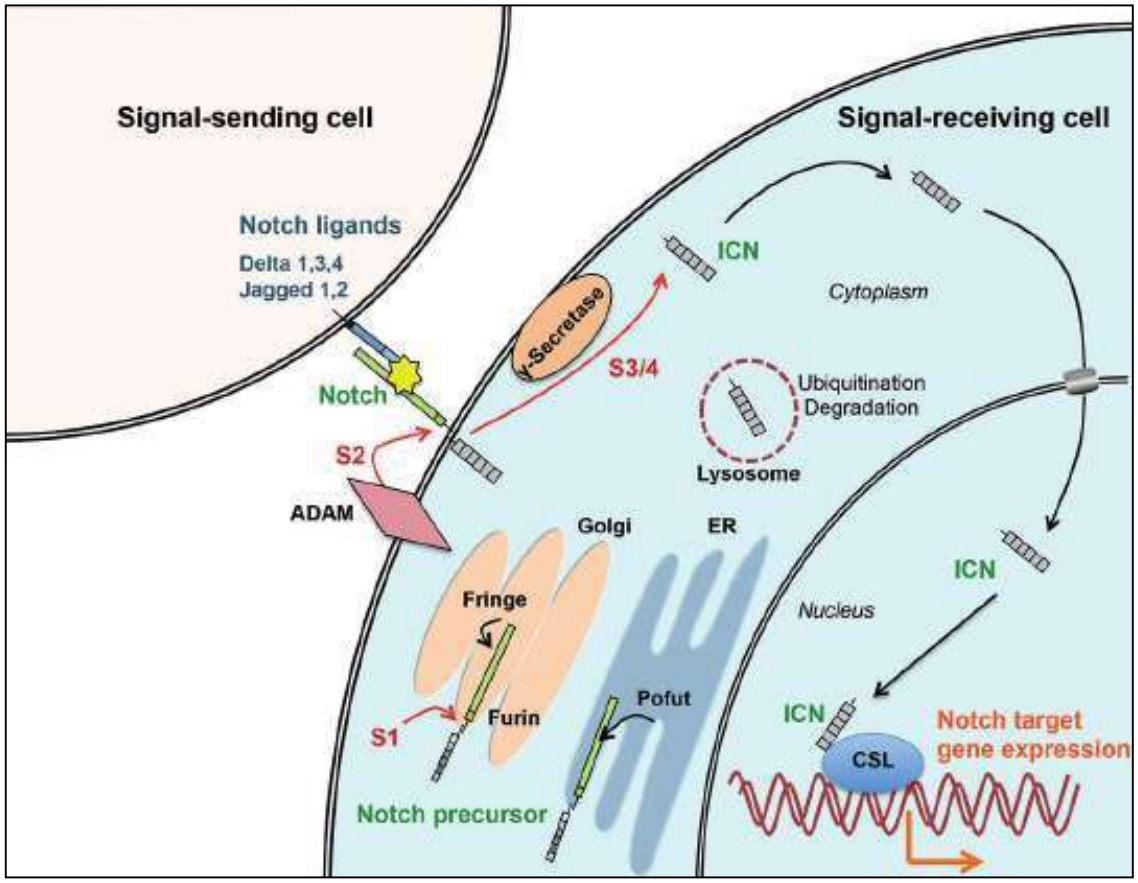

Figure 1.4: The Notch signaling pathway. In metazoan systems, POFT1 (denoted in figure as POFUT1) most impactfully functions in the Notch signaling pathway, which is a direct cell- cell communication system. POFT1 O-fucosylates the extracellular EGF repeat domains within the Notch receptor in the endoplasmic reticulum (ER). This modification is essential forfurther glycosylation events, proper ligand binding, and activation of the Notch signaling pathway. Upon Notch-ligand binding, mechanical tension induced by endocytosis of either cell surface receptor results in a conformational changes and exposes the previously protected intracellular protease site of the Notch receptor. Cleavage of the intracellular Notch domain (ICN) facilitates translocation to the nucleus and activation of CSL-mediated gene expression.Figure adapted from Melnik B.C., 2015.

receptor recognition and binding strength to its cognate ligands, tightly mediates the timing and intensity of downstream transcriptional activation as well as maintains proper receptor recycling and cell surface distribution (Kopan, 2012; Wang, 2011). Mutations or alterations in post-translational modifications, especially O-fucosylation of the Notch receptors, is intimately associated with a diverse array of severe developmental, morphological, and pathological diseases in metazoans, and of upmost current interest, a recent study implicated the Notch signaling pathway in enhancing COVID-19 (SARS-CoV2) infection, viral replication, and was most gravely linked to exacerbating cardiovascular complications observed in patients (Holdener and Haltiwanger, 2019; Breikaa and Lily, 2021).

c. Similarities and differences: Plants versus Metazoans

If not evident by now, the majority of our knowledge surrounding protein O-fucosylation and protein O-fucosyltransferases has been gleaned by studies pertaining to a discrete number of metazoan species, leaving a significant gap in our understanding of these proteins in plant systems (Hansen *et al.,* 2012). It is clear that these proteins function in the ER as critical regulators of fundamental processes underlying metazoan organismal signaling pathways as well as assist in proper protein folding and secretion. Additionally, in metazoan systems, loss-of-function or dysregulation of these enzymes imparts severe consequences to organismal heath either directly or indirectly. Nonetheless, a generalized lack of information of plant glycosyltransferases and the targets of these enzymes' modifications persists and is an area of research requiring experimental attention (Strasser *et al.,*2021).

Plants contain far more glycosyltransferases than any other form of life, and the genes that encode these enzymes represent an overall large evolutionary genome expansion event in plants (Hansen *et al.,* 2012). This genetic adaptation is postulated to be attributed to the polysaccharide-rich cell walls of plants as well as to their stationary (non-motile) existence, which mandates that they quickly integrate and adapt to their dynamic environment through complex signaling mechanisms as well as perform secondary metabolism to produce specialized compounds that are fundamental to their survival (Hansen *et al.,* 2009; Hansen *et al.,* 2010; Hansen *et al.,* 2012). For example, in the Arabidopsis genome, over 460 genes are predicted to encode glycosyltransferases compared to less than 230 genes in the human genome (Hansen *et al.,* 2010). Plant glycosyltransferases have also been proposed to be more complex in their function compared to other lifeforms due to the observation of non-catalytic domains in some of these proteins, which may function in substrate recognition and/or protein-protein interactions that facilitate protein complex formation or with protein partners necessary for specificity or functionality of the enzyme (Hansen *et al.,* 2010).

Identifying the function of plant glycosyltransferases has been recognized as a necessary, yet enormous task by the plant scientific community (Hansen *et al.,* 2010; Straser *et al.,* 2021). A central limitation to our knowledge of glycosyltransferase enzymes in plants as well as across all organisms pertains to the native subcellular localization of these proteins, which are largely type II integral transmembrane proteins that reside in the ER or Golgi-apparatus (Hansen *et al.,* 2012; Lairson *et al.,* 2008). A general deficit in our understanding of membrane proteins is also widely acknowledged and is a consequence of the challenges associated with successful isolation of these

proteins out of their preferred native hydrophobic environments without disrupting the enzyme's endogenous function, which is a prerequisite that must be achieved prior to further investigation to determine the catalytic identity of the glycosyltransferase or membrane-localized protein of interest (McKay *et al.,* 2018; Hardy *et al.,* 2018; Errasti-Murugarren *et al.,* 2021). Nonetheless, developments in the experimental approaches and platforms for isolation of membrane protein as well as novel techniques to assess the identity of membrane localized glycosyltransferases continues to progress and has assisted in identifying novel plant glycosyltransferases (Strasser *et al.,* 2021).

The identification of plant glycosyltransferases has also been assisted by computational approaches that recognize amino acid sequence conservation in the coding region in plant glycosyltransferases that show sequence homology with metazoan glycosyltransferase enzymes (Hansen *et al.,* 2009; Hansen *et al.,* 2010; Hansen *et al.,* 2012). These *in silico* classification efforts allowed for their previous Pfam database (pfam.xfam.org) classifications of genes containing a conserved DUF (Domain of Unknown Function), to be assigned to specific CAZy GT families, which has facilitated more focused research efforts surrounding glycosyltransferases, as GT familial association provides putative details for glycosyltransferase's structure and function, and thus, its potential identity (Hansen *et al.,* 2012). For example, in the *Arabidopsis thaliana* genome, 1.7% of the 27,416 encoded proteins are represented by glycosyltransferase enzymes, yet less than 20% of them have been catalytically identified (Hansen *et al.,* 2012). Furthermore, 39 genes in the Arabidopsis thaliana genome have been identified to encode putative homologs of metazoan POFT1s and are associated with the CAZy GT65

family based on sequence conservation in the catalytic *O-FucT* domain (PF10250) (Wang, 2011).

To date, SPINDLY (AtSPY, At3g11540) represents the only POFT that has been identified in Arabidopsis, and functions in the cytoplasm and nucleus to O-fucosylate the nuclear DELLA transcriptional regulatory proteins AtRGA1 (REPRESSOR OF GIBBERELLIC ACID 1, At2g01570) and ACINUS (Apoptotic Chromatin condensation Inducer in the Nucleus, At4g39680) at serine and threonine residues that do not follow a defined consensus sequence like metazoan POFTs (Zentella *et al.,* 2017; Bi *et al.,* 2021) . O-fucosylation of AtRGA1 and ACINUS mediates their independent interactions with other transcriptional elements in the nucleus that both function to regulate a large repertoire of genes that facilitate multiple phytohormone signaling pathways, including gibberellic acid (GA)-, brassinosteroid (BR)-, and abscisic acid (ABA)-mediated signaling, which have further influence in controlling almost all aspects related to plant development, double fertilization, and responses to stress and pathogen attack throughout the lifetime of the plant (Shan *et al.,* 2012; Bi *et al.,* 2021; Zentella *et al.,* 2017). However, SPINDLY is not annotated as a member of the 39 putative POFT encoding genes in Arabidopsis, nor was this gene originally predicted to encode a POFT (Zentella *et al.,* 2017; Smith *et al.,* 2018a; Smith *et al.,* 2018b). These findings suggests that the number of genes that encode POFTs in Arabidopsis may be underestimated, and/or SPINDLY represents a novel type of POFT in plant systems that is evolutionarily divergent from metazoan-like POFTs. Alternatively, the number of genes belonging to the *Arabidopsis thaliana* putative POFT family may be grossly overestimated, and the enzymes encoded by this family may function as different types of glycosyltransferases

(Hansen *et al.,* 2012; Smith *et al.,* 2018a; Smith *et al.,* 2018b). Nonetheless, all 39 genes members of the Arabidopsis putative POFT family are predicted to share structural homology with CePOFT1, and all but two members have been experimentally determined to localize to the Golgi-apparatus, where post-translational glycosylation events and biosynthesis of most cell wall polysaccharides are known to occur in plant systems (Hansen *et al.,* 2012; Nikolovski *et al.,* 2012; Wang *et al.,* 2013; Smith *et al.,* 2018a; Smith *et al.,* 2018b; Takenaka *et al.,* 2018; Neumetzler *et al.,* 2012; Verger *et al.,* 2016; Stonebloom *et al.,* 2016).

d. The *Arabidopsis thaliana* putative protein O-fucosyltransferase family

Of the 39 representative genes identified as members of the *Arabidopsis thaliana* putative POFT family, 11 genes have been investigated to some degree, however, none have demonstrated protein O-fucosyltransferase activity (Wang *et al.,* 2013; Smith *et al.,* 2018a; Smith *et al.,* 2018b; Takenaka *et al.,* 2018; Neumetzler *et al.,* 2012; Verger *et al.,* 2016; Kohorn *et al.,* 2021; Stonebloom *et al.,* 2016; Won *et al.,* 2009; Pagnussat *et al.,* 2005; Boavida *et al.,* 2009). Of these previous studies pertaining to the members of the Arabidopsis POFT family, only one report by Takenaka and team (2018) provides any biochemically data on the potential identity of these family members (Takenaka *et al.,* 2018). This research group aimed to identify glycosyltransferases that were involved in synthesizing the abundant pectic polysaccharide rhamnogalacturonan I (RG-I) in seed coat mucilage by mining two microarray datasets produced from loss-of-function mutants encoding transcription factors that are involved in this process, *TTG1 (TRANSPARENT TESTA GLABRA 1)* and *AP2 (APETALA 2).* One novel glycosyltransferase gene, which is also a member of the Arabidopsis putative POFT family, was identified for further

investigation, *At5g15740* (Takenaka *et al.,* 2018). T-DNA insertional mutants in this gene appear phenotypically wildtype, except mutant seeds produce less mucilage that is reduced in rhamnose and galacturonic acid (GalA) and exhibit irregular columellae width, suggesting this putative POFT was involved in the synthesis of RG-I (Takenaka *et al.,* 2018).

Following isolation of the protein encoded by *At5g15740,* catalytic assessment indicated that this gene encoded an RG-I RhamnosylTransferase (RRT, gene annotated as *RRT1*) that facilitated the transfer of rhamnose to the reducing end of GalA residues of the nascent RG-I backbone (Takenaka *et al.,* 2018). This team further identified and catalytically determined 3 other genes that are highly homologous to *RRT1* and are also members of the Arabidopsis putative POFT family, *At3g02250 (RRT2), At2g03289 (RRT3),* and *At1g14020 (RRT4)*, encode RRTs, and proposed these family members in addition to the other 35 genes comprising the POFT family are members of the GT106 family of UDP-β-L-rhamnose:RG-I 4-α-rhamnosyltransferases (Takenaka *et al.,* 2018). However, until composing this dissertation, a major criticism of this study resided in the authors clear acknowledgement that *RRT1-4* putatively encode POFTs and are designated as members of the GT65 family represented only by metazoan POFT1s, but completely neglect to include GDP-β-L-fucose into their analyses of donor substrate preference of these enzymes, which is this family's known and most likely utilized sugar-nucleotide, and further confounded information pertaining to these 4 genes as well as the hypothesized familial grouping (Takenaka *et al.,* 2018). Nevertheless, recent evidence has elucidated that at least RRT4 is an RRT, suggesting that further delineation of the enzymatic identities of the other members of the Arabidopsis putative POFT family is

necessary to untangle the significance and potential functions of this computationally predicted genetic association (personal communication with Debra Mohnen at the Complex Carbohydrate Research Center, University of Georgia).

Interestingly, other glycosyltransferases, specifically, the putative galacturnosyltransferases *AtGAUT11 (At1g18580), AtGALT5 (At1g02720), and QUA1 (GAUT8, At3g25140)*, demonstrate loss-of-function phenotypes related to seed mucilage defects and reductions in GalA in the different tissues examined (Caffall *et al.,* 2009; Kong *et al.,* 2013). No growth defects were observed in *gaut11* or *gaut5* T-DNA insertional mutants, but *qua1* mutant lines were severely dwarfed, sterile, and displayed a loss of cell adhesion that resulted in cell detachment, suggesting that these hypothesized glycosyltransferases are involved in pectin biosynthesis (Caffall *et al.,* 2009; Kong *et al.,* 2013; Neumetzler *et al.,* 2012; Verger *et al.,* 2016; Kohorn *et al.,* 2021) A fascinating link exists between *QUA1*, and two members of the Arabidopsis putative POFT family, *FRIABLE (AtFRB1, At5g01100) and ESMERALDA1 (AtESMD1, At2g01480).* For example, *frb1* and *qua1* T-DNA insertion mutant lines display severe cell adhesion defects that leads to cell detachment and organ fusion, which can be rescued by a second mutation in *AtESMD1* (Neumetzler *et al.,* 2012; Verger *et al.,* 2016; Kohorn *et al.,* 2021). Opposite of *qua1* mutants lines, *frb1* mutants did not display alterations in the total amount of pectic polysaccharides, but the Golgi contained less arabinose and more galactose, which lead to a net increase in galactosylated xyloglucan polysaccharides and a net decrease of other galactose containing cell wall components, such as RG-I and AGPs, as well as alterations to the xyloglucan architecture and increased expression of cell wall modification enzymes, including a pectin-methylesterase (*PME*, *At4g02330*),

EXTENSIN 4 (EXT4; At1G76930), two XyG endo-transglucosidase/hydrolases (*XTH19, At4g30290 and XTH23, At4g30290*), and *COBRA (At5g60290)* (Neumetzler *et al.,* 2012). *esmd1* mutant lines do not display any phenotypic abnormalities, and although loss-of-function of this gene in the *qua1* or *frb1* mutant backgrounds was efficient at suppressing the severe cell adhesion phenotypes displayed by single mutant *qua1* and *frb1* lines, it was not attributed to alterations to their pectin content, and further indicated that *ESMD1, FRB1*, and *QUA1* as well as its homolog, *QUA2* (TSD2, At1g78240), are involved in the same biochemical pathway (Neumetzler *et al.,* 2012; Verger *et al.,* 2016; Kohorn *et al.,* 2021).

Furthermore, Debra Mohnen and team also determined *AtFRB1* is also an RRT, suggesting this family of enzymes predicted to encode POFTs are not all grouped correctly and potentially have different glycosyltransferase activities (personal communication with Debra Mohnen at the Complex Carbohydrate Research Center, University of Georgia). Notably, proteins possessing post-translational O-glycosylation modifications in Arabidopsis include AGPs, EXTs, Leucine-Rich eXtensins (LXRs), repetitive Proline-rich Proteins (PRPs), as well as the two recently reported transcriptional regulatory proteins, AtRGA1 DELLA protein and ACINUS (Strasser *et al.,* 2021; Zentella *et al.,* 2017; Bi *et al.,* 2021). However, the O-linked sugar on all of these proteins, with the exception of AtRGA1 and ACINUS, is galactose or arabinose and not fucose (Strasser *et al.,* 2021). Nonetheless, this demonstrates that novel O-fucosylated proteins are beginning to be discovered, suggesting our understanding of the plant proteome that is post-translationally modified by O-fucose is incomplete.

One other family members of the putative POFT family in Arabidopsis also suggest these enzymes influence pectin content and/or structure, *PECTIN ARABINOGALACTAN SYNTHESIS-RELATED (AtPAGR; At3g26370)* (Stonebloom *et al.,* 2016). *AtPAGR* was identified and characterized by Stonebloom and colleagues (2016), and plays a fundamental role in plant physiology, as at least one functional copy of this allele is required in Arabidopsis, and alterations in endogenous transcript levels of this gene lead to disruptions in pectin-related cellular monosaccharide content, and further, display many pleotropic phenotypes (Stonebloom *et al.,* 2016). Homozygous Arabidopsis *pagr*$^{-/-}$ lines were not able to be generated due to this enzyme's fundamental role in pollen germination, which was illustrated by *pagr* $^{-}$ pollen grains segregating from heterozygous *pagr*$^{+/-}$ lines, which developed normally but failed to germinate or produce a PT (Stonebloom *et al.,* 2016). This experimental challenge was circumvented by investigating 2 homologs of *AtPAGR* in *Nicotiana benthamiana (N. benthi,* tobacco), *NbPAGR-A* and *NbPAGR-B* (80.2% and 80.6% sequence identity with *AtPAGR*, respectively, and 97.2% sequence similarity to each other). *NbPAGR* silencing in tobacco produced stout plants as a result of arrested internode and petiole expansion, shorter roots that were discolored, leaves that tightly grouped around the SAM and a decrease in cell wall galactose and arabinose. In *NbPAGR* overexpression lines, cell wall arabinose content was increased and displayed an enormous array of interesting phenotypes, including seedlings exhibiting dwarfism, slower rosette growth, and inflorescences displaying fasciation, increased branching, pedicels that were swollen and translucent, and defective internode expansion under long-day light conditions. Furthermore, under short-day light conditions, overexpression lines lost apical dominance and developed

rosettes with abnormal leaf morphology. The altered cell wall polysaccharide composition in these *pagr* mutant lines was associated with altered type I and type II arabinogalactan side chains on RG-I backbones (Stonebloom *et al.,* 2016). The plethora of phenotypes induced by simply altering *PAGR* expression levels, suggests a potentially larger regulatory role for this putative POFT, which is in line with the function of POFT1s in metazoans and that of SPINDLY.

In contrast to the Arabidopsis putative POFT family members that indicate a role in the synthesis or structure of cell wall pectic polysaccharides, two previously characterized and homologous gene members propose a role for these enzymes in the synthesis of cell wall hemicelluloses. *MANNAN SYNTHESIS RELATED 1* and *2 (AtMSR1, At3g21190* and *AtMSR2, At1g51630)* share 91% sequence similarity, and unlike some of the severe phenotypes displayed by mutants of the Arabidopsis putative POFT family already described, single *msr1* and *msr2* as well as double *msr1/msr2* mutant lines do not display any overt growth or developmental defects (Wang *et al.,* 2013). Additionally, these genes were both expressed ubiquitously throughout the plant and were specifically highly expressed in seedling roots, flowers, siliques, and the top region of the stem. Discrete differences in expression between *AtMSR1* and *AtMSR2* were only apparent in defined regions of a few plant structures. For example, *AtMSR1* is strongly expressed in the vascular tissue of roots, except in the basal region, while *AtMSR2* was expressed in the root epidermis. Furthermore, *AtMSR2* expression was detected in the tips of lateral roots, the socket/accessory cells surrounding the base of trichomes, and in petioles and pistil floral organs, while *AtMSR1* was strongly expressed in trichomes as well as petals (Wang *et al.,* 2013). Curiously, the only loss-of-function

phenotype detected was a significant reduction in mannan extracted from stem tissue in single *msr1* or *msr2* mutant lines (40%), and this phenotype was further exacerbated in *msr1/msr2* double mutant lines to less than 50% (Wang *et al.,* 2013). Furthermore, microsomes prepped from stems of these mutants were reduced in ManS activity, with a more severe reduction in activity observed for *msr1* mutants than *msr2,* suggesting *AtMSR1* plays a more central role in maintaining mannosyl levels in Arabidopsis. However, ManS activity was reduced even further in microsomes prepped from stems of *msr1/msr2* double mutant lines, suggesting *AtMSR2* may play a supportive role in maintaining an optimally functioning mannan biosynthetic pathway, or may reflect their different cell-specific expression patterns. Nevertheless, AtMSR1 and AtMSR2 regulate some aspect pertaining to the synthesis of mannan and further implicate a more diverse regulatory role for the Arabidopsis putative POFT family in modulating the synthesis and composition of different polysaccharide components of the cell wall (Wang *et al.,* 2013).

The final two members of this hypothesized family of POFTs in Arabidopsis only provide phenotypic information as they were identified by large-scale genetic screening or *in silico* prediction of genes involved in a general plant developmental process. For example, *EMBRYO SAC DEVELOPMENTAL ARRREST 30,* otherwise known as *TUBE GROWTH DEFECTIVE 1 (AtEDA30/AtTGD1; At3g03810)* was identified in two independent random screens of insertional mutants for genes that were associated with either male or female gametophyte development and function (Pagnussat *et al.,* 2005; Boavida *et al.,* 2009). A transposon insertional mutant in the chromosomal region encoding *AtEDA30/AtTGD1* was identified out of 130 different insertional lines that displayed female gametophyte developmental arrest prior to becoming a fertilizable

ovule due to failure of polar nuclei fusion in the central cell, resulting in a non-viable ovule (Pagnussat *et al.,* 2005).

In screening for genes involved in male gamete development, the same approach was taken for identifying genes by creating a collection of transposable element insertion lines, and the *tgd1 (eda30)* mutant developed properly but failed to produce a viable PT (Boavida *et al.,* 2009). Specifically, *in vitro,* the *tgd1 (eda30)* mutant PT was shorter than wildtype, sometimes displayed bulged regions along the tube, and had swollen tips that ballooned out as a result of isotropic growth following an initial phase of tube elongation, leading to premature growth arrest (Boavida *et al.,* 2009). Interestingly, *in vivo,* the male gamete was able to self-pollinate in heterozygous *tgd1/eda30*$^{+/-}$ lines and displayed a transmission efficiency (TE) of 0.3, which is only slightly lower than the expected TE of 0.33 due to half of the ovules being non-viable as a consequence of this mutation affecting both male and female gametes. However, in outcrosses with *tgd1/eda30*$^{+/-}$ pollen, the TE dropped to 0, suggesting that the male gamete is outraced to fertilized viable ovules every time by the wildtype-like *tgd1/eda30*$^{+}$ pollen. Interestingly, in reciprocal crosses with a *tgd1/eda30*$^{+/-}$ pistil pollinated with wildtype pollen, the TE is even lower than observed in self-pollination events (0.2 vs 0.3), suggesting that defects in the female gamete actually increase the TE of the mutant male gamete (Boavida *et al.,* 2009). The mechanism by which a mutation that deleteriously effects both male and female gametes independently but is somewhat compensated for in the case of self-pollination represents a novel and interesting phenotype and may be a unique mechanism of recognition for mutations in these putative POFT genes during the intensely coordinated process of double fertilization.

Developing roots display 3 distinct zones, including the basal meristematic zone, the elongation zone, and the differentiation zone at the most apical end of the root which correlates with 3 distinct sets of genes that are expressed under the control of a conserved *cis*- element (Won *et al.,* 2009). *ROOT HAIR-SPECIFIC 17 (AtRHS17, At4g38390)* is the final member of the Arabidopsis putative POFT family that has been previously characterized and was identified *in silico* for the purpose of illustrating how these conserved cell-specific *cis*-elements can be used to successfully identify novel root hair-specific genes (Won *et al.,* 2009). As proof that this group's *in silico* prediction method was reliable at identifying root hair specific genes, they cloned the promoter regions of the 37 novel root hair-specific genes, including *AtRHS17,* fused to GREEN FLUORESCENT PROTEIN (GFP) and visualized the fluorescent signal for each transgenic line to confirm root hair-specific expression. Surprisingly, 24 out of the 37 computationally predicted root hair genes were expressed in roots hairs, with *AtRHS17* demonstrating the least robust signal out of almost all lines (Won *et al.,* 2009). Further analysis of this report suggests expression of *AtRHS17* is the most highly expressed in pollen as well as in roots, indicating a potential role for this putative POFT in the process of double fertilization. Although further investigation must be conducted to determine if *AtRHS17* possesses novel root or PT phenotypes, this expression pattern indicates a potential role in mediating polarized tip-focused growth, which is a specialized form of cell elongation unique to PTs and root hairs (Campanoni and Blatt, 2007).

In this dissertation, we further delineate the putative POFT family in *Arabidopsis thaliana*. First, we identify and characterize a novel family member, *At3g05320*, and demonstrate its fundamental importance in facilitating pollen tube penetration through the

pistil. Phylogenetic analysis showed that this gene was more closely related to metazoan POFT1 than some of its affiliated family members. Thus, we named this gene Arabidopsis *O-FUCOSYLTRANSFERASE 1 (AtOFT1)*. Genetic analysis revealed that *oft1* mutants exhibit a marked reduction in overall fertility, however, *in vitro,* no pollen or PT-associated abnormalities were detected. Additionally, *oft1* plants display increased vegetative tissue biomass as well as increased seed size and mucilage area. Further analyses revealed that *oft1* mutant PTs are compromised in their ability to penetrate the stigma and style effectively and elongate through the TT, demonstrating a fundamental role for AtOFT1 in the process of double fertilization in pollen. We further show AtOFT1 possesses conservation in key catalytic residues important for metazoan POFT1 activity as well as in its predicted structure. Using reverse genetic techniques, we identify another gene that suppresses the PT defects of *oft1* mutants and restores its fertility, *AtGAUT14,* which additionally, may illuminate a unique pattern of regulation for the enzymes that make up the putative POFT family and the GAUT family in Arabidopsis. By developing a reliable expression and isolation platform for these enzymes, we successfully catalytically ascertain the sugar-nucleotide specificity of two other predicted family members, AtMSR1 and AtFRB1, to be GDP-β-L-fucose, providing the first evidence to date that a subset of the genes may be predicted correctly and function in protein O-fucosylation. Overall, this research establishes the Arabidopsis putative POFT family as critical regulatory enzymes governing essential plant processes, including growth and developmental processes as well as in the survival-indispensable mechanism of double fertilization.

References

Alvarez-Buylla, E. R., Benítez, M., Corvera-Poiré, A., Chaos Cador, Á., de Folter, S., Gamboa de Buen, A., Garay-Arroyo, A., García-Ponce, B., Jaimes-Miranda, F., Pérez-Ruiz, R. V., Piñeyro-Nelson, A., & Sánchez-Corrales, Y. E. (2010). Flower Development. *The Arabidopsis Book / American Society of Plant Biologists*, *8*, e0127. https://doi.org/10.1199/tab.0127

Becker, A., Alix, K., & Damerval, C. (2011). The evolution of flower development: Current understanding and future challenges. *Annals of Botany*, *107*(9), 1427–1431. https://doi.org/10.1093/aob/mcr122

Benz, B. A., Nandadasa, S., Takeuchi, M., Grady, R. C., Takeuchi, H., LoPilato, R. K., Kakuda, S., Somerville, R. P. T., Apte, S. S., Haltiwanger, R. S., & Holdener, B. C. (2016). Genetic and biochemical evidence that gastrulation defects in Pofut2 mutants result from defects in ADAMTS9 secretion. *Developmental Biology*, *416*(1), 111–122. https://doi.org/10.1016/j.ydbio.2016.05.038

Bi, Y., Deng, Z., Ni, W., Shrestha, R., Savage, D., Hartwig, T., Patil, S., Hong, S. H., Zhang, Z., Oses-Prieto, J. A., Li, K. H., Quail, P. H., Burlingame, A. L., Xu, S.-L., & Wang, Z.-Y. (2021). Arabidopsis ACINUS is O-glycosylated and regulates transcription and alternative splicing of regulators of reproductive transitions. *Nature Communications*, *12*(1), 945–945. https://doi.org/10.1038/s41467-021-20929-7

Boavida, L. C., Borges, F., Becker, J. D., & Feijó, J. A. (2011). Whole Genome Analysis of Gene Expression Reveals Coordinated Activation of Signaling and Metabolic Pathways during Pollen-Pistil Interactions in Arabidopsis. *Plant Physiology*, *155*(4), 2066–2080. https://doi.org/10.1104/pp.110.169813

Boavida, L. C., Shuai, B., Yu, H.-J., Pagnussat, G. C., Sundaresan, V., & McCormick, S. (2009). A Collection of Ds Insertional Mutants Associated With Defects in Male Gametophyte Development and Function in Arabidopsis thaliana. *Genetics (Austin)*, *181*(4), 1369–1385. https://doi.org/10.1534/genetics.108.090852

Bowman, J. L., & Eshed, Y. (2000). Formation and maintenance of the shoot apical meristem. *Trends in Plant Science*, *5*(3), 110–115. https://doi.org/10.1016/S1360-1385(00)01569-7

Boyce, C. K., & Lee, J.-E. (2017). Plant Evolution and Climate Over Geological Timescales. *Annual Review of Earth and Planetary Sciences*, *45*(1), 61–87. https://doi.org/10.1146/annurev-earth-063016-015629

Breikaa, R. M., & Lilly, B. (2021). The Notch Pathway: A Link Between COVID-19 Pathophysiology and Its Cardiovascular Complications. *Frontiers in Cardiovascular Medicine*, *8*(Journal Article), 681948–681948. https://doi.org/10.3389/fcvm.2021.681948

Caffall, K. H., Pattathil, S., Phillips, S. E., Hahn, M. G., & Mohnen, D. (2009). Arabidopsis thaliana T-DNA Mutants Implicate GAUT Genes in the Biosynthesis of Pectin and Xylan in Cell Walls and Seed Testa. *Molecular Plant*, *2*(5), 1000–1014. https://doi.org/10.1093/mp/ssp062

Campanoni, P., & Blatt, M. R. (2007). Membrane trafficking and polar growth in root hairs and pollen tubes. *Journal of Experimental Botany*, *58*(1), 65–74. https://doi.org/10.1093/jxb/erl059

Campbell, J., Davies, G., Bulone, & Henrissat, B. (1997). A classification of nucleotide-diphospho-sugar glycosyltransferases based on amino acid sequence similarities. *Biochemical Journal*, *326*(3), 929–939. https://doi.org/10.1042/bj3260929u

Cascallares, M., Setzes, N., Marchetti, F., López, G. A., Distéfano, A. M., Cainzos, M., Zabaleta, E., & Pagnussat, G. C. (2020). A Complex Journey: Cell Wall Remodeling, Interactions, and Integrity During Pollen Tube Growth. *Frontiers in Plant Science*, *11*(Journal Article), 599247–599247. https://doi.org/10.3389/fpls.2020.599247

Chantha, S.-C., Emerald, B. S., & Matton, D. P. (2006). Characterization of the plant Notchless homolog, a WD repeat protein involved in seed development. *Plant Molecular Biology*, *62*(6), 897–912. https://doi.org/10.1007/s11103-006-9064-4

Chantha, S.-C., Gray-Mitsumune, M., Houde, J., & Matton, D. P. (2010). The MIDASIN and NOTCHLESS genes are essential for female gametophyte development in Arabidopsis thaliana. *Physiology and Molecular Biology of Plants*, *16*(1), 3–18. https://doi.org/10.1007/s12298-010-0005-y

Chantha, S.-C., & Matton, D. P. (2007). Underexpression of the plant NOTCHLESS gene, encoding a WD-repeat protein, causes pleitropic phenotype during plant development. *Planta*, *225*(5), 1107–1120. https://doi.org/10.1007/s00425-006-0420-z

Chapman, L. A., & Goring, D. R. (2010). Pollen–pistil interactions regulating successful fertilization in the Brassicaceae. *Journal of Experimental Botany*, *61*(7), 1987–1999. https://doi.org/10.1093/jxb/erq021

Chen, C.-I., Keusch, J. J., Klein, D., Hess, D., Hofsteenge, J., & Gut, H. (2012). Structure of human POFUT2: Insights into thrombospondin type 1 repeat fold and O-fucosylation. *The EMBO Journal*, *31*(14), 3183–3197. https://doi.org/10.1038/emboj.2012.143

Cheung, A. Y., & Wu, H.-M. (1999). Arabinogalactan proteins in plant sexual reproduction. *Protoplasma*, *208*(1), 87–98. https://doi.org/10.1007/BF01279078

Coutinho, P. M., Deleury, E., Davies, G. J., & Henrissat, B. (2003). An Evolving Hierarchical Family Classification for Glycosyltransferases. *Journal of Molecular Biology*, *328*(2), 307–317. https://doi.org/10.1016/S0022-2836(03)00307-3

Crawford, B. C. W., Ditta, G., & Yanofsky, M. F. (2007). The NTT Gene Is Required for Transmitting-Tract Development in Carpels of Arabidopsis thaliana. *Current Biology*, *17*(13), 1101–1108. https://doi.org/10.1016/j.cub.2007.05.079

Cui, X., Wang, H., Li, Y., Chen, T., Liu, S., & Yan, Q. (2020). Epiregulin promotes trophoblast epithelial–mesenchymal transition through poFUT1 and O-fucosylation by poFUT1 on uPA. *Cell Proliferation*, *53*(2), e12745-n/a. https://doi.org/10.1111/cpr.12745

Deschuyter, M., Pennarubia, F., Pinault, E., Legardinier, S., & Maftah, A. (2020). Functional Characterization of POFUT1 Variants Associated with Colorectal Cancer. *Cancers*, *12*(6), 1430. https://doi.org/10.3390/cancers12061430

Dresselhaus, T., & Franklin-Tong, N. (J2013). Male–Female Crosstalk during Pollen Germination, Tube Growth and Guidance, and Double Fertilization. *Molecular Plant*, *6*(4), 1018–1036. https://doi.org/10.1093/mp/sst061

Endress, P. K. (2011). Evolutionary diversification of the flowers in angiosperms. *American Journal of Botany*, *98*(3), 370–396. https://doi.org/10.3732/ajb.1000299

Errasti-Murugarren, E., Bartoccioni, P., & Palacín, M. (2021). Membrane Protein Stabilization Strategies for Structural and Functional Studies. *Membranes (Basel)*, *11*(2), 155. https://doi.org/10.3390/membranes11020155

Escobar-Restrepo, J.-M., Huck, N., Kessler, S., Gagliardini, V., Gheyselinck, J., Yang, W.-C., & Grossniklaus, U. (2007). The FERONIA Receptor-like Kinase Mediates Male-Female Interactions During Pollen Tube Reception. *Science*, *317*(5838), 656–660. https://doi.org/10.1126/science.1143562

Folk, R. A., Siniscalchi, C. M., & Soltis, D. E. (2020). Angiosperms at the edge: Extremity, diversity, and phylogeny. *Plant, Cell and Environment*, *43*(12), 2871–2893. https://doi.org/10.1111/pce.13887

Foster, C. E., Martin, T. M., & Pauly, M. (2010). Comprehensive Compositional Analysis of Plant Cell Walls (Lignocellulosic biomass) Part I: Lignin. *JoVE (Journal of Visualized Experiments)*, *37*, e1745. https://doi.org/10.3791/1745

Friis, E. M., Crane, P. R., & Pedersen, K. R. (2011). *Early Flowers and Angiosperm Evolution*. Cambridge University Press. https://doi.org/10.1017/CBO9780511980206

Ge, C., & Stanley, P. (2008). The O-Fucose Glycan in the Ligand-Binding Domain of Notch1 Regulates Embryogenesis and T Cell Development. *Proceedings of the National Academy of Sciences - PNAS*, *105*(5), 1539–1544. https://doi.org/10.1073/pnas.0702846105

Ghosh, S., Brown, R., Jones, J. C. R., Ellerbroek, S. M., & Stack, M. S. (2000). Urinary-type Plasminogen Activator (uPA) Expression and uPA Receptor Localization Are Regulated by α3β1Integrin in Oral Keratinocytes. *The Journal of Biological Chemistry*, *275*(31), 23869–23876. https://doi.org/10.1074/jbc.M000935200

Hallgren, P., Lundblad, A., & Svensson, S. (1975). A new type of carbohydrate-protein linkage in a glycopeptide from normal human urine. *Journal of Biological Chemistry*, *250*(14), 5312–5314. https://doi.org/10.1016/S0021-9258(19)41182-4

Hansen, S. F., Bettler, E., Rinnan, Å., B. Engelsen, S., & Breton, C. (2010). Exploring genomes for glycosyltransferases. *Molecular BioSystems*, *6*(10), 1773–1781. https://doi.org/10.1039/C000238K

Hansen, S. F., Bettler, E., Wimmerová, M., Imberty, A., Lerouxel, O., & Breton, C. (2009). Combination of Several Bioinformatics Approaches for the Identification of New Putative Glycosyltransferases in Arabidopsis. *Journal of Proteome Research*, *8*(2), 743–753. https://doi.org/10.1021/pr800808m

Hansen, S. F., Harholt, J., Oikawa, A., & Scheller, H. V. (2012). Plant Glycosyltransferases Beyond CAZy: A Perspective on DUF Families. *Frontiers in Plant Science*, *3*. https://doi.org/10.3389/fpls.2012.00059

Hardy, D., Desuzinges Mandon, E., Rothnie, A. J., & Jawhari, A. (2018). The yin and yang of solubilization and stabilization for wild-type and full-length membrane protein. *Methods (San Diego, Calif.)*, *147*(Journal Article), 118–125. https://doi.org/10.1016/j.ymeth.2018.02.017

Haughn, G. W., & Western, T. L. (2012). Arabidopsis Seed Coat Mucilage is a Specialized Cell Wall that Can be Used as a Model for Genetic Analysis of Plant Cell Wall Structure and Function. *Frontiers in Plant Science*, *3*. https://doi.org/10.3389/fpls.2012.00064

Holdener, B. C., & Haltiwanger, R. S. (2019). Protein O-fucosylation: Structure and function. *Current Opinion in Structural Biology*, *56*(Journal Article), 78–86. https://doi.org/10.1016/j.sbi.2018.12.005

Huck, N., Moore, J. M., Federer, M., & Grossniklaus, U. (2003). The Arabidopsis mutant feronia disrupts the female gametophytic control of pollen tube reception. *Development*, *130*(10), 2149–2159. https://doi.org/10.1242/dev.00458

Jenik, P. D., & Irish, V. F. (2000). Regulation of cell proliferation patterns by homeotic genes during Arabidopsis floral development. *Development (Cambridge, England)*, *127*(6), 1267–1276.

Johnson, M. A., & Preuss, D. (2002). Plotting a Course: Multiple Signals Guide Pollen Tubes to Their Targets. *Developmental Cell*, *2*(3), 273–281. https://doi.org/10.1016/S1534-5807(02)00130-2

Kentzer, E. J., Buko, A., Menon, G., & Sarin, V. K. (1990). Carbohydrate composition and presence of a fucose-protein linkage in recombinant human pro-urokinase. *Biochemical and Biophysical Research Communications*, *171*(1), 401–406. https://doi.org/10.1016/0006-291X(90)91407-J

Khan, M. I. R., Jalil, S. U., Chopra, P., Chhillar, H., Ferrante, A., Khan, N. A., & Ansari, M. I. (2021). Role of GABA in plant growth, development and senescence. *Plant Gene*, *26*, 100283. https://doi.org/10.1016/j.plgene.2021.100283

Kohorn, B. D., Greed, B. E., Mouille, G., Verger, S., & Kohorn, S. L. (2021). Effects of Arabidopsis wall associated kinase mutations on ESMERALDA1 and elicitor induced ROS. *PloS One*, *16*(5), e0251922–e0251922. https://doi.org/10.1371/journal.pone.0251922

Kong, Y., Zhou, G., Abdeen, A. A., Schafhauser, J., Richardson, B., Atmodjo, M. A., Jung, J., Wicker, L., Mohnen, D., Western, T., & Hahn, M. G. (2013). GALACTURONOSYLTRANSFERASE-LIKE5 Is Involved in the Production of Arabidopsis Seed Coat Mucilage. *Plant Physiology*, *163*(3), 1203–1217. https://doi.org/10.1104/pp.113.227041

Kopan, R. (2012). Notch Signaling. *Cold Spring Harbor Perspectives in Biology*, *4*(10), a011213–a011213. https://doi.org/10.1101/cshperspect.a011213

Kopan, R., & Ilagan, Ma. X. G. (2009). The Canonical Notch Signaling Pathway: Unfolding the Activation Mechanism. *Cell*, *137*(2), 216–233. https://doi.org/10.1016/j.cell.2009.03.045

Lairson, L. L., Henrissat, B., Davies, G. J., & Withers, S. G. (2008). Glycosyltransferases: Structures, functions, and mechanisms. *Annual Review of Biochemistry*, *77*(1), 521–555. https://doi.org/10.1146/annurev.biochem.76.061005.092322

Lasky, J., & Wu, H. (2005). Notch signaling, brain development, and human disease. *Pediatric Research*, *57*(5), 104R-109R. https://doi.org/10.1203/01.PDR.0000159632.70510.3D

Leebens-Mack, J. H., Barker, M. S., Gitzendanner, M. A., Li, Z., Melkonian, M., Quint, M., Stevenson, D. W., Wickett, N. J., Edger, P. P., Jordon-Thaden, I. E., Joya, S., Liu, T., Melkonian, B., Miles, N. W., Pokorny, L., Quigley, C., Thomas, P., Baucom, R. S., Biffin, E., … One Thousand Plant Transcriptomes Initiative. (2019). One thousand plant transcriptomes and the phylogenomics of green plants. *Nature (London)*, *574*(7780), 679–685. https://doi.org/10.1038/s41586-019-1693-2

Li, M., Cheng, R., Liang, J., Yan, H., Zhang, H., Yang, L., Li, C., Jiao, Q., Lu, Z., He, J., Ji, J., Shen, Z., Li, C., Hao, F., Yu, H., & Yao, Z. (2013). Mutations in POFUT1, Encoding Protein O-fucosyltransferase 1, Cause Generalized Dowling-Degos Disease. *American Journal of Human Genetics*, *92*(6), 895–903. https://doi.org/10.1016/j.ajhg.2013.04.022

Li, Z., Han, K., Pak, J. E., Satkunarajah, M., Zhou, D., & Rini, J. M. (2017). Recognition of EGF-like domains by the Notch-modifying O -fucosyltransferase POFUT1. *Nature Chemical Biology*, *13*(7), 757–763. https://doi.org/10.1038/nchembio.2381

Lira-Navarrete, E., Valero-González, J., Villanueva, R., Martínez-Júlvez, M., Tejero, T., Merino, P., Panjikar, S., & Hurtado-Guerrero, R. (2011). Structural insights into the mechanism of protein O-fucosylation. *PloS One*, *6*(9), e25365–e25365. https://doi.org/10.1371/journal.pone.0025365

Liu, J., Lee, J. W., Yun, E. J., Jung, S., Seo, J., & Jin, Y. (2019). L-Fucose production by engineered Escherichia coli. *Biotechnology and Bioengineering*, *116*(4), 904–911. https://doi.org/10.1002/bit.26907

Liu, J., Zhong, S., Guo, X., Hao, L., Wei, X., Huang, Q., Hou, Y., Shi, J., Wang, C., Gu, H., & Qu, L.-J. (2013). Membrane-Bound RLCKs LIP1 and LIP2 Are Essential Male Factors Controlling Male-Female Attraction in Arabidopsis. *Current Biology*, *23*(11), 993–998. https://doi.org/10.1016/j.cub.2013.04.043

Lombard, V., Ramulu, H. G., Drula, E., Coutinho, P. M., & Henrissat, B. (2014). The carbohydrate-active enzymes database (CAZy) in 2013. *Nucleic Acids Research*, *42*(D1), D490–D495. https://doi.org/10.1093/nar/gkt1178

Luca, V. C., Kim, B. C., Ge, C., Kakuda, S., Wu, D., Roein-Peikar, M., Haltiwanger, R. S., Zhu, C., Ha, T., & Garcia, K. C. (2017). Notch-Jagged complex structure implicates a catch bond in tuning ligand sensitivity. *Science*, *355*(6331), 1320–1324. https://doi.org/10.1126/science.aaf9739

McKay, M. J., Afrose, F., Koeppe, R. E., & Greathouse, D. V. (2018). Helix formation and stability in membranes. Biochimica et Biophysica Acta. Biomembranes, 1860(10), 2108–2117. https://doi.org/10.1016/j.bbamem.2018.02.010

McMillan, B. J., Zimmerman, B., Egan, E. D., Lofgren, M., Xu, X., Hesser, A., Blacklow, S. C., & Argonne National Lab. (ANL), A., IL (United States). Advanced Photon Source (APS). (2017). Structure of human POFUT1, its requirement in ligand-independent oncogenic Notch signaling, and functional effects of Dowling-Degos mutations. *Glycobiology (Oxford)*, *27*(8), 777–786. https://doi.org/10.1093/glycob/cwx020

Melnik, B. (2015). The Potential Role of Impaired Notch Signalling in Atopic Dermatitis. *Acta Dermato Venereologica*, *95*(1), 5–11. https://doi.org/10.2340/00015555-1898

Michard, E., Lima, P. T., Borges, F., Silva, A. C., Portes, M. T., Carvalho, J. E., Gilliham, M., Liu, L.-H., Obermeyer, G., & Feijo, J. A. (2011). Glutamate Receptor—Like Genes Form Ca^{2+} Channels in Pollen Tubes and Are Regulated by Pistil D-Serine. *Science (American Association for the Advancement of Science)*, *332*(6028), 434–437. https://doi.org/10.1126/science.1201101

Mizukami, A. G., Inatsugi, R., Jiao, J., Kotake, T., Kuwata, K., Ootani, K., Okuda, S., Sankaranarayanan, S., Sato, Y., Maruyama, D., Iwai, H., Garénaux, E., Sato, C., Kitajima, K., Tsumuraya, Y., Mori, H., Yamaguchi, J., Itami, K., Sasaki, N., & Higashiyama, T. (2016). The AMOR Arabinogalactan Sugar Chain Induces Pollen-Tube Competency to Respond to Ovular Guidance. *Current Biology*, *26*(8), 1091–1097. https://doi.org/10.1016/j.cub.2016.02.040

Mollet, J.-C., Leroux, C., Dardelle, F., & Lehner, A. (2013). Cell Wall Composition, Biosynthesis and Remodeling during Pollen Tube Growth. *Plants (Basel)*, *2*(1), 107–147. https://doi.org/10.3390/plants2010107

Morris, J. L., Puttick, M. N., Clark, J. W., Edwards, D., Kenrick, P., Pressel, S., Wellman, C. H., Yang, Z., Schneider, H., & Donoghue, P. C. J. (2018). The timescale of early land plant evolution. *Proceedings of the National Academy of Sciences - PNAS*, *115*(10), E2274–E2283. https://doi.org/10.1073/pnas.1719588115

Neumetzler, L., Humphrey, T., Lumba, S., Snyder, S., Yeats, T. H., Usadel, B., Vasilevski, A., Patel, J., Rose, J. K. C., Persson, S., & Bonetta, D. (2012). The FRIABLE1 gene product affects cell adhesion in Arabidopsis. *PloS One*, *7*(8), e42914–e42914. https://doi.org/10.1371/journal.pone.0042914

Nikolovski, N., Rubtsov, D., Segura, M. P., Miles, G. P., Stevens, T. J., Dunkley, T. P. J., Munro, S., Lilley, K. S., & dupree, P. (2012). Putative Glycosyltransferases and Other Plant Golgi Apparatus Proteins Are Revealed by LOPIT Proteomics. *Plant Physiology (Bethesda)*, *160*(2), 1037–1051. https://doi.org/10.1104/pp.112.204263

Pagnussat, G. C., Yu, H.-J., Ngo, Q. A., Rajani, S., Mayalagu, S., Johnson, C. S., Capron, A., Xie, L.-F., Ye, D., & Sundaresan, V. (2005). Genetic and molecular identification of genes required for female

gametophyte development and function in Arabidopsis. *Development (Cambridge)*, *132*(3), 603–614. https://doi.org/10.1242/dev.01595

Palanivelu, R., Brass, L., Edlund, A. F., & Preuss, D. (2003). Pollen Tube Growth and Guidance Is Regulated by POP2, an Arabidopsis Gene that Controls GABA Levels. *Cell*, *114*(1), 47–59. https://doi.org/10.1016/S0092-8674(03)00479-3

Palanivelu, R., & Tsukamoto, T. (2011). Pathfinding in angiosperm reproduction: Pollen tube guidance by pistils ensures successful double fertilization. *Wiley Interdisciplinary Reviews. Developmental Biology*, *1*(1), 96.

Penton, A. L., Leonard, L. D., & Spinner, N. B. (2012). Notch signaling in human development and disease. *Seminars in Cell & Developmental Biology*, *23*(4), 450–457. https://doi.org/10.1016/j.semcdb.2012.01.010

Phokas, A., & Coates, J. C. (2021). Evolution of DELLA function and signaling in land plants. *Evolution & Development*, *23*(3), 137–154. https://doi.org/10.1111/ede.12365

Qin, Y., Leydon, A. R., Manziello, A., Pandey, R., Mount, D., Denic, S., Vasic, B., Johnson, M. A., & Palanivelu, R. (2009). Penetration of the Stigma and Style Elicits a Novel Transcriptome in Pollen Tubes, Pointing to Genes Critical for Growth in a Pistil. *PLOS Genetics*, *5*(8), e1000621. https://doi.org/10.1371/journal.pgen.1000621

Qu, L.-J., Li, L., Lan, Z., & Dresselhaus, T. (2015). Peptide signalling during the pollen tube journey and double fertilization. *Journal of Experimental Botany*, *66*(17), 5139–5150. https://doi.org/10.1093/jxb/erv275

Renault, H., El Amrani, A., Palanivelu, R., Updegraff, E. P., Yu, A., Renou, J.-P., Preuss, D., Bouchereau, A., & Deleu, C. (2011). GABA Accumulation Causes Cell Elongation Defects and a Decrease in Expression of Genes Encoding Secreted and Cell Wall-Related Proteins in Arabidopsis thaliana. *Plant and Cell Physiology*, *52*(5), 894–908. https://doi.org/10.1093/pcp/pcr041

Rotman, N., Rozier, F., Boavida, L., Dumas, C., Berger, F., & Faure, J.-E. (2003). Female Control of Male Gamete Delivery during Fertilization in Arabidopsis thaliana. *Current Biology*, *13*(5), 432–436. https://doi.org/10.1016/S0960-9822(03)00093-9

Sauquet, H., von Balthazar, M., Magallón, S., Doyle, J. A., Endress, P. K., Bailes, E. J., Barroso de Morais, E., Bull-Hereñu, K., Carrive, L., Chartier, M., Chomicki, G., Coiro, M., Cornette, R., El Ottra, J. H. L., Epicoco, C., Foster, C. S. P., Jabbour, F., Haevermans, A., Haevermans, T., … Schönenberger, J. (2017). The ancestral flower of angiosperms and its early diversification. *Nature Communications*, *8*(1), 16047. https://doi.org/10.1038/ncomms16047

Schneider, M., Al-Shareffi, E., & Haltiwanger, R. S. (2017). Biological functions of fucose in mammals. *Glycobiology (Oxford)*, *27*(7), 601–618. https://doi.org/10.1093/glycob/cwx034

Shan, X., Yan, J., & Xie, D. (2012). Comparison of phytohormone signaling mechanisms. *Current Opinion in Plant Biology*, *15*(1), 84–91. https://doi.org/10.1016/j.pbi.2011.09.006

Sigrist, C. J. A., de Castro, E., Cerutti, L., Cuche, B. A., Hulo, N., Bridge, A., Bougueleret, L., & Xenarios, I. (2013). New and continuing developments at PROSITE. *Nucleic Acids Research*, *41*(D1), E344–E347. https://doi.org/10.1093/nar/gks1067

Smith, D. K., Jones, D. M., Lau, J. B. R., Cruz, E. R., Brown, E., Harper, J. F., & Wallace, I. S. (2018a). A Putative Protein O -Fucosyltransferase Facilitates Pollen Tube Penetration through the Stigma—Style Interface. *Plant Physiology (Bethesda)*, *176*(4), 2804–2818. https://doi.org/10.1104/pp.17.01577

Smith, D. K., Harper, J. F., & Wallace, I. S. (2018b). A potential role for protein O-fucosylation during pollen-pistil interactions. *Plant Signaling & Behavior*, *13*(5), e1467687–e1467687. https://doi.org/10.1080/15592324.2018.1467687

Smyth, D. R., Bowman, J. L., & Meyerowitz, E. M. (1990). Early flower development in Arabidopsis. *The Plant Cell*, *2*(8), 755–767. https://doi.org/10.1105/tpc.2.8.755

Sprunck, S. (2020). Twice the fun, double the trouble: Gamete interactions in flowering plants. *Current Opinion in Plant Biology*, *53*(Journal Article), 106–116. https://doi.org/10.1016/j.pbi.2019.11.003

Stahl, M., Uemura, K., Ge, C., Shi, S., Tashima, Y., & Stanley, P. (2008). Roles of Pofut1 and O-Fucose in Mammalian Notch Signaling. *The Journal of Biological Chemistry*, *283*(20), 13638–13651. https://doi.org/10.1074/jbc.M802027200

Strasser, R., Seifert, G., Doblin, M. S., Johnson, K. L., Ruprecht, C., Pfrengle, F., Bacic, A., & Estevez, J. M. (2021). Cracking the "Sugar Code": A Snapshot of N- and O-Glycosylation Pathways and Functions in Plants Cells. *Frontiers in Plant Science*, *12*. https://doi.org/10.3389/fpls.2021.640919

Stonebloom, S., Ebert, B., Xiong, G., Pattathil, S., Birdseye, D., Lao, J., Pauly, M., Hahn, M. G., Heazlewood, J. L., Scheller, H. V., & Lawrence Berkeley National Lab. (LBNL), B., CA (United States). (2016). A DUF-246 family glycosyltransferase-like gene affects male fertility and the biosynthesis of pectic arabinogalactans. *BMC Plant Biology*, *16*(84), 90–90. https://doi.org/10.1186/s12870-016-0780-x

Sun, T. (2021). Novel nucleocytoplasmic protein O-fucosylation by SPINDLY regulates diverse developmental processes in plants. *Current Opinion in Structural Biology*, *68*(C), 113–121. https://doi.org/10.1016/j.sbi.2020.12.013

Takenaka, Y., Kato, K., Ogawa-Ohnishi, M., Tsuruhama, K., Kajiura, H., Yagyu, K., Takeda, A., Takeda, Y., Kunieda, T., Hara-Nishimura, I., Kuroha, T., Nishitani, K., Matsubayashi, Y., & Ishimizu, T. (2018). Pectin RG-I rhamnosyltransferases represent a novel plant-specific glycosyltransferase family. *Nature Plants*, *4*(9), 669–676. https://doi.org/10.1038/s41477-018-0217-7

Valero-Gonzalez, J., Leonhard-Melief, C., Lira-Navarrete, E., Jimenez-Oses, G., Hernandez-Ruiz, C., Pallares, M. C., Yruela, I., Vasudevan, D., Lostao, A., Corzana, F., Takeuchi, H., Haltiwanger, R. S., & Hurtado-Guerrero, R. (2016). A proactive role of water molecules in acceptor recognition by protein O-fucosyltransferase 2. *Nature Chemical Biology*, *12*(4), 240–246. https://doi.org/10.1038/NCHEMBIO.2019

van Nocker, S., & Ludwig, P. (2003). The WD-repeat protein superfamily in Arabidopsis: Conservation and divergence in structure and function. *BMC Genomics*, *4*(1), 50–50. https://doi.org/10.1186/1471-2164-4-50

Verger, S., Chabout, S., Gineau, E., & Mouille, G. (2016). Cell adhesion in plants is under the control of putative O-fucosyltransferases. *Development (Cambridge)*, *143*(14), 2536–2540. https://doi.org/10.1242/dev.132308

Wang, M. M. (2011). Notch signaling and Notch signaling modifiers. *The International Journal of Biochemistry & Cell Biology*, *43*(11), 1550–1562. https://doi.org/10.1016/j.biocel.2011.08.005

Wang, Y., Mortimer, J. C., Davis, J., Dupree, P., Keegstra, K., & Great Lakes Bioenergy Research Center (GLBRC). (2013). Identification of an additional protein involved in mannan biosynthesis. *The Plant Journal : For Cell and Molecular Biology*, *73*(1), 105–117. https://doi.org/10.1111/tpj.12019

Wigge, P., & Weigel, D. (2001). Arabidopsis genome: Life without notch. *Current Biology*, *11*(3), R112–R114. https://doi.org/10.1016/S0960-9822(01)00043-4

Windsor, J. B., Symonds, V. V., Mendenhall, J., & Lloyd, A. M. (2000). Arabidopsis seed coat development: Morphological differentiation of the outer integument. *The Plant Journal*, *22*(6), 483–493. https://doi.org/10.1046/j.1365-313x.2000.00756.x

Won, S.-K., Lee, Y.-J., Lee, H.-Y., Heo, Y.-K., Cho, M., & Cho, H.-T. (2009). Cis-Element- and Transcriptome-Based Screening of Root Hair-Specific Genes and Their Functional Characterization in Arabidopsis. *Plant Physiology (Bethesda)*, *150*(3), 1459–1473. https://doi.org/10.1104/pp.109.140905

Wu, Z. L., Ethen, C. M., Prather, B., Machacek, M., & Jiang, W. (2011). Universal phosphatase-coupled glycosyltransferase assay. *Glycobiology (Oxford)*, *21*(6), 727–733. https://doi.org/10.1093/glycob/cwq187

Zentella, R., Sui, N., Barnhill, B., Hsieh, W.-P., Hu, J., Shabanowitz, J., Boyce, M., Olszewski, N. E., Zhou, P., Hunt, D. F., Sun, T.-P., & Duke Univ., D., NC (United States). (2017). The Arabidopsis O-fucosyltransferase SPINDLY activates nuclear growth repressor DELLA. *Nature Chemical Biology*, *13*(5), 479–485. https://doi.org/10.1038/nchembio.2320

Zheng, Y.-Y., Lin, X.-J., Liang, H.-M., Wang, F.-F., & Chen, L.-Y. (2018). The Long Journey of Pollen Tube in the Pistil. *International Journal of Molecular Sciences*, *19*(11), 3529. https://doi.org/10.3390/ijms19113529

Chapter 2: Materials and methods

I. Phylogenetic and structural analysis of the Arabidopsis putative POFT family and metazoan POFT1s

The AtOFT1 amino acid sequence was used as a BLAST query to identify putative POFT homologs in the Arabidopsis genome using the WU-BLAST function on The Arabidopsis Information Resource (TAIR) website (arabidopsis.org). The amino acid sequence of *Mus Musculus* (NP_536711.3)*, Drosophila melanogaster* (NP_610931)*, Danio rerio* (AAH95289)*, Homo sapiens* (NP_056167) and *Caenorhabditis elegans* (NP_741744.2) were obtained from the National Center for Biotechnology Information (NCBI) protein sequence database (ncbi.nlm.nih.gov). Protein sequences were aligned using the multiple alignment mode in ClustalX2 (clustal.org; Larkin *et al.,* 2007), and incomplete sequences were removed. This alignment was used to create a neighbor-joining phylogenetic tree consisting of 1000 independent bootstrap trials in MEGA X (megasoftware.net; Kumar *et al.,* 2018). The resulting phylogenetic trees were viewed and analyzed in MEGA X. Similarly, evolutionary conservation between the amino acid sequences of the 39 genes in the Arabidopsis putative POFT family was similarly performed using ClustalX and the corresponding alignment was used to determine sequence conservation in 4 key catalytic residues found important for both CePOFT1 and AtOFT1 catalysis as well as was further processed in MEGA X to create a tree representing the maximum likelihood of evolutionary distance inferred using the Maximum Likelihood method and JTT matrix-based model (Jones *et al.,* 1992; Kumar *et al.,* 2018).

The molecular model of *C. elegans* POFT1 (CePOFT1) in Figure 3.23 was generated using the Visual Molecular Dynamics software (VMD) version 1.9.3. The crystal structure of this protein was generated in complex with GDP-Fucose (GDP-Fuc) by Lira- Navarette *et al.,* 2011 and accessed through the Protein Data Bank (PDB ID 3ZY5). *De novo* tertiary structure prediction for AtOFT1 was generated based on the full-length amino acid sequence in RaptorX Structure Prediction software (raptorx.uchicago.edu; Xu *et al.,* 2021; Xu, 2019; Xu and Wang, 2019; Wang *et al.,* 2017a; Wang *et al.,* 2017b; Wang *et al.,* 2018). Five models were produced as potential tertiary structures for AtOFT1, and model 2 was selected for further analysis based on it possessing the lowest RMSD (root-square-mean deviation) score of Å=6.6193. Expasy SWISS-MODEL (swissmodel.expasy.org; Waterhouse *et al.,* 2018) was also used as a second means of *in silico* structural prediction of AtOFT1 and to determine structural homology with solved protein structures as well as was used to make the structural model in Figure 3.26. Both the full length and well predicted residue region from the RaptorX model of AtOFT1 (residues 66-389) were queried in SWISS-MODEL. The crystal structure of CePOFT1 chain A crystal-form-III in complex with GDP (PDB ID 3YZ3) generated by Lira-Navarette and colleagues, 2011, demonstrated the most significant structural similarity to the *de novo* structural prediction for AtOFT1 in both the truncated and full length SWISS-MODEL alignment queries. This structure as well as the RaptorX predicted structure selected for AtOFT1 was imported into the Research Collaboratory for Structural Bioinformatics Protein Data Bank (RCSB PDB) Mol* 3D Viewer software (rcsb.org/3d-view; Sehnal *et al.,* 2021) to visualize and analyze the structural

characteristics of AtOFT1 in addition to its homology CePOFT1 (PDB ID 3ZY3) (Lira-Navarette *et al.,* 2011).

II. Plant growth and maintenance

All Arabidopsis seed used in this study were sterilized in seed cleaning solution (3% [v/v] sodium hypochlorite, 0.1 % [w/v] sodium dodecyl sulfate) for 20 minute(s) (min) at 25°C. Seeds were washed five times in sterile, deionized water and stratified at 4°C in the dark for 48 hour(s) (h) before plating. Seeds were plated on MS media (1/2× Murashige and Skoog salts, 10 mM MES-KOH pH 5.7, 1% [w/v] sucrose, and 1% [w/v] phytoagar) and grown vertically in a climate-controlled germination chamber (Percival, CU41L4) for 7 days under long-day conditions (16 h light/8 h dark) at 24°C. Following 7 days of germination and growth, seedlings were transplanted to soil and propagated in a growth chamber (Percival, AR-66L2) under long-day conditions until completion of their lifecycles. All Arabidopsis outcrosses made in this study were performed as described previously (Myers *et al.,* 2009).

III. Analysis of silique morphology

For seed set imaging, mature siliques from 6-week-old adult Arabidopsis plants were harvested and incubated for 48 h or until fully cleared at 25°C in 70% [v/v] ethanol under fluorescent light. Cleared, intact siliques were then carefully transferred to a glass microscope slide and positioned with the septum facing upright to visualize seed set that had developed in both sides of the ovary/silique. Siliques were then imaged with a Leica EZ4HD video dissecting microscope at 35X magnification. Silique length and seed set were quantified using Fiji (imagej.net). Statistical analyses were performed using GraphPad Prism(GraphPad Software, La Jolla, CA, www.graphpad.com).

IV. Isolation and verification of T-DNA lines used in this study

AtOFT1 (*At3g05320*), *At1g11990 (soft1* gene candidate), and *AtGAUT14 (At5g15470; soft2* gene*)* were queried against the Salk Institute T-DNA insertional mutant database (Alonso *et al.,* 2003), and three potential exonic T-DNA lines were identified for *AtOFT1* (*oft1-1*, SALK_072442; *oft1-2*, SALK_151675; and *oft1-3*, WiscDsLox489-492M4). Additionally, one exonic T-DNA mutant line were propagated for each suppressor gene candidates: SAIL_1174_D07 for *soft1* and SALK_000091 (*gaut14-1)* for *soft2*. These seed populations were propagated on MS media as described above, transplanted to soil, and grown under long-day conditions at 24°C. To determine the genotypes of these *oft1* mutant lines as well as all other T-DNA and transgenic lines used in this study, genomic DNA was isolated and used to perform PCR genotyping as previously described (Edwards *et al.,* 1991) with slight modifications (Villalobos *et al.,* 2015). Each genomic DNA sample was analyzed by PCR genotyping using locus or transgene-specific primers as well as the appropriate T-DNA specific left border primers, and ExTaq polymerase (Takara Bio, Mountain View, CA) (Table 2.1). Reactions were cycled under one of two conditions. Condition 1: 95°C initial denaturation for 5 min, 35 cycles of 95°C (30 seconds (sec)), 52°C (30 sec), 72°C (1 min 35 sec), and final extension at 72°C for 7 min. Condition 2: 95ºC initial denaturation for 5 min, 35 cycles of 95°C (30 sec), 55°C (30 sec), 72°C (1 min 10 sec), and final extension at 72°C for 7 min. For all *AtOFT1* associated T-DNA lines, PCR genotyping Condition 1 was used to determine line genotype as well as for determining a heterozygous genotypes for the SAIL_1174_D07 and *gaut14-1,* while all other genotyping reactions for these lines were performed under Condition 2. The resulting PCR products were separated on 1% [w/v]

Table 2.1: Oligonucleotide primers used in this study.

Primer name	primer sequence (5'→3')	Purpose
oft1-1 genotyping LP	taccaacaaaaacatccgctc	*Genotyping PCR*
oft1-1 genotyping RP	ttcgagatcgtcacatgtcag	*Genotyping PCR*
oft1-2 genotyping LP	tccaaccacttaaaaccgatg	*Genotyping PCR*
oft1-2 genotyping RP	ctgcaattgcatgcatgttac	*Genotyping PCR*
oft1-3 genotyping LP	gtgaaccgcaacaaaaggtac	*Genotyping PCR*
oft1-3 genotyping RP	atttgcatgtcaagttcgagg	*Genotyping PCR*
SALK LBb1.3	attttgccgatttcggaac	*Genotyping PCR*
WiscDsLox LB	aacgtccgcaatgtgttattaagttgtc	*Genotyping PCR*
pOFT1 -1000 pENTR F	cacccataacgcgtgaacttaaaaa	*Promoter cloning*
pOFT1 pENTR R	cggagaattcatccgagagaga	*Promoter cloning*
AttL2 sequencer R	gtaacatcagagattttgagacac	*Sequencing*
GFP sequencer R	cgctgaacttgtggccgttca	*Sequencing*
OFT1 cloning F	gaaggcgcgccagtcgacatgaattctccgttaagttctaagaatctgag	*AtOFT1 cloning*
OFT1 cloning R	agtgcggccgcacctcctccactagaacaagaaacagaatttgagccata	*AtOFT1 cloning*
OFT1-pENTR F	caccatgaattctccgttaagttct	*AtOFT1 cloning/cDNA*
OFT1-pENTR R	tccactagaacaagaaacaga	*AtOFT1 cloning/cDNA*
fMet OFT1 Δ36 pentr F	caccatgtcttactctcccagaaacgct	*AtOFT1 cloning*
OFT1+6xHis+STOP R	tcagtgatgtgtggtgatggtgatggtgatgtccactagaacaagaaacaga	*AtOFT1 cloning*
OFT1 [R51A] F	agcttattgtttgcagatcgtcacatg	*AtOFT1 SDM* [1]
OFT1 [R51A] R	catgtgacgatctgcaaacaataagct	*AtOFT1 SDM* [1]
OFT1 [H54A] F	tttcgagatcgtgccatgtcagattcc	*AtOFT1 SDM* [1]
OFT1 [H54A] R	ggaatctgacatggcacgatctcgaaa	*AtOFT1 SDM* [1]
OFT1 [H54N] F	tttcgagatcgtaacatgtcagattcc	*AtOFT1 SDM* [1]
OFT1 [H54N] R	ggaatctgacatgttacgatctcgaaa	*AtOFT1 SDM* [1]
OFT1 [R260A] F	gcggttcacatggcaatagagatagat	*AtOFT1 SDM* [1]
OFT1 [R260A] R	atctatctctattgccatgtgaaccgc	*AtOFT1 SDM* [1]
OFT1 [R260K] F	gcggttcacatgaaaatagagatagat	*AtOFT1 SDM* [1]
OFT1 [R260K] R	atctatctctattttcatgtgaaccgc	*AtOFT1 SDM* [1]
OFT1 [D264A] F	agaatagagatagcttggatgatacat	*AtOFT1 SDM* [1]
OFT1 [D264A] R	atgtatcatccaagctatctctattct	*AtOFT1 SDM* [1]
ACTIN7 F	atgggtcagaaagatgcttacgttggtga	*cDNA PCR*
ACTIN7 R	tcaggacaacggaatctctcagctccgat	*cDNA PCR*
SAIL_1174_D07 genotyping LP	aagtgacgtttggacagatgc	*Genotyping PCR*
SAIL_1174_D07 genotyping RP	ttcgggtgttagtggacaaac	*Genotyping PCR*
gaut14-1 genotyping LP	aaacatttgctcttgtgctgc	*Genotyping PCR*
gaut14-1 genotyping RP	ttaaacgctttgacatcaccc	*Genotyping PCR*
MBP pENTR F	caccatgaaaatcgaagaaggtaa	*MBP control cloning*
MBP pENTR R	ctaatggtgatggtgatggtgatggtgagtctgcgcgtctttcagggc	*MBP control cloning*
MSR1 pENTR F	caccatgggtgttgatttgaggcaa	*AtMSR1 cloning*
MSR1 pENTR R	gcaaaagcatgaataagccaa	*AtMSR1 cloning*
fMet MSR1Δ28 pENTR F	caccatgtactttgattctcttcaggag	*AtMSR1Δ28 cloning*
MSR1+6xHis+STOP R	tcagtgatggtgatggtgatggcaaaagcatgaataagccaa	*AtMSR1Δ28 cloning*
FRB1 pENTR F	caccatgtcagtcggcgttccagtg	*AtFRB1 cloning*
FRB1 pENTR R	tctcagagattgtgctcgtag	*AtFRB1 cloning*
fMet FRB1Δ144 pENTR F	caccatgagacggagaaaacacgttgag	*AtFRB1Δ144 cloning*
FRB1+6xHis+STOP R	ttagtgatggtgatggtgatgtctcagagattgtgctcgtag	*AtFRB1Δ144 cloning*

The name of each primer described in the Materials and Methods as well as their respective 5'→3' sequence and the purpose of each primer is listed. [1]SDM is abbreviation for site-directed mutagenesis.

agarose gels and documented with a Bio-Rad Gel Doc XR+ Image analysis workstation (Bio-Rad Laboratories, Hercules, CA). The *oft1-3*$^{-/-}$ line was backcrossed to Col-0 to remove a second T-DNA insertion and its associated BASTA resistance marker.

Further validation of the absence of the *OFT1* transcript in the *oft1*$^{-/-}$ T-DNA mutant lines was assessed by RNA isolation from 7-day-old seedlings from each homozygous *oft1* mutant line and Col-0 using the PureLink Plant RNA Kit (Thermo Fisher Scientific, San Jose, CA) following the manufacturer's instructions. Genomic DNA contamination was eliminated from the extracts using the Turbo DNA-*free* Kit (Ambion), and synthesis of first-strand cDNA was carried out using the Invitrogen SuperScript III First-Strand Synthesis System both according to the manufacturer's protocol (Thermo Fisher Scientific, San Jose, CA). The resulting cDNA library for each line was probed for *AtOFT1* transcript, as well as *ACTIN7* (*ACT7;* At1g33160) for amplification reference by PCR. Reactions were assembled using 24 ng cDNA as template and the respective gene-specific primers (*OFT1-pENTR F* and *OFT1-pENTR R* or *ACTIN7 F* and *ACTIN7 R;* Table 2.1). Reactions probing for the *AtOFT1* transcript were cycled under the following conditions: 98°C initial denaturation for 5 min, followed by 30 cycles of 98°C (30 sec), 55°C (30 sec), 72°C (1 min), final elongation for 5 min at 72°C. Reactions probing for the *ACTIN7* transcript were cycled under the following conditions: 98°C initial denaturation for 30 sec, followed by 30 cycles of 98°C (10 sec), 55°C (20 sec), 72°C (30 sec), final elongation for 5 min at 72°C. The resulting PCR products were separated on 1.0% (w/v) agarose gels and visualized with a Bio-Rad Gel Doc XR+ Image analysis workstation (Bio-Rad Laboratories, Hercules, CA).

V. Cloning strategies for transgenic plant lines used in this study

Construction of all plant expression vectors used to create the remaining transgenic Arabidopsis lines for this study, except for the *11p::OFT1-GFP* plasmid, were performed using the same experimental workflow. The gene of interest was first amplified out of the appropriate template source using locus specific primers (Table 2.1) and the resulting DNA amplicons were resolved on a 1.0 % (w/v) low-melting point agarose gel, excised, and gel purified with the QiaQuick gel extraction kit (Qiagen Valencia, CA). The purified amplicon of interest was then introduced into the Gateway compatible pENTR/D-TOPO entry vector following manufacturer's suggested instructions (Thermo Fisher Scientific, San Jose, CA), and subsequently transformed into chemically competent *Escherichia coli (E. coli)*. Transformation reactions were plated on Luria Broth (LB) agar media supplemented with 50 µg/mL kanamycin (Kan) and incubated for 18 h at 37ºC. Individual transformant colonies were inoculated into separate tubes containing 10 mL of liquid LB + Kan and incubated for 18 h at 37ºC. The entry plasmids were extracted from *E.coli* using the QIAprep Spin Miniprep kit (Qiagen Valencia, CA). For every plasmid constructed and described in this dissertation, Sanger dideoxy sequencing was performed by the Nevada Genomics Center (ag.unr.edu/genomics) to verify proper assembly and sequence.

Following correct sequence verification, each entry plasmid was recombined with the appropriate plant expression vector using LR Clonase II enzyme (Thermo Fisher Scientific, San Jose, CA), and transformed into electrocompetent *E.coli.* Single colonies were again propagated in liquid LB medium supplemented with the appropriate antibiotic and incubated at 37ºC for 18 h before the plasmids were purified and sequence verified as

described above. The final sequence-verified plant expression construct was introduced into the appropriate *Arabidopsis thaliana* line by agrobacterium-mediated transformation.

To construct a binary vector containing Green Fluorescent Protein (GFP) under the control of the *OFT1* promoter, an *OFT1* promoter fragment containing 1000 bp upstream of the predicted start codon and 12 bp after the start codon was cloned using genomic DNA isolated as described above, promoter-specific primers (*pOFT1 -1000 pENTR F* and *pOFT1 pENTR R*; Table 2.1), and Phusion DNA polymerase. PCR reactions were cycled under the following conditions: 98°C initial denaturation for 5 min, followed by 35 cycles of 98°C (30 sec), 52°C (30 sec), 72°C (2 min), final elongation for 7 min at 72°C. The *AtOFT1* promoter sequence was transferred into the pIGWB-504 binary vector (Nakagawa *et al.,* 2007) using LR Clonase II according to the manufacturer's instructions.

The expression vector *pUBC::OFT1-GFP,* which encodes AtOFT1 with GFP fused to the C-terminus under the control of the *Ubiquitin 10* (*UBQ10)* promoter was made by amplifying the *AtOFT1* genomic DNA sequence using gene-specific primers (*OFT1-pENTR F* and *OFT1-pENTR R*; Table 2.1). PCR reactions were cycled under the following conditions: 98°C initial denaturation for 5 min, followed by 30 cycles of 98°C (30 sec), 55°C (30 sec), 72°C (1 min), and final elongation for 5 min at 72°C. The *AtOFT1* amplicon was resolved on a 1% [w/v] low-melting-point agarose gel, introduced into the pENTR/D-TOPO entry vector, transformed into *E.coli*, and sent for sequencing as described above. Following sequence verification, the OFT1/pENTR vector was used to transfer the *AtOFT1* sequence into the plant compatible Gateway vector pUBC-GFP (Grefen *et al.,* 2010) using LR Clonase II according to the manufacturer's instructions.

Individual site-directed mutagenesis (SDM) PCR reactions were subsequently assembled using *OFT1/ pENTR-D-TOPO* as a template and nucleotide-specific mutagenic primers listed in Table 2.1 to create plasmids containing a single altered amino acid for the purposes of investigating the residue-specific catalytic activity of the encoded amino acid. For all constructs requiring SDM PCR amplification, reactions were cycled under the following conditions: 98°C initial denaturation for 5 min, followed by 35 cycles of 98°C (30 sec), 60°C (30 sec), 72°C (4.5 min), final elongation for 15 min at 72°C. Following *DpnI* digestion for 2 h at 37°C, each SDM reaction was directly transformed into chemically competent *E. coli*. Site-directed mutant expression constructs were sequenced and then individually recombined into pUBC-GFP using LR Clonase II as described above.

The *11p::OFT1-GFP* hemizygous complement line encodes AtOFT1-GFP-6xHis-TEV protease site-Halo tag-6xHis (Figure 2.1). The *AtOFT1* genomic sequence was amplified by PCR using gene-specific primers (*OFT1 cloning F* and *R*; Table 2.1) and transferred into a modified pGreenII vector system for plant expression (Hellens *et al.,* 2000), with a kanamycin selection marker for bacteria, and a hygromycin marker for plants. The DNA sequence of this construct is provided in Figure 2.1. The *11p* promoter corresponds to the upstream regulatory region for *AGP11 (At3g01700*) with the addition of a 5′ UTR region containing an intron from proton pump *AHA3* (*At5g57350*) (Frietsch *et al.,* 2007). The GFP does not contain the S65T modification for enhanced fluorescence in order to maintain a better tolerance of acidic pHs that are often found in compartments in the secretory pathway. The HaloTag® from Promega provides a tag for purification,

Figure 2.1: Sequence and relevant features of the *11p::OFT1-GFP* complement construct. The *11p::POFT1-GFP* plasmid was constructed with a modified pGreenII vector system (Hellens *et al.,* 2000). The promoter region (yellow) is from *AGP11 (At3g01700)* with an added intron in the 5' UTR(from *AHA3, At5g57350*). The promoter extends from an SbfI to an AscI restriction sites (all restriction enzyme cut sites are colored in purple/dark purple), and the *AtOFT1* open reading frame (red) is fused at the 3' end to a sequence encoding *Green Fluorescent Protein (GFP)* (green) that was modified with a silent mutation that deletes a cryptic intron splice site for plants but is otherwise equivalent to original sequence without the *S65T* modification for enhanced fluorescence. Additionalfeatures include a linker connecting *AtOFT1* to *GFP* containing a Not1 and AvrII restriction cloning site, two 6XHis affinity tags (black), a TEV protease site (gray), and a modified version of a HaloTag® from Promega (blue).

along with two 6-histidine (6xHis) epitope tags.

The binary vectors used to establish the BioID proximity labeling system for AtOFT1 protein-protein interaction analysis were kindly constructed and donated by Dr. Jeffrey Harper (University of Nevada, Reno). These vectors were constructed using the pGreen2 vector backbone (Hellens *et al.,* 2000). The *OFT1-YFP-BioID* construct contained the coding sequence for *AtOFT1* with C-terminal fusion of YFP followed by a 3X Glycine (Gly) linker and the modified biotin ligase from *Escherichia coli*, BirA, under the control of the *UBQ10* promoter. The *E. coli* BirA protein contains the R118G mutation, allowing this enzyme to promiscuously biotinylate proteins that come within a 10 nm radius of this fusion protein (Liu *et al.,* 2018). The two control constructs were made using the same vector backbone with the *YFP-BioID* vector simply lacking the *AtOFT1* coding sequence, and the *OFT1[R260A]-YFP-BioID* construct containing an altered codon at Arg260 to encode alanine, which was determined to abolish AtOFT1 activity (Smith *et al.,* 2018a*;* Smith *et al.,* 2018b*)*.

VI. Agrobacterium-mediated transformation of plant expression plasmids

Sequence verified plant binary expression plasmids were transformed into *Agrobacterium tumefaciens* GV3101 cells by electroporation and plated Luria Broth (LB) agar medium containing the necessary selection antibiotics. Transformations were incubated at 30°C for 48 h. To transfer the plant expression plasmid from *A. tumefaciens* to the desired Arabidopsis background line, a single colony of transformant *A. tumefaciens* was inoculated into a 10 mL liquid LB culture supplemented with the appropriate antibiotics and then placed in a 30°C shaking incubator for 16 h. Following incubation, the 10 mL culture was used to inoculate a 1 L LB culture containing the

appropriate antibiotics and incubated at 30°C in a shaking incubator for 16 h. The saturated culture was then centrifugation at 3,000xg for 15 min to harvest the cells, and the resulting cellular pellet was resuspended in 450 mL of 5% [w/v] sucrose supplemented with 0.05% [v/v] Silwet L-77. Five-week-old flowering Arabidopsis plants were subsequently transformed via the floral dip method (Clough and Bent, 1998) and placed back into a long-day growth chamber until reaching maximal seed set (approximately 2 weeks of additional growth when floral meristems terminate). Seed subsequently produced by the floral dipped plants was sterilized, stratified, and plated on MS media containing the appropriate plant selectable marker as well as 100 µg/ mL cefotaxime and incubated for 10 d in a germination chamber at 24° under long-day conditions. T_1 transformants seedlings were identified by growth after 10 days and were transferred to soil. Confirmation of T_1 lines, verification of the background line genotype, and all other PCR genotyping of plant lines used in this investigation was carried out by PCR genotyping. Loci or gene specific primers (Table 2.1) and ExTaq polymerase were used to identify the plant line genotypes as described above. The resulting amplified regions of interest were resolved on a 1% [w/v] agarose gel and imaged using a ChemiDoc XRS+ imaging platform (Bio-Rad Laboratories, Hercules, CA).

VII. *In vitro* pollen germination assay and data analysis

A 76 × 25mm glass slide was prepared with 750µL solid Pollen Germination Medium (PGM) (5 mM $CaCl_2$, 0.01% [w/v] boric acid, 5 mM KCl, 10% [w/v] sucrose, 1 mM $MgSO_4$; pH 7.5 (Boavida and McCormick, 2007)) containing 1.5% [w/v] low melting point agarose (PGM-agarose) cooled to 25ºC. Using fine forceps, an open flower at peak sexual maturity from 6-week-old plants of the desired genotype was removed

from the plant (Figure 2.2). While applying slight pressure with forceps just above the sepal to allow the floral organs to fan out, pollen was deposited on the surface of the PGM-agarose slide using gentle sweeping and/or blotting of the fanned-out flower (Figure 2.2; Smith and Wallace, 2020). This process was used for effectively transferring pollen for multiple experiments and was repeated until the desired amount of pollen had been transferred to the PGM-agarose slide. The pollinated PGM-agarose slide was then immediately transferred to a humidity chamber and incubated for the indicated time period in the dark at 25°C (Figure 2.3; Smith and Wallace, 2020).

Prior to imaging to assess pollen tube morphology, elongation rate, grain germination frequency, and tissue expression, PGM was applied to the surface of the PGM-agarose pad and a coverslip was added. Images for these experiments were acquired using a Keyence BZ-X700 microscope under brightfield illumination using a 10X 0.45 NA air objective and quantified using Fiji. Statistical analyses were performed in GraphPad Prism (GraphPad Software, La Jolla, CA; www.graphpad.com).

For pollen tube expression verification of AtOFT1 catalytic site-directed mutant lines, pollen from the appropriate genotype was germinated as described above, and prior to imaging, PGM was added to the surface of the PGM-agarose pad before a coverslip was applied. For confocal microscopy of AtOFT1 subcellular localization, pollen was harvested as previously described from 6-week-old *oft1-3*$^{(-/-)}$ plants expressing *11p::OFT1-GFP* or this transgenic line crossed with either Got1p-mCherry or MEMB12-mCherry Golgi marker lines (Geldner *et al.,* 2009) and germinated for 1.5 h. Prior to imaging, PGM was added to the surface of the PGM-agarose pad before a coverslip was applied. For co-localization imaging using Mitotracker Orange staining, the

Figure 2.2: Fanning out flower for pollen germination. A, An *Arabidopsis thaliana* flower at peak sexual maturity. B, Using fine forceps, apply slight pressure just above the sepal to allow for the floral structures to fan out facilitating greater access to the male reproductive structures (stamens). While simultaneously maintaining this pressure with the forceps, gently brush or blot the flower onto a PGM-agarose slide to release the pollen from the anthers for *in vitro* pollen germination analyses.

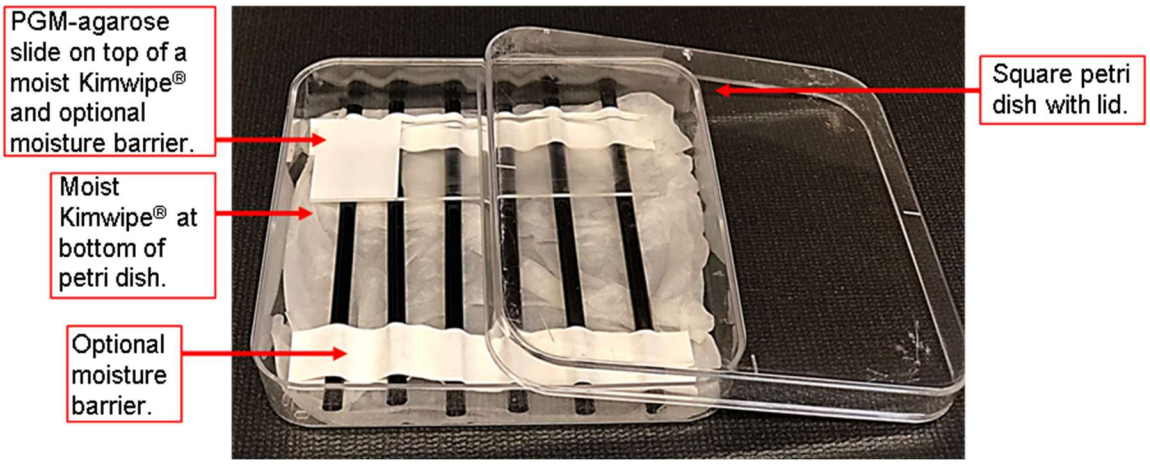

Figure 2.3: Humidity chamber setup. A humidity chamber was used to prevent the PGM- agarose media pad containing *in vitro* germinated pollen or semi-*in vivo* (*SIV*) pollinated pistils on the media surface from drying out throughout these investigations. The chamber is composed of two basic materials: 1) a square petri dish and 2) a moistened Kimwipe□. An optional, but recommended moisture barrier was inexpensively fashioned using plastic coffee straws and laboratory tape and was placed on top of the Kimwipe□ and under the microscope slide to prevent the PGM-agarose pad from being in direct contact with the moisture from the Kimwipe□. Following preparation of for the desired investigation, slides were immediately transferred to the humidity chamber, and for slides containing samples, the humidity chamber was further placed in a lightproof cardboard microcentrifuge tube storage box at 25ºC for the duration of the incubation period. Slides with samples were also immediately returned to the humidity chamber in the dark between data collection periods for the duration of the experiment. PGM-agarose slides can be prepared in advance of experimentation and stored at 4ºC for a maximum of 7 days in the humidity chamber. For storage, parafilm placed snuggly around the side edges of the closed rim of the petri dish is strongly suggested to lock in moisture and increase adherence of the PGM-agarose media pad to the glass surface of the microscope slide.

11p::OFT1-GFP pollen tubes were treated with 500 nM Mitotracker Orange for 15 min prior to coverslip addition and imaging using the tetramethyl rhodamine (TRITC) emission filter (555-615 nm), described further below.

An Olympus FluoView FV1000 line-scanning confocal microscope equipped with 40× 1.3 NA and 60× 1.4 NA oil objectives, 488 and 543 nm excitation laser lines, and emission filters for GFP (500-530 nm) and TRITC were used to acquire images for both the verification of AtOFT1 catalytic site-directed mutants and AtOFT1 colocalization analysis. Images for AtOFT1 catalytic site-directed mutants were acquired overtime simultaneously in both brightfield and GFP channels to evaluate the fluorescent expression signal, while brightfield, GFP, and TRITC channels were simultaneously used to acquire images overtime for punctate particle colocalization signal analysis. Image files for AtOFT1 catalytic site-directed mutants and AtOFT1 colocalization were processed similarly in Fiji (imagej.net) by merging their respective channels to allow for fluorescent particle visualization as well as the outline of the pollen tube. To determine the degree of fluorescent signal overlap for colocalization analyzes, time lapse images for each fluorescent channel were processed in Fiji by normalizing the channel signal intensities. The Fiji colocalization plugin, JACoP (Bolte and Cordelieres, 2006), could then be used to determine the statistical overlap of each fluorescent channel by calculating the average signal intensity overlap of the two channels and produced a Pearson's correlation coefficient for each pollen tube analyzed per pollen genotype. The Pearson's correlation coefficients determined per colocalization line were imputed into GraphPad Prism (GraphPad Software, La Jolla, CA, www.graphpad.com) and statically analyzed.

VIII. *Semi-in vivo (SIV)* pollen tube assays and quantification

Pistils from mature *Arabidopsis thaliana* homozygous *male sterile 1 (ms1)* mutant plant lines, which yield non-viable pollen (Wilson *et al.,* 2001), were used as the preferred pistil source for these assays as well as other pollen penetration experiments detailed in this study. An in-depth explanation of how to successfully perform this delicate assay is provided by Smith and Wallace, 2020.

Pollen from 6-week-old plants was collected from the indicated plant genotypes per experiment and used to pollinate mature, emasculated *ms1* stigmas (Figure 2.4). One hour after pollination (HAP), stigmas were dissected from the parental plant and placed on a glass slide with double sided tape (Figures 2.5A-C). Using an 18G needle, the stigma and style were dissected from the pistil and transferred to a PGM-agarose pad on a microscope slide as described above for *in vitro* germination analyses (Figure 2.5D). Samples were incubated at 25°C in a humidified chamber in the dark for 2 HAP, and pollen tube emergence from the cut end of the stigma-style interface was visualized using a Leica EZ4HD dissecting scope at 35X magnification over the indicated time intervals starting at 2 HAP. Following image acquisition for a given time point, the samples were immediately returned to the humidified chamber (Figure 2.3) in the dark at 25ºC until all images per time point had been collected.

Semi-in vivo assays utilizing fluorescently labeled pollen tubes were assembled identically. For these experiments, hemizygous *11p::OFT1-GFP* $^{+/-}$*; oft1-3* $^{-/-}$ transgenic lines described above or *9p::YFP* $^{+/-}$ control lines, which encodes a hemizygous copy of Yellow Fluorescent Protein (YFP) expressed under the pollen specific *AUTOINHIBITED CALCIUM ATPASE 9 (ACA9)* promoter (Schiott *et al.,* 2004) were utilized as the mature

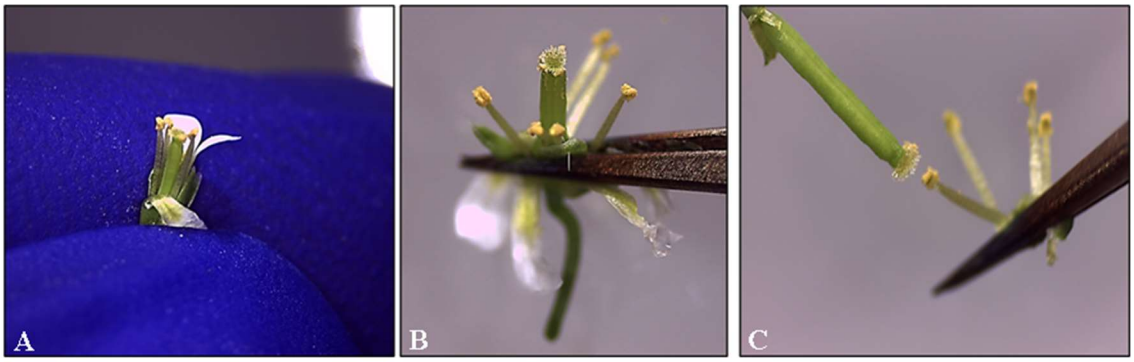

Figure 2.4: Stamen dissection for *SIV* fertilization assays**.** Demonstration of stamens dissected for fertilizing emasculated pistils for semi-*in vivo* (*SIV*) fertilization assays as well as for used for crossing. A, A hemizygous flower at peak sexual maturity grasped between thumb and index fingers of non-dominant hand. Using fine forceps in dominant hand, the floral petals are folded back and wedged between non-dominant fingers. B, Image of the flower with petals tucked out of the way and gently grasped above the sepal with fine forceps to expose the pistil and stamens for demonstration purposes, while in actual practice, the flower should remain grasped in fingers as shown in panel A. C, Using fine forceps, first remove and discard pistil from 'folded back' flower. Finally, gather stamens with forceps at base of filaments and carefully detach them from the remaining floral structures in one motion. Image showing dissected stamens grasped with fine forceps with mature pollen (yellow) atop the anther being transferred to an emasculated acceptor pistil using a gentle sweeping or blotting motion.

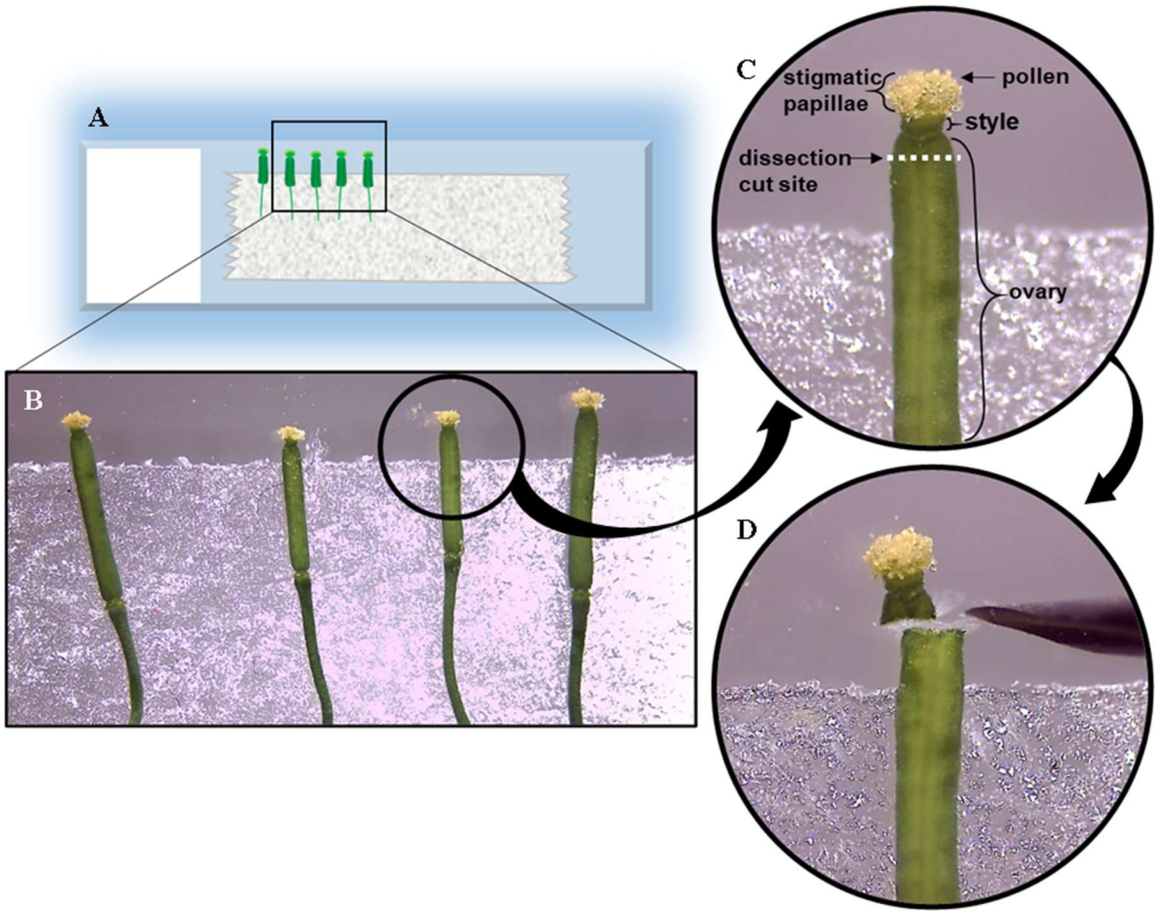

Figure 2.5: Diagram of pistil dissection for *SIV* fertilization assays**.** A, Illustration of slide setup for pistil dissection for semi-*in vivo* (*SIV*) fertilization assays. Double-sided tape is applied to glass slide in preparation for dissection. One hour after pollination (HAP), pistils are detached from the remaining plant at base of peduncle and transferred to the adhesive, ensuring the stigma and style are not in contact with tape. B, Image of real *SIV* pistils transferred to glass slide 1 HAP. C, Closeup of pistil on adhesive with important anatomical features denoted (black text and bracket) as well as the dissection cut site (white dashed line). D, The tape-immobilized pistils are cleanly dissected using a 18G needle (rightmost object) at the designated dissection site to detach the pollinated stigma-style from the remaining pistil. The stigma-style is then transferred to a PGM-agarose media slide using the fine tip of the needle and immediately placed in a humidity chamber (Figure 2.3) where the natural process of double fertilization continues in total darkness before being imaged at the indicated time points for the experiment. For fluorescent *SIVs, p*rior to imaging, PGM is applied to the media surface followed by the addition of a glass cover slip.

pollen donor source. Pollen from each line was collected and used to pollinate mature, emasculated *ms1* pistils, that had been previously dissected. Pollen tube penetration was allowed to commence for 1 HAP at 25ºC on the intact *ms1* pistil before the stigma and style were removed from the remainder of the plant and pistil, transferred to a microscope slide containing a PGM-agarose pad, and incubated as described above in a humidified chamber in the dark. Four HAP, pollen tubes emerging from the style were examined using a Keyence BZ-X700 microscope at 20X magnification. Sequential Z-stack images using brightfield illumination and GFP (ex. = 470 nm, em. = 525 nm) or YFP (ex. = 500 nm, em. = 530 nm) were collected for each *SIV* dissected stigma-style per time point. The Z-stacks were then individually processed using the Keyence BZ-X Analyzer software by first converting the Z-stack file for a single *SIV* dissected pistil into a max projection image in both the brightfield and GFP or YFP channels. The max projected images were then merged together into a single image allowing for both fluorescent and non-fluorescent pollen tubes to be visualized (Figure 2.6A). These images were subsequently used to quantify total pollen tubes emerging from the bottom of style as well as the proportion of fluorescent and non-fluorescent tubes, as this indicated the pollen tube genotype. The pollen tube genotype composition was then calculated by dividing the number of fluorescent or non-fluorescent pollen tubes per individual *SIV* pistil by the total number of pollen tubes that had penetrated through the stigma and style 4 HAP (Figure 2.6B). The emerging pollen tube composition could be predicted by Mendelian segregation of the transgene in the male gametes, which consists of a 1:1 ratio of mutant pollen: *oft1* mutant pollen that were complemented and possessed the fluorescent transgene. This expected starting pollen genotypic ratio was further verified by

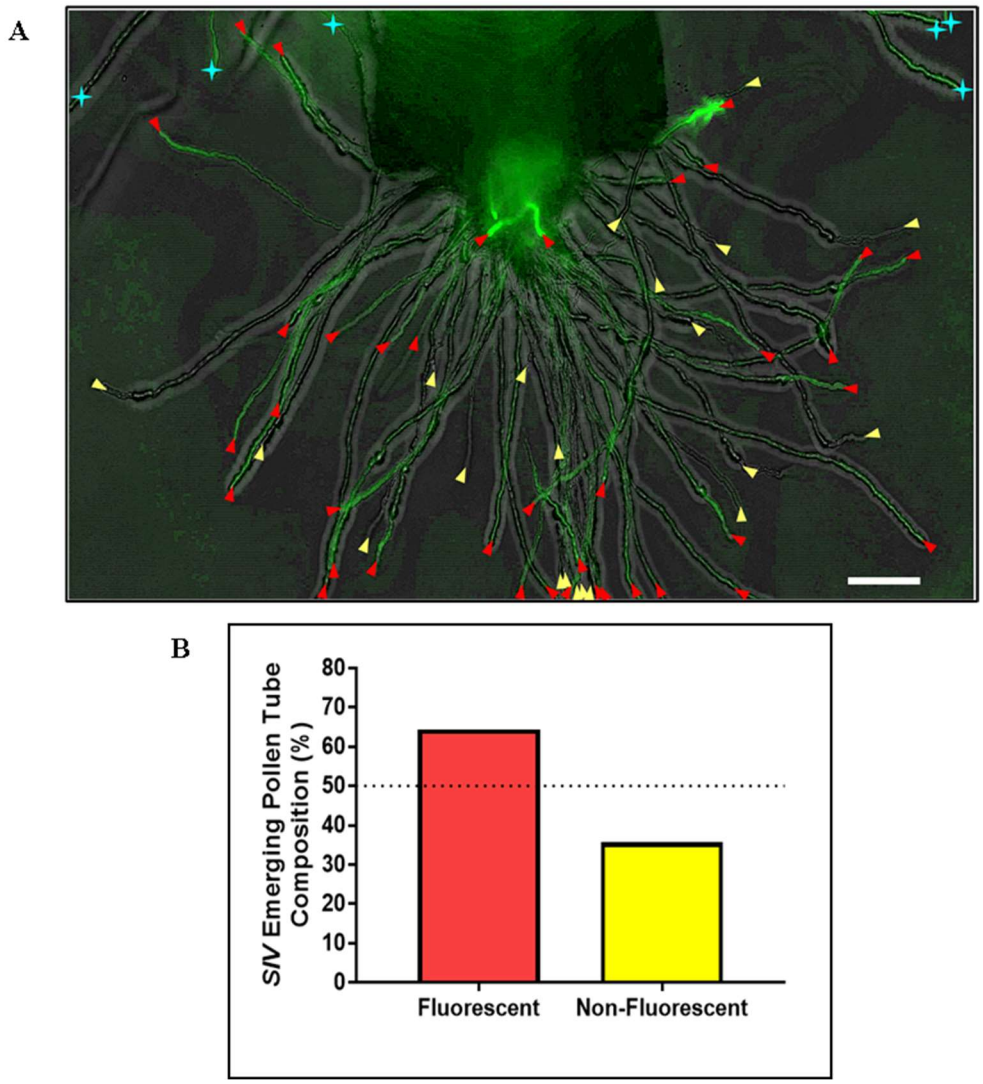

Figure 2.6: Quantification example of a fluorescent *SIV* fertilization assay using hemizygous pollen. A, A z-stack max projection overlay of both GFP and brightfield channels showing pollen tubes (PTs) emerging from the bottom of an emasculated *ms1*$^{-/-}$ style 4 HAP with hemizygous pollen. Yellow carrots indicate pollen tubes that contain the transgenic and fluorescent construct, while red carrots indicate PTs that do not contain this vector, which are not fluorescent. The vectorused in this investigation was *11p::OFT1-GFP,* which is a *oft1* mutant complement construct encoding AtOFT1 fused to GFP that effectively restored the PT defects of *oft1* PTs. The T_1 segregating gametes in this assay, in which the pollen population was 1:1 for *oft1* pollen containingthis transgene (denoted in later investigations as *oft1-3*$^{-}$*;11p::PFT1-GFP*$^{+}$, and further behaved andtreated as "wildtype" pollen) : uncomplemented regular mutant *oft1* PTs (denoted later as *oft1-3*$^{-}$*;11p::PFT1-GFP*$^{-}$). This assay was used to assess the extent of *oft1* PTs impediment in penetratingthe stigma and style compared to "wildtype" complemented pollen. Blue stars indicate PTs that didnot emerge from the bottom of the dissected stigma-style and are negated from the subsequent quantification. Bar = 100 µm. B, Quantification of emerging PT composition in (A) showing percent genotype; 64.4% (n = 38) fluorescent, transgene-containing PTs and 35.6% (n = 21) non- fluorescent, PTs. Dashed line at 50% represents expected emerging PT population percent composition if no PT penetration defect exists for a suspected PT mutant.

performing the same quantification to pollen tubes that had grown away from the top of the *SIV* stigmas for each fluorescent *SIV* stigma-style analyzed.

IX. Analine blue staining of pollen tubes

Mature, emasculated *ms1* flowers were pollinated with the indicated pollen genotype and incubated under normal long-day light conditions for either 24 h or 48 h. Following incubation, pistils were dissected and subjected to analine blue staining (Mori *et al.,* 2006). Approximately 10 emasculated, pollinated pistils were harvested and transferred to 2 mL screw cap microcentrifuge tubes containing fixative solution (1:3 ratio of acetic acid: ethanol). Using a 18G luer lock needle connected to a 10 mL syringe, a hole was punctured in the top of the microcentrifuge tube containing pistils in fixative and plunger pulled back to aspirate all of the air. The pistils were incubated in fixative solution for 2 h before the solution was discarded and pistils rehydrated for 10 min at 25ºC by sequentially adding decreasing concentrations of ethanol: 70% [v/v], 50% [v/v], and 30% [v/v]. Following the last ethanol rehydration incubation, diH_2O was added to the pistils and incubated again for 10 min at 25ºC. The diH_2O was discarded, and the pistils were subjected to alkaline treatment with 8 M NaOH at 25ºC for 18h. The alkaline treatment reaction was quenched by exchanging the 8 M NaOH solution with diH_2O and allowing the fixed pistils to soak for 10 min at 25ºC. The diH_2O wash was repeated once more before it was gently aspirated from the pistils and Decolorized Analine Blue Solution (DABS; 0.1% [w/v] analine blue, 108 mM K_3PO_4, pH 11) was carefully added. The pistils were incubated in DABS for at least 2 h in the dark at 25ºC prior to imaging.

A 76 × 25 mm glass slide was prepared for imaging analine blue stained pollinated pistils by using petroleum jelly to create a square, water impermeable

perimeter for imaging and then transferred to the in the dark for the remainder of the mounting process. Under dark conditions, the pistils were gently transferred to the center of the petroleum jelly well using fine forceps and fresh DABS that was applied before cover slip addition. Using a Leica EZ4HD video dissecting microscope at 35X magnification and working as quickly as possible, the mounted pistils were simultaneously visualized while the cover slip was carefully pressed down using fine forceps until the exterior pistil tissues protecting the ovules had sufficiently fanned opened exposing the inside of the ovary cavity. The prepared analine blue slides were then immediately returned to the dark before images were acquired at 20X magnification on a Keyence BZ-X700 epifluorescent microscope fitted with a 4',6 -diamino-phenylindole (DAPI) filter cube. Z-stacks of each pistil were acquired and subsequently processed using the Keyence BZ-X Analyzer software by converting the Z-stack files into single max-projected image allowing for visualization of pollen tube penetration throughout the entire pistil. Pollen tube penetration ability per time point was assessed by comparing the average length that wildtype Col-0 pollen tubes had traversed through the pistil compared to *oft1*$^{-/-}$ mutant pollinated pistils.

X. Pistil decapitation assay

To assess if the stigmatic and stylar tissues hypothesized to be a physical barrier to successful double fertilization events for *oft1*$^{-}$ mutant pollen, the protocol developed by Wiegand and Harper, 2020 was followed. Briefly, the stigma and style of mature, emasculated *ms1*$^{-/-}$ pistils were dissected away from the remaining plant and pistil tissues, and mature heterozygous pollen originating from a sexually mature *oft1*$^{+/-}$ plant was gently placed on the severed surfaces of each 'decapitated' *ms1*$^{-/-}$ pistil (Figure 2.7).

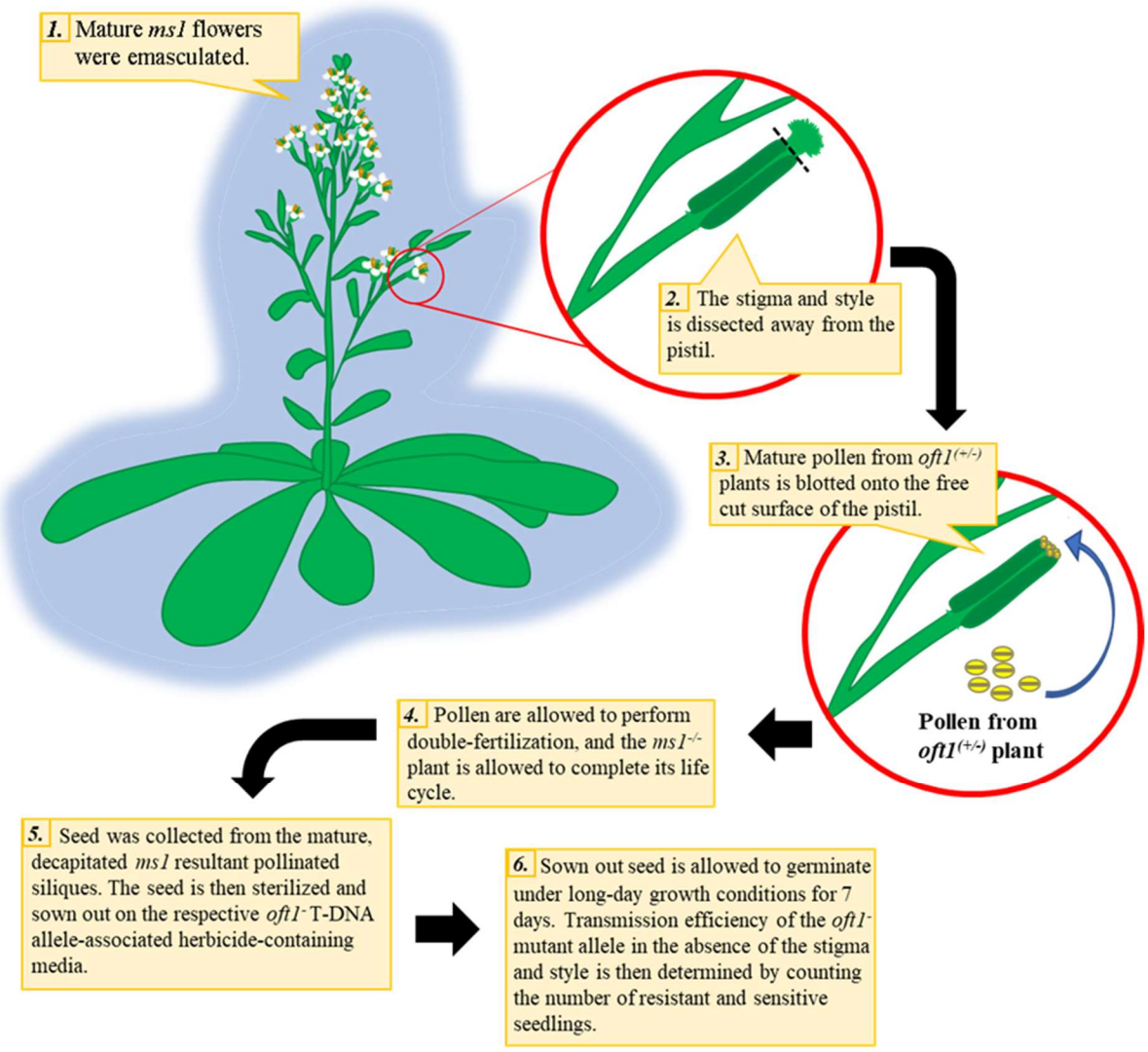

Figure 2.7: Decapitation assay experimental design. Illustration of the experimental workflow of decapitation assay experiments used to assess *oft1* mutant PT fertilization ability in the absence of the stigma and style.

The decapitated, pollinated *ms1*$^{-/-}$ plants were placed back under long-day light growth conditions, and upon senescence, the developed and mature decapitated siliques were harvested, and seed housed within these siliques collected.

The seed from the decapitated siliques was surface sterilized, stratified, plated on MS media containing the appropriate *oft1*$^{-}$ T-DNA-associated herbicide selectable marker and grown vertically under long-day light conditions. Following 7 days of growth, the resulting seedlings were scored for herbicide resistance or sensitivity. The transmission efficiency (TE) of the *oft1*$^{-}$ mutant pollen's ability to fertilize ovules in the absence of the stigma and style was determined by quantifying both the number of resulting seedlings exhibiting herbicide resistance and sensitivity.

XI. Vegetative tissue phenotypic characterization of *oft1* mutants

For all vegetative phenotypic quantification, excluding seed mucilage and area characterization, the experimental setup began by sterilization and stratification of seed from Col-0 and all three *oft1*$^{-/-}$ mutant lines as described above. Stratified seed for rosette diameter and 7-day-old root length analysis were sown on MS media, while seed intended for 7-day-old hypocotyl analysis were sown on MS media lacking sucrose. Plated seed for hypocotyl measurements were wrapped thoroughly in tin foil to prohibit light penetration, and all seedlings were grown vertically for 7 days under long-day light conditions.

For rosette diameter quantification, 7-day-old seedlings from each genotype (*oft1-1*$^{-/-}$, *oft1-2*$^{-/-}$, *oft1-3*$^{-/-}$, and Col-0 control) were individually transplanted to soil in a 4 x 4-inch pot. The seedlings were placed in a growth chamber under long day conditions as described above and rosettes were imaged after 31 days. Rosettes were imaged using a

Nikon digital camera with the camera lens placed directly over the center of each the pot. Images of each rosette were acquired by individually imaging each pot alongside a ruler at equal height with the rosette. Analysis of each image was performed using Fiji software (imagej.net) as follows. The pixel scale settings was first calibrated using the in-frame ruler, and the rosette diameter was traced using the circle tracing tool in Fiji. The resulting measurement produced the circle area, and these measurements were converted in Microsoft Excel to diameters using the equation for area of a circle, $A=\pi d$ (where A=area, π=pi=3.14, and d=diameter). Statistical analysis of the calculated diameters was performed in GraphPad Prism (GraphPad Software, La Jolla, CA, www.graphpad.com).

Root length and hypocotyl elongation quantification was carried out following 7-days of growth. The seedlings on plates were imaged on an EPSON Perfection V550 Photo Color scanner and analyzed using Fiji (imagej.net). Root and hypocotyl length were determined by using the same measurement procedure, which was very similar to rosette diameter analysis described above, by beginning each image analysis by first setting the pixel scale to the known distance of the in-frame scale provided in each image. For both 7-day-old root and hypocotyl length measurements, the Fiji line tracing tool was used. For root lengths, a line was drawn along the entire length of the root with the tracing tool from the root junction to the distal-most apical root cap. For hypocotyl measurements, the total hypocotyl length was traced from the root junction to the shoot apical meristem. The subsequent tracings could then be used to calculate the total root or hypocotyl lengths based on the known pixel distance. Statistical analyses for both root and hypocotyl measured lengths per genotype per biological replicate were performed in GraphPad Prism (GraphPad Software, La Jolla, CA, www.graphpad.com).

XII. Ruthenium red staining of *oft1* mutant seed

Approximately 20 seeds per genotype were collected from equal-age *oft1-1*$^{-/-}$, *oft1-2*$^{-/-}$, *oft1-3*$^{-/-}$, and Col-0 plants grown side-by-side and placed in separate 1.7 mL tubes containing 800 µL 50 mM EDTA (Ethylenediaminetetraacetic acid). The tubes were vortexed and incubated for 2 h at 25º C with frequent inversion to mix before the EDTA was aspirated from the tubes and replaced with 800 µL 0.01% ruthenium red stain. The seed were incubated at 25ºC for 2 h before the stain was aspirated out of the tube, and the seeds were washed 3 times with 1 mL sterile diH_2O, followed by inverting the tube containing the stained seeds gently to mix, and then discarding the supernatant. Finally, the stained seed were resuspended in 1 mL of diH_2O. The washed, stained seed were then individually transferred per genotype to a non-transparent, white 96-well microplate for imaging with a Leica EZ4HD video dissecting microscope at 35X magnification. Images were subsequently processed and seed as well as mucilage area were quantified using Fiji (imagej.net). Statistical analyses were performed using GraphPad Prism (GraphPad Software, La Jolla, CA, www.graphpad.com).

XIII. Cell wall monosaccharide profiling

Dry stem tissue collected from all three *oft1*$^{-/-}$ mutant T-DNA lines or Col-0 control line that were sown out and grown side-by-side under equivalent conditions (as described above) were harvested and placed in separate pre-weighed 2 mL screw cap microcentrifuge tubes. An Alcohol Insoluble Residue (AIR) prep of the tissue was first conducted by adding 1.5 mL of 70% [v/v] ethanol to each sample tube and incubating on a nutating shaker for 6 h at 25ºC. The samples were centrifuged at 12,000xg for 10 min, supernatant discarded, and samples resuspended with 1.5 mL of a 1:1 [v/v] chloroform:

methanol. The samples were vortexed and then placed back on the nutating shaker for 6 h at 25ºC before centrifuging again at 12,000xg for 10 min. The supernatant was discarded, and samples air dried to completion at 25ºC in a laminar flow hood. Three steel balls (2 mm diameter) were added to each completely dry tissue sample tube and ball-milled using a Retsch MM301 ball mill for 2.5 min at 25 Hz to homogenize the tissue to a fine powder. The steel balls were removed, and sample tubes reweighed to ensure at least 10 mg of tissue had been retained before being resuspended in 1 mL of 100% [v/v] acetone. The samples were transferred to clean, pre-weighed 2 mL screw cap microcentrifuge tubes and centrifuged at 12,000xg for 10 min. The supernatant was discarded, and samples were air dried again at 25ºC in a laminar flow hood for 18 h.

To de-starch the AIR prepped tissue, the samples were resuspended in 1.5 mL of 0.1 M sodium acetate buffer pH 5.0, transferred to an 80ºC heating block for 20 min and then chilled on ice for 5 min. Each sample then received 35 µL of diH_2O, 35 µL of 50 µg/mL Amylase in diH_2O, and 17 µL Pullulanase and incubated on a nutating shaker for 18 h at 25ºC. Following incubation, the reaction was quenched by heating the samples to 100ºC for 10 min and then centrifuged at 12,000xg for 12 min. The supernatant was retained for subsequent testing of the reaction efficiency and sample pellets washed 3 times by sequentially adding 1 mL of diH_2O, vertexing to thoroughly mix, centrifuging at 12,000xg for 12 min, and discarding the supernatant. Following the final wash, 500 µL of 100% [v/v] acetone was added to each sample and centrifuged at 12,000xg for 12 min. The supernatants were discarded, and samples placed in a laminar flow hood at 25ºC to completely dry.

To confirm the efficiency of the de-starching reaction, the presence of glucose in the supernatant fractions retained from the previous de-starching reaction were analyzed through an anthrone assay. Each retained supernatant as well as glucose standard were composed in duplicate, and the colorimetric analysis was performed as follows. Thirty microliters of de-starching reaction sample supernatant was combined with 70 µL of diH_2O in clean microcentrifuge tubes. Glucose standards were composed similarly with 30 µL of 0.1% [w/v] glucose diluted in 70 µL of diH_2O. The efficiency of the de-starching could be determined following the addition of 250 µL of anthrone reagent (0.2% anthrone diluted in 100% [v/v] sulfuric acid) to each sample tube and heating for 30 min in an 80ºC water bath. A colorimetric sample change to blue indicated that the de-starching reaction was efficient and further sample preparation could proceed.

The dry, de-starched, AIR prepped samples were subjected to weak acid hydrolysis before GC analysis by adding 250 µL of 2 M trifluoro acetic acid (TFA) and 100 µg of D-myo-Inositol (MP Biochemicals) to each tube. Samples were incubated at 121°C for 1.5 h, and then centrifuged at 12,000xg for 10 min. Two-hundred and fifty microliters of supernatant were transferred to an 8 mL screw cap glass vial, and TFA was evaporated under a stream of N_2 gas at 50°C. The resulting residue was dissolved in 300 µL 2-propanol and evaporated under a stream of N_2 gas at 50°C. This process was repeated two additional times. Two hundred microliters of freshly prepared reduction solution (10 mg/mL $NaBH_4$: 1 M NH_4OH) was added to each sample and incubated at 25°C for 1.5 h. The reduction reaction was quenched with 150 µL of glacial acetic acid and samples were evaporated under a stream of N_2 gas at 50°C. Two-hundred and fifty microliters of 9:1 [v/v] of methanol: acetic acid was added to the residue and evaporated

under a stream of N_2 gas. This process was repeated two additional times. Samples were then washed with 250 µL of methanol for a total of 4 times. Alditol acetylation was performed by adding 50 µL of pyridine and 50 µL of acetic anhydride to each sample, sealed tightly, and incubated at 121°C for 20 min. Samples were then placed on ice for 30 min and solvent was gently evaporated under N_2 gas at 25°C. Samples were washed with 200 µL of toluene for a total of three times. Residues containing alditol acetates were resuspended in 1 mL of ethyl acetate and 4 mL of water, and subsequently vortexed and centrifuged at 500xg for 20 min. The upper organic phase was transferred into an 8 mL screw cap glass tube and gently evaporated under N_2 gas at 25°C. Samples were prepared for gas chromatography by resuspending in 300 µL of acetone. One hundred microliters of each samples were transferred to GC vials and diluted with an additional 200 µL of acetone. Samples were then analyzed on an Agilent 7980A gas chromatography instrument (Agilent Technologies) equipped with a 30 mm x 0.25 mm x 0.25 µm SP-2380 fused silica capillary column (Supelco), under the following conditions: inlet temperature of 250°C, initial oven temperature 160°C held for 2 min, first temperature ramp at 20°C/min to 245°C, hold at 245°C for 12 min, second temperature ramp at 20°C/min to 270°C. Data was analyzed using GC Open Lab software (Agilent Technologies).

XIV. Suppressor screening

Random mutagenesis was performed using dry, mature seed collected from *oft1-1*$^{-/-}$ and *oft1-3*$^{-/-}$ plants. All material and surfaces used to perform the procedure were decontaminated before and after the mutagenesis treatment with 1 M NaOH. Five hundred microliters of seed per genotype were aliquoted into separate 50 mL tubes and

50 mL of 0.5% [v/v] ethyl methyl sulfonate (EMS) in diH_2O was added per tube. The seed was incubated in the dark for 12 h at 25ºC. The treatment was repeated by removing the EMS solution and replaced it with another 50 mL of 0.5% EMS and incubated in the dark for 2 h at 25ºC. The mutagenesis reaction was quenched by aspirating and discarding the EMS solution from the seed tubes and washing each seed line 15 times over a 3 h period by repeatedly adding and discarding 50 mL of sterile, diH_2O to the tubes. Following the final seed decontamination wash, the diH_2O was discarded and seed lines each resuspended in 1 L MS sloppy agar medium (1/2× Murashige and Skoog salts, 10 mM MES-KOH pH 5.7, 1% [w/v] sucrose, and 0.1% [w/v] phytoagar). The mutagenized seed were stratified in sloppy agar medium for 48 h at 4ºC before being directly pipetted onto the surface of premoistened prepared flats of potting soil. Flats were transferred to a growth chamber under long-day light conditions and grown to reproductive maturity to facilitate phenotypic screening of the silique morphology.

EMS treated lines that suppressed the silique and seed set phenotype of the *oft1*$^{-/-}$ lines were initially identified by visual inspection of EMS-treated plants at peak sexual maturity that displayed a “wildtype-like” silique morphology. Unsuppressed EMS-treated lines that lacked a suppressed silique morphology were used as controls lines for resequencing. Backcrossing of suspected suppressor lines and controls was performed to eliminate unrelated EMS induced point mutations by crossing treated lines with untreated *oft1-1*$^{-/-}$ or *oft1-3*$^{-/-}$ equal age plants depending on the initial pre-EMS treatment *oft1*$^{-/-}$ T-DNA line, as all lines were crossed to contain both T-DNA insertions in *AtOFT1*. Seed collected from each backcross following maturation was sterilized as described above and sown out on MS media containing both kanamycin and BASTA® related T-DNA

selectable markers for *oft1-1*$^{-/-}$ and *oft1-3*$^{-/-}$, respectively. Following 7-10 days of long-day light conditions, resistant and sensitive seedlings per backcross were quantified and then transplanted to soil as described above. Lines were further isolated following development of mature siliques and lines lacking the suppressed silique morphology were eliminated. This process was continued multiple times to reduce the number of unrelated mutations in the genomes of suspected suppressor lines before being prepped for genome resequencing.

XV. Genomic DNA extraction and genome resequencing of *soft* lines

High molecular weight genomic DNA was extracted from siliques of *soft* mutants using the Qiagen DNEasy Plant Mini Kit (Qiagen) according to the manufacturer's instructions. DNA concentrations were quantified using the PicoGreen dsDNA quantification reagent (Thermo Fisher Scientific, San Jose, CA). The resulting genomic DNA samples were sheared to a size distribution of 500-800 bp using a Covaris M220 focused ultrasonicator, and the size distribution was determined using an Agilent 2100 BioAnalyzer system. Sheared genomic DNA libraries were labeled with unique Illumina barcode tags and sequenced using a NextSeq 500 Mid Output v2 flow cell on an Illumina NextSeq 500 instrument by the Nevada Genomics Center.

XVI. Bioinformatic processing of *soft* lines

The resulting genomic resequencing data was first processed to remove Illumina adapters and low-quality sequence elements using Trimmomatic (Bolger *et al.,* 2014). Trimmed reads were aligned to the TAIR10 *Arabidopsis thaliana* genome using the Burrows-Wheeler Aligner algorithm (Li and Durbin, 2009). Single nucleotide polymorphism (SNP) and indel variants were called using SAMTOOLS (Li *et al.,* 2009;

Li, 2011) and analyzed using BCFTOOLS. The resulting SNP frequencies were used to identify an over-represented genomic interval containing the causative mutation, and each EMS-type SNP in this interval was analyzed by snpEff (Cingolani *et al.,* 2012) to determine potential effects on target genes.

XVII. Assessing hypothesized *oft1* suppressor gene candidates

A knowledge-based approach was used to assess the list of gene candidates produced following bioinformatic processing of each *soft* line, including eliminating gene candidates that did not exhibit sequence alteration predicted to be the result of EMS mutagenesis, investigating the predicted subcellular localization of the gene candidate as well as the gene expression profiles. Using this approach, a single gene candidate for each *soft* line was predicted, *At1g11990* for *soft1* and *AtGAUT14* for *soft2* lines. T-DNA homozygous insertional mutants for *AtOFT1*, *oft1-1 (SALK_072442), oft1-3 (WiscDsLox489-492M4),* were previously described by Smith *et al.,* 2018a. The homozygous exonic T-DNA insertional mutant for the *soft1* gene candidate, *At1g11990*, *SALK_1174_D07* was phenotypically assessed and showed no overt abnormalities compared to Col-0. The exonic T-DNA insertional mutant for *AtGATUT14, gaut14-1 (SALK_000091),* was previously investigated and displayed no phenotypic abnormalities when homozygous (Wang *et al.,* 2013). However, *AtGAUT14* is functionally redundant with a homologous gene, *AtGAUT13 (At3g01040),* that does also not display abnormal single mutant phenotypes, but *gaut14-1/gaut13-1*(SALK_122602) double mutant lines exhibit extreme pollen defects (Wang *et al.,* 2013). These exonic T-DNA lines were used to create double homozygous knockout lines in both *AtOFT1* and the *soft* candidate genes. Arabidopsis outcrosses were performed as described previously (Myers *et al.,*

2009) to create a double T-DNA knockout line in both *AtOFT1* and *At1g11990 (oft1/At1g11990)* as well as *AtOFT1* and *AtGAUT14 (oft1/gaut14-1).* To create these double mutant lines, *oft1-3*$^{-/-}$ pistils were emasculated and pollinated with either *SAIL_1174_D07*$^{-/-}$ or *gaut14-1*$^{-/-}$ mutant pollen. Mature F_1 seed from these crosses was collect, sterilized, stratified, and sown out on MS medium supplemented with the appropriate T-DNA-associated selectable agents for each line. Following 7 days of growth under long-day light conditions, the F_1 seedlings were transplanted to soil, grown under long-day light conditions, and allowed to self to generate an F_2 segregating population. Mature F_2 seed was bulk collected for each cross and propagated as previously described. F_2 lines were PCR genotyped to determine the individual genotypes for the *AtOFT1* allele and the target gene allele as described above. Once each double homozygous line was successfully created, it was phenotypically assessed for a restored silique phenotype as described in this chapter.

XVIII. Recombinant expression of *AtOFT1* in HEK293 cells

Cloning to attempt AtOFT1 expression in the HEK293 cell system was followed as described by Moremen *et al.,* 2018 and was initiated by setting up a gateway cloning recombination reaction as previously described above with the sequence verified *AtOFT1Δ36+10xHis/pENTR* vector with the HEK293-compatible expression plasmid, pGEn2-DEST. This expression cassette features a CMV promoter, an N-terminal 8XHis and SuperGFP epitope tags, as well as a signal sequence derived from *Trypanosoma cruzi* lysosomal α-mannosidase, facilitating secretion and subsequent purification of the recombinantly expressed protein directly out of the expression culture medium (Vandersall-Nairn *et al.,* 1998). The *beta-1,4-galactosyltransferase 1 (B_4GALT_1)* gene

from *Homo sapiens* inserted and sequence confirmed in the pGEn2-DEST plasmid was used as vector expression control, and this plasmid as well as the empty gateway compatible pGEn2-DEST vector was kindly provided by Dr. Kelley Moremen (Complex Carbohydrate Research Center, University of Georgia). The *AtOFT1Δ36/pGEn2-DEST* and *B_4GALT_1/pGEn2-DEST* plasmids were transformed into *E.coli DH5α* by electroporation, plated on LB+100 µg/mL Ampicillin (AMP) agar plates and incubated for 18 h at 37ºC. A single transformed bacterial colony that grew following the incubation period was individually isolated from each transformation bacterial plate and used to inoculate separate sterile flasks containing 500 mL liquid LB medium supplemented with 100 µg/mL ampicillin and then incubated with shaking for 18 h at 37ºC. Following incubation, each culture was centrifuged at 5,000xg for 1 h to harvest the cells before the plasmids were further isolated using the QIAGEN Plasmid Midi Prep Kit (QIAGEN, Cat. No. 12165) following the manufacturer's suggested protocol with slight modification to the final plasmid elution procedure, which was carried out by applying 500 µL 1X TE Buffer (10 mM Tris-HCl, 1 mM Ethylenediaminetetraacetic acid [EDTA], pH 7.5) to the column. The final concentrations and purity of each plasmid isolate was determined using a NanoDrop 2000 spectrophotometer (Thermo Fisher Scientific, San Jose, CA) using 260/280 nm and 260/230 nm absorbance parameters.

All solutions in the following section were warmed to 37ºC before use. Eighteen hours prior to transient transfection, the confluency of a healthy culture of adherent HEK293 cells was determined and then passed to a confluency of 50% by first gently aspirating the existing Dulbecco's Modified Eagle Medium containing high glucose and L-Glutamate (DMEM) (Gibco, Cat. No. 11965084) out of culture flask. Two milliliters of

a 1:4 ratio of new TypIE™ Express Enzyme (1X), phenol red media (Gibco, Cat. No. 12605028) : DMEM was immediately added to the cells and then aspirated. The cells were washed 4 more times as described above with 2 mL of fresh 1:4 TypIE™, phenol red media : DMEM medium before the final wash was aspirated and the determined volume of fresh TypIE™ Express Enzyme (1X), phenol red media was added to the cell culture. Cells were incubated at 25º C for 8 min and then observed under a stereoscope to verify that the cells were suspended. The reaction was quenched by the addition of 3 volumes of fresh DMEM, and the resuspended cell solution was gently pipetted up and down to further dissociate cellular aggregates before the previously calculated volume of cells and fresh DMEM to achieve 50% confluency was aliquoted into new, sterile flasks and placed in a 37ºC CO_2 incubator (13% CO_2) for 18 h.

Following the 18 h incubation, the confluency of the cultures for transient transfection was verified to be between 70-80%, and the existing DMEM medium was aspirated from each culture and replaced with prewarmed, fresh DMEM and returned to the 37ºC CO_2 incubator while the transfection reactions were prepared. The Lipofectamine™ 3000 Transfection Reagent kit (Invitrogen, Cat. No. L3000001) was used to perform separate transient transfections of *AtOFT1Δ36/pGEn2-DEST* and *B_4GALT_1/pGEn2-DEST* plasmids as well as a "sham" transfection control, which lacked plasmid. Six tubes, two for each of the 3 desired transfections, were assembled by adding 110 mL of Opti-MEM™ I Reduced Serum Medium (Gibco, Cat. No. 31985062). For each transfection reaction, one tube received 3.75 µL Lipofectamine© 3000 Transfection Reagent, while the second tube received 5 µL P3000TM Enhancer Reagent (both kit included reagents) as well as either *AtOFT1Δ36+10xHis/pGEn2-DEST* plasmid,

B_4GALT_1/pGEn2-DEST plasmid, or no plasmid. The tubes were gently mixed to combine reagents before the two respective tubes for each transfection were combined and incubated at 25º C for 20 min. Following incubation, each transient transfection was carried out quickly at the incubator by careful addition of 230 µL of the appropriate transfection reaction applied directly on top of the prepped HEK293 seeded cultures in a dropwise fashion to disperse the reaction as much as possible across the surface of the culture. Without agitation, the culture lids were replaced and incubated in a 37ºC CO_2 incubator (13% CO_2).

Thirty microliters of media from each transfected culture or sham control were collected following 24 h and 48 h, and at 72 h post-transfection, both the medium as well as the transfected or control cells were collected to assess secreted recombinant protein production overtime as well as intracellular localization of these proteins at this final time point. These extracts were used to isolate 8xHis-GFP-B4GalT1 and 8xHis-GFP-AtOFT1Δ36 recombinant proteins by nickel-nitriloacetic acid gravity affinity chromatography, and the post-purification protein isolates were separated by SDS-PAGE and expression overtime was analyzed by anti-GFP Western blot detection, as further described below.

XIX. Cloning and expression of other Arabidopsis putative POFT members

Gene specific primers were designed to amplify the *MSR1 (At3g21190)* and *FRB1 (At5g01100)* coding sequences lacking a stop codon (*MSR1 pENTR F + MSR1 pENTR R* for *AtMSR1* and *FRB1 pENTR F + FRB1 pENTR R* for *AtFRB1*; Table 2.1) out of cDNA clones (U20773 for *AtMSR1* and U88623 for *AtFRB1;* arabidopsis.org). The reactions were cycled under the following conditions: 98ºC initial denaturation for 5 min, followed

by 30 cycles of 98ºC (30 s), 55ºC (30 s), and 72ºC (1 min 30 s), and a final elongation for 5 min at 72ºC. The resulting PCR products were resolved on a 1% [w/v] low-melting-point agarose gel, and the bands corresponding with the correct molecular weight were gel extracted as previously described using the QiaQuick gel extraction kit (Qiagen). These amplicons were used as templates to further facilitate truncation of these proteins' predicted hydrophobic domain (TMHMM Server v. 2.0; Sonnhammer *et al.,*1998) as well as replaced the start and stop codons as well as add a 6xHis epitope tag to the C-terminus by PCR facilitated with gene-specific primers (*fMet MSR1Δ28 pENTR F* and *MSR1+6xHis+STOP R* for *AtMSR1; fMet FRB1Δ144 pENTR F* and *FRB1+6xHis+STOP R* for *AtFRB1*; Table 2.1*)* and Phusion DNA polymerase. The reactions were cycled under the same conditions as used in their initial amplification, and the resulting fragments were resolved and purified as described above. The purified amplicons were cloned into the pENTR/D-TOPO entry vector according to manufacturer's instructions, transformed into *E.coli*, propagated, and plasmids isolated as described above (Thermo Fisher Scientific, San Jose, CA). Following Sanger DNA sequence verification of the entry constructs, the *MSR1Δ28+6XHis+STOP* and *FRB1Δ144+6XHis+STOP* DNA fragments were individually transferred from their entry clones into the pKM596 expression vector (Fox *et al.,* 2003) by LR Clonase II (Thermo Fisher Scientific, San Jose, CA) according to the manufacturer's suggested protocol, which facilitated an N-terminus MALTOSE BINDING PROTEIN (MBP) translational fusion to increase protein solubility (Szmelcman and Hofnung, 1975). Following sequence validation, the *MSR1Δ28+6XHis /pKM596* and *FRB1Δ144+6XHis/ pKM596* expression plasmids were

individually transformed into chemically competent *E. coli* Rosetta-gami 2 chemically competent (Novagen).

Expression of MBP-MSR1Δ28-6XHis and MBP-FRB1Δ144-6XHis was carried out using the following procedure. A single colony of *E. coli* Rosetta-Gami 2 transformed with *MSR1Δ28+6xHis/pKM596* or *FRB1Δ144+6xHis/pKM596* was inoculated into10 mL LB+100ug/mL Amp and incubated at 37ºC for 18 h. The saturated starter cultures were used to seed separate 1L LB+ 50ug/mL AMP and were incubated at 37ºC until reaching an OD_{600} of approximately 0.6. The culture was induced to express either construct upon attaining this OD_{600} by the addition of isopropyl β-D-1-thiogalactopyranoside (IPTG) to a final concentration of 250 μM and incubated for 18h at 18ºC. Following expression, purification and isolation of MBP-MSR1Δ28-6XHis or MBP-FRB1Δ144-6XHis from the expression cultures was conducted by Nickel-Nitrilotriacetic acid (Ni-NTA) AC followed immediately by amylose AC as described in the following section. The final eluates were evaluated for purity by SDS-PAGE staining and anti-HIS Western blotting. Furthermore, final eluates were buffer exchanged and final concentrated protein quantified by BCA assay described in further detail below. These final protein isolates were either immediately utilized in catalytic experimentation or aliquoted into multiple pre-chilled tubes to prevent freeze-thaw protein degradation, flash frozen, and stored at -80ºC for later investigations.

XX. Protein affinity chromatography

Gravity affinity chromatography (AC) was used to isolate proteins from many recombinant expression platforms. AC always began by obtaining a crude, soluble protein extract. For isolation of 8X-GFP-AtOFT1Δ36 and 8X-GFP-B_4GalT_1 from

HEK293 cell expression medium, no cell lysis step was necessary. However, all other crude extracts, including extraction of these recombinant proteins from HEK293 cellular pellets as well as all bacterial expression of MBP-MSR1Δ28-6XHis and MBP-FRB1Δ144-6XHis, required harvesting the expression cells and performing cell lysis to obtain this crude, soluble protein fraction starting material for AC. The cellular expression culture was first centrifuged at 3000xg at 4ºC for 20 min to harvest the cells, and the supernatant was discarded, except in the case of HEK293 cells, the expression medium was retained to evaluate secreted protein expression. The pelleted cells were transferred to a 50 mL conical tube and 40 mg of lysozyme was added. The cells and lysozyme were brought up to a total volume of 40 mL with Protein Purification Buffer (PPB; 25mM Tris-HCl, 150mM NaCl, 10mM $MgCl_2$, 20mM imidazole; pH 7.5), vortexed vigorously for 10 sec, and incubated submerged in ice for 30 min. The sample was further sonicated to ensure a homogenous cell lysate using a sterilized sonification instrument performed at 4ºC in 6 consecutive cycles as follows: 30 sec of sonification, conical cap replaced and lysate inverted 6 times, and then immediately submerged in ice for 30 sec. The cell lysates as well as the HEK293 cell expression medium were fractionated using a Beckman Optima XL-80K Ultracentrifuge (Beckman Coulter Life Sciences, Brea, CA) set at 100,000xg for 1 h at 4 ºC to fractionate soluble and membrane protein fractions. Additionally, for HEK293 secreted protein expression media samples, ultracentrifugation was used to clarify the media prior to AC. The resulting soluble protein fractions were transferred to fresh, sterile 50 mL conical tubes, and 1 mL of this fraction was aliquoted into a separate microcentrifuge tube and reserved for subsequent analysis of the efficiency of the AC procedure. For experimentation that aimed to simply

evaluate recombinant protein expression in the membrane protein fraction, the insoluble membrane protein pellet was further processed by thorough resuspension in 5 mL of a denaturing solution composed of 6M urea and 50 mM Tris-HCl, pH 7.5. The membrane protein faction was then ultracentrifuged again at 100,000xg for 1 h, and the resulting supernatant retained on ice for short-term storage or flash frozen and stored at -80ºC for analyses performed later than the day of initial protein extraction.

Recombinant bacterial expression was also always carried out in 1 L expression cultures volumes. All purification steps were performed at 4ºC, and all beginning crude extraction materials and protein fractions collected throughout the purification process were kept on ice at all times or flash frozen and stored at -80ºC. All reagents used to perform AC were preprepared the day prior, stored at 4ºC, and kept on ice during the procedure. Each AC was performed using 10 mL glass gravity affinity purification columns that contained a porous polyethylene resin reservoir, which supported the agarose-conjugated purification reagent. HisPur Ni-NTA Superflow Agarose (Thermo Fisher Scientific, San Jose, CA) was used for all Nickel-Nitrilotriacetic acid (Ni-NTA) AC with translationally fused proteins containing HIS epitopes. For AC with MBP-containing expression proteins, amylose AC was directly performed following Ni-NTA AC very similarly using Amylose-Resin (New England Biolabs, Cat. No. E8021).

For Ni-NTA AC, a gravity affinity purification column containing approximately 1.5 mL of resin was equilibrated in PPB. The clarified crude expression HEK293 cell medium or crude soluble protein cell lysate was applied to the column without disrupting the resin and the column flow through was collected. Three hundred and fifty milliliters of PPB was passed over the column to wash the resin, and then the final resin-bound

protein was eluted from the column in eight 1 mL fractions with Ni-NTA elution buffer (25mM Tris-HCl, 150mM NaCl, 10mM $MgCl_2$, 300mM imidazole; pH 7.5).

For amylose AC following Ni-NTA AC, the Ni-NTA elution fractions were combined in a 50 ml conical tube and 200µL was reserved for subsequent analysis. The combined elution fractions were diluted in 10 mL PPB and transferred to a 50 mL conical tube containing 500 µL amylose resin that had been pre-equilibrated in PPB. The diluted Ni-NTA eluate and resin were incubated for 30 min on ice with gentle, manual inversion of the sample tube 3-5 times every 5 min. An AC column was equilibrated with PPB prior to the incubated resin-protein sample being applied directly to the column. The column flow-through was collected, and column was washed with 200 mL of PPB before 10 mL of amylose elution buffer (25mM Tris-HCl, 150mM NaCl, 10mM $MgCl_2$, 20mM imidazole, 10mM maltose; pH 7.5) was applied to the column and incubated on the column for 5 min. The final protein was eluted following incubation in eight 1 mL fractions.

All final protein samples were quantified by bicinchoninic acid (BCA) assay using the Pierce™ Protein Assay Kit (Thermo Fisher Scientific, San Jose, CA, Cat. No. 23225) following the manufacturer's protocol. Final protein samples were always additionally evaluated by separation on an SDS-PAGE gel, which was subsequently stained for visualization of proteins or transferred to a nitrocellulose membrane for Western blot analysis as described in further detail in the following section of this chapter.

Protein isolates used for subsequent catalytic analyses, such as MBP-MSR1Δ28-6XHis and MBP-FRB1Δ144-6XHis, were further processed by column concentration and

buffer exchange following AC using 2 mL Pierce™ Protein Concentrator microcentrifuge column featuring a polyether sulfone (PES) membrane and 5K MWCO (Thermo Fisher Scientific, San Jose, CA). The column was pre-equilibrated with 500 µL of exchange buffer (25mM Tris-HCl, 150mM NaCl, 10mM $MgCl_2$, pH 7.5) and centrifugation for 5 min at 15,000xg at 4ºC. The exchange buffer column flow through was discarded, and the eight 1 mL eluate fractions that had been placed on ice following AC were sequentially applied to the column as follows. Five hundred µL of final protein AC eluate was added to the column, centrifuged at 15,000xg for 5 min at 4ºC, and flow through collected. This process was repeated until all eluate fractions had been applied to the column. The column was continuously ensured to not run completely dry during this process, and prior to a new addition of eluate, the column was visually inspected for signs of protein precipitation/aggregation. Following the final application of AC eluate and collection of the column flow through, the column was washed three times by sequentially applying 500 µL of exchange buffer to the column, centrifuging at 15,000xg for 5 min at 4ºC, and discarding the column flow through. Following the final wash spin, the column retentate was pipetted off of column and transferred to a sterile 1.5 mL microcentrifuge tube before being brought up to a final volume of 500 µL with Exchange Buffer and immediately placed on ice.

XXI. Western blot analysis

To visualize the success of a protein extraction or efficiency to homogenously isolate a protein following AC, aliquots of the samples of interest were prepared for loading on a 4-20% SDS-PAGE Mini-PROTEAN® TGX™ Precast Gel alongside 10 µL Precision Plus Protein™ Dual Color Standards for gels intended for western blot analysis

or 10 µL of Precision Plus Protein™ Unstained Protein Standards (Bio-Rad Laboratories, Hercules, CA) for gels intended for protein staining by combining with the appropriate volume of 6X SDS-PAGE protein loading buffer (375 mM Tris-HCl, pH 6.8, 9% [w/v] SDS, 50% [v/v] glycerol, 0.05% [w/v] bromophenol blue, 9% β-mercaptoethanol) and loaded into individual wells on the gel. SDS-PAGE gels were run at 200V in a Mini-PROTEAN Tetra Vertical Electrophoresis Cell (Bio-Rad Laboratories) until the dye front had almost reached the bottom of the gel. Gels were carefully removed from their molds and rehydrated in diH_2O if intended for staining with GelCode™ Blue Safe Protein Stain (Thermo Fisher Scientific, Cat. No. 24594) following the manufacturer's suggested instructions. Gels intended for immunoblotting were integrated into the traditional western blot "sandwich" for protein transfer to a nitrocellulose membrane using the Bio-Rad Trans-Blot® Turbo™ Transfer System (Bio-Rad Laboratories) and were composed of 2 sheets of kit provided transfer filter paper and nitrocellulose membrane pre-soaked in western transfer buffer (125 mM Tris, 192 mM glycine, 20% [v/v] methanol). The gel was successfully transferred to the nitrocellulose membrane following manufacturer's suggested instructions. The membrane was removed from the sandwich, transferred to a light-poof container, and washed for 10 min in 1X PBS (phosphate-buffered saline; 137 mM NaCl, 2.7 mM KCl, 10 mM Na_2HPO_4, 1.8 mM KH_2PO_4; pH 7.4). The 1X PBS was discarded and replaced with 15 mL of 5% blocking buffer (1X PBS, 5% non-fat milk) and incubated on an orbital shaker at 25ºC for 18 h. The blocking buffer was discarded from the membrane and washed with 1X PBS for 10 min at 25ºC. The 1X PBS was discarded and primary antibody diluted in 1% blocking buffer (1X PBS, 1% [w/v] dry nonfat milk) was applied to the membrane for 1 h at 25ºC on an orbital shaker. The

primary antibody was gently poured off of the membrane and washed with 1X PBS-T (1X PBS, 0.1% Tween-20) three times for 10 min each at 25ºC on an orbital shaker. Following the final wash, the 1X PBS-T was discarded and the secondary antibody diluted in 1% blocking buffer was applied to the membrane. Following a 1 h incubation at 25ºC on an orbital shaker, the secondary antibody was discarded, and the membrane washed again three times for 10 min with 1X PBS-T. For anti-GFP probed western membranes, the primary polyclonal Rabbit Anti-GFP antibody (Thermo Fisher Scientific, San Jose, CA, Cat. No. A11122) was diluted 1:1000 and followed by secondary Goat Anti-Rabbit Horseradish peroxidase (HRP) conjugated secondary antibody (Thermo Fisher Scientific, San Jose, CA, Cat. No. 32460) was diluted 1:3000. For anti-His probed western membranes the primary Mouse Anti-His monoclonal antibody (Sigma Aldrich, St. Louis, MO, Cat. No. SAB1305538) was diluted 1:10,000 and then the secondary Goat Anti-Mouse-HRP conjugated secondary antibody (Thermo Fisher Scientific, San Jose, CA, Cat. No. 32430) was diluted 1:3000. For anti-MBP probed western membranes, the primary Mouse Anti-MBP monoclonal antibody (Thermo Fisher Scientific, San Jose, CA, Cat. No. MA514122) was diluted 1:10,000 and then the secondary Goat Anti-Mouse-HRP conjugated secondary antibody (Thermo Fisher Scientific, San Jose, CA, Cat. No. 32430) was diluted 1:3000. For biotinylated protein probed membranes, the Pierce™ High Sensitivity Streptavidin-HRP conjugated antibody (Thermo Fisher Scientific, San Jose, CA, Cat. No. PI21130) was diluted 1:50,000 in 3% TBS supplemented with 4 mg Bovine Serum Albumin (BSA).

Detection of probed proteins on the nitrocellulose probed western membranes was facilitated by chemiluminescent developer solutions that reacted with the secondary

antibodies conjugated to HRP protein allowing for luminescent signal readout. Two developer solutions were made: Developer I (90 mM Tris-HCl, pH 8.5, 2.24 mM luminol, 363 µM p-coumaric acid) and Developer II (90 mM Tris-HCl, pH 8.5 and 0.008% H_2O_2). Membranes were developed following the final 1X TBS-T wash as follows: 1X TBS-T discarded, developer solutions mixed 1:1 and applied to the membrane, agitated in the developer for 45 sec at 25º. The actively developing membrane was then transferred to the imaging dock of a ChemiDoc XRS+ imaging platform (Bio-Rad Laboratories, Hercules, CA) for detection of luminescent signal following for 1 min exposure. SDS-PAGE gels de-stained following manufacturer's suggested instructions using GelCode™ Blue Safe Protein Stain were imaged using the same imaging platform using the appropriate image settings.

XXII. Mass spectrometry verification of AtMSR1

Mass spectrometry was further used in this study to confirm successful expression and purification of MBP-MSR1Δ28-6xHis. Sample preparation began by first precipitating the protein out of solution by adding 4 volumes of 100% methanol (MeOH) directly to the AC purified, concentrated, and quantified protein sample, and vortexed to mix. One volume of 100% chloroform was added, and again, the sample was vortexed to mix. Three volumes of sterile diH2O were added to the sample, vortexed to mix, and then centrifuged for 2 min at 12,000xg. Following centrifugation, the top aqueous layer was carefully aspirated from the sample and replaced with 4 volumes of 100% MeOH. The sample was vortexed to homogenize the precipitated protein aggregate, centrifuged at 12,000xg for 3 min, and supernatant discarded. The sample was then placed in a laminar

flow hood until the protein pellet was completely dry before being resuspended in 100 µL of 25mM Ammonium bicarbonate, 8.5 M urea.

Following precipitation, the protein sample was further prepared for mass spectrometry by undergoing reduction of cystine bonds and alkylation to prevent them from reforming. This was achieved by adding dithiothreitol (DTT) to a final concentration of 5 mM and incubating the sample in a 37ºC water bath for 30 min. Iodoacetamide (IAA) was then added to a final concentration of 15 mM and incubated at 25º C in the dark for 30 min. DTT was added to the sample once more to a final concentration of 5 mM and incubated for 15 min at 25ºC in the dark before the sample was diluted in 25mM Ammonium bicarbonate to a final concentration of 1.5 mM urea. The sample was then digested using a 1:50 ratio of trypsin: the sample final volume and incubated at 25ºC for 16 h.

The subsequent digested peptides were further processed to remove residual salts, buffer components, and unreacted reagents by reverse-phase chromatography using a C18 SepPak column (Thermo Fisher Scientific, San Jose, CA). First, the trypsinized sample was acidified by the addition of 10% [v/v] trifluoroacetic acid (TFA) to achieve a pH < 2 and centrifuged for 10 min at 12,000xg. The supernatant was transferred to a clean microcentrifuge tube, and the column was primed by sequential 1 mL aliquots, while also ensuring the column never ran dry as follows: 3 applications of 100% acetonitrile (ACN), 1 application of 70% [v/v] ACN, 1 application of 40% [v/v] TFA, and 3 additions of 0.1% [v/v] TFA. The sample supernatant was applied to the column and then washed with 1 mL 0.1% [v/v] TFA three times. The column was then quickly transferred to a clean 2 mL screw top microcentrifuge tube, and 1.75 mL of 70% [v/v]

ACN was used to elute the peptides off of the column membrane. The liquid in the final eluate was evaporated using SpeedVac vacuum concentrator to dry the sample completely before being thoroughly resuspended in 20 µL 0.1% formic acid. The prepped sample was sent for mass spectrometry analysis at the Mick Hitchcock, Ph.D. Nevada Proteomics Center (unr.edu/proteomics).

XXIII. Extraction and purification of AtOFT1 out of Arabidopsis seedlings

Recombinant expression and isolation of AtOFT1-GFP began by sterilizing and plating seed from *oft1-2*$^{-/-}$ and *pUBC::OFT1-GFP;oft1-2*$^{-/-}$ *T*$_3$ plant lines as described above and grown under long-day light conditions for 10 days. The resulting seedlings were separately collected off of their MS medium plates and individually homogenized to a fine powder by macerating with prechilled mortars and pestles in liquid nitrogen (LN_2). The homogenized seedlings were transferred to separate 50 mL conical tubes, 20 mL of Plant Protein Extraction Buffer (PPEB; 50 mM HEPES-NaOH, 150 mM NaCl, 10 mM $MgCl_2$, 10 mM ascorbic acid, 5 mM β-mercaptoethanol, 1% [w/v] PVP-40, pH 7.0 and supplemented with a broad spectrum, EDTA-free protease inhibitor (Thermo Fisher Scientific, San Jose, CA, Cat. No. A32955)) was added to each tube of homogenized seedlings, and vortexed vigorously to mix. The resuspended plant extracts were then individually passed through a dual layer of miracloth to eliminate insoluble plant material and eluates were collected in separate sterile 50 mL conical tubes. The plant total seedling extracts were brought up to a final volume of 20 mL by the addition of PPEB and centrifuged at 12,000xg for 20 min at 4 ºC to further clarify the samples. The supernatants were transferred to fresh 50 mL conical tubes and ultracentrifuged at 100,000xg for 1 h at 4 ºC to fractionate the soluble and insoluble protein. The resulting

insoluble membrane protein pellets were each resuspended in 10 mL chilled 1X PBS and ultracentrifuged again at 100,000xg for 1 h, while the soluble protein supernatant fractions were collected in fresh tubes and stored either on ice for immediate use or at -80ºC for later analyses. Following ultracentrifugation, the supernatants were discarded, and the final membrane protein pellets were resuspended in 500 µL chilled 1X PBS, transferred to fresh microcentrifuge tubes, and either placed on ice for immediate use or stored at -80ºC. Before further experimentation was performed on the final membrane fractions, Western blot analysis was carried out to ascertain the presence of OFT1-GFP only in the membrane fraction originating from the *pUBC/OFT1-GFP* expression line seedlings. Additionally, the protein concentration was determined using a Pierce™ Protein Assay Kit (Thermo Fisher Scientific, San Jose, CA, Cat. No. 23225) as described above.

Following Western blot analysis and determining protein concentration of the seedling membrane protein extracts, 60 µL of resuspended membrane extract was aliquoted into separate, prechilled micro-ultracentrifuge tubes. Using a Beckman Avanti J-20XP ultracentrifuge fitted with a TLA120.1 rotor, the samples were pelleted for 1 h at 100,000xg. The supernatants were discarded without disrupting the membrane protein pellet and 60 µL of one of the 12 kit-contained solutions of the Membrane Protein Extraction Kit Plus (Profoldin, Hudson, MA; Cat. No. MPE01-12P) or 1X PBS for the control sample was used to resuspend the pellet thoroughly. The resuspended membrane protein extracts were incubated on ice for 1 h and centrifuged at 100,000xg for 1 h as before. The detergent-solubilized supernatants were individually collected, while the membrane protein pellets were resuspended thoroughly in 60 µL of 1X PBS and

transferred to separate tubes. To assess the success of the detergent treatment solutions, an anti-GFP Western blot was performed following running an SDS-PAGE gel that was loading with individual side-by-side lanes with an equal volumes of detergent solubilized protein and its post-treatment resuspended membrane protein pellet counterpart, as further described below. The efficacy of each detergent and kit solution was determined by comparing the signal intensity produced by the solubilized supernatant with that emanating from its associated post-treatment membrane protein resuspended pellet and untreated control samples.

XXIV. Malachite green phosphate detection assay and analysis

Thirty microliter reactions containing 100 µM sugar-nucleotide, 7 µg MBP-MSR1Δ28-6xHis or MBP-FRB1Δ144-6xHis, 0.2 µg CD39L3 (NTPDase 3, R & D Systems), 6.67 mM $MnCl_2$, and brought up to final volume with Exchange Buffer were composed to assess the sugar-nucleotide specificity of these proteins of interest. Following a 3 h incubation at 25 ºC, reactions were quenched by heating at 100 ºC for 5 min. Free phosphate resulting from sugar-nucleotide hydrolysis was detected using a Malachite Green Phosphate Detection Kit (R & D Systems, Cat. No. DY996) and the resultant 620 nm colorimetric readout was measured using a Spectramax M5 Microplate Reader. Nanomolar phosphate concentrations for each sugar-nucleotide assayed were normalized to negate false signal detected in control samples lacking sugar-nucleotide or no purified, hypothesized protein O-fucosyltransferase.

XXV. Strategies to identify O-fucose protein modifications: Lectins and DSF

Lectins are plant derived glycan-recognition probes commonly used in glycan investigations due to their ability to selectively discriminate between a wide range of

glycan structures (Cummings and McEver, 2015). Biotinylated lectins that specifically recognize fucose modification in protein isolates were used as a means of identifying fucosylated proteins in wildtype samples using streptavidin western blot analysis. Three biotinylated fucose-specific lectins from *Aleuria aurantia* (AAL), *Ulex europaeus* agglutinin I (UEA I), and *Lotus tetragonolobus* lectin (LTL) (Vector Laboratories, Burlingame, CA) were initially tested to assess their efficiencies to detect protein fucosylation in 12-day-old Col-0 seedling protein extracts. Probing Col-0 protein isolates with each lectin was initially performed to assess its the efficacy and specificity to detect fucose moieties on proteins within the seedling protein extracts.

Initially, membrane and soluble protein isolates from 12-day-old Col-0 seedlings were extracted as previously described, except for slight modification as all mentions of the use of 1X PBS were replaced with 1X TBS (Tris-Buffered Saline; 50 mM Tris-HCl, pH 7.5, 150 mM NaCl) at an equivalent volume. Following extraction, 40 µL of soluble and membrane Col-0 seedling protein extracts were assessed in triplicate by loading on a 4-20% SDS-PAGE gel, and the separated gel-immobilized proteins were transferred to a nitrocellulose membrane as previously described in this chapter. The nitrocellulose membrane was carefully trisected following transfer resulting in 3 separate, identical membranes that contained the same protein samples at equivalent concentrations for subsequent western blotting with either lectin, control for the primary lectin, or secondary streptavidin-HRP antibody control. All membranes were blocked with 1X TBS supplemented with 3% BSA for 18 h at 4ºC before the blocking solution was discarded and membranes washed for 10 min with 1X TBS. The 1X TBS was discarded, and lectin solution (2 µg lectin, 4 µg/mL BSA, 1 mM $CaCl_2$ diluted in 1X TBS) was applied to the

treatment membrane, while the primary control membrane received 10 mL primary lectin solution that had been pre-incubated for 2 h with 200 mM L-fucose at 25ºC, and the secondary control membrane incubated in a 10 mL solution of 1X TBS containing 4 µg/mL BSA, 1 mM $CaCl_2$ and incubated for 30 min on an orbital shaker at 25ºC. Following incubation, the solutions were discarded, and the membranes were washed 3 min twice in 1X TBS-T (50 mM Tris-HCl, pH 7.5, 150 mM NaCl, 0.1% [v/v] Tween-20). Following discarding the second wash solution, all three membranes were treated with a 1:5000 dilution of streptavidin-HRP conjugated secondary antibody diluted in 1X TBS supplemented with 4 µg/mL BSA. The membrane was incubated for 30 min at 25ºC on an orbital shaker before being washed again two times with 1X TBST for 3 min. Blots were developed as described previously with chemiluminescent developer solutions and luminescence detected and captured using a Bio-Rad Gel Doc XR+ Image analysis workstation (Bio-Rad Laboratories, Hercules, CA).

AAL was determined to be the best lectin for detection of fucosylation events on membrane- immobilized 12-day-old Col-0 seedling protein isolates by western blotting and was further utilized to selectively purify fucosylated proteins by gravity affinity chromatography using AAL-agarose resin, and all steps were carried out at 4ºC. Twelve-day-old Col-0 seedling soluble protein isolate was passed over a glass protein affinity chromatography column containing 500 µL of 1X TBS pre-equilibrated AAL-agarose resin (Vector Laboratories, Burlingame, CA. The flow through was collected, and the protein bound resin washed by passing 100 mL of 1X TBS through the column. The lectin-bound fucosylated proteins were eluted from the resin in 0.5 mL fractions with 2.5 mL 1X TBS containing 100mM L-fucose. Detection of fucosylated proteins in the

eluates was evaluated by western blotting and staining with GelCode™ Blue Safe Protein Stain (Thermo Fisher Scientific, San Jose, CA) following separation on a 4-20% SDS-PAGE gel as described above in this section. The AAL lectin is not specific to N- or O-linked protein fucosylation, thus the N-linked glycosidase, PNGase F, was used to remove N-linked glycans from 50 µg of precipitated 12-day-old Col-0 seedling soluble AAL-agarose purified protein eluate. The precipitated proteins were resuspended in 100 µL of 1X TBS and 2 units of PNGase F (Sigma Aldrich) was added to cleave N-linked glycans from the proteins. The digestion reaction was performed in a 37ºC water bath for 18 h prior to analyzing the difference in enzyme treated protein abundance compared to untreated control samples, again, using AAL+streptavidin-HRP western blotting as described in this section.

Differential scanning fluorimetry (DSF) is a common technique to experimentally determine enzyme-substrate binding specificity and kinetics (Gao *et al., 2*020) and was implemented in this study as a second means of testing the sugar nucleotide specificity of catalytic dependence of $MnCl_2$ for MBP-MSR1Δ28-6XHis. The method was also established to allow for future assessment of sugar-nucleotide substrate specificities with other purifiable Arabidopsis putative POFT members in a high-throughput manner. To initially establish this method, Maltose Binding Protein (MBP) was utilized as its K_d had been previously determined in the absence and presence of its ligand, maltose (Szmelcman and Hofnung, 1975). Twenty-five microliter reactions containing 50 mM Tris-HCl (pH 7.5), 50 mM NaCl, 5 mM MgCl, 5 µM protein, 4X SYPRO Orange (Thermo Fisher Scientific, San Jose, CA), and varying substrate concentration were aliquoted in a 96 well PCR plate. Reactions were measured with a Bio-Rad CFX96

Touch Real-Time PCR Detection System equipped with a FRET filter cube (Bio-Rad Laboratories, Hercules, CA) for detection of thermal shift upon addition of a maltose or sugar-nucleotide using the following reaction conditions: 25-80°C temperature ramp in 0.5º C increments with 5 sec fluorescent measurement acquisition intervals. Following verifying this technique for MBP, the T_m of MBP-MSR1Δ28-6XHis alone was determined. The ΔT_m in the presence of sugar-nucleotide is correlated to a change in ΔG and is also related to its substate affinity as ΔG increases as a result of increased stability of the protein-substate complex (Gao *et al.,* 2020). Therefore, assessing the necessity of the hypothesized metal cofactor for MBP-MSR1Δ28-6XHis, $MnCl_2$, as well as its preferred sugar-nucleotide donor substrate could be evaluated by the resultant calculated thermal shift (ΔT_m) in the presence of at 5 mM $MnCl_2$ and a concentration range of 100 µM and 1mM for the sugar-nucleotides tested, including GDP-fucose, GDP-mannose, UDP-glucose, GDP-glucose, UDP-galactose, UDP-glucuronic acid, and UDP-N-acetylglucosamine.

References

Agarwala, R., Barrett, T., Beck, J., Benson, D. A., Bollin, C., Bolton, E., Bourexis, D., Brister, J. R., Bryant, S. H., Canese, K., Cavanaugh, M., Charowhas, C., Clark, K., Dondoshansky, I., Feolo, M., Fitzpatrick, L., Funk, K., Geer, L. Y., Gorelenkov, V., … NCBI Resource Coordinators. (2018). Database resources of the National Center for Biotechnology Information. *Nucleic Acids Research*, *46*(D1), D8–D13. https://doi.org/10.1093/nar/gkx1095

Alonso, J. M., Stepanova, A. N., Leisse, T. J., Kim, C. J., Chen, H., Shinn, P., Stevenson, D. K., Zimmerman, J., Barajas, P., Cheuk, R., Gadrinab, C., Heller, C., Jeske, A., Koesema, E., Meyers, C. C., Parker, H., Prednis, L., Ansari, Y., Choy, N., … Ecker, J. R. (2003). Genome-Wide Insertional Mutagenesis of Arabidopsis thaliana. *Science (American Association for the Advancement of Science)*, *301*(5633), 653–657. https://doi.org/10.1126/science.1086391

Bank, R. P. D. (n.d.). *RCSB PDB - 3ZY5: Crystal structure of POFUT1 in complex with GDP-fucose (crystal-form-I)*. Retrieved April 28, 2021, from https://www.rcsb.org/structure/3ZY5

Boavida, L. C., & McCormick, S. (2007). Temperature as a determinant factor for increased and reproducible in vitro pollen germination in Arabidopsis thaliana. *The Plant Journal : For Cell and Molecular Biology*, *52*(3), 570–582. https://doi.org/10.1111/j.1365-313X.2007.03248.x

Bolger, A. M., Lohse, M., & Usadel, B. (2014). Trimmomatic: A flexible trimmer for Illumina sequence data. *Bioinformatics (Oxford, England)*, *30*(15), 2114–2120. https://doi.org/10.1093/bioinformatics/btu170

Bolte, S., & Cordelières, F. P. (2006). A guided tour into subcellular colocalization analysis in light microscopy. *Journal of Microscopy (Oxford)*, *224*(3), 213–232. https://doi.org/10.1111/j.1365-2818.2006.01706.x

Cingolani, P., Platts, A., Wang, L. L., Coon, M., Nguyen, T., Wang, L., Land, S. J., Lu, X., & Ruden, D. M. (2012). A program for annotating and predicting the effects of single nucleotide polymorphisms, SnpEff: SNPs in the genome of Drosophila melanogaster strain w1118; iso-2; iso-3. *Fly (Austin, Tex.)*, *6*(2), 80–92. https://doi.org/10.4161/fly.19695

Clough, S. J., & Bent, A. F. (1998). Floral dip: A simplified method for Agrobacterium -mediated transformation of Arabidopsis thaliana. *The Plant Journal : For Cell and Molecular Biology*, *16*(6), 735–743. https://doi.org/10.1046/j.1365-313x.1998.00343.x

Cummings, R. D., & McEver, R. P. (2015). C-Type Lectins. In A. Varki, R. D. Cummings, J. D. Esko, P. Stanley, G. W. Hart, M. Aebi, A. G. Darvill, T. Kinoshita, N. H. Packer, J. H. Prestegard, R. L. Schnaar, & P. H. Seeberger (Eds.), *Essentials of Glycobiology* (3rd ed.). Cold Spring Harbor Laboratory Press. http://www.ncbi.nlm.nih.gov/books/NBK453028/

Edwards, K., Johnstone, C., & Thompson, C. (1991). A simple and rapid method for the preparation of plant genomic DNA for PCR analysis. *Nucleic Acids Research*, *19*(6), 1349.

Fox, J. D., Routzahn, K. M., Bucher, M. H., & Waugh, D. S. (2003). Maltodextrin-binding proteins from diverse bacteria and archaea are potent solubility enhancers. *FEBS Letters*, *537*(1–3), 53–57. https://doi.org/10.1016/S0014-5793(03)00070-X

Frietsch, S., Wang, Y.-F., Sladek, C., Poulsen, L. R., Romanowsky, S. M., Schroeder, J. I., & Harper, J. F. (2007). A Cyclic Nucleotide-Gated Channel Is Essential for Polarized Tip Growth of Pollen. *Proceedings of the National Academy of Sciences - PNAS*, *104*(36), 14531–14536. https://doi.org/10.1073/pnas.0701781104

Gao, K., Oerlemans, R., & Groves, M. R. (2020). Theory and applications of differential scanning fluorimetry in early-stage drug discovery. *Biophysical Reviews*, *12*(1), 85–104. https://doi.org/10.1007/s12551-020-00619-2

Geldner, N., Dénervaud-Tendon, V., Hyman, D. L., Mayer, U., Stierhof, Y., & Chory, J. (2009). Rapid, combinatorial analysis of membrane compartments in intact plants with a multicolor marker set. *The Plant Journal : For Cell and Molecular Biology*, *59*(1), 169–178. https://doi.org/10.1111/j.1365-313X.2009.03851.x

GraphPad Prism (Version 8). [Computer software]. GraphPad Software Inc., La Jolla California USA. www.graphpad.com

Grefen, C., Donald, N., Hashimoto, K., Kudla, J., Schumacher, K., & Blatt, M. R. (2010). A ubiquitin-10 promoter-based vector set for fluorescent protein tagging facilitates temporal stability and native

protein distribution in transient and stable expression studies. *The Plant Journal : For Cell and Molecular Biology*, *64*(2), 355–365. https://doi.org/10.1111/j.1365-313X.2010.04322.x

Hellens, R. P., Edwards, E. A., Leyland, N. R., Bean, S., & Mullineaux, P. M. (2000). pGreen: A versatile and flexible binary Ti vector for Agrobacterium-mediated plant transformation. *Plant Molecular Biology*, *42*(6), 819–832. https://doi.org/10.1023/A:1006496308160

Huala, E., Dickerman, A. W., Garcia-Hernandez, M., Weems, D., Reiser, L., LaFond, F., Hanley, D., Kiphart, D., Zhuang, M., Huang, W., Mueller, L. A., Bhattacharyya, D., Bhaya, D., Sobral, B. W., Beavis, W., Meinke, D. W., Town, C. D., Somerville, C., & Rhee, S. Y. (2001). The Arabidopsis Information Resource (TAIR): A comprehensive database and web-based information retrieval, analysis, and visualization system for a model plant. *Nucleic Acids Research*, *29*(1), 102–105.

Humphrey, W., Dalke, A., & Schulten, K. (1996). VMD: Visual molecular dynamics. *Journal of Molecular Graphics*, *14*(1), 33–38. https://doi.org/10.1016/0263-7855(96)00018-5

Jones, D. T., Taylor, W. R., & Thornton, J. M. (1992). The rapid generation of mutation data matrices from protein sequences. *Bioinformatics*, *8*(3), 275–282. https://doi.org/10.1093/bioinformatics/8.3.275

Kumar, S., Stecher, G., Li, M., Knyaz, C., & Tamura, K. (2018). MEGA X: Molecular Evolutionary Genetics Analysis across Computing Platforms. *Molecular Biology and Evolution*, *35*(6), 1547–1549. https://doi.org/10.1093/molbev/msy096

Larkin, M. A., Blackshields, G., Brown, N. P., Chenna, R., McGettigan, P. A., McWilliam, H., Valentin, F., Wallace, I. M., Wilm, A., Lopez, R., Thompson, J. D., Gibson, T. J., & Higgins, D. G. (2007). Clustal W and Clustal X version 2.0. *Bioinformatics*, *23*(21), 2947–2948. https://doi.org/10.1093/bioinformatics/btm404

Li, H. (2011). Improving SNP discovery by base alignment quality. *Bioinformatics (Oxford, England)*, *27*(8), 1157–1158. https://doi.org/10.1093/bioinformatics/btr076

Li, H., & Durbin, R. (2009). Fast and accurate short read alignment with Burrows-Wheeler transform. *Bioinformatics*, *25*(14), 1754–1760. https://doi.org/10.1093/bioinformatics/btp324

Li, H., Handsaker, B., Wysoker, A., Fennell, T., Ruan, J., Homer, N., Marth, G., Abecasis, G., Durbin, R., & 1000 Genome Project Data Processing Subgroup. (2009). The Sequence Alignment Map format and SAMtools. *Bioinformatics*, *25*(16), 2078–2079. https://doi.org/10.1093/bioinformatics/btp352

Li, Z., Han, K., Pak, J. E., Satkunarajah, M., Zhou, D., & Rini, J. M. (2017). Recognition of EGF-like domains by the Notch-modifying O-fucosyltransferase POFUT1. *Nature Chemical Biology*, *13*(7), 757–763. https://doi.org/10.1038/nchembio.2381

Lira-Navarrete, E., Valero-Gonzalez, J., Villanueva, R., Martinez-Julvez, M., Tejero, T., Merino, P., Panjikar, S., & Hurtado-Guerrero, R. (2011). Structural Insights into the Mechanism of Protein O-Fucosylation. *PloS One*, *6*(9), e25365–e25365. https://doi.org/10.1371/journal.pone.0025365

Liu, X., Salokas, K., Tamene, F., Jiu, Y., Weldatsadik, R. G., Ohman, T., & Varjosalo, M. (2018). An AP-MS- and BioID-compatible MAC-tag enables comprehensive mapping of protein interactions and subcellular localizations. *Nature Communications*, *9*(1), 1188–1188. https://doi.org/10.1038/s41467-018-03523-2

McMillan, B. J., Zimmerman, B., Egan, E. D., Lofgren, M., Xu, X., Hesser, A., Blacklow, S. C., & Argonne National Lab. (ANL), A., IL (United States). Advanced Photon Source (APS). (2017). Structure of human POFUT1, its requirement in ligand-independent oncogenic Notch signaling, and functional effects of Dowling-Degos mutations. *Glycobiology (Oxford)*, *27*(8), 777–786. https://doi.org/10.1093/glycob/cwx020

Moremen, K. W., Ramiah, A., Stuart, M., Steel, J., Meng, L., Forouhar, F., Moniz, H. A., Gahlay, G., Gao, Z., Chapla, D., Wang, S., Yang, J.-Y., Prabhakar, P. K., Johnson, R., Rosa, M. D., Geisler, C., Nairn, A. V., Seetharaman, J., Wu, S.-C., … Argonne National Lab. (ANL), A., IL (United States). (2018). Expression system for structural and functional studies of human glycosylation enzymes. *Nature Chemical Biology*, *14*(2), 156–162. https://doi.org/10.1038/nchembio.2539

Mori, T., Kuroiwa, H., Higashiyama, T., & Kuroiwa, T. (2006). GENERATIVE CELL SPECIFIC 1 is essential for angiosperm fertilization. *Nature Cell Biology*, *8*(1), 64–71. https://doi.org/10.1038/ncb1345

Myers, C., Romanowsky, S. M., Barron, Y. D., Garg, S., Azuse, C. L., Curran, A., Davis, R. M., Hatton, J., Harmon, A. C., & Harper, J. F. (2009). Calcium-dependent protein kinases regulate polarized tip

growth in pollen tubes. *The Plant Journal : For Cell and Molecular Biology*, *59*(4), 528–539. https://doi.org/10.1111/j.1365-313X.2009.03894.x

Nakagawa, T. (Shimane Univ., Matsue (Japan). Center for Integrated Research in Science), Suzuki, T., Murata, S., Nakamura, S., Hino, T., Maeo, K., Tabata, R., Kawai, T., Tanaka, K., Niwa, Y., Watanabe, Y., Nakamura, K., Kimura, T., & Ishiguro, S. (2007). Improved Gateway binary vectors: High-performance vectors for creation of fusion constructs in transgenic analysis of plants. *Bioscience, Biotechnology, and Biochemistry*, *71*(8), 2095–2100. https://doi.org/10.1271/bbb.70216

Schindelin, J., Arganda-Carreras, I., Frise, E., Kaynig, V., Longair, M., Pietzsch, T., Preibisch, S., Rueden, C., Saalfeld, S., Schmid, B., Tinevez, J.-Y., White, D. J., Hartenstein, V., Eliceiri, K., Tomancak, P., & Cardona, A. (2012). Fiji: An open-source platform for biological-image analysis. *Nature Methods*, *9*(7), 676–682. https://doi.org/10.1038/NMETH.2019

Schiøtt, M., Romanowsky, S. M., Bækgaard, L., Jakobsen, M. K., Palmgren, M. G., Harper, J. F., & Chrispeels, M. J. (2004). A Plant Plasma Membrane Ca2+Pump Is Required for Normal Pollen Tube Growth and Fertilization. *Proceedings of the National Academy of Sciences - PNAS*, *101*(25), 9502–9507. https://doi.org/10.1073/pnas.0401542101

Sehnal, D., Bittrich, S., Deshpande, M., Svobodová, R., Berka, K., Bazgier, V., Velankar, S., Burley, S. K., Koča, J., & Rose, A. S. (2021). Mol Viewer: Modern web app for 3D visualization and analysis of large biomolecular structures. *Nucleic Acids Research*, *Journal Article*. https://doi.org/10.1093/nar/gkab314

Smith, D. K., Harper, J. F., & Wallace, I. S. (2018b). A potential role for protein O-fucosylation during pollen-pistil interactions. *Plant Signaling & Behavior*, *13*(5), e1467687–e1467687. https://doi.org/10.1080/15592324.2018.1467687

Smith, D. K., Jones, D. M., Lau, J. B. R., Cruz, E. R., Brown, E., Harper, J. F., & Wallace, I. S. (2018a). A Putative Protein O-Fucosyltransferase Facilitates Pollen Tube Penetration through the Stigma–Style Interface1[OPEN]. *Plant Physiology*, *176*(4), 2804–2818. https://doi.org/10.1104/pp.17.01577

Smith, D. K., & Wallace, I. S. (2020). Internally Controlled Methods to Quantify Pollen Tube Growth and Penetration Defects in Arabidopsis thaliana. *Methods in Molecular Biology (Clifton, N.J.)*, *2160*, 129–147. https://doi.org/10.1007/978-1-0716-0672-8_9

Sonnhammer, E. L., von Heijne, G., & Krogh, A. (1998). A hidden Markov model for predicting transmembrane helices in protein sequences. *Proceedings. International Conference on Intelligent Systems for Molecular Biology*, *6*(Journal Article), 175.

Szmelcman, S., & Hofnung, M. (1975). Maltose transport in Escherichia coli K-12: Involvement of the bacteriophage lambda receptor. *Journal of Bacteriology*, *124*(1), 112–118.

Vandersall-Nairn, A., Merkle, R., O'Brien, K., Oeltmann, T., & Moremen, K. (1998). Cloning, expression, purification, and characterization of the acid alpha-mannosidase from Trypanosoma cruzi. *Glycobiology (Oxford)*, *8*(12), 1183–1194. https://doi.org/10.1093/glycob/8.12.1183

Villalobos, J. A., Yi, B. R., & Wallace, I. S. (2015). 2-Fluoro-L-Fucose Is a Metabolically Incorporated Inhibitor of Plant Cell Wall Polysaccharide Fucosylation. *PloS One*, *10*(9), e0139091–e0139091. https://doi.org/10.1371/journal.pone.0139091

Wang, L., Wang, W., Wang, Y.-Q., Liu, Y.-Y., Wang, J.-X., Zhang, X.-Q., Ye, D., & Chen, L.-Q. (2013). Arabidopsis Galacturonosyltransferase (GAUT) 13 and GAUT14 Have Redundant Functions in Pollen Tube Growth. *Molecular Plant*, *6*(4), 1131–1148. https://doi.org/10.1093/mp/sst084

Wang, S., Li, Z., Yu, Y., & Xu, J. (2017a). Folding Membrane Proteins by Deep Transfer Learning. *Cell Systems*, *5*(3), 202.

Wang, S., Sun, S., Li, Z., Zhang, R., & Xu, J. (2017b). Accurate De Novo Prediction of Protein Contact Map by Ultra-Deep Learning Model. *PLoS Computational Biology*, *13*(1), e1005324–e1005324. https://doi.org/10.1371/journal.pcbi.1005324

Wang, S., Sun, S., & Xu, J. (2018). Analysis of deep learning methods for blind protein contact prediction in CASP12. *Proteins, Structure, Function, and Bioinformatics*, *86*(S1), 67–77. https://doi.org/10.1002/prot.25377

Waterhouse, A., Bertoni, M., Bienert, S., Studer, G., Tauriello, G., Gumienny, R., Heer, F. T., de Beer, T. A. P., Rempfer, C., Bordoli, L., Lepore, R., & Schwede, T. (2018). SWISS-MODEL: homology modelling of protein structures and complexes. *Nucleic Acids Research*, *46*(W1), W296–W303. https://doi.org/10.1093/nar/gky427

Weigand, C., & Harper, J. (2020). Decapitation Crosses to Test Pollen Fertility Mutations for Defects in Stigma-Style Penetration. *Methods in Molecular Biology (Clifton, N.J.)*, *2160*(Journal Article), 29. https://doi.org/10.1007/978-1-0716-0672-8_3

Wilson, Z. A., Morroll, S. M., Dawson, J., Swarup, R., & Tighe, P. J. (2001). The Arabidopsis MALE STERILITY1 (MS1) gene is a transcriptional regulator of male gametogenesis, with homology to the PHD-finger family of transcription factors. *The Plant Journal : For Cell and Molecular Biology*, *28*(1), 27–39. https://doi.org/10.1046/j.1365-313X.2001.01125.x

Xu, J. (2019). Distance-based protein folding powered by deep learning. *Proceedings of the National Academy of Sciences - PNAS*, *116*(34), 16856–16865. https://doi.org/10.1073/pnas.1821309116

Xu, J., McPartlon, M., & Li, J. (2021). Improved protein structure prediction by deep learning irrespective of co-evolution information. *Nature Machine Intelligence*, *Journal Article*. https://doi.org/10.1038/s42256-021-00348-5

Xu, J., & Wang, S. (2019). Analysis of distance-based protein structure prediction by deep learning in CASP13. *Proteins, Structure, Function, and Bioinformatics*, *87*(12), 1069–1081. https://doi.org/10.1002/prot.25810

Chapter 3: Results

I. *Arabidopsis thaliana* OFT1 is a member of a large gene family that is predicted to encode a protein O-fucosyltransferase

The function of numerous plant glycosyltransferase enzymes remains an open question in plant biology, and predictions about glycosyltransferase activities are often made through investigating the identified catalytic domains of metazoan biochemically characterized enzymes to facilitate a putative understanding of their potential function using the Carbohydrate Active Enzyme Database ((CAZy); www.cazy.org, Lombard *et al.,* 2014). Using this classification database, the *Arabidopsis thaliana* POFT gene family has been phylogenetically related to the metazoan GT65 family of enzymes through their amino acid sequence conservation in the O-fucosyltransferase domain (Hansen *et al.,* 2012). This domain is best represented by metazoan Protein O-FucosylTransferase 1 (POFT1) enzymes, and to examine the phylogenetic relationship between plant and metazoan POFT1s, the full-length amino acid sequences of *M. musculus*, *D. melanogaster*, *D. rerio*, *C. elegans*, and *H. sapiens* POFT1 were used as BLAST queries against the Arabidopsis genome. In each case, a previously uncharacterized Arabidopsis gene (*At3g05320*) exhibited weak (18–21%) amino acid sequence identity to these metazoan POFT1s. In contrast, the queried metazoan POFT1s did not identify previously characterized putative Arabidopsis POFTs, such as FRB1 (Neumetzler *et al.,* 2012) and ESMD1 (Verger *et al.,* 2016). To further understand the phylogenetic relationships between At3g05320, other putative Arabidopsis POFTs, and established metazoan POFT1s, a phylogenetic tree containing these protein sequences was constructed (Figure 3.1). The Arabidopsis genome contains 39 proteins that are annotated as putative POFTs,

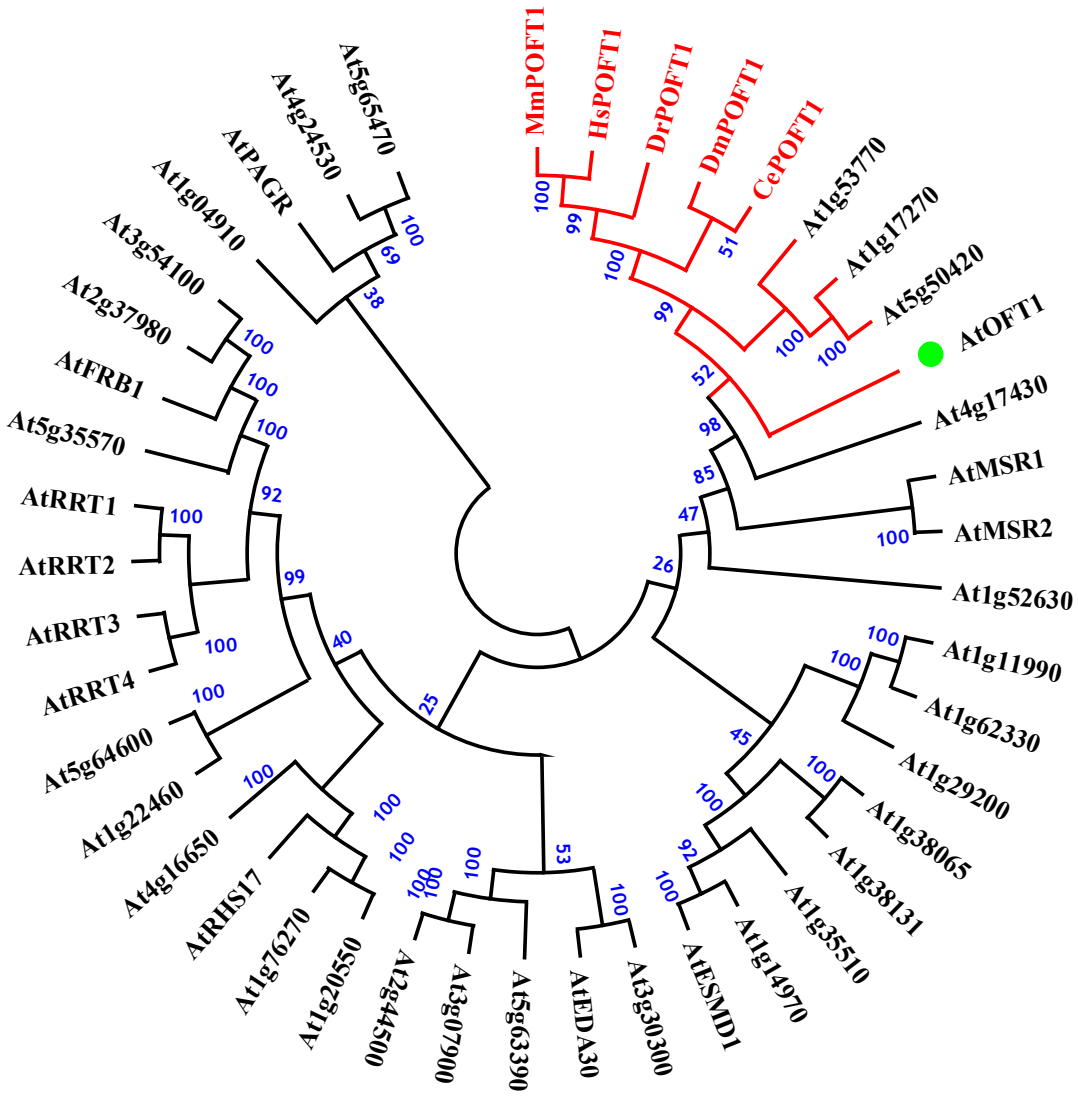

Figure 3.1: Phylogenetic analysis of the Arabidopsis putative POFT family. A neighbor-joining phylogenetic tree was constructed based on the amino acid sequences of members of the putative Arabidopsis protein O-fucosyltransferase (POFT) family as well as various metazoan POFT1 sequences . Labels at nodes represent bootstrap values based on 1,000 bootstrap trials. The metazoan POFT1 sequences are labeled in red as well as with red branches that include the closest related Arabidopsis putative POFTs (black labels). The position of AtOFT1 is designated by a green dot. Evolutionary distances are denoted in blue text next to corresponding node.

in agreement with previous analyses (Neumetzler *et al.,* 2012). At3g05320 was most phylogenetically similar to a subgroup of POFTs that included three other unidentified Arabidopsis genes (*At1g53770*, *At1g17270*, and *At5g50420*), and the metazoan POFT1 family. Interestingly, these protein sequences preferentially clustered with metazoan POFT1s and were only distantly related to previously identified Arabidopsis putative POFTs, suggesting that At3g05320 and its homologues are more similar to metazoan POFT1s in amino acid sequence and potentially in enzymatic function. In light of this phylogenetic similarity, the *At3g05320* gene was named *Arabidopsis thaliana O-FUCOSYLTRANSFERASE 1* (*AtOFT1*).

II. *oft1* mutants display abnormal silique morphology and seed production

Based on the observation that the AtOFT1 protein sequence is closely related to metazoan POFT1s, and that the function of AtOFT1 had not been previously studied, a genetic approach was pursued to examine the physiological role of this gene. Three independent *AtOFT1* T-DNA insertions were identified (Figure 3.2A) in the Arabidopsis T-DNA insertional mutant database (Alonso *et al.*, 2003), and homozygous T-DNA insertions in these mutants were verified by PCR genotyping (Figure 3.2B). These insertional mutant alleles were renamed *oft1-1* (SALK_072442), *oft1-2* (SALK_151675), and *oft1-3* (WiscDsLox489-492M4) (Figure 3.2). RT-PCR analysis confirmed that the *AtOFT1* transcript was not expressed in these mutants, suggesting that each of these T-DNA lines contain null alleles (Figure 3.2C).

oft1 mutant lines were phenotypically evaluated at various stages of Arabidopsis development (Figure 3.3A). At the reproductive stage, *oft1* mutants flowered normally, but developed 65% shorter siliques compared to those of wild-type Col-0 control plants

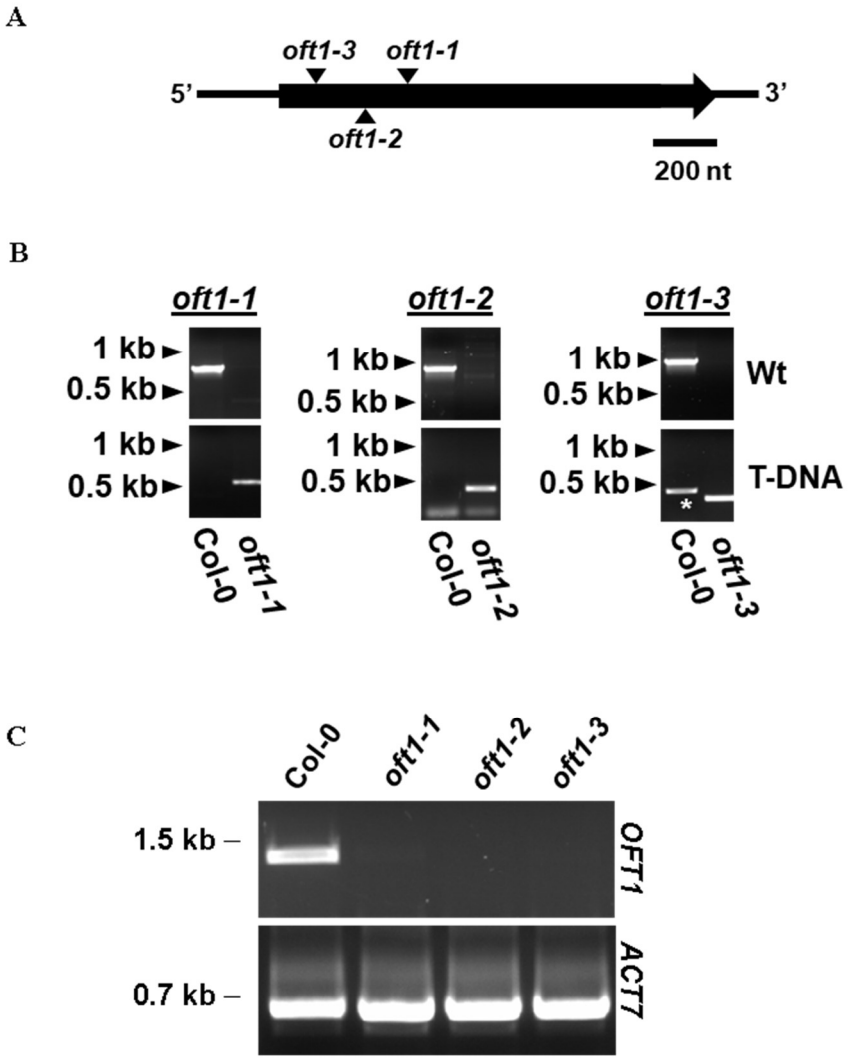

Figure 3.2: Verification of *oft1* T-DNA insertions and *AtOFT1* transcript abundance. A, A model of the Arabidopsis *OFT1* gene (*AtOFT1; At3g05320*) is shown with the T-DNA insertion position for each knockout line indicated with a black arrowhead. A scale bar of 200 nucleotides is shown for reference. B, PCR products from wild-type Col-0 (top panels) and independent T-DNAs (bottom panels). PCR reactions are shown for *oft1-1* (left panel), *oft1-2* (middle panel), and *oft1-3* (right panel) and the positions of the 0.5 and 1 kb markers are indicated to the left of each panel. A non-specific amplicon amplified by the *oft1-3* primer set in wild-type genomic DNA is indicated with a white asterisk. C, Total RNA was extracted from 7-day-old Col-0 or the indicated *oft1* mutant genotype seedlings, converted to cDNA, and probed with either *OFT1* (top) or *ACT7* (bottom) gene-specific primers as described in Materials and Methods. The positions of relevant molecular weight markers are indicated to the left of each gel.

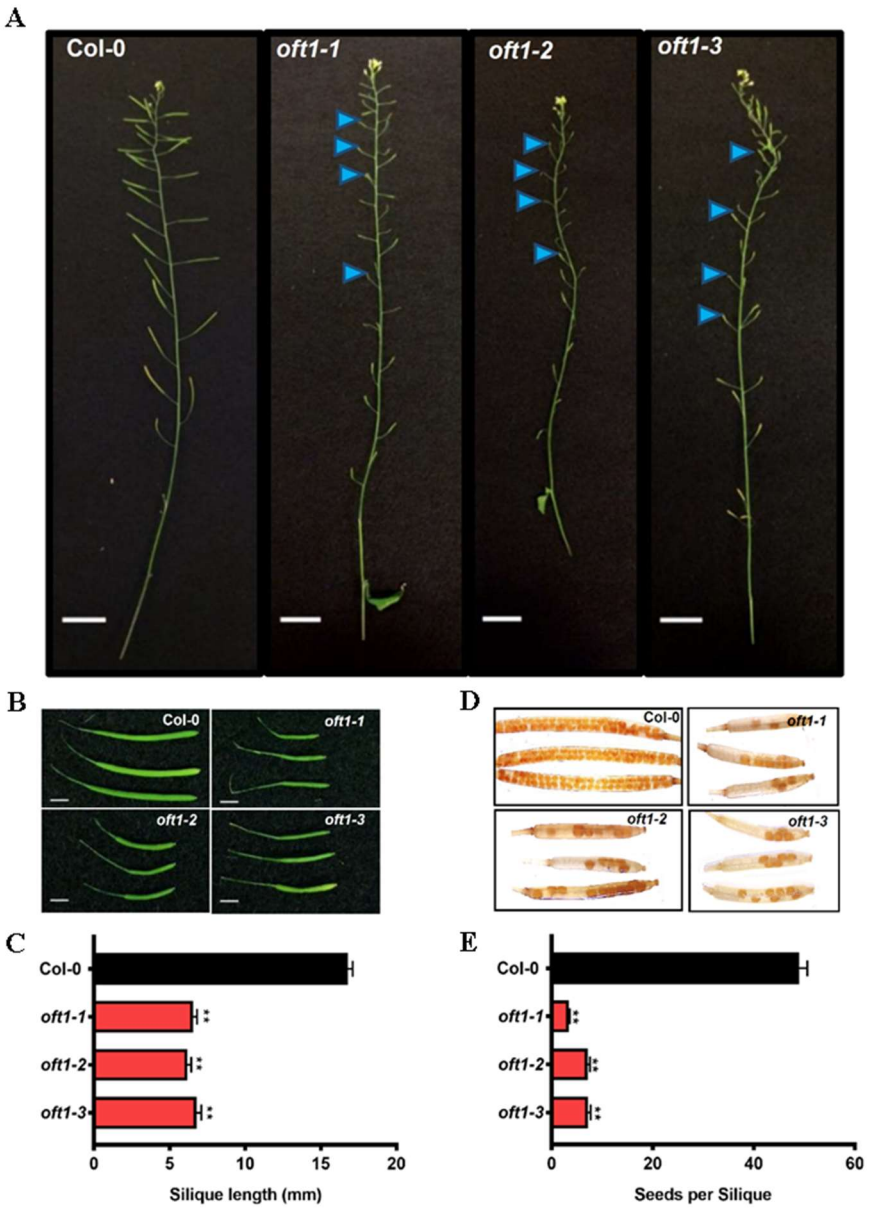

Figure 3.3: Phenotypic characterization of *oft1* mutant lines. A, Inflorescence morphology of 6-week-old *oft1* mutants and wild-type Col-0 controls. Blue arrowheads indicate improperly developed siliques. Bars = 1 cm. B, Representative images of fully developed siliques harvested from 6-week-old *oft1* mutant or wild-type Col-0 control plants. The genotypes of siliques are indicated in the top right corner of each image. Bars = 2 mm. C, Quantification of 6-week-old Col-0 (black bar) and *oft1* mutant (red bars) silique lengths. Data are means ± SE (n = 23). One-way ANOVA indicated a significant difference between Col-0 and *oft1* mutants (**, $P < 0.01$ by Tukey's post hoc analysis). D, Fully developed siliques of the indicated genotypes were harvested from 6-week-old plants and cleared in 70% (v/v) ethanol as described in "Materials and Methods." Representative siliques from each genotype are shown. E, Quantification of Col-0 (black bar) and *oft1* mutants (red bars) seed set. Data are means ± SE (n = 12-22 siliques). One-way ANOVA indicated a significant difference between Col-0 and *oft1* mutants (**, $P < 0.01$ by Tukey's post hoc analysis).

(Figure 3.3A-C). Seed sets of the *oft1* mutants were examined by clearing fully developed siliques and quantifying the number of seed produced. In contrast to wild-type Col-0 control plants, which produced 45–60 seeds per silique, *oft1* mutants produced 5–10-fold fewer seeds (Figure 3.3D-E), indicating that these mutants are reproductively compromised. Due to the more severe reproductive implications determined in the *oft1* mutant lines, this phenotype was investigated in greater detail.

III. Reduced fertility in *oft1* mutants is due to the male gamete

The observed reproductive defects in *oft1* mutants could be a result of the male gamete, female reproductive tissues, or both. To investigate this aspect in more detail, self-fertilization and reciprocal outcrossing experiments were performed. Following repropagation of the mature seed from these crosses, the transmission efficiency of the *oft1* mutant allele in each T-DNA mutant line could be evaluated by their resistance to the plant medium supplemented with the T-DNA associated herbicide marker for *oft1-1* plants (kanamycin resistance) and *oft1-3* (BASTA resistance) at the seedling stage, while the *oft1-2* mutant line was evaluated by PCR genotyping following transplanting to soil. Selfing $oft1^{+/-}$ mutants would be expected to produce 75% progeny containing the *oft1* T-DNA insertion, but *oft1* mutant alleles were transmitted to only 51% (*oft1-1*), 47% (*oft1-2*), and 52% (*oft1-3*) of progeny (Table 3.1). The frequency of homozygotes recovered in these selfing events was also estimated by propagating a population of the progeny and visually phenotyping the plants at the reproductive stage. Homozygous mutants were recovered at much lower frequencies than the expected 33% progeny (*oft1-1* [3.7% homozygotes, n = 108], *oft1-2* [0.9% homozygotes, n = 108], *oft1-3* [1.4% homozygotes,

Table 3.1: Segregation distortion analysis of *oft1* mutant lines

Parents (♂ x ♀)[a]	#R[b]	#S[b]	Total	%R	TE[c]	χ^{2d}	P value
oft1-1$^{+/-}$ self	258	247	505	51.1	1.04	38.5	<0.00001
oft1-2$^{+/-}$ self	51	57	108	47.2	0.89	11.1	0.0009
oft1-3$^{+/-}$ self	369	328	697	52.9	1.13	45.2	<0.00001
Col-0 x oft*1-1*$^{+/-}$	57	52	109	52.3	1.10	0.11	0.74
oft1-1$^{+/-}$ x Col-0	0	116	116	0	0	58	<0.00001
Col-0 x *oft1-3*$^{+/-}$	364	340	704	51.7	1.07	0.41	0.52
oft1-3$^{+/-}$ x Col-0	1	1871	1872	0.05	5.3 x10^{-4}	934	<0.00001

[a] The parental lines of each cross are indicated. [b] The total number of resistant (#R) and sensitive (#S) individuals in each cross F_1 progeny are indicated. The transmission of alleles were scored as described in "Chapter 2": *oft1-1* (kanamycin resistance), *oft1-2* (PCR genotyping), and *oft1-3* (BASTA resistance). [c] Transmission efficiency (TE) was calculated as #R/#S. [d] χ^2 was calculated based on the expectation of a 1:1 segregation of transgenes in the resulting F_1 progeny.

n = 72]), indicating that while homozygous mutants can be obtained from self-fertilization events, they are much less common than expected by Mendelian inheritance.

To further investigate whether this observed segregation distortion was due to defects in the male or female gametophyte, reciprocal crosses were performed using *oft1*$^{+/-}$ parents, and the transmission of mutant alleles was evaluated in the F1 progeny (Table 3.1). The resulting F1 progeny would be expected to inherit the *oft1* allele at a frequency of 50%, and when *oft1*$^{+/-}$ pistils accepted Col-0 pollen, 52% (*oft1-1*) and 51% (*oft1-3*) of the resulting progeny exhibited herbicide resistance (Table 3.1). In contrast, when *oft1*$^{+/-}$ pollen was used to fertilize Col-0 pistils, only 1 transmission event was detected out of 1872 *oft1-3* F1 progeny, and no transmission events were observed for *oft1-1* F_1 progeny, indicating a nearly 2000-fold reduction in *oft1* pollen transmission efficiency (Table 3.1). These results suggest that *oft1* mutants exhibit segregation distortion specifically attributed to a defective male gamete.

IV. *AtOFT1* is expressed in the pollen tube

To investigate whether *AtOFT1* was expressed in developing pollen or other reproductive tissues, public microarray data was examined using the Pollen RCN Heat Tree expression viewer (arabidopsis-heat-tree.org). This analysis revealed that *AtOFT1* expression was not observed in various female tissues (Figure 3.4A). However, *AtOFT1* expression was observed in dry pollen, and transcript abundance increased after pollen tube germination. Interestingly, the highest *AtOFT1* transcript abundance was observed in 4 h semi-*in vivo (SIV)* germinated pollen tubes that had penetrated through dissected stigmatic tissue (Qin et al., 2009), suggesting that *AtOFT1* expression increases as the pollen tube interacts with the female tissues. This analysis also revealed that

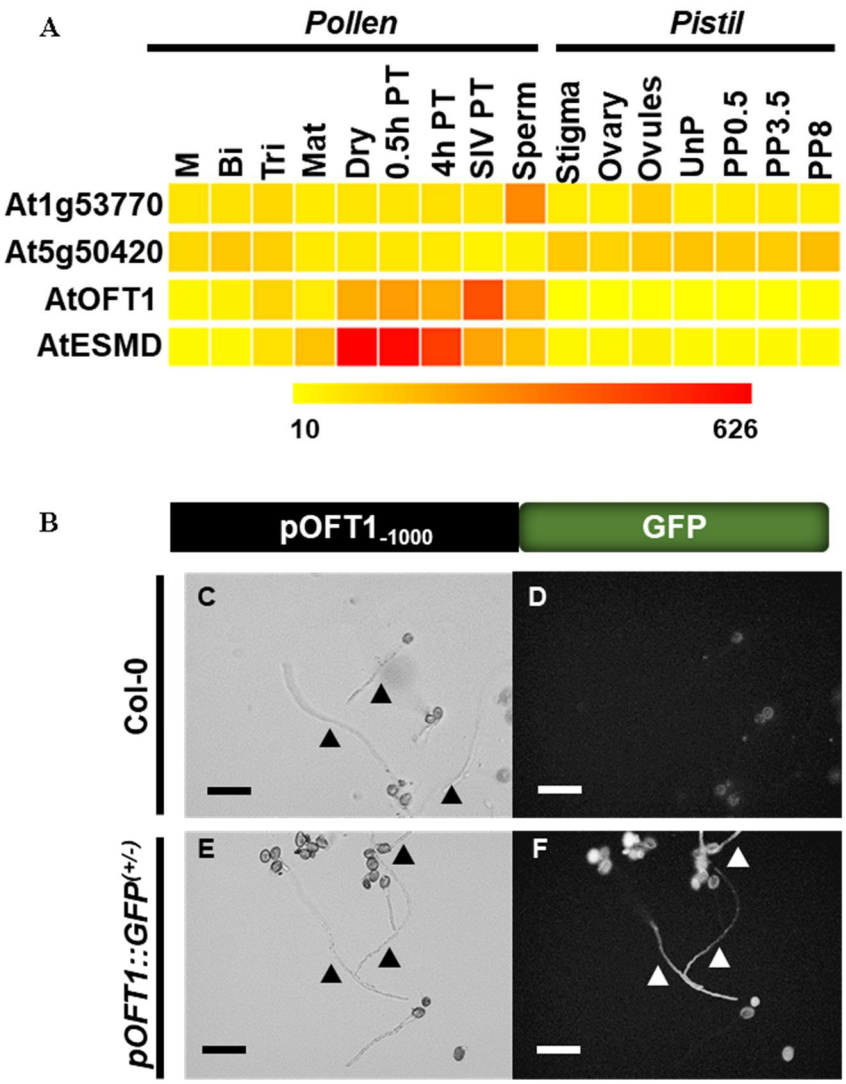

Figure 3.4: Tissue expression analysis of *AtOFT1*. A, A heat-map of expression values for *AtOFT1* as well as the OFT-like genes *At1g53770*, *At5g50420*, and *AtESMD* is shown for reproductive tissues. The scale for raw expression values is shown below the heatmap. Abbreviations for the expression conditions are as follows: M = Uninucleate microspore, Bi = Bicellular pollen, Tri = Tricellular pollen, Mat = Mature pollen grain, Dry = Dry pollen grain, 0.5h PT = 0.5h pollen tubes germinated in vitro, 4h PT = 4h pollen tube in vitro, SIV = Semi-*in vivo* pollen tubes, Sperm = sperm cells, Stigma = stigma, Ovary = ovary, Ovule = ovule, UnP = unpollinated pistil, PP0.5, 3.5, and 8 = pollinated pistil after 0.5, 3.5, and 8 h, respectively. B, The DNA sequence encompassing 1000 bp upstream of the *AtOFT1* start codon was used to drive GFP expression. This construct was transformed into wild-type Col-0 Arabidopsis plants and pollen tubes from the resulting transgenic lines and wild-type Col-0 controls were germinated under *in vitro* conditions for 4 h. Brightfield (C and E) and GFP-channel (D and F) images of germinated Col-0 (C and D) as well as a *pOFT1::GFP*$^{(+/-)}$ transgenic line (E and F) pollen tubes. Black arrowheads in C and E indicate the position of pollen tubes. White arrowheads in F indicate the position of fluorescent pollen tubes. Scale bars in C-F represent 100µm.

At1g53770 and *At5g50420*, two other genes that are closely phylogenetically related to *AtOFT1*, exhibited very different expression profiles in reproductive tissues (Figure 3.4A). *At1g53770* was strongly expressed in sperm cells, with lower but significant expression in ovule tissue. *At5g50420* was expressed throughout the pistil tissue but was not expressed in the male gametophyte tissues after pollen maturity, suggesting that AtOFT1-like genes may play distinct roles in Arabidopsis reproductive tissues due to their non-overlapping expression patterns.

To additionally confirm *AtOFT1* pollen tube expression, 1000 base pairs of the putative *AtOFT1* promoter was fused to a GFP reporter (Figure 3.4B), and this construct was transformed into wild-type Col-0 plants. Subsequent fluorescence imaging of pollen derived from T_1 transformants revealed substantial GFP signal in *in vitro* germinated pollen tubes (Figure 3.4B), confirming that *AtOFT1* is expressed in growing pollen tubes.

V. AtOFT1 facilitates pollen tube penetration through the stigma-style interface

The reciprocal outcross results suggested that *oft1* mutants were specifically compromised in some aspect of pollen tube physiology. Mutations that compromise pollen tube elongation often exhibit reduced fertility, so *oft1* mutant pollen was germinated *in vitro* to compare their relative elongation rates and morphology to wild-type Col-0 control pollen as described in Chapter 2 as well as demonstrated in Figure 2.2 and 2.3. As illustrated in Figure 3.5A *in vitro* germinated pollen tubes from all three *oft1* mutant lines appeared phenotypically indistinguishable from wild-type Col-0 pollen tubes in terms of overall length and morphology. Pollen tube growth rates from the *oft1* mutant lines and wild-type Col-0 control pollen tubes were further evaluated (Figure 3.5B). This analysis revealed that under *in vitro* conditions, *oft1* mutant pollen tubes grew at similar

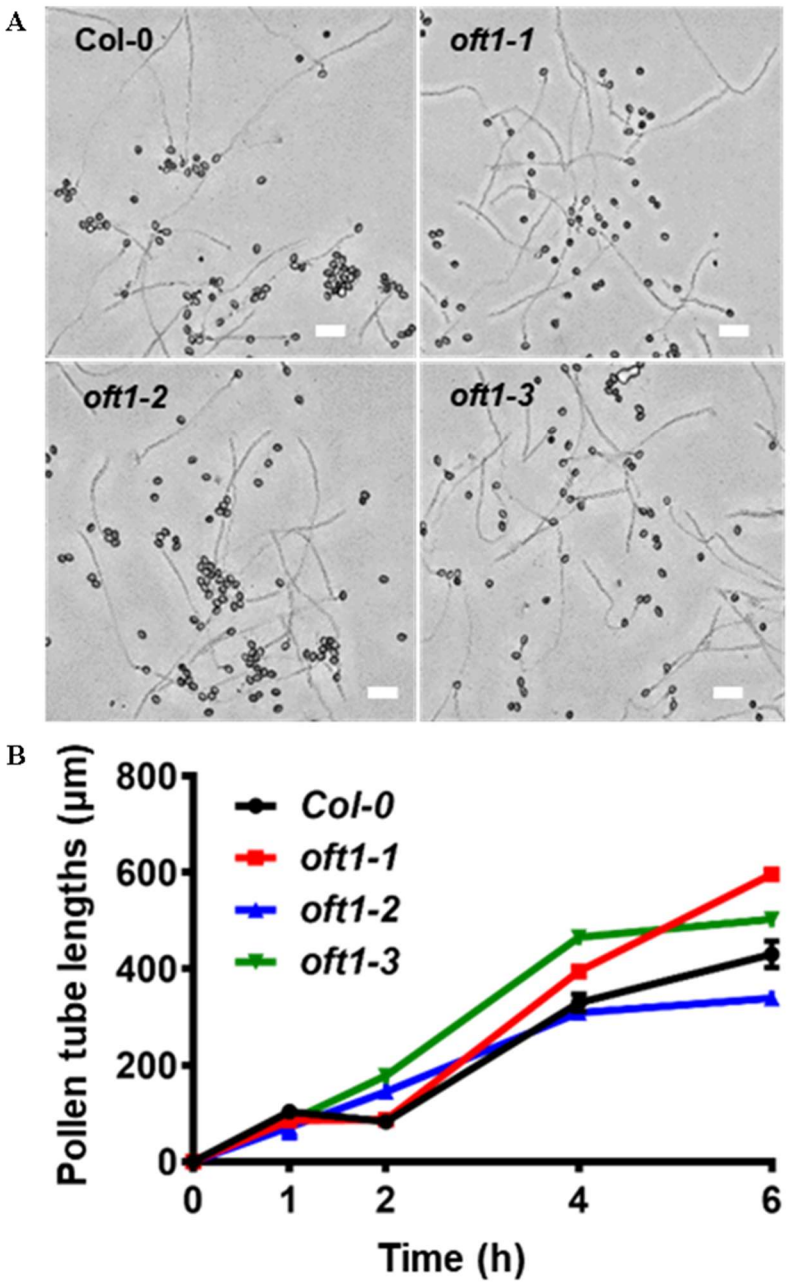

Figure 3.5: *In vitro* pollen tube growth behavior of *oft1* mutants. A, Representative images of wild-type Col-0 or *oft1*$^{-/-}$ mutant pollen after 6 h of growth. The pollen tube genotype is indicated at the top left corner of each image. Bar = 100 µm. B, Lengths of Col-0 (black line), *oft1-1*$^{-/-}$ (red line), *oft1-2*$^{-/-}$ (blue line), and *oft1-3*$^{-/-}$ (green line) pollen tubes were quantified at the indicated time points. Data are means ± SE (n = 30-240).

rates to control pollen tubes. Overall, these observations indicate that *oft1* mutant pollen tubes germinate and develop normally, suggesting that these factors cannot explain the reduced transmission of *oft1* pollen.

To further investigate the mechanistic basis of the compromised *oft1* reproductive phenotype, pollen tube elongation in the pistil was initially examined. Col-0 or *oft1-1*$^{-/-}$ mutant pollen was applied to intact, emasculated *male sterile 1* (*ms1*; Wilson *et al.,* 2001) mutant pistils. These pistils were harvested 24 hours after pollination (HAP) and stained with analine blue as described in Chapter 2. Subsequent fluorescence microscopy imaging to examine pollen tube penetration through the pistil revealed that Col-0 pollen tubes had largely traversed the stigma–style interface and extended into the ovary cavity at this timepoint (Figure 3.6, left), while *oft1-1* pollen tubes were largely retained in the stigma–style interface (Figure 3.6, right).

To more closely examine this phenomenon, a *SIV* fertilization assay was utilized to examine the initial stages of pollen tube growth at the stigma–style interface. Emasculated *ms1* mutant pistils were pollinated with Col-0 control or homozygous *oft1* mutant pollen, dissected from the remainder of the pistil 1 HAP and maintained on PGM-agarose as described in Chapter 2 and demonstrated in Figure 2.4 and Figure 2.5. Pollinated *SIV* stigmas were imaged over time to determine the rate of pollen tube emergence from the transmitting tract (TT) and the total number of pollen tubes exiting the TT (Figure 3.7A). In four independent trials, the percentage of stigmas that exhibited at least one pollen tube exiting the TT over the course of the assay was quantified (Figure 3.7B). Wild-type Col-0 pollen tubes exited the TT of 50% of the stigmas by 3 h after pollination (HAP), and 100% of stigmas pollinated with Col-0 pollen exhibited pollen

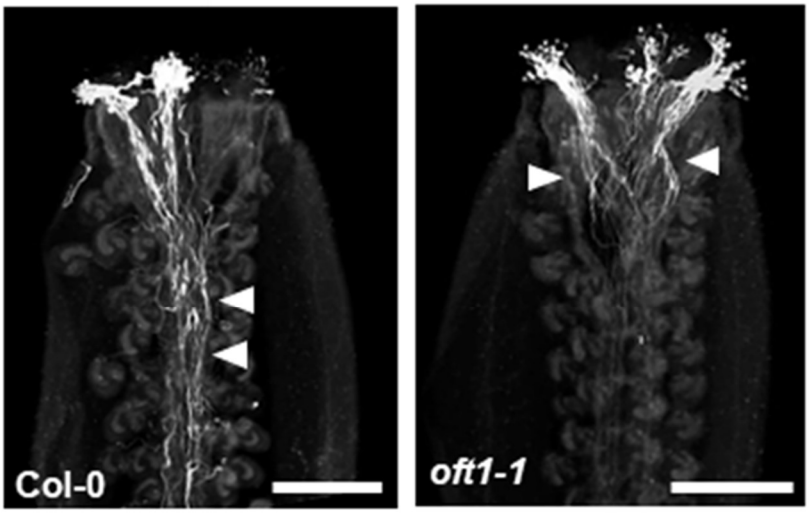

Figure 3.6: *In vivo* behavior of *oft1* mutant pollen tubes. Analine blue staining of *ms1* pistils pollinated with either Col-0 (top panel) or *oft1-1* (bottom panel) pollen. Scale bars represent 300 μm. White arrowheads indicate pollen tube trajectories through the pistil.

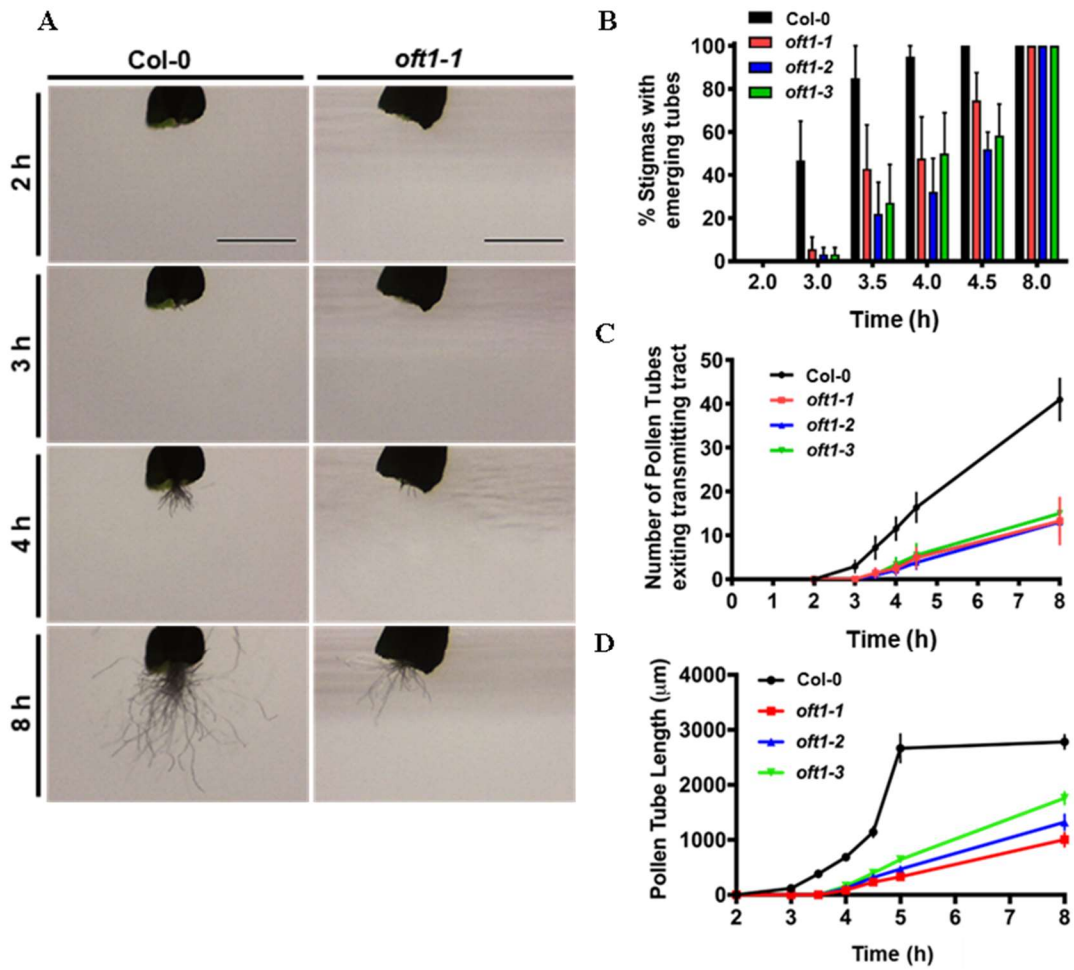

Figure 3.7: *Semi-in vivo* fertilization assay of *oft1* mutant pollen tube behavior at the stigma-style interface. A, Representative images of pollen tube emergence from the transmitting tract in *ms1* pistils dissected at the indicated timepoints following pollination with either wild-type Col-0 (top row panels) or *oft1-1*$^{-}$ (bottom row panels) pollen. Scale bars represent 0.5 mm. B, Quantification of *ms1* stigmas exhibiting pollen tubes emanating from the transmitting tract following pollination with Col-0 (black bars), *oft1-1*$^{-}$ (red bars), *oft1-2*$^{-}$ (blue bars), or *oft1-3*$^{-}$ (green bars) homozygous pollen. Data are means ± SEM (n = 4 independent trials with 4–8 stigmas per experimental group per trial). C, Quantification of pollen tube number emerging from *ms1* stigmas at the indicated time points following pollination with Col-0 (black line), *oft1-1*$^{-}$ (red line), *oft1-2*$^{-}$ (blue line), or *oft1-3*$^{-}$ (green line). Data are means ± SEM (n = 4 biological replicates). D, The growth rate of pollen tubes following emergence from the bottom of dissected *ms1* stigmas pollinated with Col-0 (black line), *oft1-1*$^{-}$ (red line), *oft1-2*$^{-}$ (blue line), or *oft1-3*$^{-}$ (green line) pollen were individually tracked following emergence from the transmitting tract. Error bars represent SEM (n=4 biological replicates).

tubes exiting the TT by 3.5–4.0 HAP (Figure 3.7A-B). In contrast, *oft1* mutant pollen tubes had only exited the TT of 5% of stigmas by 3 HAP, and only 50–75% of *oft1* pollinated stigmas exhibited pollen tube emergence 4.5 HAP (Figure 3.7A-B). The number of pollen tubes exiting the TT over time was also quantified. Wild-type Col-0 pollen tubes were first observed exiting the TT at 3 HAP, and a linear increase in pollen tube number was observed over the course of the experiment to a maximum of approximately 40 pollen tubes at 8 HAP (Figure 3.7C). In contrast, *oft1* mutant pollen tubes exhibited a substantial temporal delay in exiting the TT. Approximately 5 pollen tubes were observed exiting the TT at 4 HAP, and a maximum of 12 pollen tubes were observed 8 HAP (Figure 3.7C). The growth rate of pollen tubes exiting the stigma–style interface was also quantified (Figure 3.7D). While Col-0 control pollen tubes exhibited a rapid growth rate that eventually plateaued at 4 HAP, *oft1* mutant pollen tubes exhibited a much slower elongation rate that remained linear over the course of the assay. These mutant pollen tubes also achieved a much shorter final length. These observations suggest that *oft1* mutant pollen tubes are compromised in their ability to penetrate the stigma–style interface, despite their ability to elongate normally under *in vitro* conditions.

VI. Complementation lines verify and further define the *oft1* pollen tube defect

To further verify that *AtOFT1* loss-of-function was responsible for reproductive consequences in the *oft1* mutants and characterize its loss-of-function phenotype in greater depth, hemizygous complement lines were developed. The hemizygous complement lines were first constructed using the *11p::OFT1-GFP* complement construct, which contained the *AtOFT1* genomic DNA sequence fused to the N-terminus of green fluorescent protein (*GFP)* under the control of the pollen tube-specific

ARABINOGALACTAN PROTEIN 11 (*AGP11*) promoter (Levitin *et al.,* 2008). This construct was transformed into the *oft1-3*$^{-/-}$ mutant background as described in Chapter 2 and Figure 2.1. Creation of *oft1-3*$^{-/-}$*;11p::OFT1-GFP* $^{+/-}$ lines provided an endogenous pollen control due to the predictable 1:1 genotypic segregation of the male gametes, as each anther of these transgenic lines produces a pollen population containing 50% pollen expressing the complement construct and exhibiting its associated transgene GFP fluorescence and 50% pollen that was the original *oft1-3* mutant pollen that did not exhibit fluorescence. The seed produced from these plants was collected, selected on hygromycin containing media, and the resulting seedlings transplanted to soil. Following PCR genotyping to confirm the presence of the transgene, T_1 lines were further assessed for hemizygosity through *in vitro* germination of the pollen produced by each line upon reaching sexual maturity. Hemizygous complemented *oft1-3*$^{-/-}$*; 11p::OFT1-GFP*$^{+/-}$ T_1 lines possessing a single copy of the transgenic construct were identified by *in vitro* germination of the pollen followed by imaging using fluorescence microscopy and quantifying the pollen tube genotypes per line. Verified hemizygous complement lines were then implemented in the following experiments.

Quantification of seed set produced by independent T_1 hemizygous *oft1-3*$^{-/-}$*; 11p::OFT1-GFP*$^{+/-}$ lines demonstrated a single copy of the *11p::OFT1-GFP* complement construct fully or partially complemented the seed set phenotype of *oft1-3*$^{-/-}$ mutants in multiple independent transgenic lines (Figure 3.8). Reciprocal crosses were then performed with three independent *oft1-3*$^{-/-}$*; 11p::OFT1-GFP*$^{+/-}$ lines (Table 3.2). In this assay, all of the pollen were mutant, and the transmission test evaluated how well the hemizygous pollen harboring the transgene competed with pollen that do not contain the

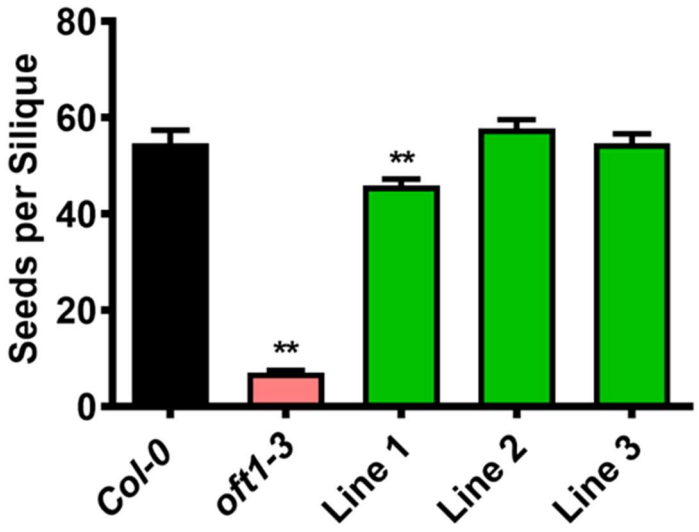

Figure 3.8: Seed set quantification of *oft1* hemizygous complement lines. Siliques were harvested from 6-week-old *oft1-3*$^{(-/-)}$ mutant plants (red bar) or three independent *oft1-3*$^{(-/-)}$*; 11p::OFT1-GFP*$^{(-/+)}$ complement lines (green bars). Wild-type Col-0 siliques (black bar) were used as controls. Siliques were cleared in 70% ethanol as described in Chapter 2, and seed set was quantified. Error bars represent SEM (n = 12-22; ** indicates $P < 0.01$ compared to wild-type by one way ANOVA and Tukey's post-hoc analysis).

Table 3.2: Segregation distortion analysis of *oft1* hemizygous complement lines

Parents (♂ x ♀)[a]	#R[b]	#S[b]	Total	%R	TE[c]	χ^{2d}	P value
Col-0 x *oft1-3*$^{-/-}$; *11p::OFT1-GFP*$^{+/-e}$	84	102	186	45.2	0.82	0.87	0.35
oft1-3$^{-/-}$; *11p::OFT1-GFP*$^{+/-}$ x *oft1-3*$^{-/-e}$	494	0	494	0	ND	247	<0.00001
Col-0 x *oft1-3*$^{+/-}$; *11p::OFT1-GFP*$^{+/-e}$	161	158	319	50.5	1.02	0.014	0.91
oft1-3$^{+/-}$; *11p::OFT1-GFP*$^{+/-}$ x Col-0[e]	771	1688	2459	31.4	0.46	171.0	<0.00001

[a] The parental lines of each cross are indicated. Hemizygous transgenic lines containing the *11p::OFT1-GFP* construct are abbreviated as *11p::OFT1-GFP* with the indicated genotype. [b] The total number of resistant (#R) and sensitive (#S) individuals in each cross F_1 progeny are indicated. The transmission of the transgene was scored as described in "Chapter 2" using hygromycin selection to detect the complement construct. [c] Transmission efficiency (TE) was calculated as #R/#S. [d] χ^2 was calculated based on the expectation of a 1:1 segregation of transgenes in the resulting F_1 progeny. [e] The aggregate number of progeny from at least three independent hemizygous complement lines are reported.

complement transgene. While an expected 50% transmission was observed through the female gametophyte, a near 100% transmission was observed through the pollen (Table 3.2). These results indicate that *oft1-3*$^{-}$ pollen tubes containing the *11p::OFT1-GFP* transgene significantly outcompete *oft1-3*$^{-}$ pollen tubes in a direct competition assay.

To measure the simultaneous transmission of wild-type, mutant, and complemented *oft1* pollen tubes, the transmission efficiency of *oft1-3*$^{-}$ and *11p::OFT1-GFP* alleles in outcrosses between Col-0 and *oft1-3*$^{+/-}$*; 11p::OFT1-GFP*$^{+/-}$ were evaluated. For these experiments, the BASTA resistance cassette associated with the *oft1-3* T-DNA allele was utilized to evaluate transmission. When *oft1-3*$^{+/-}$*; 11p::OFT1-GFP*$^{+/-}$ females were used with Col-0 pollen, 50% of the resulting F_1 progeny inherited the *oft1-3* mutant allele, consistent with the expected value of 50% (Table 3.2). However, when *oft1-3*$^{+/-}$*; 11p::OFT1-GFP*$^{+/-}$ pollen was used to pollinate Col-0 pistils, only 31% of the F_1 progeny inherited the *oft1-3* T-DNA allele, which was significantly less than the expected 50% inheritance (Table 3.2). This result was consistent with the hypothesis that only *oft1-3*$^{-}$*; 11p::OFT1-GFP*$^{+}$ pollen is able to successfully compete with wild-type pollen (Table 3.2), suggesting that *oft1-3*$^{-}$ mutant pollen tubes could only successfully fertilize ovules if they also contained a functional complement copy of the *11p::OFT1-GFP* transgene. Overall, these results provide compelling evidence to support the hypothesis that AtOFT1 plays a significant role in pollen tube physiology and that the male gametophyte is solely responsible for the reduction in *oft1* fertility.

To further compare pollen tube elongation rates and verify that the *oft1* mutant pollen defect was not a result of an overall reduction in pollen tube germination, pollen harvested from hemizygous *oft1-3*$^{-/-}$*; 11p::OFT1-GFP*$^{+/-}$ lines were germinated *in vitro*

and visualized using both epifluorescent and brightfield microscopy, facilitating the simultaneous examination of rescued and non-rescued pollen tube elongation rates. Pollen germination rates of complemented and *oft1* mutant pollen tubes were indistinguishable (Figure 3.9A). As shown in Figure 3.9B, pollen tube growth rates of *oft1-3^{-}; 11p::OFT1-GFP^{+}* and *oft1-3^{-}; 11p::OFT1-GFP^{-}* were also essentially identical, further indicating that pollen tube elongation is not compromised in the *oft1* mutant. Again, these results suggest that *oft1* mutant pollen tubes germinate and develop normally and that these factors cannot account for the reduced transmission of *oft1* pollen.

To further test the hypothesis that *oft1* mutants are unable to efficiently penetrate the stigma–style interface, a *semi-in vivo* competitive pollen tube penetration assay was also developed. Pollen was harvested from 6-week-old *oft1-3$^{-/-}$;11p::OFT1-GFP$^{+/-}$* T_1 hemizygous lines and used to pollinate emasculated *ms1* pistils following the aforementioned *SIV* setup. Four HAP, the dissected stigmas were observed by fluorescence microscopy (Figure 3.10A). Fluorescent pollen tubes containing the *11p::OFT1-GFP* transgene and non-fluorescent *oft1-3^{-}* mutant pollen tubes would be expected to exit the TT at equal frequencies, but fluorescent pollen tubes were observed to exit the TT at a much higher frequency (85–90%) (Figure 3.10B). As a control, similar *SIV* penetration competition assays were performed with pollen expressing a hemizygous copy of Yellow Fluorescent Protein (YFP) under the control of the pollen tube specific *AUTOINHIBITED CALCIUM ATPASE 9* (*ACA9*) promoter, which we refer to as *9p::YFP* (Schiott *et al.,* 2004). The pollen tubes emerging from the TT were quantified, and 45% of emerging pollen tubes exhibited *9p::YFP*-associated fluorescence

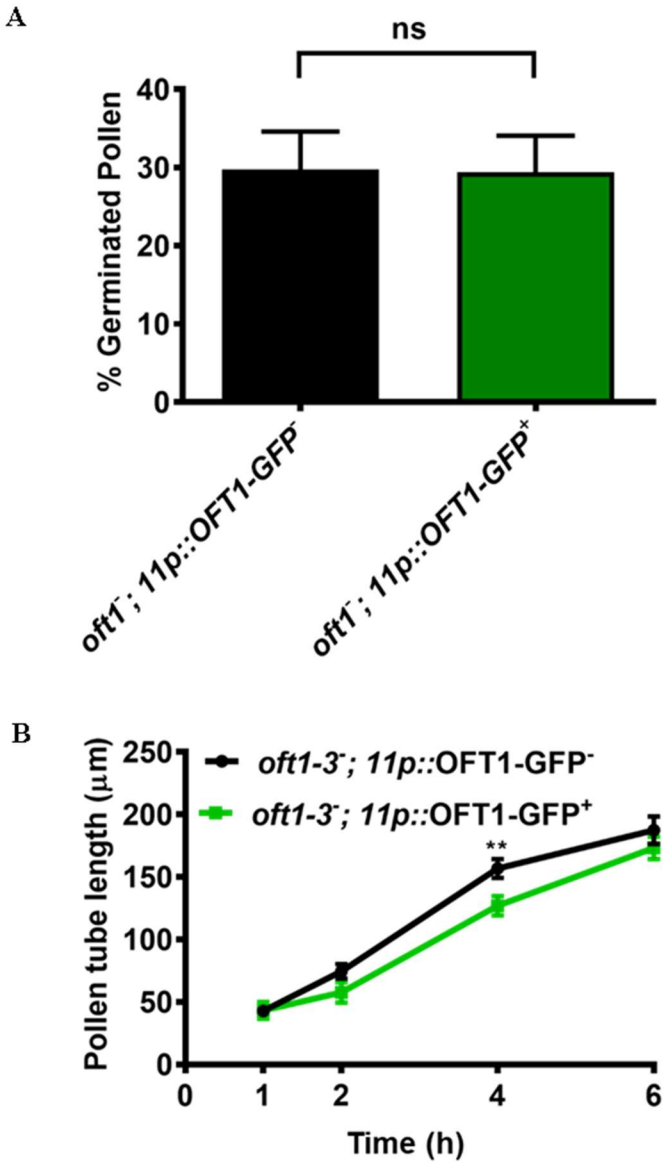

Figure 3.9: *In vitro* germination and tube elongation rate comparison of hemizygous *oft1* pollen. Pollen derived from *oft1-3$^{-/-}$; 11p::OFT1-GFP$^{+/-}$* plants was germinated for the indicated time period on pollen germination medium as described in Chapter 2. Pollen tubes were visualized using epi-fluorescence and brightfield microscopy at each time point to identify GFP positive and negative pollen tubes. A, Pollen tube germination frequency was quantified after 6 h. These data represent aggregate measurements of 7 independent transgenic lines. Error bars represent SEM (n = 7; ns indicates not significant by Student's t-test. B, Pollen tube lengths of *oft1-3^{-}; 11p::OFT1-GFP^{-}* (black line) and *oft1-3^{-}; 11p::OFT1-GFP^{+}* (green line) were measured using ImageJ at the indicated time point. Error bars represent SEM (n = 36-306; ** indicates $P < 0.01$ by Student's t-test). These data were collected and averaged from 7 independent transgenic lines.

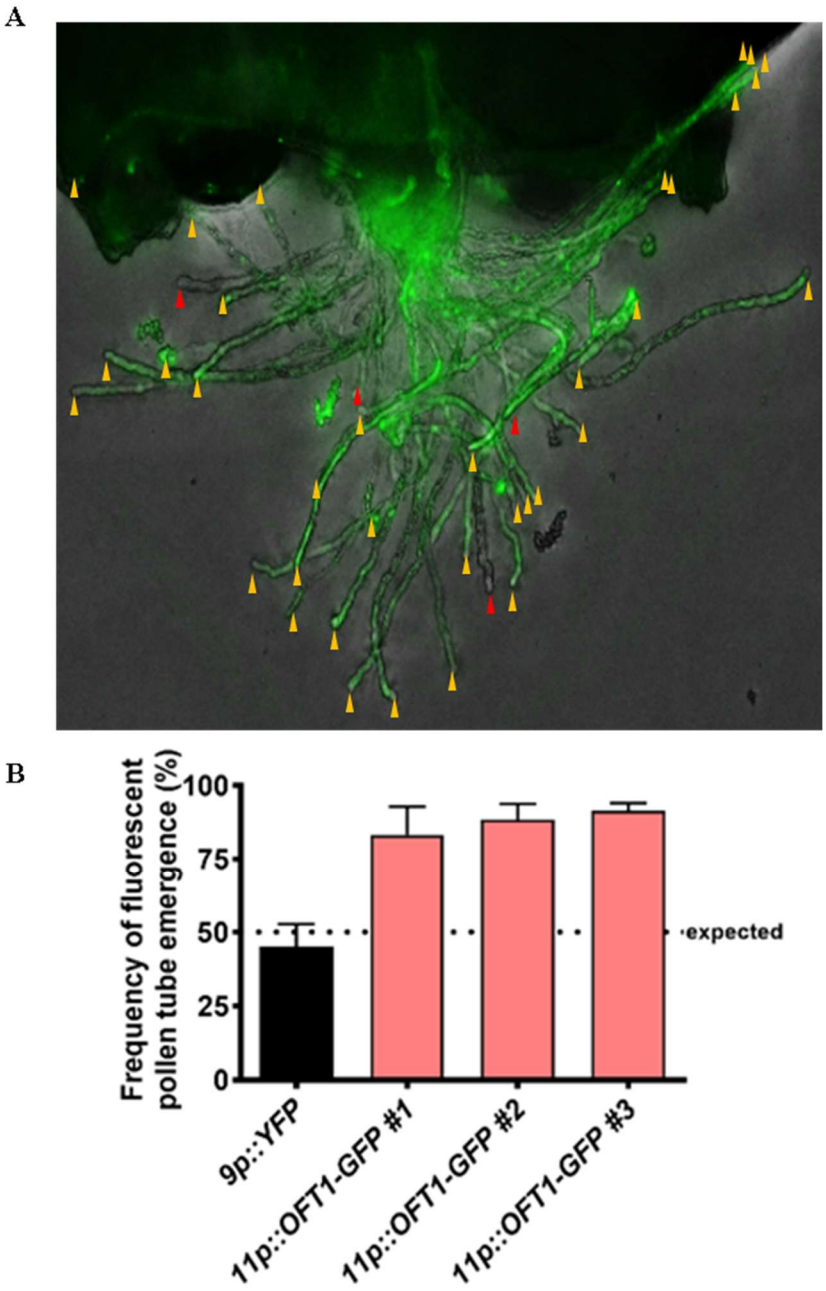

Figure 3.10: *SIV* penetration assay behavior of hemizygous AtOFT1 hemizygous complemented pollen. Fluorescent *SIV* penetration competition assay of mutant and complement pollen tubes through the stigma-style interface. A, GFP and brightfield overlaid representative image depicting the bottom of an *oft1-3*$^{-/-}$*;11p:OFT1-GFP*$^{+/-}$ pollenated *ms1*$^{-/-}$ stigma displaying complemented (fluorescent) and mutant (non-fluorescent) penetrating pollen tubes. Red arrowheads indicate non-fluorescent pollen tubes and yellow arrowheads indicate fluorescent pollen tubes. B, Quantification of the percentage of fluorescent, complemented PTs emerging from the transmitting tract 4 h after pollination. Three independent *oft1-3*$^{-/-}$*;11p:OFT1-GFP*$^{+/-}$ transgenic lines (red bars) were assessed. *9p::YFP*$^{+/-}$ pollen tubes (black bar) served as a negative control. Data are means ± SD ($n \geq 7$).

(Figure 3.10B), suggesting that this control transgene had little influence on pollen tube penetration. Overall, these results suggest that *oft1-3*$^{-}$ pollen tubes containing the *11p::OFT1-GFP*$^{+}$ construct outcompete *oft1-3*$^{-}$ mutant pollen tubes for penetration through the stigma–style interface and exit into the TT. Due to the fact that *oft1* mutant pollen tubes are capable of normal elongation under *in vitro* conditions, these results strongly support the hypothesis that *oft1* mutant pollen tubes are compromised in their ability to physically penetrate through the stigma–style interface.

VII. <u>The stigma–style interface is a critical barrier for *oft1* pollen tubes</u>

While the stigma–style interface is often considered essential for plant sexual reproduction, fertilization events have been observed in the absence of this interface in tobacco, Lilly, and eucalyptus (van Tuyl *et al.,* 1991; Goldman *et al.,* 1994; Trindade *et al.,* 2001). Our results suggest that *AtOFT1* plays a significant role in pollen tube penetration through the stigma–style interface, and to test this hypothesis in more detail, we adapted a "decapitation" fertilization assays for use in Arabidopsis as described by Weigand and Harper, 2020. In this assay, mature *ms1* flowers were emasculated, and the stigma–style interface was excised from the remainder of the pistil. Pollen derived from *oft1-3*$^{+/-}$ parent plants was applied to the dissected pistil (Figure 2.7). The pollen germinated and successfully fertilized ovules, resulting in the production of seed. While this process was inefficient compared to normal outcrosses in the presence of a stigma, sufficient seed (19 ± 7 seeds per silique) was produced in these assays to examine *oft1-3* mutant allele transmission in the absence of a stigma. Interestingly, transmission of the *oft1-3* mutant allele increased dramatically under these conditions, with 29.1% of the resulting progeny inheriting the *oft1-3* T-DNA allele (TE = 0.41). While this result did

not reach the 50% progeny that would be expected from Mendelian inheritance, removal of the stigma and style increased transmission efficiency by 773-fold compared to the < 0.1% transmission, which was observed when *oft1-3*$^{+/-}$ pollen was utilized to pollinate intact pistils. We additionally postulated that this assay format represented a limited pollination scenario that could yield different transmission rates compared to full pollination experiments carried out above. To examine this possibility, intact *ms1* stigmas were pollinated with limiting amounts of *oft1-3*$^{+/-}$ pollen, and *oft1-3* mutant allele transmission was assayed in the resulting F_1 progeny. Under limiting pollination conditions, 2% of the resulting progeny inherited the *oft1-3* mutant allele (n = 86), suggesting that *oft1* mutant pollen are more competitive under limiting pollination conditions, but still ineffective compared to full pollination conditions or pollination in the absence of an intact stigma–style interface. These results suggest that *oft1-3* mutant pollen tubes are capable of fertilizing ovules, but the stigma–style interface represents a critical barrier that slows their penetration through these female tissues.

VIII. *Oft1* mutants display additional phenotypic abnormalities

Although initial efforts were focused on quantifying the *oft1* mutant lines pollen defect, we additionally hypothesized that *oft1* may possess other interesting phenotypes that could lend insight into the overall function of *AtOFT1* in Arabidopsis. We initially aimed to determine if any abnormalities were present in the seed produced by the *oft1* mutant lines. Seed size and mucilage area were initially characterized by harvesting mature seed from equal aged *oft1-1*$^{-/-}$, *oft1-2*$^{-/-}$, *oft1-3*$^{-/-}$, and Col-0 plants that were grown under equal conditions. Seeds were stained with ruthenium red to visualize the seed mucilage and were imaged (Figure 3.11A). Subsequent quantification revealed that

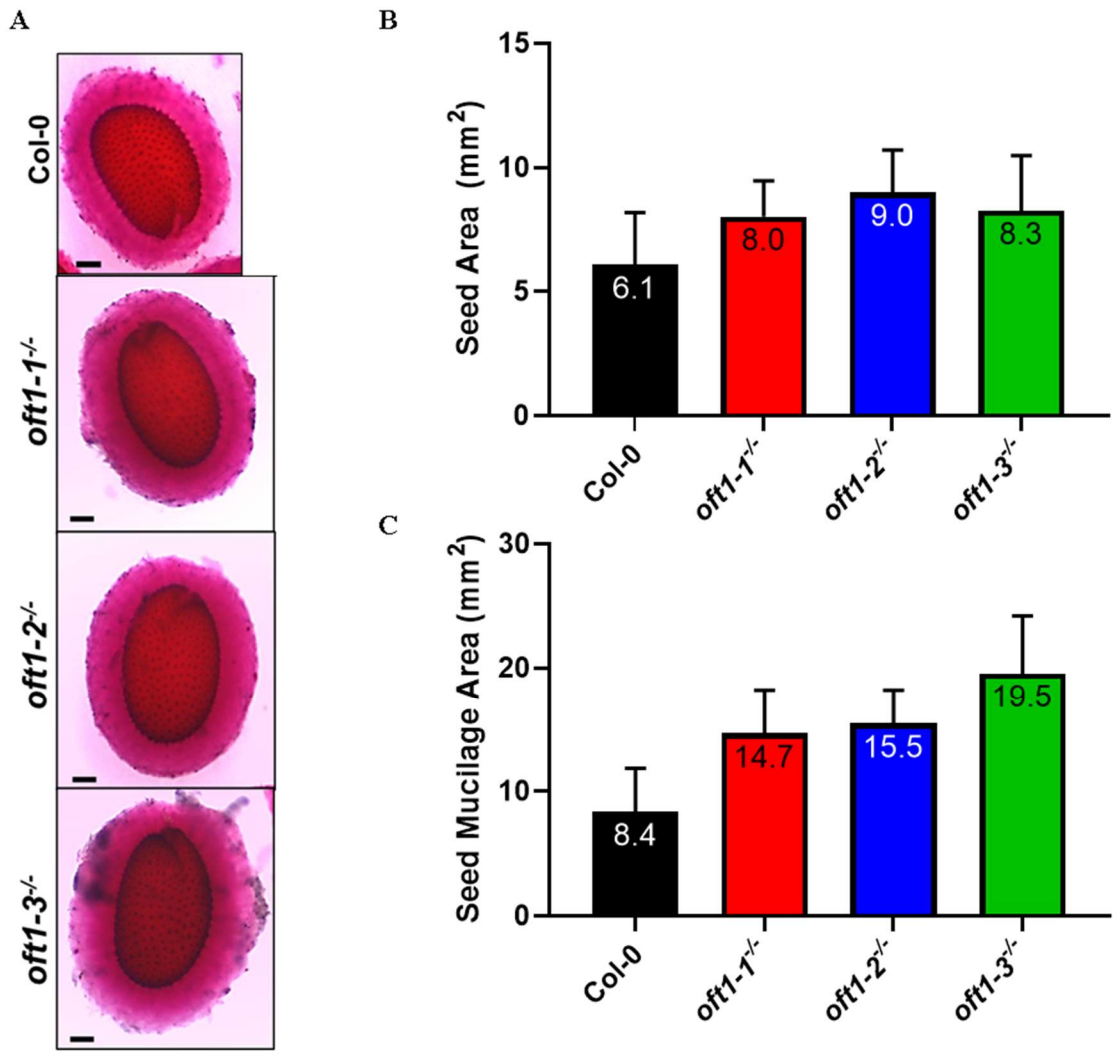

Figure 3.11: Phenotypic quantification of the o*ft1* mutant seed and mucilage area. Seed used for analysis was derived from plants sown out at the same time and grown under equal conditions. Mature seed was harvested from each indicated genotype and subsequently used to assess seed and mucilage area following ruthenium red staining. A, Representative images of seed size and mucilage following stain washout and imaged with a Leica EZ4 HD stereo microscope at 35X magnification. Black scale bar=100µm. Top to bottom: Wildtype Col-0 control seed and three independent exonic T-DNA *oft1* mutants line seeds. B & C, Quantification of Col-0 (black bar) and *oft1* T-DNA mutants (red-pink bars) mucilage area and seed area following ruthenium red staining. Data are representative means ± range of two independent biological replicates with ≥ 18 seeds per replicate. Value denoted within respective bars in bar graphs is mean of both data sets. Averaging these values across all three *oft1* mutant lines, suggests seed area is increased by 11% and *oft1* seed mucilage area is increased by 85% compared to Col-0 seed.

across all three *oft1* homozygous mutant lines, the seed area as well as mucilage area were increased compared to wildtype Col-0 controls (Figure 3.11B-C). These results indicated that *oft1* seed exhibited abnormal seed architecture as well as inefficient pollen tube penetration. Alterations in seed area can be attributed to inequivalent dosages between maternal and paternal genomes following double fertilization, which can alter both embryo and endosperm development (Garcia *et al.,* 2003). Seed mucilage is a specialized layer of extracellular matrix that is primarily composed of cell wall polysaccharides and are specifically rich in pectic polysaccharides (Tsai *et al.,* 2017). The increased seed size and seed mucilage area of *oft1* mutants may suggest that these mutants display altered seed development following fertilization and additionally indicates that this may be a result of dysregulation in polysaccharide composition of seed coat mucilage.

To investigate whether *oft1* mutants display vegetative tissue phenotypic abnormalities as well and further gain insight into a potential dysregulated growth and developmental phenomenon in these mutants, both light grown seedling root length and dark grown seedling hypocotyl lengths in the *oft1* mutant lines were characterized. Both root and hypocotyl length assays were carried out by first sowing out Col-0, *oft1-1*$^{-/-}$, *oft1-2*$^{-/-}$, and *oft1-3*$^{-/-}$ seed on plant medium with no selection. Seed intended for seedling root length analysis were subjected to long-day light conditions, while seeds plated for hypocotyl analysis were grown in the dark. Following 7 days of growth, both the light- and dark-grown seedlings were imaged (Figure 3.12). Quantification of the root lengths of light grown 7-day-old seedlings showed a significantly increased root length compared to Col-0 seedlings (Figure 3.12A-B). Additionally, the hypocotyl lengths in 7-day-old

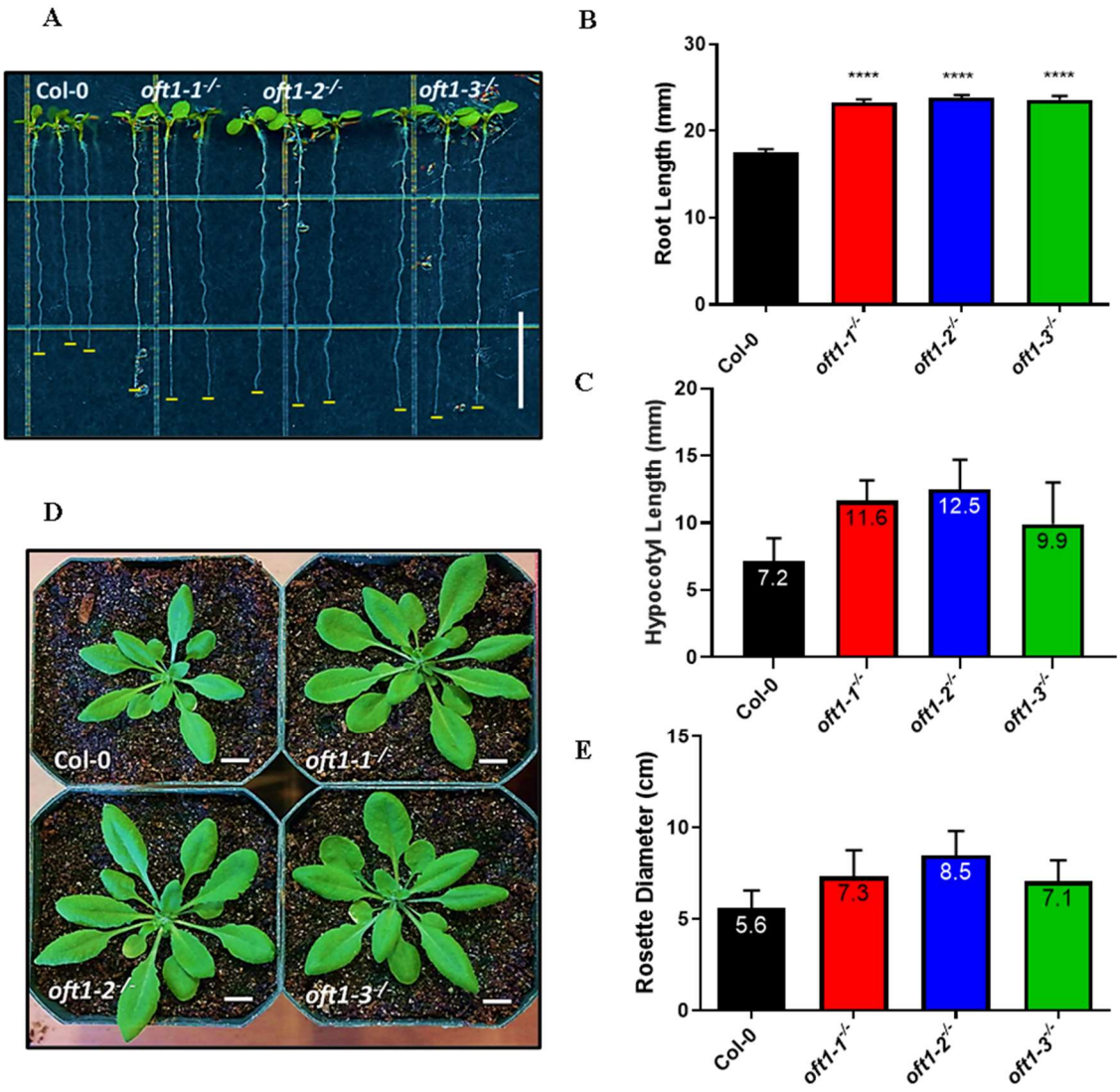

Figure 3.12: Vegetative tissue phenotypic characterization of *oft1* mutant lines. A, Representative image of 7-day-old root lengths of light grown root lengths of Col-0 and *oft1* mutant lines. Scale bar = 1cm with yellow line denotes total lengths achieved following 7 days of growth. B, Quantification of 7-day-old seedling root lengths means ± SEM across 4 biological replicates with ≥ 30 seedlings analyzed per replicate. One-way ANOVA analysis comparison of *oft1* mutants root length compared to wildtype Col-0 control indicated statistical significance (****, $P < 0.0001$ by Tukey's post hoc analysis). C, Quantification dark growth hypocotyls across 2 biological replicates ≥ 11 seedlings analyzed per replicate. Bars are representative of means ± range with means denoted within respective bar. D, Representative image of rosette diameter of Col-0 and *oft1* mutant lines of equal age. Scale bar = 1cm and genotypes denoted next to each respective rosette. E, Quantification rosette diameters across 2 biological replicates with ≥ 11 rosettes analyzed per replicate. Bars are representative of means ± range with means denoted within respective bar. Averaging the values across all three *oft1* mutant lines in C and E, suggests *oft1* hypocotyl length are increased by 58% as well as a 36% increase in rosette diameter compared to Col-0.

dark-grown seedlings illustrated a similar outcome as they were also significantly longer than that of the control Col-0 (Figure 3.12C). Plant cell growth is a result of increasing the number of cells through cell division and/or increasing the size of the existing cell population, which requires a coordinated effort to synthesize and arrange new cell wall polysaccharides to both expand and make new cells (Wang and Ruan, 2013). Taken together, these results suggest that *oft1* mutants display a pattern of general dysregulated growth that may be attributed to cell wall polysaccharide biosynthesis and deposition.

To gain further insight into the *oft1* increased cell proliferation and expansion phenotype observed in both its seed and seedlings as well as determine if this increased growth characteristic was carried through to later stages of plant development, rosette diameter was measured prior to bolting. In this analysis, all three *oft1* mutant seed lines as well as Col-0 controls were propagated, and 7-day old seedlings were transplanted to individual pots. Following 31 days of total growth, the rosettes were imaged (Figure 3.12D). Analysis of these images demonstrated that the rosette diameters calculated across all three *oft1* mutant T-DNA lines produced a larger rosette compared to Col-0 prior to bolting (Figure 3.12D-E) and indicated that *oft1* mutant lines are further dysregulated in regard to plant cell growth in later stages of development. Overall, these results suggest that *AtOFT1* facilitates additional functions pertaining to biomass accumulation throughout many stages of development following fertilization, which we hypothesized was a consequence of altered cell wall polysaccharide composition in the *oft1* mutant lines.

To evaluate the abnormal developmental phenotype of increased biomass in seed and pre-sexually mature plants tissues and to test our hypothesis that this was a

consequence of altered cell wall matrix polysaccharide composition, cell wall monosaccharide analysis was conducted on mature stems to determine the matrix sugar profiles of stems collected from equal aged *oft1-1*$^{-/-}$, *oft1-2*$^{-/-}$, *oft1-3*$^{-/-}$, and Col-0 plants that were grown under equal conditions (Figure 3.13). The results of this analysis demonstrated that xylose content in the *oft1* mutant lines was increased compared to Col-0 in all three lines. Additionally, minor increases in all queried matrix sugars except for fucose were observed in the *oft1-3* mutant line as well as a slight increase in rhamnose for *oft1-2* and a decrease in glucose was observed in *oft1-1*. Most shocking was the observation that *oft1* mutants did not show any appreciable attenuation in fucose content compared to Col-0. Xylose is a major component in the pectic polysaccharide composition of the plant cell wall and are particularly abundant polymers in growing and dividing cells (Mohnen, 2008). Moreover, all pectic polysaccharides contain or are largely composed of xylose and function in a wide range of fundamental plant processes, including plant growth, development, wall structure, cell-cell adhesion, signaling, expansion, growth factors and associated enzymes, pollen tube growth, and seed hydration (Mohnen, 2008). Thus, it could be surmised that the diverse phenotypes displayed by the *oft1* mutants may be a result of dysregulation of the biosynthetic or restructuring enzymes that facilitate xylose integration into pectic polysaccharides.

IX. Subcellular localization of AtOFT1

Metazoan POFTs are localized to the endoplasmic reticulum where they modify target substrates before being further glycosylated in the Golgi apparatus (Luo and Haltiwanger, 2005). To further understand the function of AtOFT1 and determine organelle or intracellular location in which it performs its catalytic activity, the

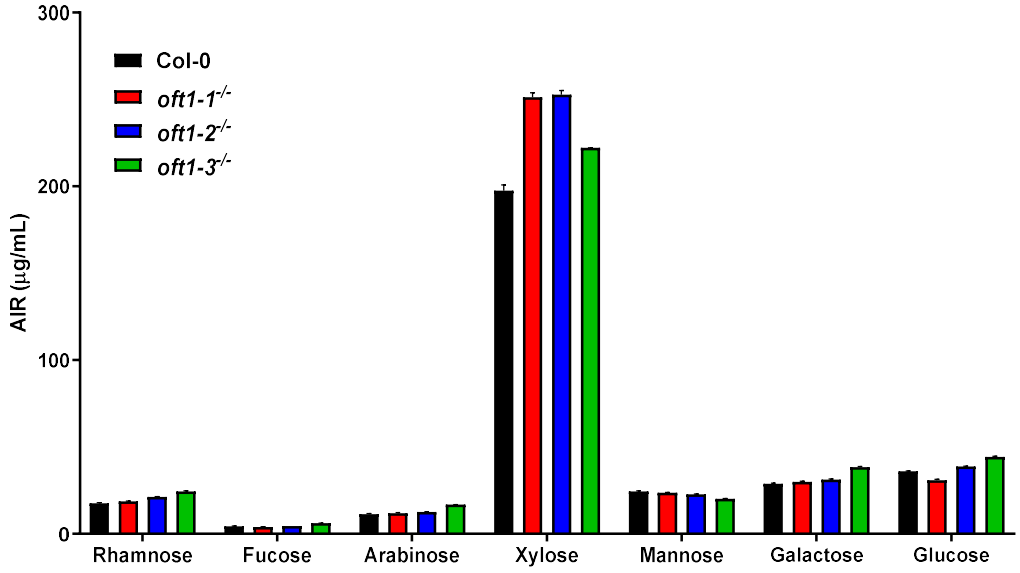

Figure 3.13: Cell wall monosaccharide profile of *oft1* mutant lines. Eight-week-old plant stems from Col-0 and three *oft1*$^{-/-}$ T-DNA mutant lines were harvested and analyzed by gas chromatography. Soluble sugars, proteins, lipids, and nucleic acid were extracted from homogenized plant stems before undergoing destarching and weak acid hydrolysis. Insoluble cell wall material was subsequently subjected to Seeman hydrolysis before being injected onto a gas chromatograph fitted with flame ionization detector. Monosaccharide data is represented as the mean ± range. Averaging the values across all three *oft1* mutant lines, suggested a 22% increase in xylose in *oft1* stems.

previously described *11p::OFT1-GFP* transgenic lines were used to investigate the subcellular localization of this protein. Pollen tubes were germinated under *in vitro* conditions and examined by confocal microscopy 1.5 h after germination. AtOFT1-associated GFP signal was localized to punctate motile intracellular organelles (Figure 3.14).

To further investigate this subcellular localization pattern, the predicted subcellular localization of AtOFT1 was examined using the SUBcellular localization database of Arabidopsis proteins (SUBA; Tanz et al., 2013). AtOFT1 was predicted to be mitochondrially-localized by SUBA, so *11p::OFT1-GFP* expressing pollen tubes were germinated *in vitro* and stained with 500 nM MitoTracker Orange. As shown in Figure 3.14A (top panel), AtOFT1-GFP signal did not overlap with MitoTracker Orange-stained mitochondria, and quantitative co-localization analysis using JACoP (Bolte and Cordelieres, 2006) revealed a Pearson's correlation coefficient of only 0.21 between the AtOFT1-GFP and MitoTracker Orange signals (Figure 3.14B), suggesting that AtOFT1 is not localized to pollen tube mitochondria as predicted.

Subcellular localization studies previously determined that other members of the Arabidopsis putative protein O-fucosyltransferase family, including FRB1 and ESMD1, were localized to the Golgi apparatus in interphase cells (Neumetzler *et al.,* 2012; Verger et al., 2016), suggesting that AtOFT1 may also localize to this organelle. To test this hypothesis, the *11p::OFT1-GFP* transgenic construct was introgressed into transgenic plants expressing the established Golgi markers MEMBRIN12 (MEMB12) or GOLGI TRANSPORT1 (Got1p) fused to mCherry (Geldner *et al.,* 2009). Pollen harvested from 6-week-old F_1 progeny was germinated *in vitro* and examined by confocal fluorescence

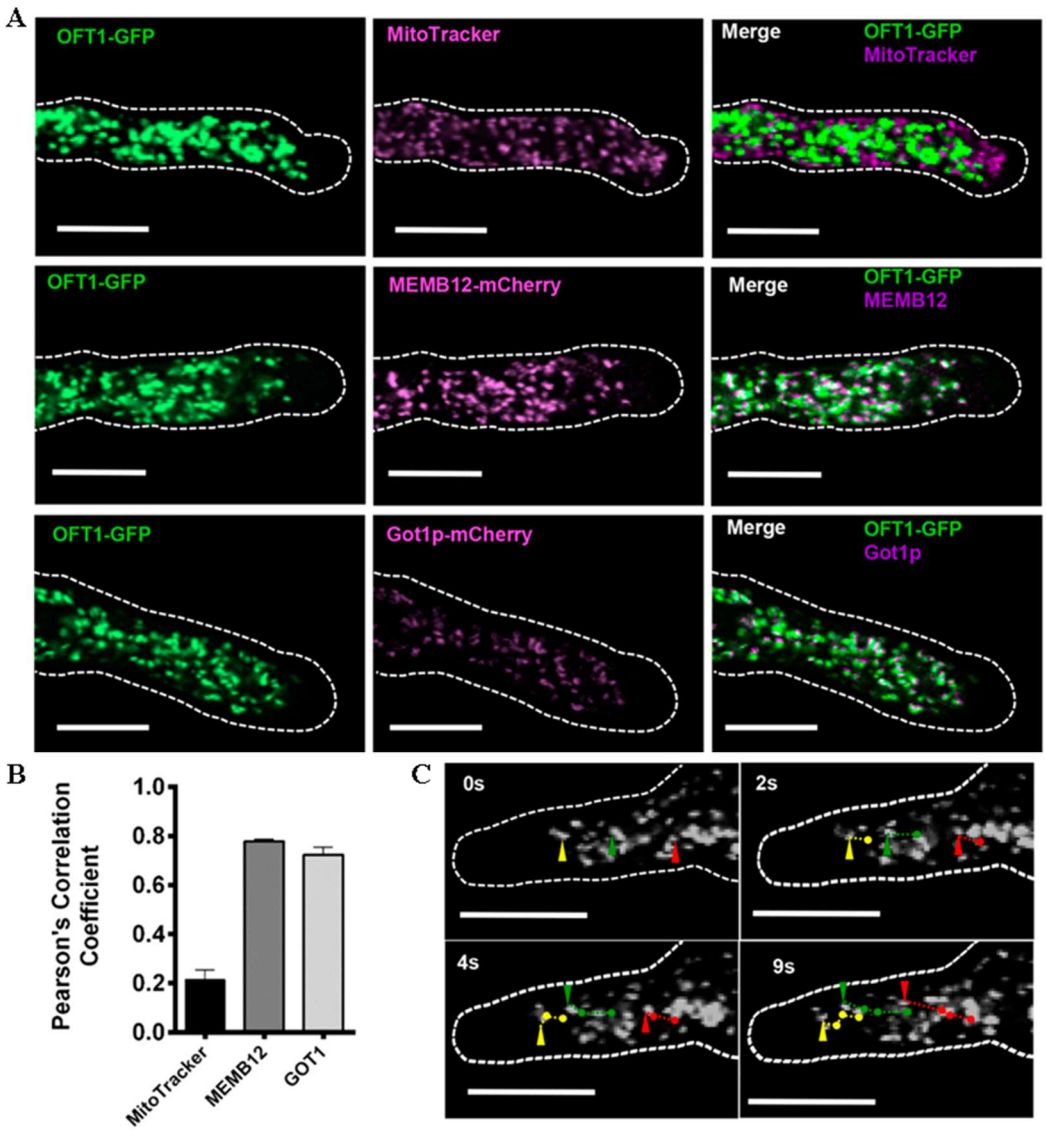

Figure 3.14: Subcellular localization of AtOFT1. A, Pollen tubes from *11p::OFT1-GFP*-expressing plants stained with 500 nM MitoTracker Orange for 15 min (top row) and *11p::OFT1-GFP* and MEMB12- or GOT1-mCherry- (Geldner *et al.,* 2009) coexpressing plants (middle and bottom rows, respectively. Pollen tubes were germinated and visualized as described in Chapter 2. The outline of each pollen tube is shown as a dashed white line. OFT1-GFP (left column, green signal), the colocalization marker (middle column, magenta signal), and the merge of each image set (right column, overlap of merged channels shown as white signal). Bars = 10 µm. B, Quantitative colocalization analysis of each image set was performed using JACoP (Bolte and Cordelières, 2006), and the Pearson correlation coefficient between OFT1-GFP and MitoTracker (black bar), MEMB12-mCherry (charcoal bar), or GOT1-mCherry (gray bar) was calculated. Data are means ± SE (n = 6-15 independent images per colocalization marker). C, Live-cell confocal imaging of OFT1-GFP subcellular localization in a growing pollen tube over time. The outline of the pollen tube is indicated with a dashed white line. Image time points are indicated in the top left corner of each image. The trajectories of three representative fluorescent particles are indicated individually at their current positions for each indicated time point by green, red, and yellow arrowheads, and their corresponding trajectories in successive images are indicated with green, red, and yellow dashed lines, respectively. Scale bars represent 10 µm.

microscopy. These experiments revealed significant localization overlap between AtOFT1-GFP and Golgi marker fluorescent signals (Figure 3.14A). Quantitative co-localization analyses revealed that both the MEMB12- and Got1p-mCherry markers respectively co-localized with AtOFT1-GFP signal with a Pearson's correlation coefficients of 0.79 and 0.72 (Figure 3.14B), suggesting a high degree of co-localization between AtOFT1-GFP and known Golgi-resident proteins. These results suggest that AtOFT1 localizes to the Golgi apparatus and potentially participates in cellular glycosylation events in this organelle.

X. Random mutagenesis to identify AtOFT1 pathway protein-protein interactions

To gain insight into the proteins AtOFT1 may be modifying as well as to identify the pathways this protein may be participating in, a suppressor screen was carried out to determine if mutation in other genes could effectively restore the *oft1*$^{-/-}$ pollen tube penetration defect. These experiments were performed by treating *oft1-1*$^{-/-}$ and *oft1-3*$^{-/-}$ seed with EMS and propagating the mutagenized seed to sexual maturity. The M_1 lines were initially phenotypically screened for a wildtype-like silique morphology compared to the *oft1*$^{-/-}$ mutant alone. Two EMS lines that maintained a robust silique length and seed set following backcrossing were identified for further investigation and were named *suppressor of oft1* line 1 *(soft1)* and *suppressor of oftt1* line 2 *(soft2).* To ensure the *soft* mutant phenotypes were not due to contamination by wildtype Col-0 pollen and to eliminate unassociated genome mutations induced by EMS that were not related to the restored silique phenotypes of these lines, *soft1* and *soft2* were backcrossed multiple times with the *oft1-1*$^{-/-}$ and *oft1-3*$^{-/-}$ background lines and repropagated.

To evaluate the ability of the suppressor lines to restore the silique morphology and seed set defects related to the *oft1* mutant, mature siliques were collected from *soft1* and *soft2* lines for analysis. Initial observations of s*oft1* siliques were no different in length to that of equal age Col-0 siliques (Figure 3.15A-B). Following clearing mature *soft1* siliques in 70% [v/v] ethanol, the seed set per silique could be visualized and quantified (Figure 3.15C-D). This analysis additionally demonstrated a seed set that was not significantly different to that of the wildtype Col-0 control and indicated that *soft1* sufficiently suppressed the male-specific reproductive defects induced by the *oft1*$^{-/-}$ mutant lines (Figure 3.15D).

The *soft2* EMS line was characterized in a similar manner by first examining the mature silique lengths of these mutants (Figure 3.16A). Similar to our observations of *soft1* silique morphology, the silique lengths of the *soft2* mutants were significantly longer than that of the *oft1* mutants (Figure 3.16B). However, the *soft2* mutant did not fully rescue the silique length compared to that of the wildtype control Col-0 line (average length Col-0 = 11.2 mm vs *soft2* = 9.8 mm). Mature siliques from equal age Col-0, *oft1-1*$^{-/-}$, *oft1-3*$^{-/-}$, and *soft2* plants were collected and cleared in ethanol to evaluate the number of seeds per silique produced by each of these lines (Figure 3.16C). As Figure 3.16D illustrates, the seed set of *soft2* lines was increased compared to *oft1-1* and *oft1-3* (42.8 for *soft2* vs. 7.1 and 7.4 for *oft1-1* and *oft1-3,* respective mean seed sets). However, the *soft2* silique seed set was still reduced compared to that of Col-0 (Col-0=62.0 average seed set). Nonetheless, both *soft1* and *soft2* EMS lines exhibited quantitative fertility enhancement compared to the *oft1* mutants with respect to both their silique lengths and seed set, suggesting that these lines represent stable suppressor mutants. Taking these

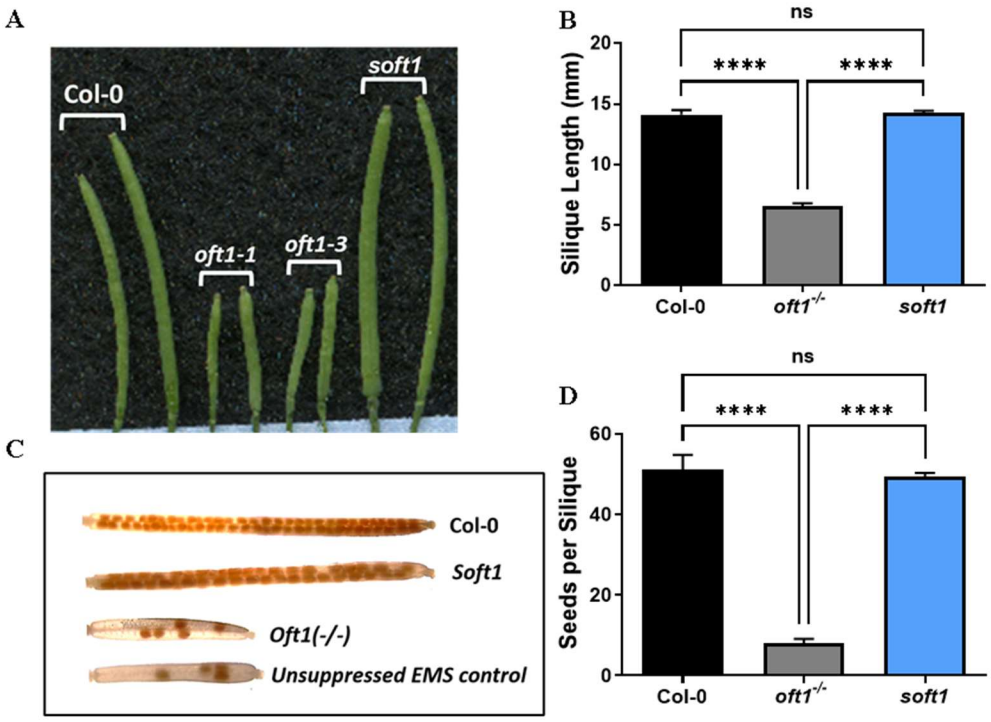

Figure 3.15: Phenotypic identification and quantification of silique length and seed set of *soft1*.Fully developed siliques from 6-week-old plants were harvested from the indicated genotypes. A, Picture of fresh, whole siliques not yet cleared. B, Quantification of 6-week-old Col-0 (black bar), two independent *oft1*$^{-/-}$ exonic T-DNA mutants (dark gray bar) and 3 *soft1* EMS lines (blue bar) silique lengths. Data are means ± SEM calculated over 3 biological replicates (n=14-84 siliques per genotype per replicate). C, Representative image of fully developed siliques of the indicated genotypes, including unsuppressed EMS control that were harvested from 6-week-old plants and cleared in 70% (v/v) ethanol as described in Chapter 2. D, Quantification of 6-week-old Col-0 (black bar), two independent *oft1*$^{-/-}$ T-DNA mutant lines (dark gray bar) and *soft1* (blue bar) seeds per silique. Data are means calculated over 3 biological replicates ± SEM (n ≥80 siliques per genotype). One-way ANOVA analysis performed separately on B and D data sets indicated a significant difference when comparing Col-0 and *oft1*$^{-/-}$ but not when compared to *soft1* EMS mutants for silique length as well as seed set (****, $P < 0.0001$ by Tukey's multiple comparisons test).

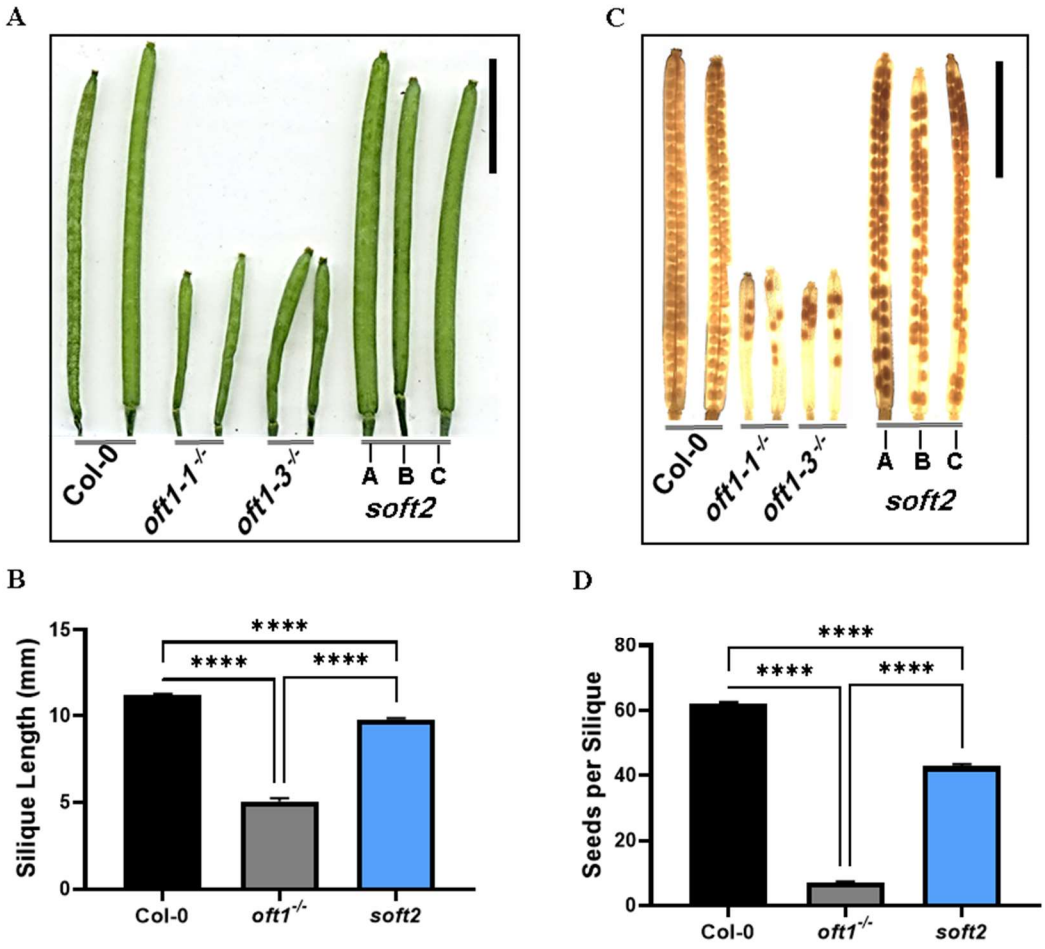

Figure 3.16: Phenotypic identification and quantification of silique length and seed set of *soft2*. Fully developed siliques from 6-week-old plants were harvested from the indicated genotypes. A, Picture of fresh, whole siliques not yet cleared. B, Quantification of 6-week-old Col-0 (black bar), two independent *oft1* exonic T-DNA mutants (dark gray bar), and 3 *soft2* EMS lines (blue bar) silique lengths. Data are means ± SEM calculated over 3 biological replicates with 80-202 siliques per genotype. C, Representative image of mature siliques of the indicated genotypes were harvested from 6-week-old plants and cleared in 70% [v/v] ethanol as described in Chapter 2. Representative siliques from each genotype are shown. Black bar= 5 mm. D, Quantification of 6-week-old seed sets produced by the indicated genotype. Data are means ± SEM calculated over 3 biological replicates (n ≥80 siliques per genotype). Bar graphs produced for both C and D depict Col-0 with black bar, two independent *oft1*$^{-/-}$ T-DNA mutant lines with dark gray bar, and *soft1* in blue bar. One-way ANOVA analysis performed separately on C and D data sets indicated a significant difference when comparing Col-0, *oft1*$^{-/-}$, and *soft2* EMS mutants for silique length as well as seed set (****, $P < 0.0001$ by Tukey's multiple comparisons test).

results into consideration, we postulated that *soft1* and *soft2* mutants would produce pollen tubes that more effectively penetrated through the stigma-style interface, as this was the main phenotypic defect of *oft1* single mutants that resulted in near-sterile plants.

To investigate if the suppressor lines increased pollen tube penetration through the stigma style interface compared to the *oft1* mutant, analine blue staining of 24 h emasculated pistils was performed using *soft1* pollen (Figure 3.17A). Surprisingly, 24 HAP, *soft1* pollen tubes had effectively penetrated through the stigma style interface and had elongated approximately half of the way into ovary compared to Col-0 pollen tubes that had traversed the entire pistil body. At this same time point, *oft1* pollen tubes had been largely retained in the transmitting tract of the style and few pollen tubes were observed in the ovary cavity, in agreement with previous investigations (Smith *et al.,* 2018a). The results of analine blue pollen tube analysis suggested that *soft1* mutant pollen tubes penetrate the stigma-style interface more efficiently compared to the *oft1* mutant, and that the disrupted gene in *soft1* lines somehow plays a role in pollen tube elongation as postulated.

To investigate this pollen tube penetration phenotype in more detail for *soft1* EMS lines, a *SIV* fertilization assay was performed using mature, emasculated Col-0 pistils pollinated with either mature pollen from Col-0, *oft1*$^{-/-}$, or *soft1* equal age plants (Figure 3.17B). Following 3 HAP, Col-0 pollen tubes began emerging from the bottom of the dissected style, while *soft2* pollen tubes first appeared at 4 HAP (Figure 3.17C). This was represented a drastic increase for pollen tube penetration as *oft1*$^{-}$ pollen tube emergence was only observed following 8 HAP. These results indicate that *soft1* pollen tubes still exhibited a temporal delay in exiting the TT of the style but were significantly faster at

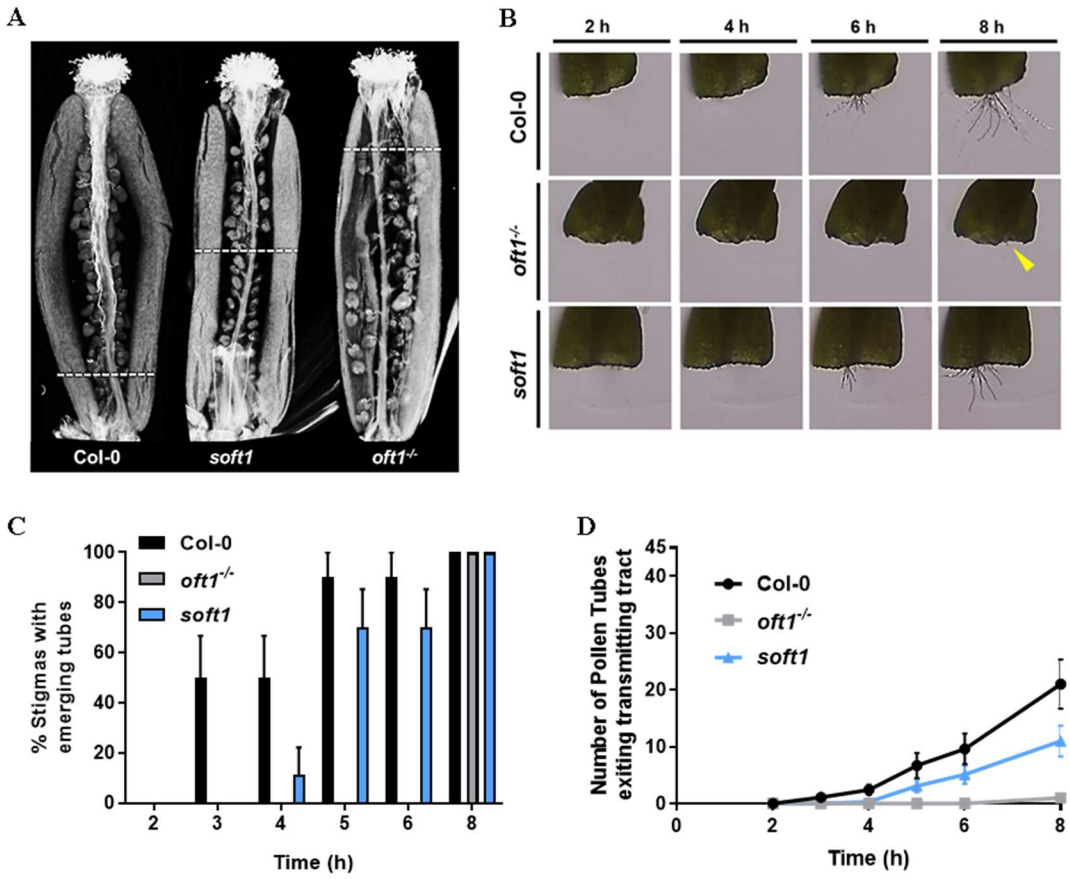

Figure 3.17: *Soft1 in vivo* pollen tube penetration behavior. A, Col-0 emasculated pistils pollinated with the indicated genotype and stained with analine blue to visualize pollen tube penetration. Images were acquired at 10X magnification on a Keyence BZ-X700 fluorescence microscope fitted with DAPI filter cube (ex=1/15s), as described in Chapter 2. White dashed line indicates the total distance pollen tubes were observed at following 24 HAP. B, Representative images of *SIV* assays showing pollen tube emergence from the bottom of the TT style of mature, emasculated Col-0 pistils dissected at the indicated time points following pollination with either wild-type Col-0 (top row) , *oft1*$^{-/-}$ (middle row), or *soft1* EMS pollen (bottom row) Yellow carrot points to the only PT emerging from *oft1* pollinated *SIV* pistil. C, Quantification of the % stigmas with emerging pollen tubes at the indicated time point after pollination. D, Quantification of the number of pollen tube number emerging from Col-0 stigmas at the indicated time points following pollination with the indicated pollen genotype. Both C and D are means ± SEM calculated over 3 biological replicates with Col-0 depicted by black bar/trend line, *oft1*$^{-/-}$ *by* gray bars/trend line, or *soft1* suppressor pollen by blue bars/trend line.

penetrating through the stigma-style interface compared to *oft1*$^{-}$ mutant pollen. To additionally assess the results of the *SIV* fertilization assay, the number of pollen tubes per genotype per time point were quantified, which revealed that the number of pollen tubes for *soft1* was also significantly increased compared to *oft1* mutant pollen, although, across all time points, the number of *soft1* emerging pollen tubes was approximately 50% greater than that of *oft1* pollen tube emergence in *SIV* assays but was also consistently lower than that of Col-0 with mean pollen tube averages 8 HAP for Col-0 = 21 versus *soft1* = 11 versus *oft1*$^{-/-}$ = 1 (Figure 3.17D). These results indicate that *soft1* pollen penetrates through the stigma-style interface more efficiently than *oft1* mutant pollen but are only about half as robust compared to Col-0. In considering the rescued silique length and seed set of the *soft1* mutant, which was not significantly different from Col-0, these data further suggest that pollen tubes do not have to fertilize ovules as robustly as Col-0 pollen to effectively restore the fertility of the plant that were induced by *AtOFT1* loss-of-function in situations where there is no competition with wildtype pollen.

SIV fertilization assays were also performed to assess the penetration behavior of the *soft2* EMS line (Figure 3.18A). These assays revealed that both *soft2* and Col-0 pollen tubes began emerging from the transmitting tract of the style 2 HAP, while *oft1* pollen began appearing 3 HAP (Figure 3.18B). Interestingly, the results of these assays indicated only a slight increase in the number of pollen tubes emerging from the stigma-style interface for *soft2* pollinated *SIV* pistils compared to the *oft1* mutant alone. The number of pollen tubes exiting the bottom of the style for *soft2* was also insignificant across all time points with an average number of 9 PTs for *soft1* and 5 PTs for *oft1* exiting 8 HAP compared to 33 PTs for Col-0 (Figure 3.18C). Additionally, between the 6

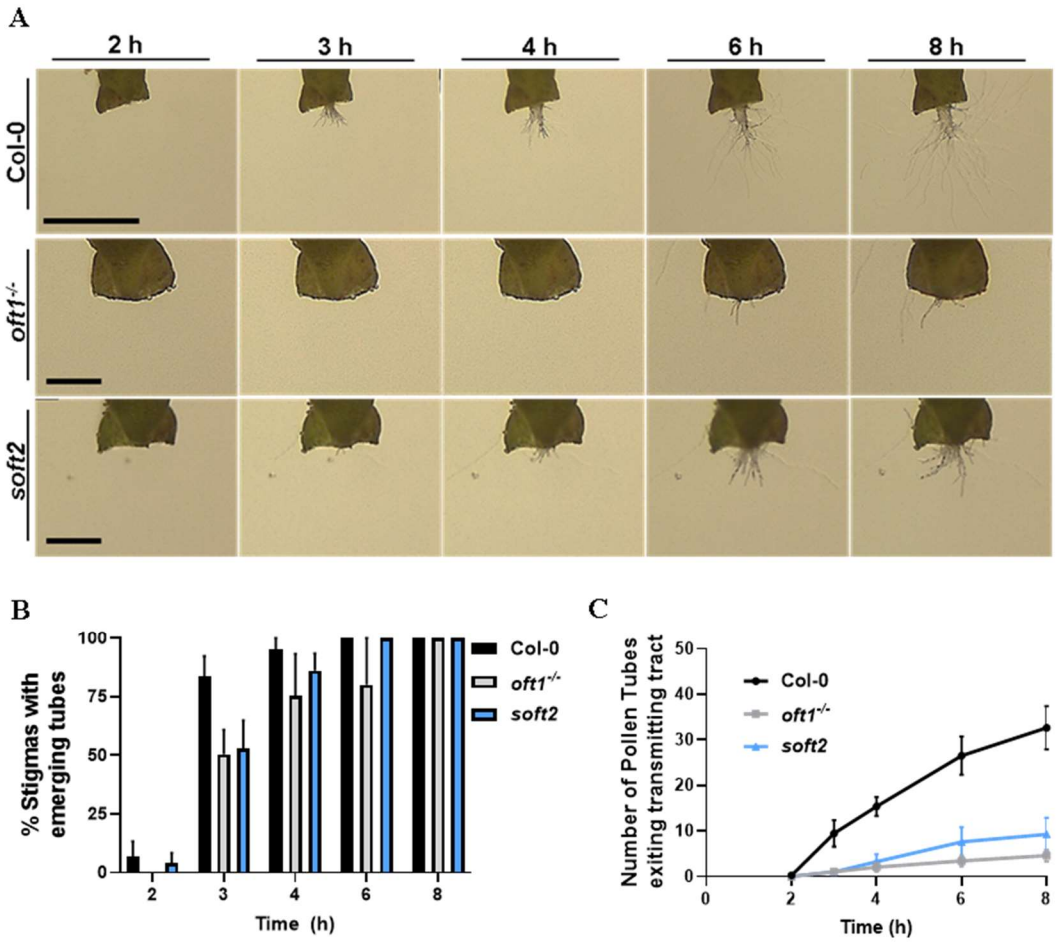

Figure 3.18: *Soft2 in vivo* pollen tube penetration behavior. A, Representative images *SIV* assays showing pollen tube emergence from the bottom of the TT style of mature, emasculated Col-0 pistils pollinated with either wild-type Col-0 (top row) , *oft1*$^{-/-}$ (middle row), or *soft1* pollen (bottom row) over an 8-hour time course. B, Quantification of Col-0 stigmas exhibiting pollen tubes emanating from the TT following pollination with Col-0 (black bars) , *oft1*$^{-/-}$ (gray bars), or *soft1* suppressor pollen (blue bars) homozygous pollen. C, Quantification of the number of pollen tubes emerging from Col-0 stigmas at the indicated time points following pollination with Col-0 (black line) , *oft1*$^{-/-}$ (gray line), or *soft1* suppressor pollen (blue line). Both B and C are means ± SEM (n = 3 independent biological replicates with 5-8 stigmas per genotype per replicate).

to 8 HAP time points, the number of emergent *soft2* pollen tubes seemed to plateau as only a slight increase was observed, while the existing pollen tubes elongated further, suggesting that *soft2* PTs may still have considerable difficulty traversing the stigma-style interface. Taken together, the results of the pollen tube penetration behavior of the suppressor lines indicate that *soft2* is less robust compared to *soft1* in its ability to penetrate through the sigma-style interface, and additionally accounts for the *soft2* silique phenotype not being fully restored back to that of wildtype. Although the silique length and seed set of the *soft1* and *soft2* mutants was greatly increased compared to the *oft1* mutants, their abilities to penetrate through the pistil were only marginally to moderately increased.

XI. Identification of the disrupted genes in *oft1* suppressor lines

To identify gene candidates that were responsible for the increased fertilization efficiency observed in the *soft1* and *soft2* EMS lines, gDNA was extracted from segregating suppressed mutants as well as unsuppressed controls that had been treated with EMS but did not restore the reproductive defects of *oft1* mutants and were sent for paired end Illumina genome resequencing. Bioinformatic processing of each sample was performed by 1) concatenating the forward and reverse sequence reads for both suppressed and unsuppressed control data, 2) assessing the raw data read quality with FastQC, 3) eliminating poor quality reads in Trimmomatic, 4) assessing the quality of the trimmed read data again with FastQC, 5) indexing the quality reads to the *Arabidopsis thaliana* reference genome (arabidopsis.org) with BWA (Burrows–Wheeler Alignment), 6) calculating read coverage and position against the reference genome with bcftools, and then 7) filtering out non-specific SNPs with vcfutils (Andrews, 2010; Bolger *et al.,* 2014;

Li and Durban, 2009; Li *et al.,* 2009; Li, 2011; Danecek *et al.,* 2011). The SNP variant list produced from this analysis produced a list of SNPs present on each of the five Arabidopsis chromosomes for both suppressor lines. The SNPs and their associated alternative allele frequencies were plotted against their position on their respective chromosome to allow for centromeric regions to be identified as well as SNPs in the genomic interval containing each *soft* mutation. SNPs identified in both the suppressor lines and controls were negated. Chromosomal regions of interest that were hypothesized to contain the gene candidate disrupted in the suppressor mutants were predicted to display a bell-shaped curve of individual SNPs plotted across a specific chromosomal region and possess a maximum alternative SNP allele frequency of approximately 0.5 due to these lines being outcrossed to the parental lines (*oft1-1* and *oft1-3)* and segregating 50:50. A single chromosome-specific region exhibiting these expected characteristics was identified for both *soft1* and *soft2. Soft1* showed an interval spanning on chromosome 1 (position 3025334-7675677 bp), while *soft2* displayed a region on chromosome 5 (position 3790766-7498566 bp). These regions were further examined using SnpEff (Cingolani *et al.,* 2012) to predict the effects of the genetic variants on the coding regions contained within the chromosomal interval of interest, which produced a defined list of gene candidates that included the specific amino acid variant induced by EMS, the variant frequency, the gene ID, and the predicted consequence of each mutation on the associated gene.

EMS is an alkylating agent that induces guanine to adenine and cytosine to thymine genome alterations following DNA replication, and this knowledge could be further applied to reduce the list of gene candidates. Additionally, the list of candidates

was narrowed to include only protein coding regions with an approximate expected alternative allele frequency of 0.5. The gene candidates were also filtered to only include SNPs that induced a missense or nonsense mutation in the protein sequence. The final group of gene candidates produced by this processing method narrowed the relevant possible mutations to approximately 20 candidate genes of interest for both *soft1* and *soft2.* A knowledge-based approach was then implemented to identify the best gene candidate in each suppressor line by prioritizing nonsense mutations over missense mutations and querying the expression profiles of candidate genes produced for *soft1* and *soft2*. The *soft1* gene candidate list contained only proteins possessing a SNP that induced a nonsense mutations, and shockingly, a nonsense mutation in another Arabidopsis putative POFT family member, *At1g11990,* was selected as the target candidate gene for this EMS line. The specific mutation in *At1g11990* induced by EMS treatment was identified as a cytosine to thymine alteration at the 1310th bp of its nucleotide sequence that created an Alanine 434→Valine nonsense mutation within its putative catalytic domain, which we postulated would disrupt the function of the At1g11990 protein. The *soft2* mutant contained various nonsense mutations as well as one SNP-induced missense candidate in the *GALACTURNOSYL TRANSFERASE 14* (*AtGAUT14; At5g15470*) gene. *AtGAUT14* was selected as the target candidate gene disrupted in the *soft2* EMS line and possessed a cytosine to thymine SNP at the 165th base pair position within its nucleotide coding sequence creating a Leucine 55→STOP missense mutation. These gene candidates were chosen for *soft1 and soft2* as a similar regulatory mechanism of mutant phenotype suppression had previously been reported for two other Arabidopsis putative POFT family members (Neumetzler *et al.,* 2012, Verger *et al.,* 2016). Thus, we

hypothesized that our bioinformatic and knowledge-based approaches to identify the second disrupted genes in the *soft1* and *soft2* EMS lines were correct due to this workflow producing a list of logical gene candidates, and we further postulated a similar mechanism of suppression was potentially playing out in the suppressor mutants that allowed for suppression of the *oft1* mutant reproductive phenotype.

XII. Verification of the hypothesized disrupted genes in *oft1* suppressor lines

To verify that our hypothesis that *At1g11990* was the disrupted gene in *sotf1* and that *AtGAUT14 (At3g25140)* was the disrupted gene in *soft2,* exonic T-DNA mutants were acquired and used to create double knockout mutants in *AtOFT1* and *At1g11990* or *AtGAUT14*. The mutant phenotype *At1g11990* had not been previously investigated, so we propagated an exonic T-DNA mutant for this gene, *SAIL_1174_D07*, to homozygosity and characterized its silique morphology, which did not display any overt phenotypic abnormalities. T-DNA exonic mutants for *AtGAUT14* had been previously investigated and both the *gaut14-1 (SALK_000091)* and *gaut14-2 (SALK_029525)* mutants were reported to display no overt phenotypic abnormalities (Wang, *et al.,* 2013). However, Wang and colleagues demonstrated that the *GALACTURONOSYLTRANSFERASE 13* (*AtGAUT13; At3g01040)* gene was redundant with *AtGAUT14,* as they shared high amino acid sequence homology (93% identical) and their single mutants alone did not display overt defects, but their double T-DNA mutant, *gaut14-1*$^{-/-}$*;gaut13-1*$^{-/-}$ *(SALK_122602),* displayed severe pollen tube-specific abnormalities that specifically compromise plant reproduction, similar to *oft1* mutants (Wang *et al.,* 2013). In taking this previous information into consideration, the *gaut13-1*

T-DNA line was included in our creation of double mutant lines to evaluate these gene candidates.

To investigate genetic interactions between *oft1* and the genes outlined above, *oft1-3*$^{-/-}$ pistils were emasculated and pollinated with either homozygous *SAIL_1174_D07* or *gaut14-1* pollen. The resulting F_1 progeny were allowed to self-pollinate, and F_2 plants were genotyped by PCR.. The double mutant lines, *oft1-2*$^{-/-}$*; SAIL_1174_D07*$^{-/-}$ and *oft1-3*$^{-/-}$*; gaut14-1*$^{-/-}$*,* were evaluated at reproductive maturity to assess their silique length and seed set. The *oft1-2*$^{-/-}$*; SAIL_1174_D07*$^{-/-}$ double mutant silique seed set was no different from that of the *oft1-2*$^{-/-}$ mutant alone indicating that this gene may be redundant with another Arabidopsis putative POFT family member, or the gene candidate predicted for the *soft1* EMS line was incorrect (Figure 3.19). Mature siliques were collected from the double mutant created for the *soft2* EMS line, *oft1-3*$^{-/-}$*; gaut14-1*$^{-/-}$, and silique length quantified (Figure 3.19B). Excitingly, there was no difference in silique length between this double mutant and Col-0 (Figure 3.20A-B). Mature siliques from this double mutant line were then collected and placed in ethanol to examine seed set (Figure 3.20C), which was comparable to that of wildtype Col-0 controls, however, were still not completely restored (Figure 3.20D). These results indicated that *AtGAUT14* was the gene disrupted in the *soft2* EMS line. Nonetheless, *AtGAUT14* sufficiently rescued the mutant silique phenotype of *oft1* mutants and was used for further investigation.

To assess the ability of the *oft1-3*$^{+/-}$*; gaut14-1*$^{-/-}$ line to transmit the *oft1*$^{-}$ mutant allele, mature pollen from three independent lines were used to pollinate emasculated *ms1* pistils. The outcrossed seed was collected and sown on MS medium containing BASTA for the *oft1-3*$^{-}$ associated T-DNA. This experiment revealed an increased

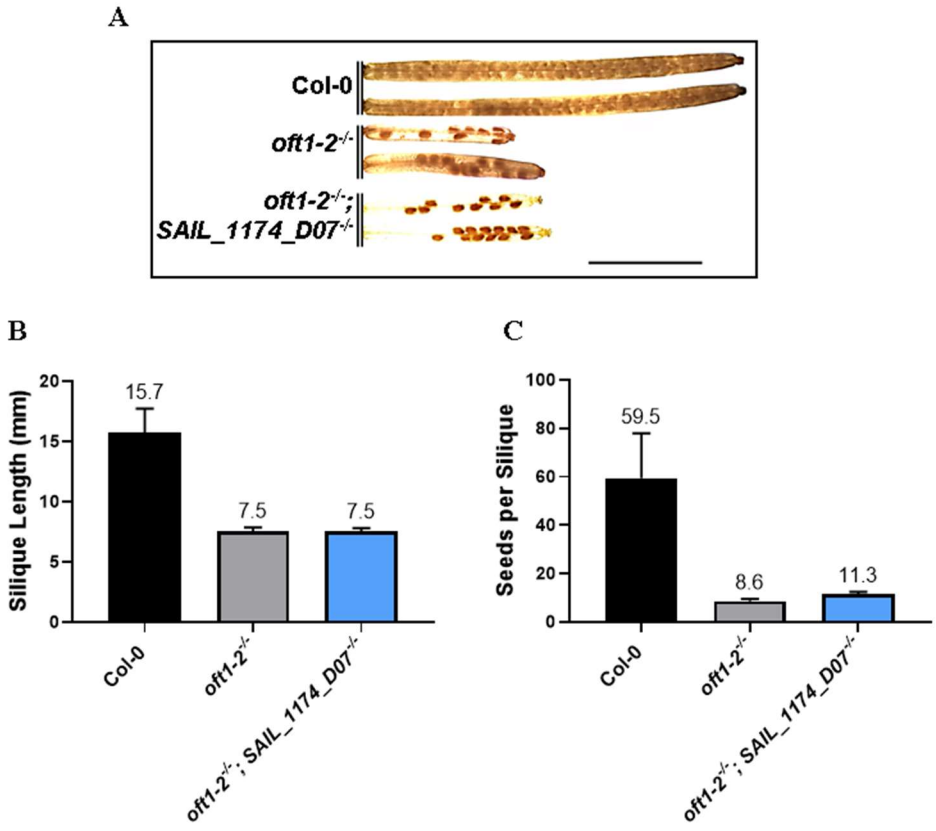

Figure 3.19: Silique morphology of the *soft1* double T-DNA mutant. Fully developed siliques were harvested from equal age 6-week-old homozygous recessive exonic T-DNA double mutant *oft1-2*$^{-/-}$; *SAIL_1174_D07*$^{-/-}$ lines as well as control genotypes, Col-0 and *oft1-2*$^{-/-}$. A, Image of siliques cleared in 70% (v/v) ethanol as described in Chapter 2. Representative siliques from each genotype are shown, and black scale bars = 5 mm. B, Quantification of silique lengths graphed as mean of data set per genotype ± range. C, Quantification of seeds per individual silique genotype graphed as mean of data set per genotype ± range. For both B and C, data are means calculated over 1 biological replicate (n =11-25 siliques per line) and Col-0 represented by black bar, *oft1-2*$^{-/-}$ by gray bar, and 2 independent *oft1-2*$^{-/-}$; *SAIL_1174_DO7*$^{-/-}$ double mutant lines are depicted by a blue bar in each graph with mean values per genotype denoted above range bar.

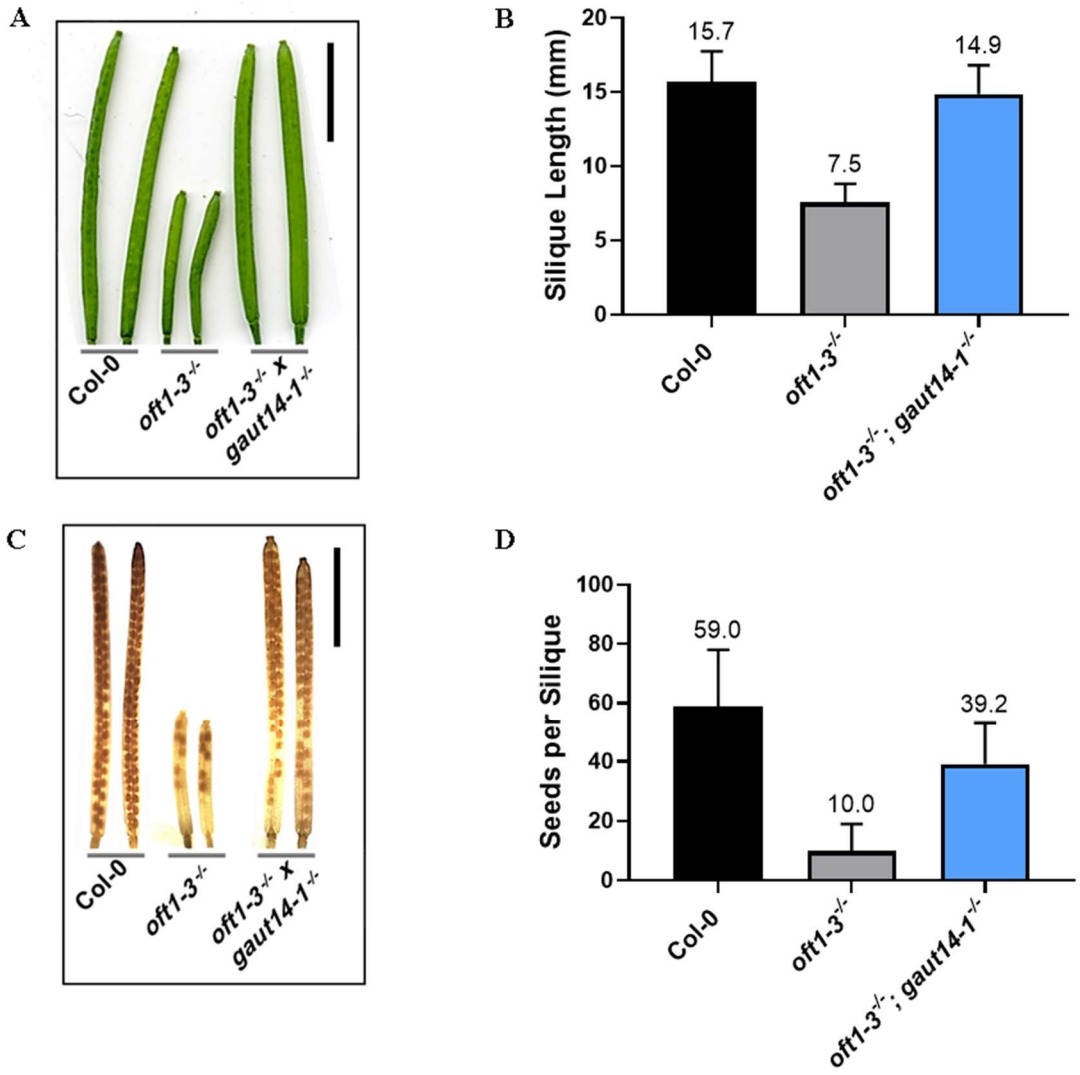

Figure 3.20: *AtGAUT14* suppresses the fertility defects of *oft1* mutant lines. Fully developed siliques were harvested from equal age 6-week-old homozygous recessive exonic T-DNA double mutant *oft1-3*$^{-/-}$ *x gaut14-1*$^{-/-}$ lines as well as control genotypes, Col-0 and *oft1-3*$^{-/-}$. A, Image of fresh, whole siliques not yet cleared. B, Quantification of silique lengths and bar graph is representative of means ± range with mean values denoted above respective range bar. C, Image of siliques cleared in 70% [v/v] ethanol as described in Chapter 2. Representative siliques from each genotype are shown. Scale bars = 5 mm and 11-13 siliques analyzed per line replicate per genotype in both A and C. D, Quantification of seed per silique and bar graph is representative of mean ± range with mean values denoted above respective range bars.

transmission efficiency of 0.1, which represented a significant increase compared to the observed transmission efficiency of *oft1-3*$^{+/-}$ pollinated Col-0 pistils of 5.3x10^{-4} (Figure 3.21). Nonetheless, this cross did not fully restore the transmission efficiency to 50% predicted by Mendelian inherence, further suggesting that the *AtGAUT13* gene may be interfering with inheritance of the *oft1* mutant allele as well as this double mutant's ability to fully restore the seed set to that of wildtype.

XIII. Establishing a proximity labeling system to identify transient protein-protein interactions

As an additional means of identifying proteins that stably or transiently interact with AtOFT1 and to gain further insight into the pathways that AtOFT1 may be participating in, we created a BioID-based proximity labeling system in the *oft1-2*$^{-/-}$ background. Three plasmids were kindly created and donated by Dr. Jeffrey Harper (University of Nevada, Reno). These plasmids were constructed using the pGreen2 vector backbone (Hellens *et al.,* 2000) and included the *AtOFT1* coding sequence translationally fused to YELLOW FLUORESCENT PROTEIN (YFP) and the BirA biotin ligase from *Escherichia coli* expressed under the *Ubiquitin 10* promoter. The BirA coding sequence additionally contains a site-specific amino acid modification, Arginine118→Glycine, which facilitates its promiscuity to biotinylate any protein within 10 nm of the expressed OFT1-YFP-BioID fusion protein (Liu *et al.,* 2018). Two other vectors constructed using the same vector with modifications were implemented as controls. The *UBQ10::YFP-BioID* vector lacked the coding sequence for *AtOFT1*, while the *UBQ10::OFT1*^{R260A}*-YFP-BioID* construct contained a site-specific amino acid alteration, Arginine260→Alanine, in the AtOFT1 coding sequence, which was previously shown to

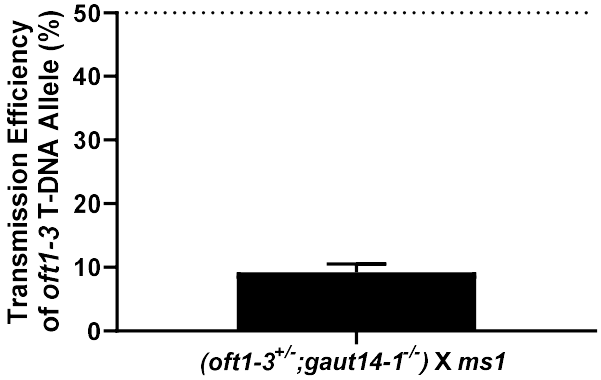

Figure 3.21: Increased transmission efficiency of the *oft1-3*$^{-}$ T-DNA allele by knockout of *AtGAUT14*. Quantification was performed by crossing pollen from three independently verified, equal-aged ♂*oft1-3*$^{+/-}$*;gaut14-1*$^{-/-}$ double mutant lines with *Male Sterile 1 (ms1)* immaculate pistils. Mature seed produced from each cross was plated on glufosinate-ammonium (Basta®)-containing medium due to the herbicide specificity associated with the *oft1-3* mutant T-DNA allele. Seedlings were grown for 7 days under long-day-light condition before inheritance of the *oft1-3*$^{-}$ allele was quantified by counting the total number of seedlings resistant and sensitive to the herbicide per plate per cross. Bar graph represent the mean transmission efficiencies (TE) ± SEM across 16 independent crosses with ≥ 79 seedlings per plate. TE was calculated by dividing the number of resistant seedlings per plate by the total number of seedlings per plate and is represented in graph as a percent. Dashed line in graph depicts expected TE of a heterozygous cross.

abolish AtOFT1 activity in Arabidopsis (Smith *et al.,* 2018a). All three plasmids were individually introduced into the *oft1-2*$^{-/-}$ background and successful isolation of independent lines for *oft1-2*$^{-/-}$*;UBQ10-OFT1-YFP-BioID*, *oft1-2*$^{-/-}$*;UBQ10-OFT1*^{R260A}*-YFP-BioID,* and *oft1-2*$^{-/-}$*;UBQ10- YFP-BioID* transgenic plant constructs allowed for evaluation of this system as an experimental approach to identify other proteins that interact with AtOFT1.

To evaluate the effects of these plasmids in the *oft1-2*$^{-/-}$ background, *oft1-2*$^{-/-}$*;UBQ10-OFT1-YFP-BioID*, *oft1-2*$^{-/-}$*;UBQ10-OFT1*^{R260A}*-YFP-BioID, oft1-2*$^{-/-}$*;UBQ10-YFP-BioID*, as well as Col-0 and *oft1-2*$^{-/-}$ seed was sown out, transplanted to soil, PCR genotyped to verify the transgene, and grown to sexual maturity before mature siliques were harvested from each of these lines to assess silique length (Figure 3.22A). Analysis of the silique lengths from each line demonstrated that the *oft1-2*$^{-/-}$*;UBQ10-OFT1-YFP-BioID* line was not significantly different in length compared to wildtype Col-0, while the silique lengths of the control lines, *UBQ10-OFT1*^{R260A}*-YFP-BioID* and *oft1-2*$^{-/-}$*;UBQ10-YFP-BioID,* maintained the same length as the *oft1-2*$^{-/-}$ line (Figure 3.22B). Clearing mature siliques from all three BioID transgenic lines as well as *oft1-2*$^{-/-}$ and Col-0 controls lines in ethanol revealed the seed set of the mature siliques (Figure 3.22C). In quantifying the seed sets of each line, the active *oft1-2*$^{-/-}$*;UBQ10-OFT1-YFP-BioID* displayed a seed set that was not significantly different from that of Col-0, indicating that it had effectively rescued the seed set of the *oft1-2*$^{-/-}$ background with its functional copy of *AtOFT1* (Figure 3.22D). Evaluating the seed sets of *UBQ10-OFT1*^{R260A}*-YFP-BioID* and *oft1-2*$^{-/-}$*;UBQ10- YFP-BioID* transgenic lines showed that they did not rescue the silique morphology of *oft1-2*$^{-/-}$ and were not significantly different from the original *oft1*

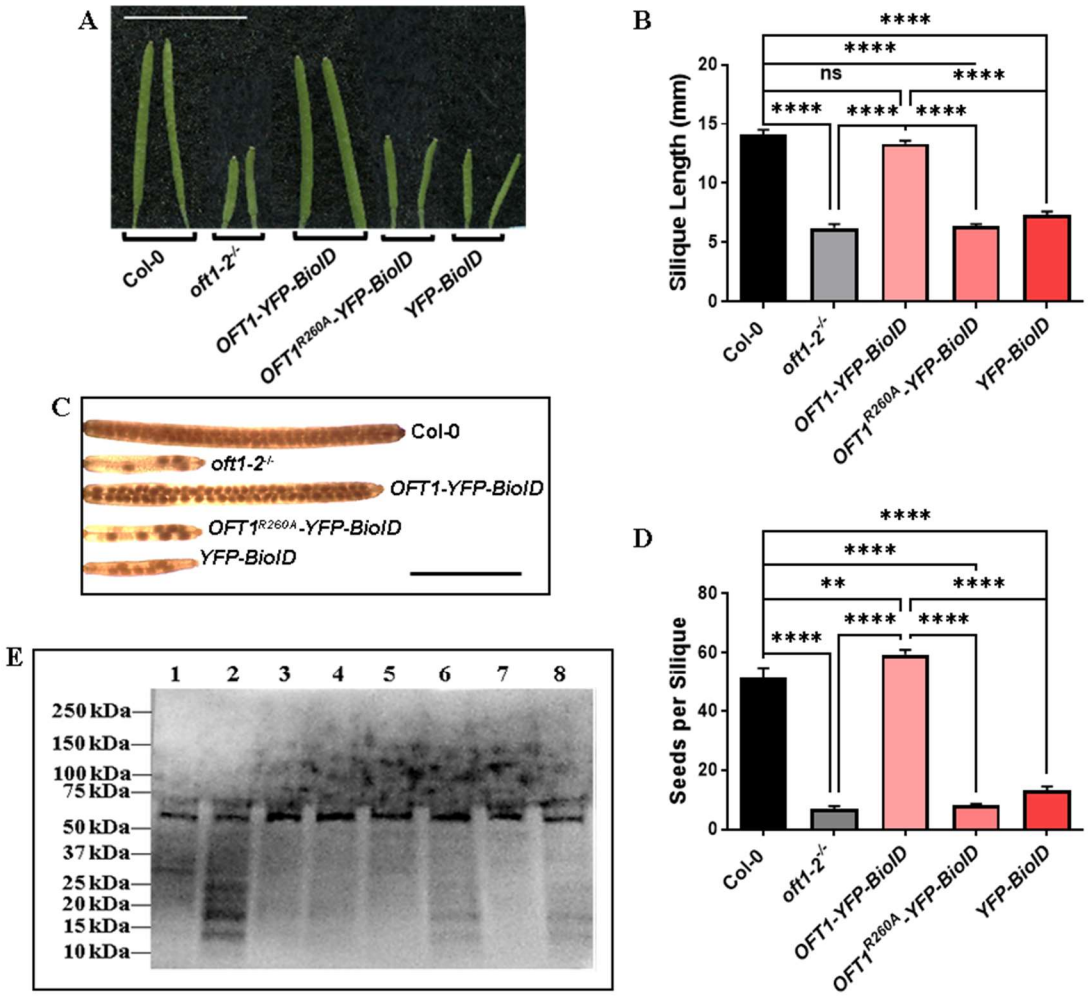

Figure 3.22: Establishment of a proximity labeling system for identification of protein partners of AtOFT1. Fully developed siliques from 6-week-old plants were harvested from the indicated genotypes and the three transgenic BioID constructs: 1) The active OFT1-YFP-BioID, 2) the catalytically dead AtOFT1(R2060A) control construct, and 3) the YFP-BioID empty vector control . A, Picture of fresh, whole siliques not yet cleared. Scale bar= 10mm. B, Quantification of 6-week-old silique lengths from Col-0 (black bar), *oft1-2* control (dark gray bar), and the three transgenic BioID constructs (pink to red shaded bars). Bar graph represents mean ± SEM across three independent biological replicates. C, Representative images of mature siliques cleared in 70% [v/v] EtOH to reveal seed set of each indicated genotype. Bar=5mm. D, Quantification of the seeds produced per indicated silique genotype with graph representing mean ± SEM across three independent biological replicates. One-way ANOVA analysis (multiple comparisons) are shown for both B and D (****, $P \leq 0.0001$). NS= no statistically significant difference (ns) difference. E, Streptavidin immunoblot of 10-day old seedlings in the absence of exogenously supplemented biotin of each transgenic line BioID construct and control *oft1-2*$^{-/-}$ seedlings that was developed for 5 seconds by chemiluminescence. Lane 1: *oft1-2*$^{-/-}$*;UBQ10::OFT1-YFP-BioID* soluble fraction protein (SP), Lane 2: *oft1-2*$^{-/-}$*;UBQ10::OFT1-YFP-BioID* Membrane Protein fraction (MP), Lane 3: *oft1-2*$^{-/-}$*;UBQ10::OFT1*^{R260A}*-YFP-BioID* SP, Lane 4: *oft1-2*$^{-/-}$*;UBQ10::OFT1*^{R260A}*-YFP-BioID* MP, Lane 5: *oft1-2*$^{-/-}$*;UBQ10::YFP-BioID* SP, Lane 6: *oft1-2*$^{-/-}$*;UBQ10::YFP-BioID* MP, Lane 7: *oft1-2*$^{-/-}$ SP, and Lane 8: *oft1-2*$^{-/-}$ MP.

mutant background, as expected (Figure 3.22D). These results suggested that the BioID proximity labeling system had been successfully integrated into the *oft1* mutant background for detection of protein interaction partners with AtOFT1.

To further validate the BioID proximity labeling system, we aimed to identify natively biotinylated proteins in these developed lines to establish a baseline for this proximity labeling system. This analysis was performed by extracting total protein from 7-day-old seedlings grown on MS media that was not supplemented with biotin from all three BioID transgenic lines as well as *oft1-2*$^{-/-}$ seedlings. Differential centrifugation was used to fractionate soluble and insoluble protein for each sample, and equal amounts of each protein per line were run on an SDS-PAGE gel and immunoblotted using a streptavidin conjugated HRP antibody. Following chemiluminescent development of the probed Western membrane, it was apparent that many natively biotinylated proteins were present across all lines analyzed (Figure 3.22E). Interestingly, membrane fractions produced more signal compared to their equivalent genotype soluble protein fractions, suggesting membrane proteins contain more biotin modifications. Additionally, the signal produced from the active OFT1-YFP-BioID expression constructs was more robust than that of the control lines, indicating that the active form of this plasmid was utilizing endogenously supplied biotin to label proteins in both fractions and was functional. Moreover, the active *oft1-2*$^{-/-}$*;OFT1-YFP-BioID* expression line produced the greatest signal across all fractions with the highest signal coming from the membrane fraction of this expression line, again indicating that this construct was functionally active and utilizing endogenous free biotin to label proteins. Overall, these results further validate the transgenic lines established for identification of other protein-protein interactions with

AtOFT1 in Arabidopsis using the BioID proximity labeling system providing a reliable platform for future identification of AtOFT1 protein partners in its native organism and facilitating insights into the pathway this protein participates in.

XIV. Catalytically important POFT1 residues are functionally important for AtOFT1

To investigate the activity of AtOFT1 the amino acid sequence similarities between previously characterized metazoan POFT1s and AtOFT1 were further examined. Initially, we compared the conservation of AtOFT1 amino acid residues with known metazoan POFT1 residues that participate in the POFT1 active site. The X-ray crystal structure of *C. elegans* POFT1 (CePOFT1; PDB ID 3ZY5) was previously determined in the presence of GDP-Fucose (GDP-Fuc), and this crystal structure illustrates the network of amino acid residues that participate in CePOFT1 substrate selectivity as well as catalysis (Figure 3.23A) (Lira-Navarette et al., 2011). The crystal structure of CePOFT1 revealed that the β-phosphate and fucose moieties of GDP-Fuc are coordinated by a critical arginine residue, CePOFT1^{R240}. CePOFT1^{N43} was also shown to position the hydroxyl group of the incoming protein substrate in proximity to the fucosyl moiety of GDP-Fuc, hydrogen bond to the fucose ring, and interact with the α-phosphate of GDP-Fuc. CePOFT1^{R40} interacts with the ribose ring of GDP-Fuc and also hydrogen bonds to the fucose ring. Finally, CePOFT1^{D244} was implicated as a residue which potentially stabilizes the GDP-Fuc bound conformation of the enzyme. Importantly, *in vitro* assays indicated that each of these residues are critical for POFT activity and GDP-Fuc binding (Lira-Navarette *et al.,* 2011; Figure 3.23A). Amino acid sequence alignments between AtOFT1 and metazoan POFT1s revealed that many of these critical residues are conserved in AtOFT1 (Figure 3.23B). AtOFT1^{R260} aligned with CePOFT1^{R240}, the critical

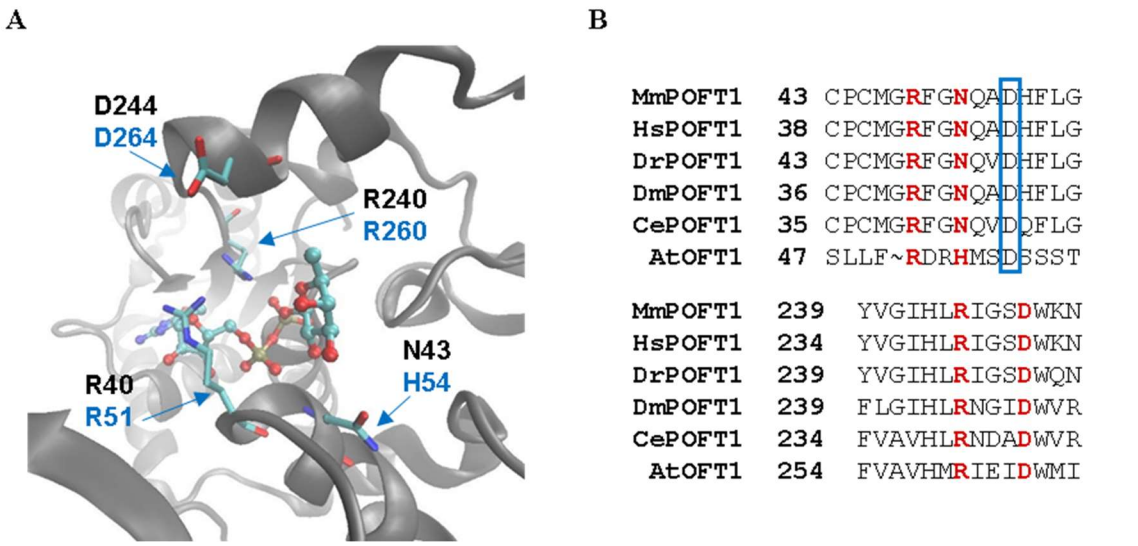

Figure 3.23: Structure-function analysis of AtOFT1 putative catalytic residues. A, The active site of *C. elegans* POFT1 bound to GDP-Fucose (PDB ID 3ZY5) is shown with critical catalytic residue indices in black font, and the corresponding AtOFT1 residues shown in blue font. B, Sequence alignments of the AtOFT1 N-terminal (upper panel) and C-terminal (lower panel) regions compared to multiple metazoan POFT1s. Critical catalytic residues are highlighted in red, and the beginning residues for each alignment segment are indicated for reference. An aspartic acid residue used to propose an alternative alignment of the N-terminal domain is boxed in blue.

arginine residue required for catalysis. Similarly, conserved residues corresponding to CePOFT1^{R40} and ^{D244} were identified (AtOFT1^{R51} and ^{D264}). Interestingly, CePOFT1^{N43} was not conserved in AtOFT1, and this residue position contained a histidine substitution. Based on the hydrogen bonding function of this residue in the CePOFT1 mechanism (Lira-Navarette *et al.,* 2011), we postulated that AtOFT1^{H54} could serve a similar function.

To functionally assess the importance of these conserved catalytic residues in AtOFT1 (R51, H54, R260, and D264), site-directed mutagenesis was performed to individually alter these residues in the vector *pUBQ10::OFT1-GFP*. Expression of each site-directed mutant was verified by RT-PCR and by confocal microscopy of *in vitro* germinated pollen tubes to confirm proper subcellular localization of these site-directed mutants (Figure 3.24A-B). The functional importance of each residue was assessed by evaluating the ability of each mutant construct to complement the *oft1* seed set phenotype (Figure 3.24C). When residues R51, H54, R260, and D264 were individually mutated to encode alanine, seed set was not significantly restored compared to the homozygous *oft1* mutant background, which suggested these residues contribute important structural or catalytic roles in AtOFT1. Similar to CePOFT1, an AtOFT1^{R260K} mutant was also unable to complement the *oft1*$^{-/-}$ seed set phenotype, which indicated this residue was fundamentally important in AtOFT1 catalysis due to its stringent requirement for an arginine residue at this position. Interestingly, when AtOFT1^{H54} was mutated to Asparagine, the aligned and catalytically relevant residue in CePOFT1, full complementation of the mutant seed set phenotype was observed. Overall, these observations demonstrate the functional importance of catalytically conserved residues

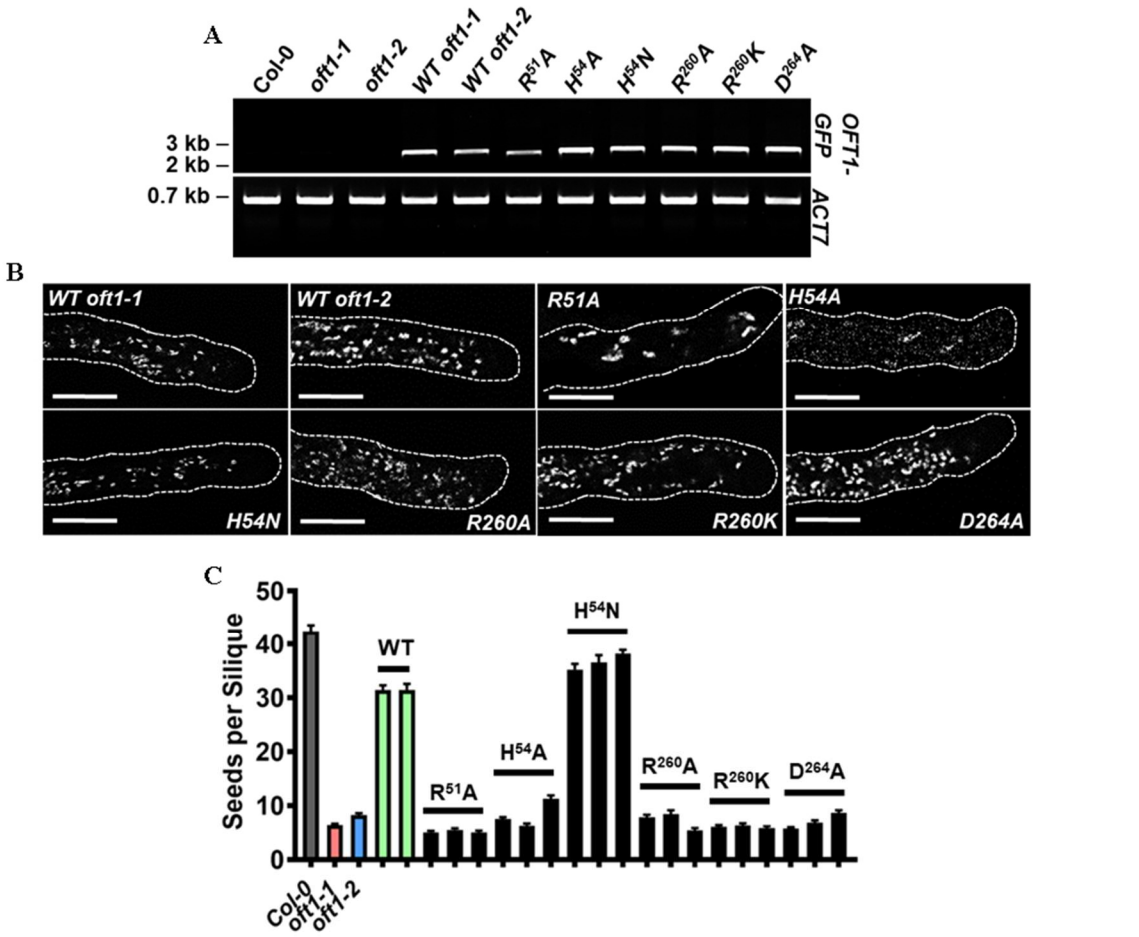

Figure 3.24: AtOFT1 key catalytic residue site-directed mutant construct lines *in vivo* expression verification and enzymatic importance. A, Total RNA was extracted from 7-day-old seedlings of the indicated genetic background or expressing the indicated site-directed mutant constructs of *AtOFT1* under the control of the *UBQ10* promoter. Isolated RNA was converted to cDNA and probed for the expression of GFP-tagged *OFT1* transgenes (top) and *ACT7* (bottom) as described in Chapter 2. The positions of relevant molecular weight markers are indicated to the left of each gel. B, Pollen from transgenic plants expressing *AtOFT1-GFP* or the indicated site-directed mutant construct of *AtOFT1-GFP* under the control of the *UBQ10* promoter were germinated for 1.5 h on separate PGM-agarose microscope slides and visualized by confocal microscopy at 60X magnification. AtOFT1-GFP fluorescence patterns are shown in grayscale images, and the outline of each pollen tube is shown as a dashed white line. Scale bars in all images indicate 10 µm. C, Seed set in *oft1-1*$^{-/-}$ plants expressing the indicated site-directed mutant constructs of *AtOFT1* (black bars). Seed sets of Col-0 (gray bar), *oft1-1*$^{-/-}$ (red bar), *oft1-2*$^{-/-}$ (blue bar), and *oft1-1*$^{-/-}$ lines expressing wild-type *AtOFT1* (green bars) are shown for reference. Data are means ± SEM (n = 29–71).

between CePOFT1 and AtOFT1, which additionally suggests these enzymes may share a conserved biochemical mechanism.

To determine if these four key catalytic residues are conserved in other Arabidopsis putative POFT family members, the amino acid sequences of all 39 proteins were aligned in ClustalX and a tree of evolutionary maximum likelihood was created in MEGA X (Figure 3.25 left). The resulting alignment indicated 4 predicted family members are conserved with AtOFT1^{R51}, and 11 additional family members display a residue of similar chemical composition (Lys/K or His/H) at this position (Figure 3.25 right). Six family members share a His (H) or Asn (N) residue aligning with AtOFT1^{H54} and an additional 9 members displayed a residue of similar chemical composition at this site (Lys, Asp, or Gln). Asparagine was considered a conserved residue at this position as it **w**as shown to effectively complement the *oft1* mutant phenotype when the *UBQ10::AtOFT1^{H54N}* site-directed mutant transgene was present (Figure 3.24C), and potentially suggests the amino group substituent present on these alternative residues may facilitate a similar molecular function. The most conserved key catalytic residue across the Arabidopsis hypothetical POFT family was with AtOFT1^{R260}, as 35 other members displayed conservation of an arginine residue aligning with this position, representing approximately 92.3% conservation in this amino acid in the Arabidopsis putative POFT family. Furthermore, no substitutions for amino acids of any similar chemical composition or gaps in the alignment were determined at this position for the 3 sequences that did not contain an arginine at this position, indicating this residue may be extremely important for Arabidopsis POFTs as this residue is fundamentally important for both metazoan POFT1 and AtOFT1 catalysis (Lira-Navarette *et al.,* 2011; Smith *et al.,* 2018a).

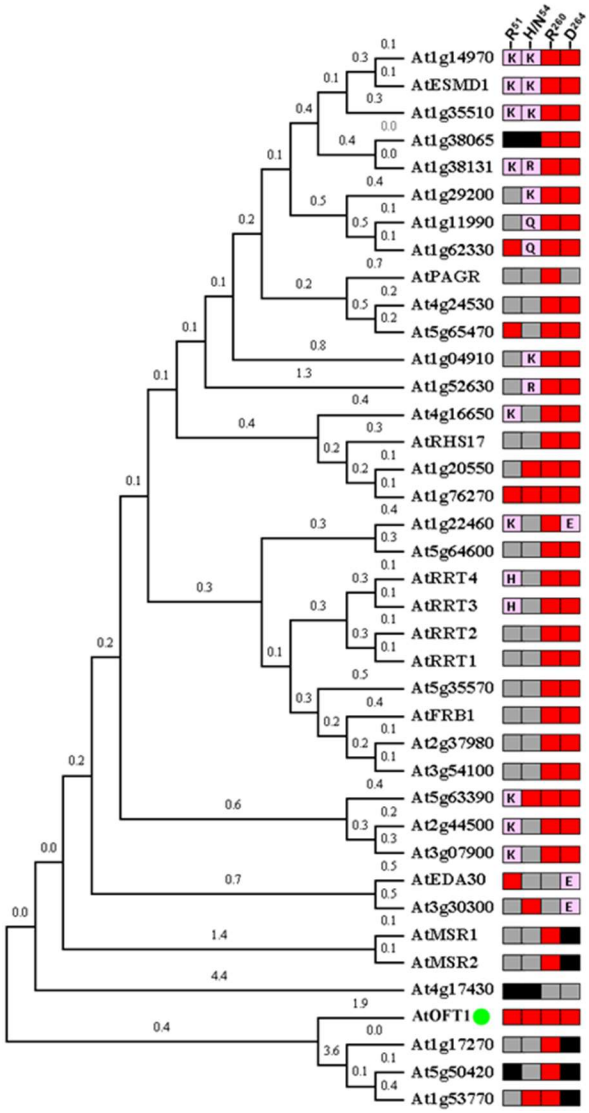

Figure 3.25: Sequence similarity and catalytic residue conservation between the Arabidopsis putative POFT family. Multisequence alignment was performed on all 39 *Arabidopsis thaliana* hypothesized POFT family members in ClustalX2 and MEGA X was used to perform the heuristic search by applying Neighbor-Join and BioNJ algorithms to a matrix of pairwise distances estimated using the JTT (Jones–Thornton–Taylor) model and then selecting the topology with superior log likelihood value. A total of 966 positions were in the final dataset. The evolutionary history was inferred by using the Maximum Likelihood method and JTT matrix-based model. The tree with the highest log likelihood (-39803.86) is shown, and a green dot denotes the location of AtOFT1 (left panel). The ClustalX2 multisequence alignment results were further used to determine sequence-specific conservation in the 4 key catalytic residues shown to be critical for both metazoan POFT1s and AtOFT1(R^{51}, H/N^{54}, R^{260}, D^{264}) in other hypothesized Arabidopsis POFT members (right panel). Residue position relative to AtOFT1 is denoted at the top of boxes (top right panel), and conservation per sequence for the indicated residue is illustrated by color-coded boxes adjacent to the corresponding sequence ID on tree. Red box indicates complete residue conservation, pink box with one-letter amino acid code indicates a residue with similar chemical composition is retained at the position, gray box denotes a non-conserved residue, and black box indicates a gap in the sequence at the specific residue position within the multisequence alignment.

Additionally, an astonishing 28 Arabidopsis putative POFT family members possessed an aspartic acid residue aligning with AtOFT1^{D264} , and 3 members maintained a glutamic acid at this position. Conservation in this critical catalytic aspartic acid represents ~74.4% total residue conservation at this site within the Arabidopsis POFT family, indicating this amino acid may also be fundamentally important for facilitating catalysis in other Arabidopsis POFT family members akin to CePOFT1^{R244} and AtOFT1^{R260} (Lira-Navarette *et al.,* 2011; Smith *et al.,* 2018a; Smith *et al.,* 2018b). Altogether, At4g17430 was the only sequence that did not demonstrate any conservation in the 4 residues assessed, while At1g76270 was the only member other than AtOFT1 that possessed complete conservation in all residues. Furthermore, the majority of the Arabidopsis putative POFT family (24 members) were conserved in 2 out of the 4 catalytic residues investigated, 8 members were conserved at only one residue position, and 4 members demonstrate conservation in 3 of 4 catalytic residues. These results suggest that other putative members of the Arabidopsis POFT family are more likely to maintain key catalytic amino acids known to facilitate metazoan POFT1 and AtOFT1 catalysis, and further hints that these residues may also play fundamental roles in maintaining the catalytic activity in other Arabidopsis family members.

XV. Structure-function investigation of the Arabidopsis POFT family and metazoan POFT1s

To more clearly define AtOFT1's conservation with metazoan POFT1s, *in silico* tertiary structure prediction was performed by imputing the full length 445 amino acid sequence of AtOFT1 into RaptorX *de novo* structural prediction software (raptorx.uchicago.edu; Xu *et al.,* 2021; Xu, 2019; Xu and Wang, 2019; Wang *et al.,*

2017a; Wang *et al.,* 2017b, Wang *et al.,* 2018). Five potential models for AtOFT1 were generated, and model 2 was selected for analysis as it had the lowest RMSD(Å) (root-square-mean deviation) score of 6.6193 and residue resolution range of 0.34-25.85Å (Figure 3.26). The putative structure of AtOFT1 begins with a poorly predicted (Å>3) 65 aa long segment encompassing a N-terminal disordered region followed by a 46.04 Å long α-helix that elongates into another disordered segment. From amino acids 66-389, the structure is well defined (Å<3), and this region takes on the typical characteristics of a GT-B type fold topology with defined N- and C-terminal domains (α1-α5/β1-β4 and α6-α9/β5-β7) that adopt a Rossmann-like fold architecture, as the central β-sheets are surrounded on both sides by α-helices. The structure further elucidates at least 3 disulfide bridges. Cys^{19} and Cys^{20} form the first disulfide bridge in α1, which is considered an unusual bond that is a signature of metazoan POFT1 structure (Lira-Navarrete *et al.,* 2011) (Figure 3.26). Cys^{90} on β6 and Cys^{135} on α3 form the second putative disulfide bridge, and the third bond is formed between Cys^{269} and Cys^{135} within α7 where the helix becomes slightly disordered creating a loop region.

To further investigate the structural similarities between AtOFT1 and metazoan POFT1s, the protein sequence for AtOFT1 was assessed in Expasy SWISS-MODEL (swissmodel.expasy.org) as a second means of evaluating the observed tertiary structure conservation (Waterhouse *et al.,* 2018). AtOFT1 was queried against known protein structures, and 9 representative model templates of known proteins with a GMQE (Global Model Quality Estimation) score ≥ 0.3 were determined , which included the 4 structures of CePOFT1 (PDB ID 3ZY4.1.A, 3ZY3.2.A, 3ZY2.1.A, 3ZY3.1), 3 from MmPOFT1 (PDB ID 5KXQ.1.A, 5KY7.1.A, 5KY0.1.A), and 2 from HsPOFT1

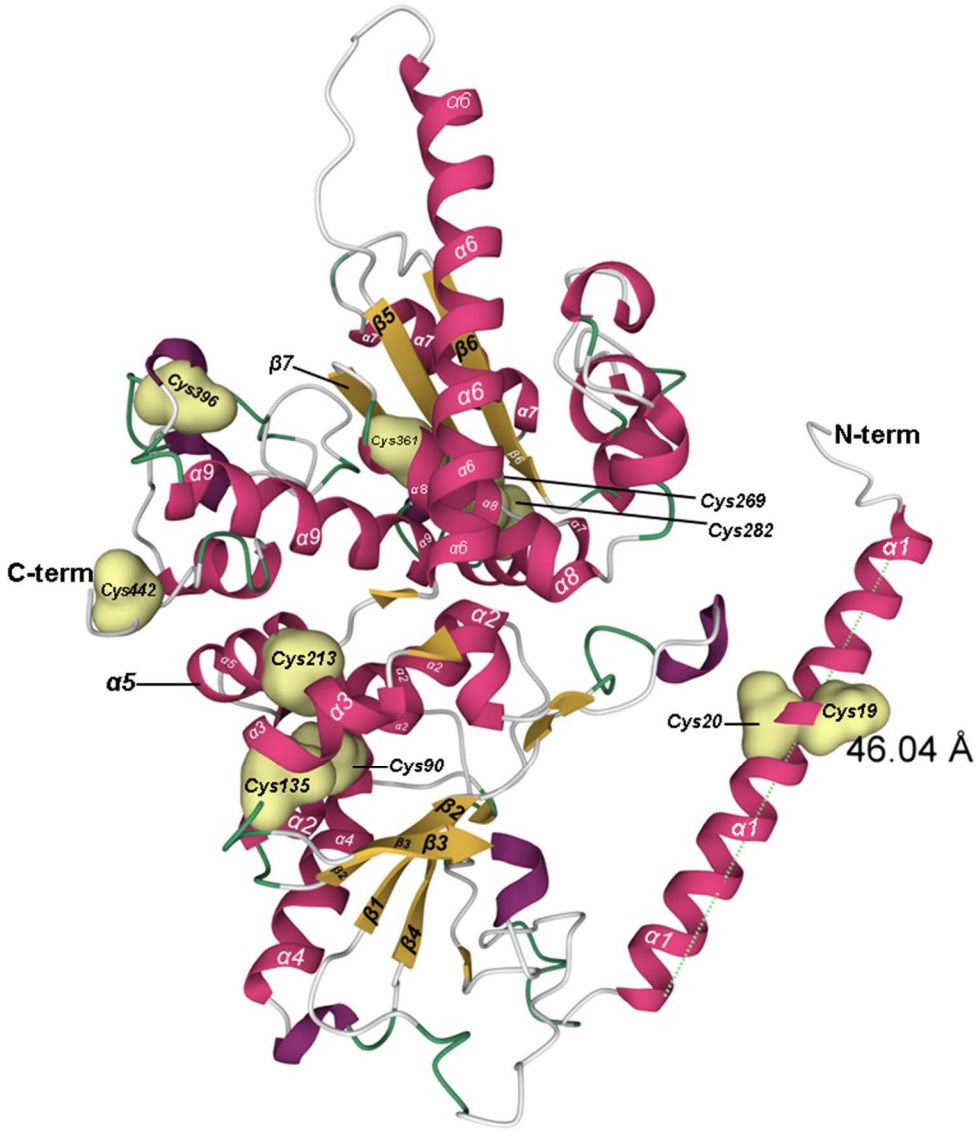

Figure 3.26: AtOFT1 *in silico* structure prediction. Computational structural prediction of AtOFT1 was performed in RaptorX using the full-length amino acid sequence of AtOFT1. The best structure (model 2) was visualized in PDB Mol* 3D Viewer and further used to measure the length of α-helix 1 as described in Chapter 2. The 9 well-defined α-helices (magenta-purple coils) and 7 β-sheets (golden yellow flat arrows) in AtOFT1's structure are shown. The measured length of AtOFT1's putative α-helix 1 in Angstroms (46.04) is depicted next to this structural feature and cystine residues are depicted as light-yellow molecular surface projections. All relevant features and amino acid positions of this model of AtOFT1 are either denoted in or are associated with a black line next to the feature of interest within the structural model with black or white text.

(PDB ID 5KU6.1.A and 5KU6.1.A). Interestingly, CePOFT1 crystal form III in complex with GDP (PDB ID 3ZY3) determined by Lira-Navarette *et al.,* 2011 was the most homologous to AtOFT1 with a QMQE score of 0.32. The determined conservation of AtOFT1 tertiary structure modeled against these known structures was aligned to the corresponding sequences of the models with AtOFT1, which illustrated AtOFT1 not only shares secondary and tertiary homology with metazoan POFT1s but additionally elucidated further primary sequence homology that was not before detected (Figure 3.27). Interestingly, AtOFT1 Cys^{269} and Cys^{282} aligned with CePOFT1 Cys^{249} and Cys^{281}, respectively. In CePOFT1, these residues form the third disulfide bridge and participate in the fundamental architecture of the binding site for GDP-fucose as well as houses the key catalytic residues, $CePOFT^{R240}$ and $CePOFT^{D244}$, which aligned with $AtOFT1^{R260}$ and $AtOFT1^{D264}$ and were demonstrated to be critical for the functionally of this protein in Arabidopsis (Lira-Navarrete *et al.,* 2011; Smith *et al.,* 2018a). Overall, these data indicate that AtOFT1 may possess a similar protein structure to metazoan POFT1s and strongly supports our hypothesis that AtOFT1 is a protein O-fucosyltransferase.

To more clearly visualize the structural similarities between AtOFT1 and metazoan POFT1s, the structure of CePOFT1 crystal form III in complex with GDP determined by Lira-Navarette *et al.,* 2011 (PDB ID 3ZY3) was used to compare to AtOFT1's predicted structure (Figure 3.28). The basic ribbon diagram of these proteins in the same orientation illustrated conservation of the structural GT-B fold motif with two distinct N- and C-terminal domains that are formed by central β-sheets encompassed by α-helices (Figure 3.28A-B). AtOFT1 and CePOFT1 were further examined in the same orientation as molecular surface projections color coded for hydrophobicity, and both

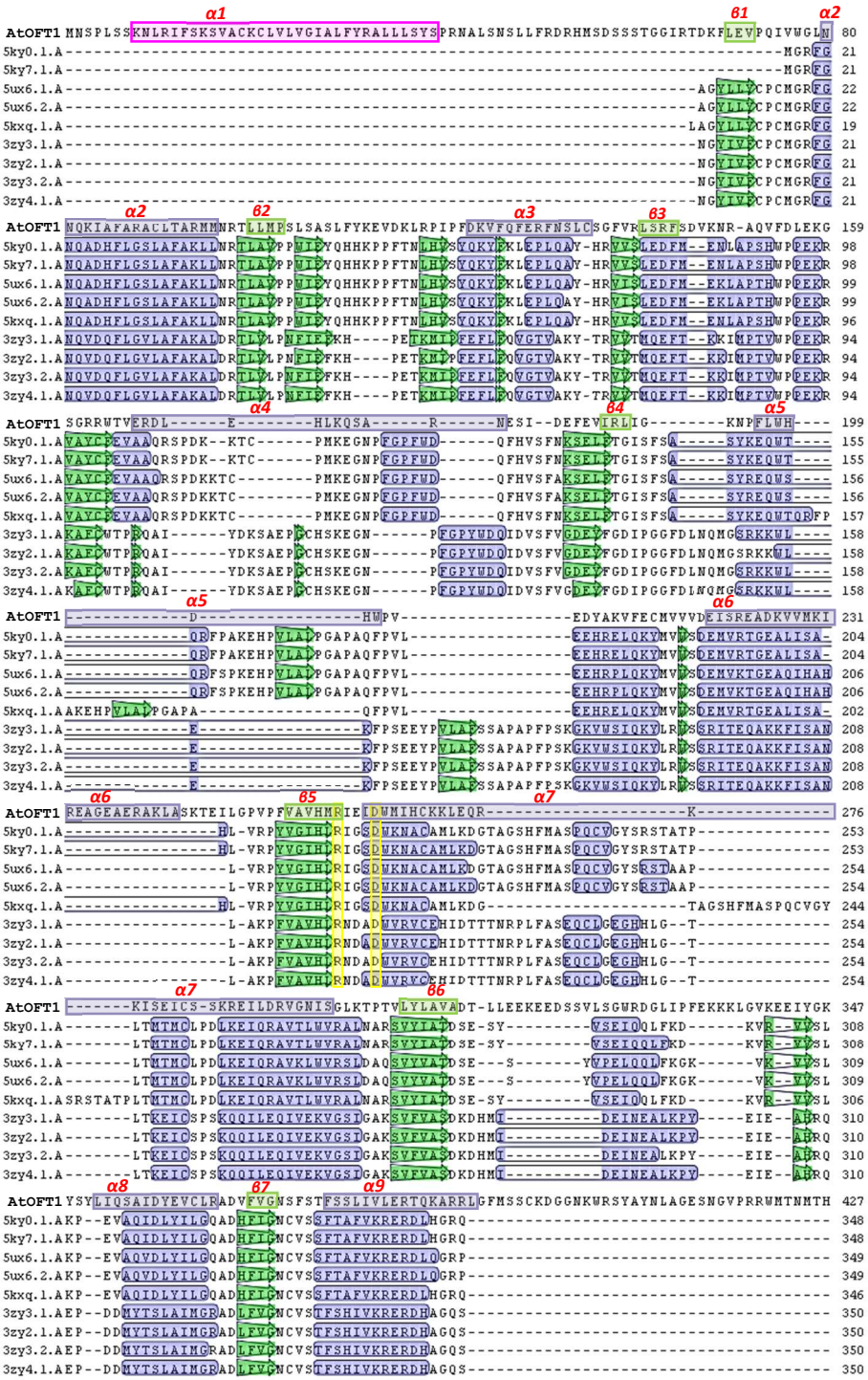

Figure 3.27: AtOFT1 secondary structure conservation with top metazoan POFT1 solved structures. The amino acid sequence of AtOFT1 was queried in Expasy SWISS-MODEL (Waterhouse *et al*., 2018), which further determined the 7 most homologous structures and alignment to AtOFT1, which were only metazoan POFT1s. The alignment was further annotated using AtOFT1's RaptorX *de novo* tertiary structure prediction with color coded boxed portions of its sequence showing structural homology. Red text above AtOFT1 denotes structural features of AtOFT1, and for all sequences, purple boxes indicate α-helices, green for β-strands, yellow for conserved residues (AtOFT1$^{R260\ \&\ D264}$), and a pink box indicates AtOFT1's putative α-helix 1. Metazoan POFT1 sequences are denoted by their PDB IDs to the left of their corresponding sequence, and their sequence position within the alignment is noted at far right.

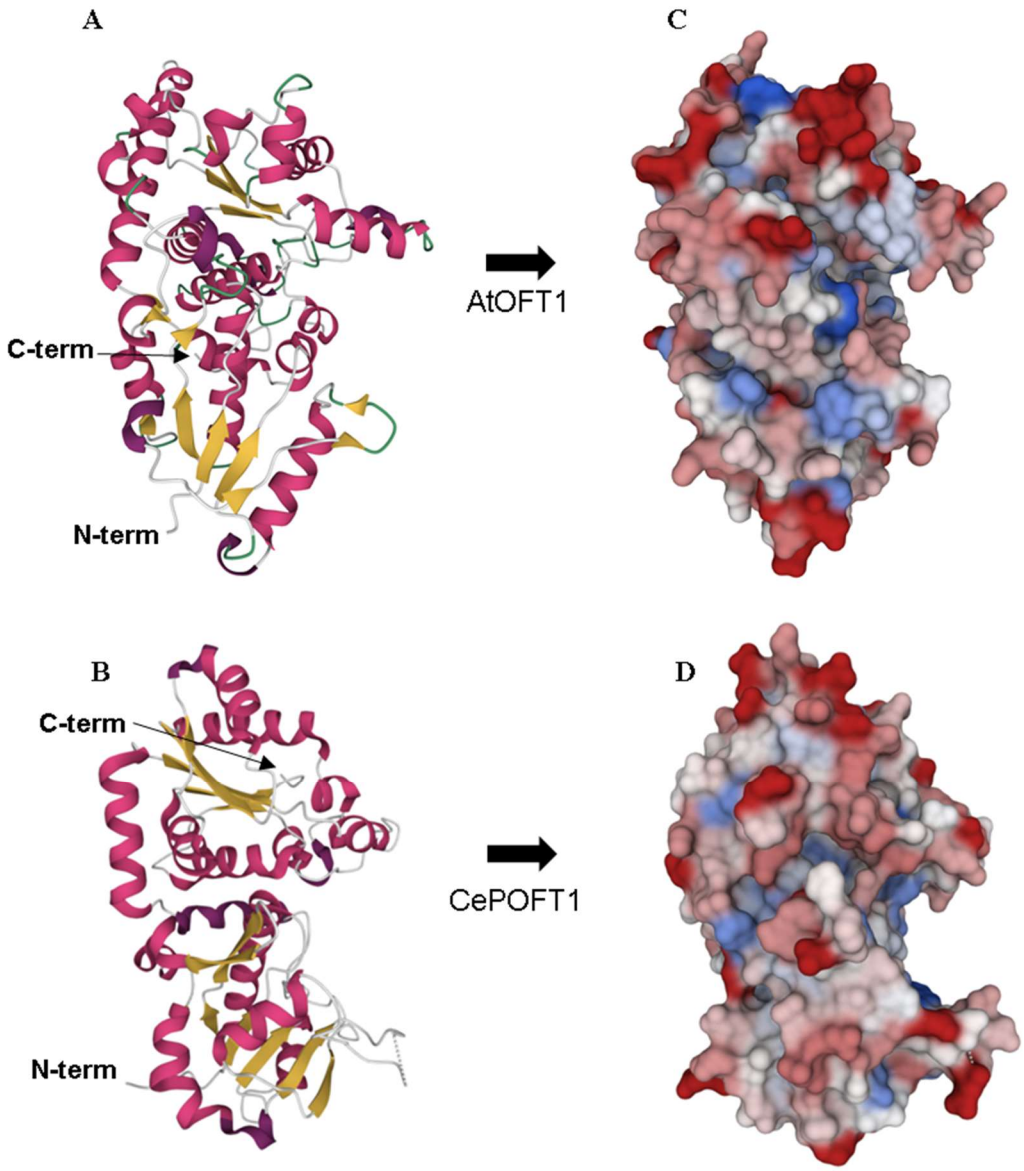

Figure 3.28: Structural similarities between AtOFT1 and *C. elegans* POFT1. A, RaptorX *de novo* structure prediction for AtOFT1 excluding the first 65 amino acids determined to be poorly predicted by this *in silico* database. B, The structure of *C. elegans* POFT1 (CePOFT1) (PDB 3ZY3) with α-helices in magenta-purple coils and β-sheets shown as golden yellow flat arrows. C and D, molecular surface projections of C, AtOFT1 and D, *C.* CePOFT1 (Lira-Navarrete *et al*., 2011) in same orientation as corresponding cartoons in A and B, respectively. The molecular surface projection models are color-coded to show surface hydrophobicity on a scale of red-white-blue, where red hues are most hydrophobic, white is neutral, and blue indicates hydrophilic surfaces. Models were constructed in PDB Mol* 3D Viewer as described in Chapter 2.

proteins demonstrated correlative interface microenvironments at distinct sites (Figure 3.28C-D). Additionally, both proteins displayed a deep cleft at the division of the two protein domains that face other one another, which is not only a fundamental characteristic of GT-B fold glycosyltransferases, but this large pocket is the reported catalytic site for metazoan POFT1s (Figure 3.28 C-D) (Lairson *et al.,* 2008; Lira-Navarrete *et al.,* 2011; Li *et al.,* 2017; McMillan *et al.,* 2017). Taken together, the putative structure of AtOFT1 shows structural characteristics that are in line with all known architectures of GT-65 enzymes, including CePOFT1, *Mouse musculus* POFT1 (MmPOFT1), and *Homo sapiens* POFT1 (HsPOFT1) (cazy.org; Lairson *et al.,* 2008; Lira-Navarrete *et al.,* 2011; Li *et al.,* 2017; McMillan *et al.,* 2017).

XVI. Expression of AtOFT1

Due to the observation that AtOFT1 contains the same functionally important catalytic amino acid residues that are necessary for metazoan POFT1 catalysis, and its predicted structure is most similar to these enzymes, we hypothesized it additionally functioned as a protein O-fucosyltransferase. To test this hypothesis, we aimed to express and purify AtOFT1 to homogeneity and catalytically assess if it shared the same sugar-nucleotide donor substrate as metazoan POFT1's, GDP-Fucose (GDP-Fuc). None of the members 39 genes in the Arabidopsis putative POFT family had been biochemically assessed as expression of glycosyltransferases is known to be challenging (Schmid *et al.,* 2016; Moremen *et al.,* 2017). Previously, expression of AtOFT1 in Arabidopsis and immunoblotting seedling protein extracts demonstrated that this protein was strongly associated with the membrane fraction as no signal was detected in the soluble protein fractions and signal solely originating from the membrane protein fraction in western blot

analyses. Furthermore, we determined that AtOFT1 was a Golgi-resident protein and most likely membrane bound to this organelle, which indicated AtOFT1 would need to be re-engineered to facilitate increased solubility without disrupting its native activity for characterizing its preferred sugar-nucleotide substrate. We initially approached this challenge by querying the amino acid sequence of AtOFT1 to identify its hydrophobic transmembrane domain using the TMHMM hydrophobic domain prediction software (www.cbs.dtu.dk/services/TMHMM; Version 2.0; Sonnhammer *et al.,* 1998). The results of this analysis indicated the first 36 amino acids in AtOFT1's N-terminal domain were strongly hydrophobic, and we theorized that soluble, recombinant protein expression may be possible by removing these residues from its coding sequence. To test our theory that AtOFT1's first 36 amino acids were causing trans-Golgi membrane integration and reducing the solubility of AtOFT1, PCR amplification was used to remove amino acids 1-36 from the *AtOFT1* coding sequence as well as replace the start codon. The truncated amplicon was then cloned into multiple expression plasmids containing different epitopes for affinity purification as well as different promoters and even secretion signals to facilitate soluble AtOFT1Δ36 expression in bacterial and yeast expression platforms. Following each expression trial, protein expression was evaluated by fractionating total protein using differential centrifugation to separate the soluble protein fraction from the membrane fraction, and the analyzing these fractions following running an SDS-PAGE gel and staining for protein or transferring protein fractions to a western membrane and probing for AtOFT1Δ36 expression. The results of each attempt indicated that AtOFT1 was being expressed across all systems but was consistently observed only in the membrane protein or insoluble protein fraction across all expression trials.

To attempt solubilization of AtOFT1Δ36 out of these membrane fractions without denaturing the protein, many non-denaturing ionic detergents were implemented, including CHAPS (3-[(3-Cholamidopropyl)dimethylammonio]-1-propanesulfonate hydrate), sodium deoxycholate, Tween 20 (polyoxyethylene (20) sorbitan monolaurate), Triton X-100, and sarkosyl (sodium lauroyl sarcosinate). The ability of the non-denaturing detergent treatments to solubilize AtOFT1Δ36 out of the membrane fractions from many different expression trials was compared to controls that always included the untreated membrane fraction as well as a denaturing solution treatment using SDS (sodium dodecyl sulfate) or Resuspension Buffer (25mM ammonium bicarbonate, 8.5 mM Urea). Following re-fractionation of the resuspended, detergent treated membranes, the soluble fraction as well as the membrane fractions were analyzed by western blotting. In all attempts to solubilize AtOFT1Δ36 using the aforementioned non-denaturing ionic detergents, signal from the western blot was only observed in the membrane fraction compared to denaturing control treatments that allowed for the release of AtOFT1Δ36 in its denatured form. These results indicated that AtOFT1 was still being retained in the membrane or insoluble protein fraction in yeast and bacterial expression systems following removal of its putative hydrophobic domain and treatment with a wide range of non-denaturing detergents to attempt to solubilize it out of this protein fraction. However, these results did not deter testing expression of AtOFT1 in other platforms.

We next examined Moremen and colleagues' successes using HEK293 cells in combination with their unique expression plasmids that allowed them to express, isolate, and characterize many human glycosyltransferases, glycosyl hydrolases, sulfotransferases, and other glycan modifying enzymes as well as determine a crystal

structure of the first Neu5Ac-α2,6GalNAcII sialyltransferase superfamily member protein, ST6GalNAcII (Moremen *et al.,* 2017). This team designed five unique Gateway compatible vector cassettes for mammalian cell expression which featured a secretion signal from *Trypanosoma cruzi*, allowing for the translated fusion protein to be isolated from the cell culture medium. Thus, we postulated that this system could effectively facilitate expression of AtOFT1. Dr. Kelley Moremen kindly provided us with their empty pGEn2-dest vector as well as an expression control vector, *B_4GALT_1/pGEn2-dest,* that encodes the human *beta-1,4-galactosyltransferase 1 (B_4GALT_1)* gene and was successfully secreted in a soluble and stable form using this HEK293 cell expression platform (Moremen *et al.,* 2017). The pGEn2 plasmid features an N-terminal fusion of the *Trypanosoma cruzi* signal sequence, an 8xHis epitope, and superfolder GREEN FLUORESCENT PROTEIN (sGFP) expressed under the human cytomegalovirus (CMV) promoter, which was used to create the *AtOFT1Δ36/pGEn2* plasmid for testing expression in HEK293 cells. Both plasmids were individually used to transiently transfect HEK293 cell cultures for a total of 72 h. The cell culture medium and cells were collected following 72 h of incubation and expression of the target proteins 8xHis-sGFP-AtOFT1Δ36 and 8xHis-sGFP-B_4GALT_1 control was evaluated using an anti-GFP immunoblot. Expression of 8xHis-sGFP-AtOFT1Δ36 was not detectable in the cell culture media, while robust signal was detected for the 8xHis-sGFP-B_4GALT_1 control sample, indicating that this system was functional but did not result in efficient secretion of recombinant AtOFT1 into the expression medium. We also attempted to isolate small amounts of secreted recombinant 8xHis-sGFP-AtOFT1Δ36 using Ni-NTA affinity chromatography (AC). The pre- and post- AC fractions were separated on an SDS-PAGE

gel along with ¼ the original quantity of 8xHis-sGFP-B_4GALT_1 control samples and stained for protein. These results further demonstrated that 8xHis-sGFP-AtOFT1Δ36 was not present in the medium, while 8xHis-sGFP-B_4GALT_1 was evidently isolated. As a final assessment of this expression platform, we aimed to understand if AtOFT1 was expressible at all in HEK293 cells in the pGEn2 plasmid. To evaluate this, the cellular pellets of both 8xHis-sGFP-AtOFT1Δ36 and 8xHis-sGFP-B_4GALT_1 collected 72 h post transfection were extracted for total cellular protein, protein fractionated into soluble and insoluble fractions, and immunoblotted. 8xHIS-sGFP-AtOFT1Δ36 signal was detected in the insoluble protein fraction (Figure 3.29), indicating that HEK293 cells did express *AtOFT1,* but the fusion protein was not being secreted into the medium and was being integrated into the membrane of the cell. Based on these observations, we concluded that expression of AtOFT1Δ36 was possible in HEK293 cells, but it was not a viable solution to our experimental goals because very limited amounts of protein were being produced that could not satisfy the input requirements of downstream assays.

Due to the consistent observation that AtOFT1 was expressed in an insoluble form and was not efficiently solubilized out of these membrane fractions using a range of non-denaturing ionic detergents. we also attempted to express this protein using a cell-free *in vitro* transcription and translation expression platform. Using the PURExpress *in vitro* Protein Synthesis Kit (New England Biolabs, Cat. No. E6800), which contained all of the necessary enzymes from *E. coli* to facilitate transcription and translation of the *AtOFT1Δ36+6XHis/pKM596* vector as well as a positive control plasmid, which contained the coding sequence for human *DIHYDROFOLATE REDUCTASE* (*DHFR)* expressed under the control of the T7 promoter, we attempted *in vitro* transcription/

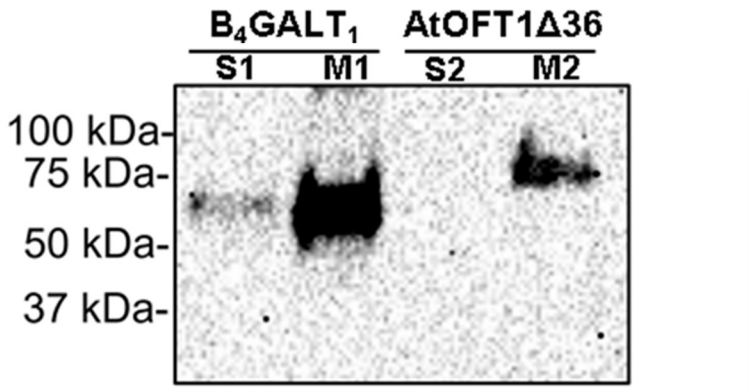

Figure 3.29: AtOFT1 HEK293 cell expression immunoblot. AtOFT1Δ36-GFP and B4GalT1-GFP control constructs cellular extracts following transient transfection in HEK293 cells that were lysed, fractionated, immunoblotted with anti-GFP antibody, and chemiluminescently developed to determine expressibility of AtOFT1 using the HEK293 cell expression platform developed by Moremen *et al.,* 2017. Soluble protein fractions (S1 and S2) and membrane fractions M1 and M2, each respectively for control and AtOFT1, respective fractions. The relevant molecular weight markers are denoted to the right of the blot.

translation of these proteins. Following the reaction, the protein was precipitated and was assessed by loading onto an SDS-PAGE gel and staining for total protein. This experiment indicated that the control vector was produced as the appropriate protein band was observed at approximately 22 kDa, however the expected protein band for MBP-AtOFT1Δ36-6XHis was not observed, indicating this system failed to produce the target protein in this cell-free expression platform or was produced at such low levels, that it was not evident on the stained SDS-PAGE gel.

To further troubleshoot recombinant expression of AtOFT1 in a soluble and functionally active form, a translational fusion ofAtOFT1 to MALTOSE-BINDING PROTEIN (MBP) was assessed. MBP is a widely utilized epitope tag that is natively produced by many bacterial as well as archaea species and facilitates increased yield and solubility of translationally fused proteins when expressed in bacterial systems (Fox *et al.,* 2003; Fox and Waugh, 2003; Szmelcman and Hofnung, 1975). Three different gateway compatible N-terminal MBP fusion plasmids all expressed under the control of the lac operon from *E.coli* were evaluated for expression of soluble AtOFT1Δ36, and all expression was performed in the novel *E. coli* strain Rosetta-Gami 2 (Novagen). This specific bacterial strain possesses mutations in its *glutaredoxin reductase* and *thioredoxin reductase* genes that facilitate a more oxidizing cytoplasmic environment, which promotes disulfide bond formation and is more conducive for enhanced expression of eukaryotic proteins (Zarkar *et al.,* 2020). The pDEST-HIS-MBP (Nallamsetty *et al.,* 2005) featured a 6xHis epitope tag followed by MBP from *E.coli*, while the pKM596 vector was MBP from *E. coli* only (Fox and Waugh, 2003), and the pKM839 vector was MBP from *Pyrococcus furiosus* (Fox *et al,,* 2003). Evaluating these plasmids for their

ability to express soluble AtOFT1Δ36 was initially approached by cloning *AtOFT1Δ36* into these plasmids. Modification to add a hexahistidine epitope tag to the 3' end of the *AtOFT1Δ36* DNA fragment was required prior to cloning into the pKM596 and pKM839 vectors to allow for subsequent Ni-NTA affinity chromatography. Expression was induced after the culture had reached logarithmic growth by the addition of a low concentrations of IPTG and performing expression under low temperature conditions (18ºC) for 18 h. The soluble protein fraction of the cell expression lysate was purified by Ni-NTA affinity chromatography and protein expression was evaluated by separating the membrane protein fraction as well as pre- and post-affinity chromatography soluble protein fractions by SDS-PAGE and staining the gel for protein. In all cases, AtOFT1 was not expressed in the soluble fraction or at the correct molecular weight. However, a band was evident in all fractions of the soluble protein originating from the expression of the *AtOFT1Δ36/pDEST-His-MBP* expression that corresponded with the approximate molecular weight of MBP alone, indicating that cleavage of ATOFT1Δ39 from its fused 10xHis-MBP epitopes was occurring.

Following these failed attempts at successful purification of AtOFT1, we returned to overexpression in Arabidopsis seedlings, as the lab had experienced success in solubilizing membrane proteins using the Profoldin Membrane Protein Extraction Kit (Profoldin). Membrane microsomes were prepared from *oft1-2$^{-/-}$;UBQ10::OFT1-GFP* 10-day-old light grown transgenic seedlings and then the 12 kit supplied propriety non-denaturing detergents were tested for solubilization of AtOFT1-GFP. Solubilization efficiency of AtOFT1-GFP was determined by anti-GFP Western blot analysis on the soluble and insoluble fractions after detergent treatment. Surprisingly, the proprietary

zwitterionic detergent solution #8 (Profoldin) successfully solubilized AtOFT1-GFP out of Arabidopsis seedlings (Figure 3.30). To isolate AtOFT1-GFP, affinity chromatography using GFP-Trap Magnetic Agarose beads (Chromotek; Cat. No. gtma-20) was performed. However, following western blot analysis of the pre- and post- affinity chromatography fractions on an anti-GFP western blot, it was apparent that the elution fractions did not contain AtOFT1-GFP following attempted final protein elution with 50µL 6X SDS-PAGE loading buffer (375 mM Tris-HCl pH 6.8, 9% [w/v] SDS, 50% [v/v] glycerol, 0.05% [w/v] bromophenol blue, 9% β-mercaptoethanol) applied directly to the AC medium and heating for 20 min at 65ºC or 95ºC for 15 min as well as attempted dissociation by the addition of 50µL of acidic glycine elution buffer (200mM glycine, pH 2.5) to the AC medium followed by neutralizing the eluate fraction with 5µL of 1M Tris (pH 10.4). To dissociate captured protein off of the AC medium as well as identify if AtOFT1 was contained within the eluate, on-bead trypsin digestion was performed for 16 h following methanol: chloroform precipitation as well as reduction and alkylation of the AC medium final bound protein sample. The trypsin-digested peptides were cleaned up and desalted on a C18 SepPak column, dried down completely, and then resuspending in 0.1% [v/v] formic acid. The peptide eluate was sent to the Mick Hitchcock, Ph.D. Nevada Proteomics Center at the University of Nevada, Reno. AtOFT1was present in the resulting mass spectrometry analysis (data not shown).. These results suggest that expression and purification of AtOFT1 is difficult but possible, and that the most effective means of isolating AtOFT1 may be through expression in Arabidopsis seedlings following modification of the affinity purification procedure to allow for efficient elution of the protein. While this approach may be suitable for some applications, it would be

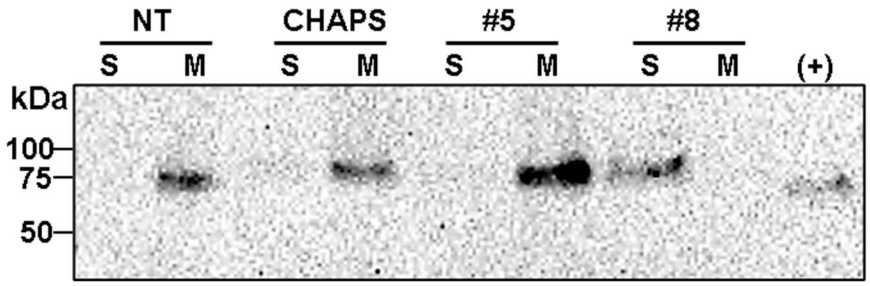

Figure 3.30: AtOFT1 membrane solubility following non-denaturing detergent treatment. Total protein was extracted from 10-day old T_3 seedlings expressing the *UBQ10::OFT1-GFP* complement construct transformed in the *oft1-2*$^{-/-}$ mutant background and fractionated by ultracentrifugation to separate soluble and membrane protein fractions. AtOFT1 is endogenously localized to the Golgi-apparatus membrane (Figure 3.14), therefore, the membrane protein fraction was parsed into separate aliquots containing equal quantities of protein prior to being treated with CHAPS or one of the 12 detergent solutions included in the Profoldin Membrane Protein Extraction Kit (Profoldin, Cat. No. MPEO1-12P) compared to 2% [w/v] CHAPS solution as described in Chapter 2. No treatment (NT) control samples were processed in line with detergent treated samples with an equal volumes of 1X PBS as supplemented for detergent solution and protein. Following treatment, the samples were again fractionated to retrieve the detergent solubilized protein, while the remaining membrane protein pellet was resuspended in an equal volume of 1X PBS. To assess the efficacy of each detergent to solubilize AtOFT1-GFP out of the membrane protein fraction, an equal volume of detergent soluble (S) and associated post-treatment resuspended membrane protein pellet (M) counterpart were loaded onto an SDS-PAGE gel side by side and B_4GalT_1-GFP was used as a positive control (+). The gel was transferred to a nitrocellulose membrane that was then probed with anti-GFP antibody. Shown above are the results of the chemiluminescent developed anti-GFP Western membrane. Notice that the kit-supplied detergent solution #8 (Profoldin MEOP8) was able to completely solubilize AtOFT1 out of the membrane fraction in lane #8S compared to the Profoldin solution #5 and CHAPS. The expected molecular weight of AtOFT1-GFP is approximately 77.5 kDa. Out of all 12 solutions in the Profoldin kit as well as with all other non-denaturing detergents attempted for solubilizing AtOFT1-GFP out of membranes, solution #8 was by far the most efficient (data not shown).

prohibitively difficult to obtain large quantities of purified AtOFT1 for downstream biophysical analyses.

XVII. Other putative Arabidopsis POFT family members are expressible

To simultaneously circumvent the challenges faced with expression of AtOFT1 in a soluble form that retains its catalytic activity as well as to gain insight into other members of the Arabidopsis putative POFT family, we postulated that other Arabidopsis putative POFT members could be more amenable to overexpression and purification procedures. Our decision to investigate the other related family members of AtOFT1 was based on the fact that these proteins were predicted to share the same catalytic function, and we hypothesized that because these proteins share high sequence homology as well as a conserved catalytic domain, successful expression and catalytic analysis of any Arabidopsis OFT-like protein would lend insight into their associated functions. Therefore, recombinant expression of 5 members was performed. Four of the five family members, *AtMSR1 (At3g21190), AtFRB1 (At5g01100), AtESMD1 (At2g01480),* and *AtEDA30 (At3g03810)* were chosen for expression testing due to their previously characterized phenotypes. *At1g04910* had not been previously phenotypically characterized but was selected for expression following surveying the entire 39 membered family for the lowest number of cysteine resides in the encoded protein as well as the smallest hydrophobic domain. All 5 genes were prepared for expression by truncating the coding region to remove their hydrophobic domains and then integrating them into the pDEST-His-MBP vector. Each vector was transformed into *E. coli* Rosetta-Gami 2 and expressed under the same conditions attempted for expressing AtOFT1Δ36 using this vector and expression system with a low concentration of IPTG (250 μM) and

slow (18 h), low temperature (18ºC) expression conditions. Protein was extracted and the soluble protein fraction was purified by Ni-NTA affinity chromatography. To evaluate the expression of each protein, an anti-His western blot was performed to investigate the expression of the protein in the membrane protein fraction as well as the pre- and post Ni-NTA fractions. Surprisingly, three of the five tested family members were expressed and purified, including AtMSR1Δ28, AtFRB1Δ144, and AtESMD1Δ94, with AtMSR1Δ28 and AtFRB1Δ144 exhibiting the highest soluble protein yield. AtEDA30Δ31 as well as At1g04910Δ45 were retained in the insoluble membrane fraction. Nonetheless, these results demonstrated that purification of other Arabidopsis putative POFTs was feasible, so we pursued a more detailed enzymatic characterization of these proteins.

XVIII. Biochemical characterization of AtMSR1

We initially focused our enzymatic characterization efforts on AtMSR1Δ28 as it showed the highest soluble protein yield compared to the other 2 family members following Ni-NTA chromatography. The pDEST-His-MBP vector had previously exhibited cleavage of the HIS-MBP from the AtOFT1. To circumvent this issue, a 6xHis tag was amplified onto the 3' end of *AtMSR1Δ28* and recloned into the pKM596 vector. The *AtMSR1Δ28+6xHis/pKM596* plasmid was introduced into *E. coli* Rosetta-Gami 2 and expressed as before with a low concentration of IPTG (250 μM) and low temperature conditions (18ºC) for 18 h. Sequential Ni-NTA and amylose affinity chromatography were used to isolate the protein, the elution fractions were concentrated and buffer exchanged, and the pre- and post-affinity chromatography fractions as well as column concentrated protein was evaluated on a stained SDS-PAGE gel. Shockingly, MBP-AtMSR1Δ28-6xHis was purified to homogeneity (Figure 3.31A). Furthermore, following

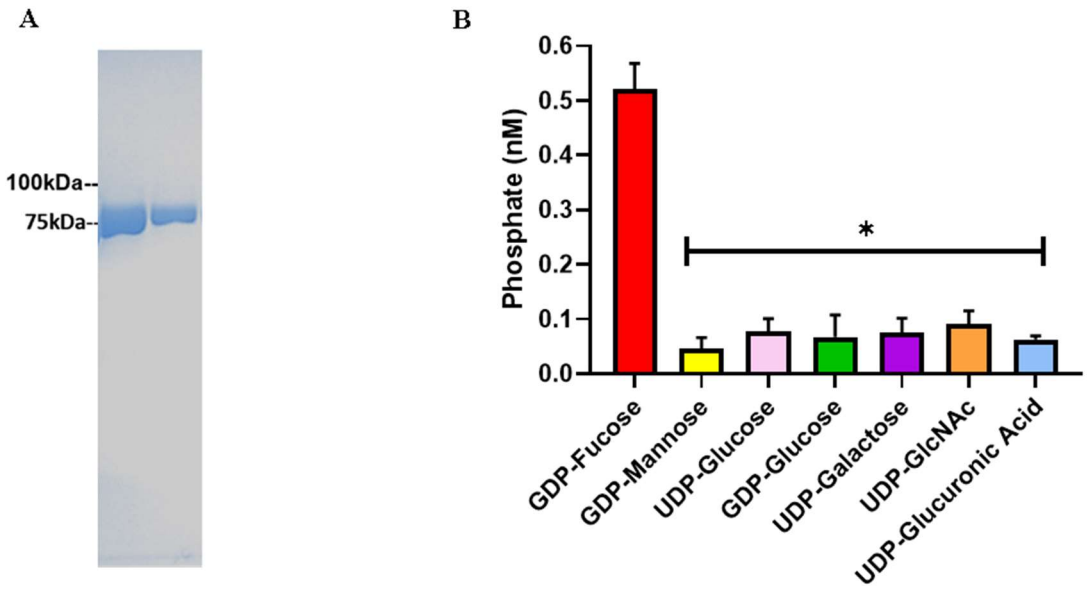

Figure 3.31: AtMSR1 is expressible and utilizes GDP-fucose. A, Coomassie stained SDS-PAGE gel of recombinantly expressed AtMSR1Δ28 following Ni-NTA and amylose affinity chromatography purification. The two lanes (left to right) show the post-Amylose AC eluate fractions 1 and 2, demonstrating AtMSR1Δ28 can be purified to homogeneity. B, Following buffer exchange and column concentration of AC purified AtMSR1Δ28, the enzyme was catalytically assessed for sugar-nucleotide substrate specificity against 7 potential substate donors by malachite green phosphate assays as described in Chapter 2. Bar graph represents means of 3 independent purifications ± SEM. One-Way ANOVA indicated a significant difference between GDP-fucose compared the other substrates evaluated (*, $P \leq 0.0332$ by Tukey's post hoc analysis).

BCA assay of the concentrated, buffer exchanged, column concentrated MBP-AtMSR1Δ28-6xHis, this protein consistently produced high yields (≥600 μg protein per 1 L expression culture). These results were not only exciting but indicated that MBP-AtMSR1Δ28 -6xHis could be further evaluated to assess the catalytic activity and sugar nucleotide specificity of the protein.

To approach this question, we performed sugar nucleotide hydrolysis assays. When a glycosyltransferase is in the presence of its preferred sugar-nucleotide donor substrate and not its acceptor substrate, the enzyme will hydrolyze off the nucleotide from the sugar (Wu *et al.,* 2011). The exposed phosphate moieties of the hydrolyzed nucleotide can then be attacked by the human nucleoside triphosphate diphosphohydrolase enzyme (NTPDase), which will cleave the terminal phosphate from the di-nucleotide creating free inorganic phosphate in the reaction (Robson *et al.,* 2006). The malachite green phosphate assay can then measure the concentration of free inorganic phosphate in a colorimetric assay allowing for the sugar-nucleotide donor substrate of the glycosyltransferases to be determined (Wu *et al.,* 2011). To assess the sugar-nucleotide donor specificities of the purified MBP-MSR1Δ28-6xHis protein, individual reactions containing NTPDase, equal amounts of MBP-MSR1Δ28-6x in the presence or absence of either GDP-Fucose, GDP-Mannose, UDP-Glucose, UDP-N-Acetylglucosamine (GlcNAc), or UDP-Galacturonic acid were composed. Following a 3 h incubation with the individual sugar-nucleotide, the free phosphate in the reaction was detected using malachite green phosphate detection. In multiple independent biological and technical replicates, MBP-MSR1Δ28-6xHis in the presence of GDP-Fucose was the only sugar-nucleotide that produced significant amounts of free phosphate in solution

(Figure 3.31B). The results represent the first biochemical evidence to indicate that MSR1 was not only active, but that its sugar-nucleotide substrate was GDP-fucose and no other sugar-nucleotide tested. Metazoan POFT1's sugar-nucleotide substate is also GDP-fucose, which further suggested that AtMSR1 potentially is a protein O-fucosyltransferase, and that the hypothetical grouping of this family is potentially correct.

To further characterize the catalytic requirements of AtMSR1, we examined whether its catalytic activity required the addition of $MnCl_2$, as *C. elegans* POFT1 acts independently of this metal cofactor, but other metazoan POFTs, such as POFT2, are dependent on the presence of manganese(II) chloride (Lira-Navarette et al., 2011). To test this hypothesis, differential scanning fluorimetry (DSF) was implemented in combination with SYPRO® Orange (Molecular Probes), which specifically binds to exposed hydrophobic regions on the protein causing increased fluorescence intensity (Bai *et al.,* 2019).

To determine AtMSR1's dependence with $MnCl_2$ for efficient fucosyltransferase activity, DSF reactions were assembled with equal concentrations of MBP-AtMSR1Δ28-10XHis and SYPRO® Orange supplemented with or without 5 mM $MnCl_2$ and placed in a Bio-Rad CFX96 Touch Real-Time PCR Detection System. Following the reaction, the T_m of MBP-AtMSR1Δ28-10XHis in the absence of $MnCl_2$ was determined to be 53.5ºC, while the T_m of MBP-AtMSR1Δ28-10XHis in the presence of $MnCl_2$ was observed at 51.5ºC (Figure 3.32). These results indicated that the observed decrease in T_m of 2ºC in the presence on this metal cofactor lead to a decrease in the stability of MSR1, suggesting that AtMSR1 may function independently of this additive. However, MSR1 should be catalytically evaluated in the presence and absence of $MnCl_2$, such as in a sugar-

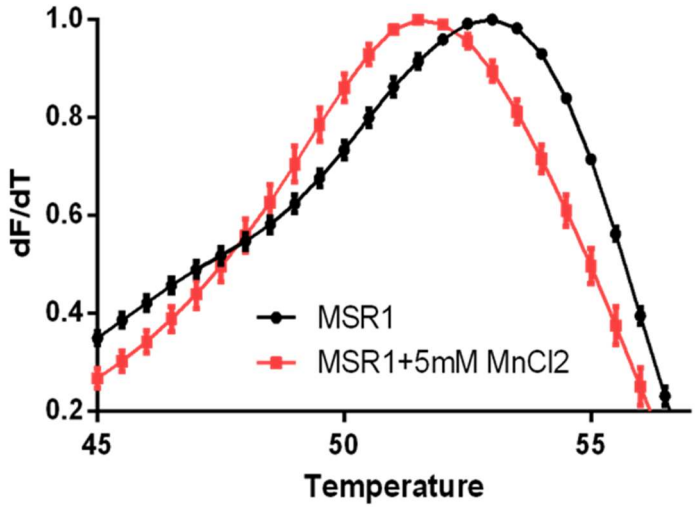

Figure 3.32: AtMSR1 may be metal cofactor independent**.** MSR1 Tm shift in the presence or absence of 5mM Manganese(II) chloride (MnCl2) and determined by DSF described in Chapter 2. The T_m of catalytically processed recombinant MSR1Δ28 shifted from 53.5°C in the absence (black trend line) to 51.5°C in the presence of this metal cofactor (red trend line), which was similarly observed for CePOFT1 by Lira-Navarette *et al.,* 2016.

nucleotide hydrolysis assay format, to determine if this protein is truly metal-cofactor independent. Furthermore, a similar decrease in T_m was observed for CePOFT1 in the presence of 5 mM $MnCl_2$ with and without the addition of GDP-fucose, which indicated that this enzyme functioned independently of this metal cofactor as the thermal stability decreased in the presence of the metal-cofactor alone and did not increase the rate of sugar-nucleotide hydrolysis (Lira-Navarette *et al.,* 2011. Taken together, these results draw additional similarities between metazoan POFT1 and AtMSR1's catalytic requirements for catalysis and add weight to our theory that the putative Arabidopsis POFT familial grouping is correct, and these enzymes may indeed be protein O-fucosyltransferases.

XIX. FRIABLE utilizes GDP-fucose as one of its donor substrates

To understand whether Arabidopsis putative POFTs that are phylogenetically distant from MSR1 have similar sugar nucleotide substrate specificity, we examined whether AtFRB1 also utilized GDP-Fucose or other sugar-nucleotide substrates. *FRB1Δ144* was amplified to add a 6xHis tag onto the 3' end of its coding sequence and recloned into the pKM596 vector as done for AtMSR1. The *AtFRB1Δ144+6xHis/pKM596* vector was introduced into *E. coli* Rosetta-Gami 2 and expressed as described above for expression of *AtMSR1Δ28+6xHis/pKM596* in this expression host. Ni-NTA as well as amylose affinity chromatography were used to isolate the protein, and then the elution fractions were concentrated and buffer exchanged, and then the pre- and post-affinity chromatography fractions as well as column concentrated protein was evaluated on a stained SDS-PAGE gel. MBP-AtFRB1Δ144-6xHis, was

consistently produced at high yield using this approach, indicating that MBP-AtFRB1Δ144 -6xHis could be further evaluated using sugar nucleotide hydrolysis assays.

To test our hypothesis that AtFRB1 also utilized GDP-Fucose, the malachite green phosphate detection assay was again implemented to assess the sugar-nucleotide specificity of this protein. Reactions were composed of MBP-FRB1Δ144-6xHis protein and NTPDase supplemented with and without either GDP-Fucose, GDP-Mannose, UDP-Glucose, UDP-GlcNAc, or UDP-Galacturonic acid. Following a 3 h incubation with the individual sugar-nucleotide, the free phosphate in the reaction was detected using malachite green phosphate detection kit (R&D Systems). Interestingly, MBP-FRB1Δ144-6xHis in the presence of GDP-Fucose was the only sugar-nucleotide that produced significant amounts of free phosphate in solution (Figure 3.33). The results demonstrate that AtFRB1 can also be isolated in a functionally active form and its sugar-nucleotide donor substrate was GDP-Fucose and no other sugar-nucleotide tested. Additionally, this result not only adds significance to the hypothetical grouping of these enzymes, but also suggests that these enzymes are protein O-fucosyltransferases, as two of its family members selectively utilize the same sugar-nucleotide substrate as metazoan POFT1's.

XX. Lectins provide additional tools for the profiling of O-fucosylated proteins in Arabidopsis

To investigate the proteins that may be the acceptor substrates of Arabidopsis putative POFTs, fucose-specific lectins were employed. Lectins are glycan-recognition probes that can selectively discriminate between a wide range of glycan structures (Cummings & McEver, 2009). We previously determined that the biotinylated fucose-specific lectin from *Aleuria aurantia* (AAL) was the most efficient at detecting fucosylated

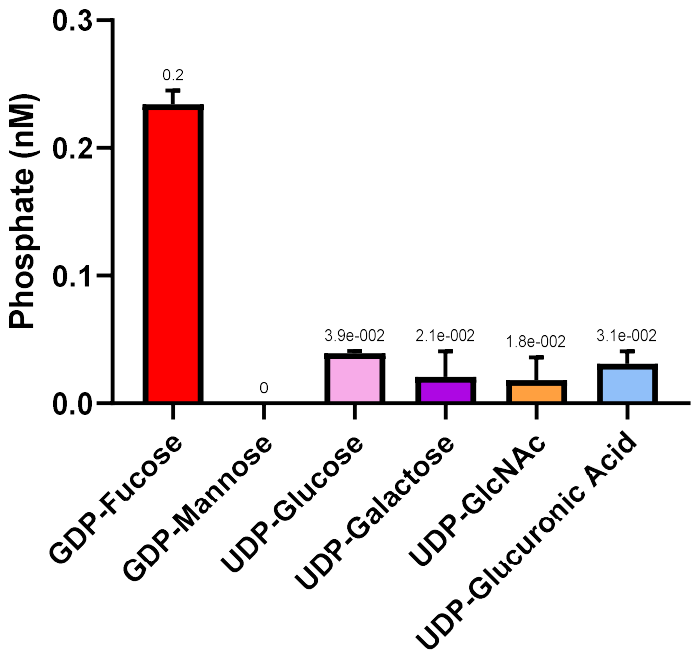

Figure 3.33: AtFRB1 also utilizes GDP-fucose as a preferred sugar-nucleotide donor substrate. Recombinantly purified and catalytically prepared FRB1Δ144 was assessed for sugar-nucleotide specificity as described in Chapter 2 by malachite green phosphate detection colorimetric assay. Data representative of means replicates ± range of 2 independent biological replicates with mean values denoted above corresponding range bars.

proteins by streptavidin western blotting. To initially understand the degree of fucosylation in Arabidopsis seedlings, total protein was extracted from Col-0 seedlings, and separated into soluble and membrane protein fractions. Equal quantities of soluble and membrane protein were separated by SDS-PAGE, transferred to a nitrocellulose membrane, and trisected to allow for 3 membranes containing the same protein fractions to be probed differently as 2 of these membranes were used as controls. One control consisted of the AAL lectin preincubated with fucose to control for the primary antibody, while the second control membrane was only treated with the secondary streptavidin conjugate to control for biotinylated proteins. The third membrane was treated with AAL lectin followed by the secondary streptavidin conjugate and all three membranes were developed and imaged for analysis (Figure 3.34). These results demonstrated that the AAL lectin was extremely efficient at identifying proteins as the robust signal produced in both the soluble and insoluble membrane fractions compared to controls was extremely high with fucosylated proteins detected at almost at every molecular weight, suggesting that in Arabidopsis, the protein population is heavily fucosylated. Furthermore, the highest signal was observed in the membrane protein fraction indicating that the majority of the fucosylated proteins are either actively being modified by POFTs in the Golgi-apparatus and/or the majority of fucosylated proteins are membrane localized.

To isolate the population of soluble fucosylated proteins, AAL-agarose was used as an affinity purification medium to selectively isolate these fucose-modified proteins. Streptavidin western blotting with the AAL lectin as described above was performed on the pre-purified soluble protein and post-AAL isolated protein to visualize the success of this affinity chromatography medium to isolate fucosylated soluble protein from

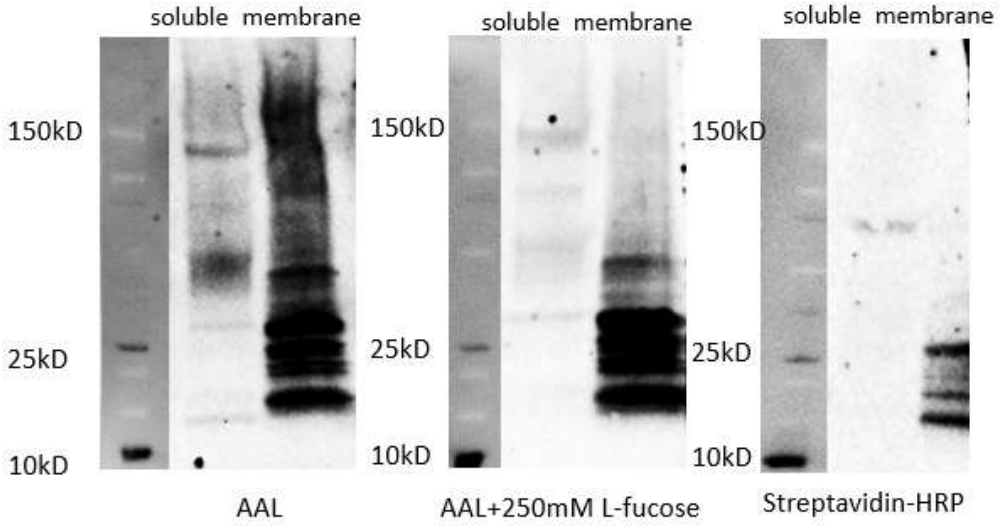

Figure 3.34: Col-0 seedlings protein extraction reveals a high degree of fucosylated proteins**.** Col-0 soluble and total membrane protein prepped from 10-day old seedlings and probed on Western membranes with either AAL lectin (left), AAL lectin incubated with 250 mM L-fucose used for AAL control (middle), or streptavidin-HRP used for Streptavidin false detection control (right). The increased signal in the AAL probed blot (left blot) indicates the presence of fucosylated proteins.

Arabidopsis seedlings (Figure 3.35 top panel). These results demonstrate that AAL is an effective medium for isolating soluble fucosylated protein from the total soluble protein fraction of Arabidopsis seedlings as the signal produced for the AAL eluate fraction was significantly greater than that of the total soluble protein fraction alone, indicating these proteins were concentrated following AAL affinity chromatography. Additionally, purification of the soluble protein using the purification medium was able to reduce the simultaneous detection of biotinylated proteins compared to the pre-purified soluble protein fraction, indicating biotinylation and fucosylation of proteins are not linked as very little signal was observed in the streptavidin control blot for the AAL eluate protein fraction, while a consistent signal of biotinylated proteins was detected in the pre-purification soluble protein fraction.

Lectins are not specific to the type of linkage of sugar moiety, thus, to visualize O-fucosylated protein s, PNGase F (Peptide:N-glycosidase F) was used to digest away N-linked glycans from the proteins to allow fir only O-linked fucosylated proteins to be isolated, AAL Following AAL affinity chromatography, the eluates were treated with PNGase F for 18 h. To visualize the success of the PNGase treatment to identify the population of proteins that contained only O-linked fucosylation events, digested and undigested affinity purification isolates were immunoblotted as previously described (Figure 3.35 bottom panel). Following development of the western membranes, the PNGase digested eluate exhibited a reduction in signal compared to an equivalent amount of undigested protein sample, indicating that PNGase F treatment reduced the amount of N-linked fucose modifications from the protein eluates allowing for only O-linked fucose modification on proteins to be visualized. Overall, these results indicate that lectins are

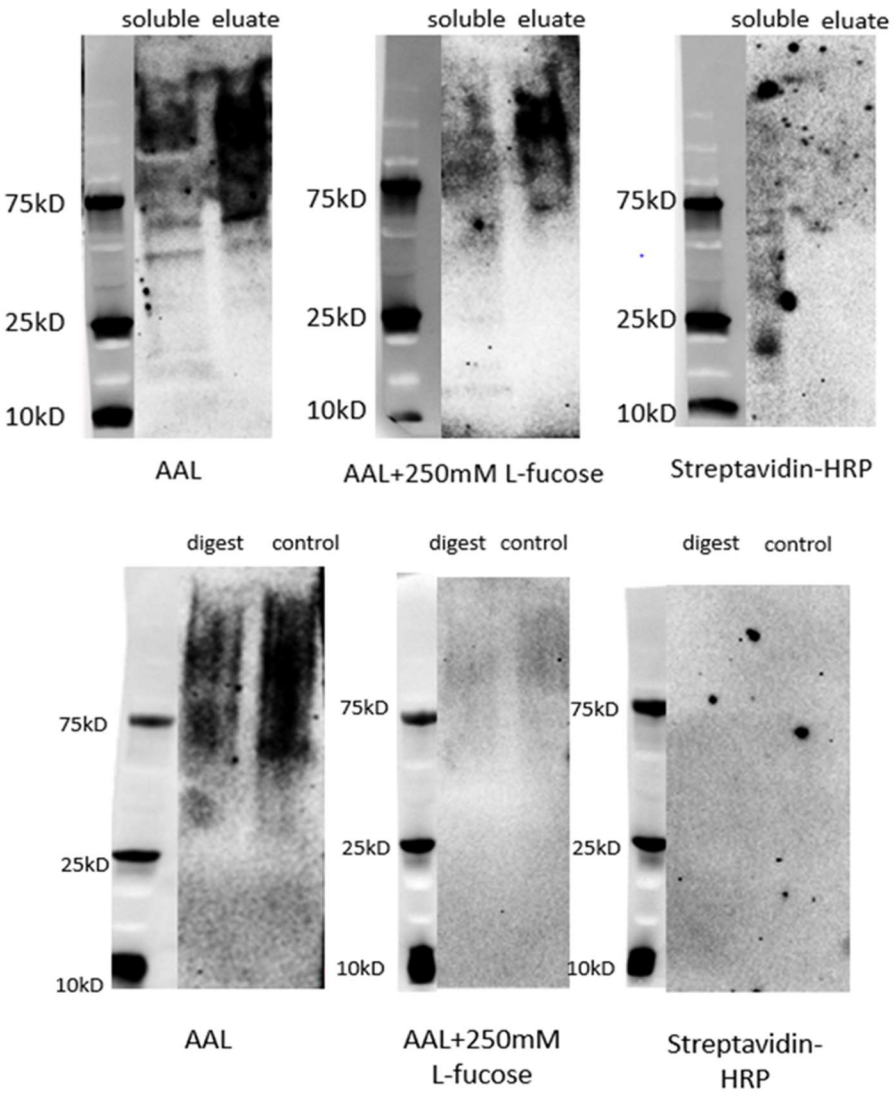

Figure 3.35: AAL-agarose selectively and effectively isolates endogenously fucosylated proteins in Arabidopsis. Top blots: AAL probed Western blot of 10-day old Col-0 seedlings total soluble protein and post-AAL-agarose AC eluted protein probed with AAL lectin on Western membranes and developed by chemiluminescence (top left), or AAL incubated with 250 mM L-fucose and streptavidin-HRP control blots (top middle and top right, respectively). The increased signal in the AAL probed eluate column indicates the presence of fucosylated proteins. Bottom blots: Western blot of PNGase F digested soluble fucosylated proteins that were enriched by AAL-agarose AC and digested with PNGase F to release N-linked glycans as described in Chapter 2. AAL, AAL+250mM L-fucose, and streptavidin-HRP were used to probe digested and undigested proteins on Western blot membrane developed and detected by chemiluminescence (bottom left blot, bottom middle blot, and bottom right blot, respectively). Note the decreased signal in the digested lane of AAL membrane (bottom left) versus controls, indicating PNGase F cleaved some N-linked fucose residues. PNGase A (NEB Cat. No. P0707) should be used for future N-linked glycan cleavage reactions, as this enzyme cleaves N-linked glycans with or without α(1,3)-linked core fucose residues.

not only an effective means of identifying proteins containing fucose modifications, but also demonstrates their efficacy in isolating and purifying the population of O-fucosylated proteins. This probing and isolation methodology will be invaluable as a high throughput method of determining the acceptor protein substrates of the 39 enzymes of the Arabidopsis putative POFT and for facilitating further understanding of the role of protein O-fucosylation and POFTs in plant systems as well as the pathways and functions of they participate in.

References

Alonso, J., Stepanova, A., Leisse, T., Kim, C., Chen, H., Shinn, P., Stevenson, D., Zimmerman, J., Barajas, P., Cheuk, R., Gadrinab, C., Heller, C., Jeske, A., Koesema, E., Meyers, C., Parker, H., Prednis, L., Ansari, Y., Choy, N., … Ecker. (2003). Genome-Wide Insertional Mutagenesis of Arabidopsis thaliana. *Science (American Association for the Advancement of Science)*, *301*(5633), 653–657. https://doi.org/10.1126/science.1086391

Andrews, S. (2010). *FastQC: A Quality Control Tool for High Throughput Sequence Data*. http://www.bioinformatics.babraham.ac.uk/projects/fastqc/

Bai, N., Roder, H., Dickson, A., & Karanicolas, J. (2019). Isothermal Analysis of ThermoFluor Data can readily provide Quantitative Binding Affinities. *Scientific Reports*, *9*(1), 2650–2650. https://doi.org/10.1038/s41598-018-37072-x

Bolger, A. M., Lohse, M., & Usadel, B. (2014). Trimmomatic: A flexible trimmer for Illumina sequence data. *BIOINFORMATICS*, *30*(15), 2114–2120. https://doi.org/10.1093/bioinformatics/btu170

Bolte, S., & Cordelières, F. P. (2006). A guided tour into subcellular colocalization analysis in light microscopy. *Journal of Microscopy (Oxford)*, *224*(3), 213–232. https://doi.org/10.1111/j.1365-2818.2006.01706.x

Cingolani, P., Platts, A., Wang, L. L., Coon, M., Nguyen, T., Wang, L., Land, S. J., Lu, X., & Ruden, D. M. (2012). A program for annotating and predicting the effects of single nucleotide polymorphisms, SnpEff: SNPs in the genome of Drosophila melanogaster strain w1118; iso-2; iso-3. *Fly (Austin, Tex.)*, *6*(2), 80–92. https://doi.org/10.4161/fly.19695

Cummings, R. D., & McEver, R. P. (2009). C-type Lectins. In A. Varki, R. D. Cummings, J. D. Esko, H. H. Freeze, P. Stanley, C. R. Bertozzi, G. W. Hart, & M. E. Etzler (Eds.), *Essentials of Glycobiology* (2nd ed.). Cold Spring Harbor Laboratory Press. http://www.ncbi.nlm.nih.gov/books/NBK1943/

Danecek, P., Auton, A., Abecasis, G., Albers, C. A., Banks, E., DePristo, M. A., Handsaker, R. E., Lunter, G., Marth, G. T., Sherry, S. T., McVean, G., Durbin, R., & 1000 Genomes Project Analysis Group. (2011). The variant call format and VCFtools. *Bioinformatics*, *27*(15), 2156–2158. https://doi.org/10.1093/bioinformatics/btr330

Fox, J. D., Routzahn, K. M., Bucher, M. H., & Waugh, D. S. (2003). Maltodextrin-binding proteins from diverse bacteria and archaea are potent solubility enhancers. *FEBS Letters*, *537*(1–3), 53–57. https://doi.org/10.1016/S0014-5793(03)00070-X

Fox, J. D., & Waugh, D. S. (2003). Maltose-binding protein as a solubility enhancer. *Methods in Molecular Biology (Clifton, N.J.)*, *205*(Journal Article), 99.

Garcia, D., Saingery, V., Chambrier, P., Mayer, U., Jürgens, G., & Berger, F. (2003). Arabidopsis haiku Mutants Reveal New Controls of Seed Size by Endosperm. *Plant Physiology (Bethesda)*, *131*(4), 1661–1670. https://doi.org/10.1104/pp.102.018762

Geldner, N., Dénervaud-Tendon, V., Hyman, D. L., Mayer, U., Stierhof, Y., & Chory, J. (2009). Rapid, combinatorial analysis of membrane compartments in intact plants with a multicolor marker set. *The Plant Journal : For Cell and Molecular Biology*, *59*(1), 169–178. https://doi.org/10.1111/j.1365-313X.2009.03851.x

Goldman, M. H. S., Goldberg, R. B., & Mariani, C. (1994). Female sterile tobacco plants are produced by stigma-specific cell ablation. *The EMBO Journal*, *13*(13), 2976–2984. https://doi.org/10.1002/j.1460-2075.1994.tb06596.x

Hansen, S. F., Harholt, J., Oikawa, A., Scheller, H. V., & Joint Bioenergy Institute (JBEI). (2012). Plant glycosyltransferases beyond CAZy: A perspective on DUF families. *Frontiers in Plant Science*, *3*(Journal Article), 59–59. https://doi.org/10.3389/fpls.2012.00059

Hellens, R. P., Edwards, E. A., Leyland, N. R., Bean, S., & Mullineaux, P. M. (2000). pGreen: A versatile and flexible binary Ti vector for Agrobacterium-mediated plant transformation. *Plant Molecular Biology*, *42*(6), 819–832. https://doi.org/10.1023/A:1006496308160

Lairson, L. L., Henrissat, B., Davies, G. J., & Withers, S. G. (2008). Glycosyltransferases: Structures, functions, and mechanisms. *Annual Review of Biochemistry*, *77*(1), 521–555. https://doi.org/10.1146/annurev.biochem.76.061005.092322

Levitin, B., Richter, D., Markovich, I., & Zik, M. (2008). Arabinogalactan proteins 6 and 11 are required for stamen and pollen function in Arabidopsis. *The Plant Journal : For Cell and Molecular Biology*, *56*(3), 351–363. https://doi.org/10.1111/j.1365-313X.2008.03607.x

Li, H. (2011). A statistical framework for SNP calling, mutation discovery, association mapping and population genetical parameter estimation from sequencing data. *Bioinformatics*, *27*(21), 2987–2993. https://doi.org/10.1093/bioinformatics/btr509

Li, H., & Durbin, R. (2009). Fast and accurate short read alignment with Burrows–Wheeler transform. *Bioinformatics*, *25*(14), 1754–1760. https://doi.org/10.1093/bioinformatics/btp324

Li, H., Handsaker, B., Wysoker, A., Fennell, T., Ruan, J., Homer, N., Marth, G., Abecasis, G., Durbin, R., 1000 Genome Project Data Proc, & 1000 Genome Project Data Processing Subgroup. (2009). The Sequence Alignment/Map format and SAMtools. *Bioinformatics*, *25*(16), 2078–2079. https://doi.org/10.1093/bioinformatics/btp352

Li, Z., Han, K., Pak, J. E., Satkunarajah, M., Zhou, D., & Rini, J. M. (2017). Recognition of EGF-like domains by the Notch-modifying O-fucosyltransferase POFUT1. *Nature Chemical Biology*, *13*(7), 757–763. https://doi.org/10.1038/nchembio.2381

Lira-Navarrete, E., Valero-González, J., Villanueva, R., Martínez-Júlvez, M., Tejero, T., Merino, P., Panjikar, S., & Hurtado-Guerrero, R. (2011). Structural insights into the mechanism of protein O-fucosylation. *PloS One*, *6*(9), e25365–e25365. https://doi.org/10.1371/journal.pone.0025365

Liu, X., Salokas, K., Tamene, F., Jiu, Y., Weldatsadik, R. G., Ohman, T., & Varjosalo, M. (2018). An AP-MS- and BioID-compatible MAC-tag enables comprehensive mapping of protein interactions and subcellular localizations. *Nature Communications*, *9*(1), 1188–1188. https://doi.org/10.1038/s41467-018-03523-2

Lombard, V., Ramulu, H. G., Drula, E., Coutinho, P. M., & Henrissat, B. (2014). The carbohydrate-active enzymes database (CAZy) in 2013. *Nucleic Acids Research*, *42*(D1), D490–D495. https://doi.org/10.1093/nar/gkt1178

Luo, Y., & Haltiwanger, R. S. (2005). O-Fucosylation of Notch Occurs in the Endoplasmic Reticulum. *The Journal of Biological Chemistry*, *280*(12), 11289–11294. https://doi.org/10.1074/jbc.M414574200

McMillan, B. J., Zimmerman, B., Egan, E. D., Lofgren, M., Xu, X., Hesser, A., Blacklow, S. C., & Argonne National Lab. (ANL), A., IL (United States). Advanced Photon Source (APS). (2017). Structure of human POFUT1, its requirement in ligand-independent oncogenic Notch signaling, and functional effects of Dowling-Degos mutations. *Glycobiology (Oxford)*, *27*(8), 777–786. https://doi.org/10.1093/glycob/cwx020

Mohnen, D. (2008). Pectin structure and biosynthesis. *Current Opinion in Plant Biology*, *11*(3), 266–277. https://doi.org/10.1016/j.pbi.2008.03.006

Moremen, K. W., Ramiah, A., Stuart, M., Steel, J., Meng, L., Forouhar, F., Moniz, H. A., Gahlay, G., Gao, Z., Chapla, D., Wang, S., Yang, J.-Y., Prabhakar, P. K., Johnson, R., dela Rosa, M., Geisler, C., Nairn, A. V., Seetharaman, J., Wu, S.-C., … Argonne National Lab. (ANL), A., IL (United States). (2017). Expression system for structural and functional studies of human glycosylation enzymes. *Nature Chemical Biology*, *14*(2), 156–162. https://doi.org/10.1038/NCHEMBIO.2539

Nallamsetty, S., Austin, B. P., Penrose, K. J., & Waugh, D. S. (2005). Gateway vectors for the production of combinatorially-tagged His6-MBP fusion proteins in the cytoplasm and periplasm of Escherichia coli. *Protein Science*, *14*(12), 2964–2971. https://doi.org/10.1110/ps.051718605

Neumetzler, L., Humphrey, T., Lumba, S., Snyder, S., Yeats, T. H., Usadel, B., Vasilevski, A., Patel, J., Rose, J. K. C., Persson, S., & Bonetta, D. (2012). The FRIABLE1 Gene Product Affects Cell Adhesion in Arabidopsis. *PloS One*, *7*(8), e42914–e42914. https://doi.org/10.1371/journal.pone.0042914

Qin, Y., Leydon, A. R., Manziello, A., Pandey, R., Mount, D., Denic, S., Vasic, B., Johnson, M. A., & Palanivelu, R. (2009). Penetration of the Stigma and Style Elicits a Novel Transcriptome in Pollen Tubes, Pointing to Genes Critical for Growth in a Pistil. *PLoS Genetics*, *5*(8), e1000621–e1000621. https://doi.org/10.1371/journal.pgen.1000621

Robson, S. C., Sévigny, J., & Zimmermann, H. (2006). The E-NTPDase family of ectonucleotidases: Structure function relationships and pathophysiological significance. *Purinergic Signalling*, *2*(2), 409–430. https://doi.org/10.1007/s11302-006-9003-5

Schiott, M., Romanowsky, S., Baekgaard, L., Jakobsen, M., Palmgren, M., & Harper, J. (2004). A Plant Plasma Membrane Ca2+Pump Is Required for Normal Pollen Tube Growth and Fertilization. *Proceedings of the National Academy of Sciences - PNAS*, *101*(25), 9502–9507. https://doi.org/10.1073/pnas.0401542101

Schmid, J., Heider, D., Wendel, N. J., Sperl, N., & Sieber, V. (2016). Bacterial Glycosyltransferases: Challenges and Opportunities of a Highly Diverse Enzyme Class Toward Tailoring Natural Products. *Frontiers in Microbiology*, *7*(Journal Article), 182–182. https://doi.org/10.3389/fmicb.2016.00182

Smith, D. K., Harper, J. F., & Wallace, I. S. (2018b). A potential role for protein O-fucosylation during pollen-pistil interactions. *Plant Signaling & Behavior*, *13*(5), e1467687–e1467687. https://doi.org/10.1080/15592324.2018.1467687

Smith, D. K., Jones, D. M., Lau, J. B. R., Cruz, E. R., Brown, E., Harper, J. F., & Wallace, I. S. (2018a). A Putative Protein O-Fucosyltransferase Facilitates Pollen Tube Penetration through the Stigma-Style Interface. *Plant Physiology (Bethesda)*, *176*(4), 2804–2818. https://doi.org/10.1104/pp.17.01577

Sonnhammer, E. L., von Heijne, G., & Krogh, A. (1998). A hidden Markov model for predicting transmembrane helices in protein sequences. *Proceedings. International Conference on Intelligent Systems for Molecular Biology*, *6*(Journal Article), 175.

Szmelcman, S., & Hofnung, M. (1975). Maltose transport in Escherichia coli K-12: Involvement of the bacteriophage lambda receptor. *Journal of Bacteriology*, *124*(1), 112–118.

Tanz, S. K., Castleden, I., Hooper, C. M., Vacher, M., Small, I., & Millar, H. A. (2013). SUBA3: A database for integrating experimentation and prediction to define the SUBcellular location of proteins in Arabidopsis. *Nucleic Acids Research*, *41*(D1), D1185–D1191. https://doi.org/10.1093/nar/gks1151

Trindade, H., Boavida, L. C., Borralho, N., & Feijó, J. A. (2001). Successful Fertilization and Seed Set from Pollination on Immature Non-dehisced Flowers of Eucalyptus globulus. *Annals of Botany*, *87*(4), 469–475. https://doi.org/10.1006/anbo.2000.1359

Tsai, A. Y.-L., Kunieda, T., Rogalski, J., Foster, L. J., Ellis, B. E., & Haughn, G. W. (2017). Identification and Characterization of Arabidopsis Seed Coat Mucilage Proteins. *Plant Physiology (Bethesda)*, *173*(2), 1059–1074. https://doi.org/10.1104/pp.16.01600

Van Tuyl, J. M., Van Diën, M. P., Van Creij, M. G. M., Van Kleinwee, T. C. M., Franken, J., & Bino, R. J. (1991). Application of in vitro pollination, ovary culture, ovule culture and embryo rescue for overcoming incongruity barriers in interspecific Lilium crosses. *Plant Science (Limerick)*, *74*(1), 115–126. https://doi.org/10.1016/0168-9452(91)90262-7

Verger, S., Chabout, S., Gineau, E., & Mouille, G. (2016). Cell adhesion in plants is under the control of putative O-fucosyltransferases. *Development (Cambridge)*, *143*(14), 2536–2540. https://doi.org/10.1242/dev.132308

Wang, L., & Ruan, Y.-L. (2013). Regulation of cell division and expansion by sugar and auxin signaling. *Frontiers in Plant Science*, *4*(Journal Article), 163–163. https://doi.org/10.3389/fpls.2013.00163

Wang, L., Wang, W., Wang, Y.-Q., Liu, Y.-Y., Wang, J.-X., Zhang, X.-Q., Ye, D., & Chen, L.-Q. (2013). Arabidopsis Galacturonosyltransferase (GAUT) 13 and GAUT14 Have Redundant Functions in Pollen Tube Growth. *Molecular Plant*, *6*(4), 1131–1148. https://doi.org/10.1093/mp/sst084

Wang, S., Li, Z., Yu, Y., & Xu, J. (2017a). Folding Membrane Proteins by Deep Transfer Learning. *Cell Systems*, *5*(3), 202.

Wang, S., Sun, S., Li, Z., Zhang, R., & Xu, J. (2017b). Accurate De Novo Prediction of Protein Contact Map by Ultra-Deep Learning Model. *PLoS Computational Biology*, *13*(1), e1005324–e1005324. https://doi.org/10.1371/journal.pcbi.1005324

Wang, S., Sun, S., & Xu, J. (2018). Analysis of deep learning methods for blind protein contact prediction in CASP12. *Proteins, Structure, Function, and Bioinformatics*, *86*(S1), 67–77. https://doi.org/10.1002/prot.25377

Waterhouse, A., Bertoni, M., Bienert, S., Studer, G., Tauriello, G., Gumienny, R., Heer, F. T., de Beer, T. A. P., Rempfer, C., Bordoli, L., Lepore, R., & Schwede, T. (2018). SWISS-MODEL: homology modelling of protein structures and complexes. *Nucleic Acids Research*, *46*(W1), W296–W303. https://doi.org/10.1093/nar/gky427

Weigand, C., & Harper, J. (2020). Decapitation Crosses to Test Pollen Fertility Mutations for Defects in Stigma-Style Penetration. *Methods in Molecular Biology (Clifton, N.J.)*, *2160*(Journal Article), 29.

Wilson, Z. A., Morroll, S. M., Dawson, J., Swarup, R., & Tighe, P. J. (2001). The Arabidopsis MALE STERILITY1 (MS1) gene is a transcriptional regulator of male gametogenesis, with homology to the PHD-finger family of transcription factors. *The Plant Journal : For Cell and Molecular Biology*, *28*(1), 27–39. https://doi.org/10.1046/j.1365-313X.2001.01125.x

Wu, Z. L., Ethen, C. M., Prather, B., Machacek, M., & Jiang, W. (2011). Universal phosphatase-coupled glycosyltransferase assay. *Glycobiology (Oxford)*, *21*(6), 727–733. https://doi.org/10.1093/glycob/cwq187

Xu, J. (2019). Distance-based protein folding powered by deep learning. *Proceedings of the National Academy of Sciences - PNAS*, *116*(34), 16856–16865. https://doi.org/10.1073/pnas.1821309116

Xu, J., McPartlon, M., & Li, J. (2021). Improved protein structure prediction by deep learning irrespective of co-evolution information. *Nature Machine Intelligence*, *Journal Article*. https://doi.org/10.1038/s42256-021-00348-5

Xu, J., & Wang, S. (2019). Analysis of distance-based protein structure prediction by deep learning in CASP13. *Proteins, Structure, Function, and Bioinformatics*, *87*(12), 1069–1081. https://doi.org/10.1002/prot.25810

Zarkar, N., Nasiri Khalili, M. A., Khodadadi, S., Zeinoddini, M., & Ahmadpour, F. (2020). Expression and purification of soluble and functional fusion protein DAB 389 IL-2 into the E. coli strain Rosetta-gami (DE3). *Biotechnology and Applied Biochemistry*, *67*(2), 206–212. https://doi.org/10.1002/bab.1833

Chapter 4: Discussion

I. AtOFT1 facilitates efficient pollen tube penetration during double fertilization

Data mining of amino acid sequences to identify sequence homology with known catalytic glycosyltransferase domains and glycan modifying enzymes mainly from metazoan systems has facilitated predictive familial groupings and essential insights into the potential functions of uncharacterized proteins that resemble carbohydrate active enzymes (Hansen *et al.,* 2012). Perpetuating the ambiguity of these proteins are the overwhelming difficulties in experimentally investigating these enzymes across all organisms, which has further stifled our understanding. Nonetheless, these predictive efforts have provided fascinating insights into the potential function of unknown proteins and has allowed for more focused scientific studies. In general, land plants display an overall genome expansion in putative glycan-associated proteins, and in *Arabidopsis thaliana,* 39 unique genes display sequence conservation in the known domain responsible for GDP-fucose Protein O-fucosyltransferase 1 catalytic activity (Pfam ID PF10250; InterPro ID IPR019378). These genes comprise the Arabidopsis putative POFT family, which are alternatively classified as Glycosyltransferase 65 (GT 65; cazy.org) and DUF264 proteins. These enzymes are best represented by metazoan Protein O-FucosylTransferase 1's (POFT1s), which are most notable for their function in the Notch Signaling Pathway. Interestingly, plant systems do not contain the necessary proteins to perform canonical Notch signaling, and in Arabidopsis, the SPINDLY (SPY, At3g11540; Zentella *et al.,* 2017) protein is the only biochemically defined POFT,. However, SPINDLY was not initially predicted to be a protein O-fucosyltransferase, does not contain a canonical POFT domain, and is not included in the hypothesized familial

grouping of the *Arabidopsis thaliana* putative POFT family. The research detailed in this dissertation aids in delineating the relationship between metazoan POFT1s and the putative POFT family of enzymes in Arabidopsis.

We began our investigation of the *Arabidopsis thaliana* putative POFT family by determining the relative amino acid sequence relationship between the 39 Arabidopsis proteins included in this family and known model metazoan POFT1s by performing a multiple sequence alignment. This analysis demonstrated that some Arabidopsis POFTs are more similar to metazoan POFT1s at the amino acid level than to some of their putative homologous genes. AtOFT1 is a novel family member that demonstrates this phylogenetic relationship and was investigated due to its striking mutant silique morphology, indicating that this gene is involved in some process underlying plant sexual reproduction. *AtOFT1* T-DNA insertional mutants (*oft1)* exhibit shortened silique lengths as well as a significant reduction in seed set. Outcross analysis determined that this phenotype was associated with the male gamete (pollen), and an examination of public expression analysis as well as promoter::GFP fusions demonstrated that *AtOFT1* is highly expressed in germinated pollen tubes (PT(s)).

Further investigation of the *oft1* mutant phenotype surprisingly demonstrated that under *in vitro* germination conditions, no morphological defects between *oft1* PTs and Col-0 wildtype control PTs exist. However, in the presence of female tissues, *oft1's* pollen defects become evident, as mutant pollen tubes are mainly retained at the stigma-style interface and routinely failed to efficiently penetrate beyond this barrier into the ovary. These results provided a basic explanation for the observed reduction in silique

length and seed set of *oft1* mutants lines, as PTs must continue to directionally grow into the transmitting tract and eventually into the ovary where unfertilized ovules reside.

Investigating the extent of *oft1* mutant PTs inability to traverse the stigma-style interface was assessed by *SIV* fertilization analyses, which demonstrated *oft1* PTs penetrate through these initial female tissues at a slower rate compared to Col-0 PTs and overall, fewer PTs emerge from the bottom of the style. Notably, following emergence from the bottom of the style, *oft1* PT elongation rate is slower than that of wildtype after emergence from the style in these assays. Overall, these analyses suggest that *oft1* mutant PTs are defective at penetrative growth through the stigma and style of the pistil and rarely make it into the ovary to fertilize ovules.

Passage through the style represents a critical checkpoint for the PT before it progresses into the ovary, as this tissue-specific male-female interaction alters gene expression in the PT, which enables the PT to perceive guidance signals and induces rapid PT growth (Palanivelu and Tsukamoto, 2011). Rare amino acids, such as D-serine and gamma-aminobutyric acid (GABA), are present in the style and exhibit dual functionality to both facilitate cross-talk between the PT and pistil and increase the growth rate of PTs (Michard *et al.,* 2011). For example, GABA applied at low concentrations to *in vitro* germinated PTs stimulates growth, while the Arabidopsis *POLLEN ON PISTIL 2 (At3g22200)* gene that natively encodes a GABA transaminase, which acts to degrade this amino acid, is proposed to establish a chemical positional guidance gradient that extends into the ovary, and loss-of-function mutants *(pop2-1)* exhibit reproductive defects associated with PT growth arrest (Palanivelu *et al.,* 2003).

Generating hemizygous complement lines allowed for *oft1's* mutant PT penetration defect to be more thoroughly investigated and ruled out other possible pollen-related abnormalities that could have accounted its phenotype. These lines facilitated an endogenous control to evaluate mutant and complemented pollen as the segregation of male gametes at each anther on each flower of these plants predictably produced a 1:1 ratio of complemented *oft1* pollen: uncomplemented *oft1* mutant pollen. These hemizygous rescue lines allowed us to determine that only a single copy of the endogenous *AtOFT1* gene reintroduced into the mutant *oft1* background was sufficient to restore the seed set back to that of wildtype. An alternative explanation of *oft1's* fertilization defect could be explained by a reduction in *oft1's* ability to produce a pollen tube. However, *in vitro* germination of pollen from hemizygous lines showed no abnormalities pertaining to this theory, as the germination frequency between complemented and uncomplemented *oft1* pollen was equivalent. Furthermore, hemizygous pollen was assessed to ensure that the lack of an *in vitro* PT phenotype was maintained between complemented and uncomplemented *oft1* mutant pollen from hemizygous lines, which allowed us to consider complemented *oft1* pollen as "wildtype" in *in vivo assays.* Outcrosses were performed using pollen from these lines, and further confirmed loss of *AtOFT1* specifically impacted the pollen and complemented pollen effectively restored the TE expected of the *oft1* mutant allele, as *oft1* pollen containing the complement construct were able to achieve 100% TE compared to the same outcross with uncomplemented to $oft1^{+/-}$ mutant pollen ($TE=5.3x10^{-4}$). These results indicated that only *oft1* pollen containing the complement construct beat uncomplemented *oft1* pollen to fertilize ovules in every cross made with this pollen population.

Following these evaluations, we implemented *oft1-3*$^{-/-}$*;11p::OFT1-GFP*$^{+/-}$ hemizygous pollen in *SIV* fertilization assays to precisely evaluate the severity of the *oft1* mutant PT penetration defect. In these direct competition assays, the intensity of *oft1* mutant's delay in penetrating the stigma-style interface was illustrated, as >90% of PTs emerging from the bottom of the style were complemented *oft1* PTs. These results showed that uncomplemented *oft1* PTs were indeed being outcompeted to fertilize the limited number of ovules contained within the ovary by complemented *oft1* PTs due to their difficulties in penetrating through the stigma-style interface. Taken together, creation of this rare endogenous control line not only allowed us to determine a single copy of the endogenous gene was adequate to restore the mutant reproductive phenotype but allowed us to rule out the possibility of a pollen grain germination defect and fully demonstrated the severe barrier that the stigma-style interface poses to *oft1's* ability to fertilize ovules.

In acknowledgment that the stigma and style is a critical impediment to *oft1's* capacity to fertilize ovules, we dissected these tissues away from pistils and applied *oft1*$^{+/-}$ pollen to the decapitated surface. Surprisingly, in the absence of the stigma-style interface, *oft1*$^{-}$ mutant pollen tubes are over 700-fold more successful at fertilizing ovules. Although this result further defined the stigma and style as an extreme barrier to *oft1* PT fertilization, the transmission of the mutant allele in the absence of these tissues did not achieve that expected if these female tissues are the sole cause of *oft1's* PT penetration defect and indicated *oft1* retains fertilization defects in the later tissues of the pistil. After exiting the style, PTs must continue to penetratively grow into the TT before emergence into the ovary cavity (Johnson and Preuss, 2002). Thus, one explanation that

could explain why *oft1* mutant PTs lack of ability to reach the expected TE in decapitation assays may be due to the continued requirement of penetrative growth in the TT prior to being able to reach the ovary cavity, as this mechanism of growth was demonstrated to be ineffective for *oft1* PT elongation through the stigma and style.

Amidst our investigations, we noticed that *oft1* mutant lines additionally display abnormal vegetative phenotypes, including longer root lengths and etiolated hypocotyls as well as increased rosette diameters compared to control lines. Furthermore, total plant height and delayed senescence were noted as additional potentially interesting vegetative phenotypes of *oft1* mutant lines, but experimental verification of the significance of these characteristics requires experimental evaluation. Seed size and mucilage area of homozygous *oft1* mutant seed is also increased in *oft1* mutant lines, suggesting a potential defect in cell wall composition and or a dysregulation in cell wall polysaccharide biosynthesis or deposition. However, assessing the monosaccharide profiles of *oft1* stems, showed increased xylose is the only cell wall sugar that differs across all three *oft1* mutant lines. This result suggests that xylose in the secondary cell walls of *oft1* stems is related to an increase in xylan in the secondary cell wall, which is the second most abundant polysaccharide in this cellular layer (Zhong *et al.,* 2019). Xylan is composed of β-1,4-linked xylose arranged linearly, and acts to strengthen the secondary cell wall through hydrogen bonding with cellulose microfibrils as well as aids in biomass recalcitrance, plant protection, and regulation of cell expansion (Hummel, 2008; Zhong *et al.,* 2019). Moreover, xylose is present in seed mucilage in the predominant form of xylan at low but appreciable concentrations in seed mucilage, as it functions as a critical mediator of an adherent mucilage layer and proper polysaccharide distribution through its

branching with rhamnogalacturonan I (RG-I) chains that interact with innermost cellulose mucilage layer, which anchors the mucilage to the seed coat (Ralet *et al.,* 2016). Xyloglucan (XyG) is composed of a backbone of β-1,4-linked glucosyl residues substituted on the 6-position by α-linked xylose, which can be further substituted with galactose and fucose residues and is the major hemicellulose in angiosperm primary cell walls (Oikawa *et al.,* 2013; Kim *et al,.* 2020). Although the function of XyG in primary cell walls seems to remain dynamic and debatable, mutant lines have demonstrated the importance of XyG in cell wall rigidity under stress conditions as well as cell expansion and adhesion (Young *et al.,* 2008; Voinicuic *et al.,* 2015).

Furthermore, the presence of these arabinose and fucose substitutions on XyG mediates its interactions with cellulose microfibrils, which can be further O-acetylated on galactose residues. In PTs, XyG shows high levels of fucosylation that is distributed evenly around the cell wall and notably, is absent in regions of the PT that changed directions or diameter (Chebli *et al.,* 2012). Additionally, O-acetylation and fucosylation of XyG in the PT is thought to mediate its interactions with cellulose and other pistil cell wall components at the apical tip allowing for rapid growth during the process of double fertilization (Mollet *et al.,* 2013).

The sum of the phenotypic traits that *oft1* exhibits make for a potential agronomically attractive gene to probe in other plant species for increased plant biomass and seed size. Plant biomass is considered one of the most sustainable bioresources that is utilized for the production of numerous industrial important products, such as clothing, biofuels, and therapeutics (Yang and Li, 2021; Fernando, 2012). For plants that are cultivated for their vegetative tissue biomass, such as hemp, the fertility defects that are imparted by loss-of-

function of *AtOFT1* would not be a limitation. However, increasing biomass and retaining the ability to efficiently perform double fertilization would make for a generally elite crop, which could be achieved by simply expressing *AtOFT1* or its species-specific genetic homolog under a pollen specific promoter, such as *AGP11,* in the mutant background (Levitin *et al.,* 2008).

II. Biochemical characterization of *Arabidopsis thaliana* putative POFT family members

We began to investigate AtOFT1 at the molecular level by subcellular colocalization analysis and determined that AtOFT1 is localized to the trans-Golgi apparatus. Interestingly, all 39 *Arabidopsis thaliana* putative POFT family genes, except for two genes that share the high sequence homology with AtOFT1 (*At5g50420* and *At1g17270*), have been localized to the Golgi-apparatus by either confocal microscopy, LOPIT proteomic investigation, or both techniques (Nikolovski *et al.,* 2012; Takenaka *et al.,* 2018; Stonebloom *et al.,* 2016; Verger *et al.,* 2016). The Golgi-apparatus represents a fundamental organelle in all eukaryotic life forms, but in plant systems is especially critical for synthesizing all cell wall polysaccharide components, except for cellulose, and the most important enzymes involved in this process are glycosyltransferases (Oikawa *et al.,* 2013). This result further suggests that AtOFT1 as well as its family members were potentially correctly grouped and may function as protein O-fucosyltransferases in the Golgi-*trans*-Golgi-apparatus.

We then aimed to understand which pathways AtOFT1 participates in by performing a random mutagenesis suppressor screen using EMS. We phenotypically identified two mutants that effectively restored the fertilization defects of *oft1* mutants and refer to them *soft1* and *soft2*. *soft1* EMS mutants did not show any deviations from

Col-0 controls with regards to silique length and seed set, while *soft2* EMS lines were increased in these metrics compared to *oft1* mutant lines but were still significantly different than wildtype Col-0 controls. EMS induced mutations in an Arabidopsis seed population can occur at a frequency of 4.4×10^7 bp, which is why extensive backcrossing is required to rid the genome of unrelated mutations (Jander *et al.,* 2003). The incomplete restoration of silique length and fertility observed in the *soft2* lines, was initially believed to be caused by residual EMS mutations that inferred with seed set production. Interestingly, when we investigated the PT penetration ability of the *soft* EMS lines *in vivo,* both lines display only a marginal increase in PT penetration ability, which we infer to be adequate for restoring the seed set defects of *oft1* mutants. Furthermore, this result suggests the virility of Col-0 PTs is not necessary to effectively fertilize ovules in the absence of competition from wildtype pollen.

Genome resequencing the *soft1* and *soft2* EMS lines was conducted and following bioinformatic processing of these data in combination with a knowledge-based approach to filtering potentially disrupted gene disrupted in each *soft* line, we postulated *At1g11990* was the disrupted gene in *soft1* lines and *AtGAUT14* was compromised and responsible for the *soft2* EMS fertility phenotype. To verify these were the correct gene targets, double mutant T-DNA lines facilitating loss-of-function in *At1g11990* and *AtOFT1* as well as *AtGAUT14* and *AtOFT1* were created. The *At1g11990/oft1* double mutant seed set was equal to that of *oft1,* indicating that this gene was not responsible for the suppression of the *oft1* silique length and seed set phenotype, and the list of potential gene candidates must be reevaluated to determine the genetic target in *soft1* EMS lines. On the other hand, *AtGAUT14* was the correct gene candidate, as the double mutant lines

almost completely restored the fertility phenotype of *oft1* mutants back to that of wildtype. We postulate that the silique lengths and seed set of the *gaut14/oft1* mutant line did not completely achieve that of wildtype due to *AtGAUT14's* function redundancy with *AtGAUT13,* which was demonstrated by no apparent phenotype in single homozygous loss-of-function mutants in *AtGAUT13 (gaut13-1)* and *AtGAUT14 (gaut14-1, gaut14-2)* but *gaut13/gaut14* homozygous double mutant lines are severely reproductively compromised due to an abnormal distribution of methyesterified homogalacturonan (HG) in the PT cell wall, which impairs PT morphology and growth (Wang, L. *et al.,* 2013). Therefore, we postulate that triple homozygous knockout lines in *AtOFT1, AtGAUT14,* and *AtGAUT13,* which are currently being developed, will fully restore the seed set of these mutants, elucidate another gene involved in *AtOFT1's* mechanistic pathway in PTs, as well as reemphasize the redundancy of *AtGAUT13* and *AtGAUT14*. Nonetheless, outcrosses with *oft1-3*$^{+/-}$*/gaut14-1*$^{-/-}$ lines to Col-0 emasculated pistils substantially increased the TE of the *oft1*$^{-}$ mutant allele by approximately 19,000 % compared to the same outcross scheme using *oft1-3*$^{+/-}$ pollen (TE 0.101 vs 5.3 x 10^{-4}), indicating that AtGAUT14 interacts with the same pathway that AtOFT1 participates in in PTs. Furthermore, these results strongly suggest that the *oft1* mutant phenotype may be related to a disrupted pectic polysaccharide composition that cannot dynamically accommodate the rapid and targeted PT growth necessary to effectively fertilize ovules during the process of double fertilization.

Additional pathway interactions with AtOFT1 will undoubtably be illuminated by using the successfully established BioID proximity labeling system in *Arabidopsis*

thaliana, as this system can identify both transient and stable interacting proteins that come within a 10 nm radius of the expressed fusion protein (Liu *et al.,* 2018).

A more detailed analysis of the specific amino acid sequence conservation between model metazoan POFT1s and AtOFT1, indicated residues known to participate in the protein O-fucosyltransferase catalysis in metazoan were conserved in AtOFT1. We evaluated the functional importance of these conserved catalytic residues by creating complement constructs containing a site-specific alteration at the conserved residue site to encode a null or synonymous residue and then tested each constructs' ability to complement the reproductive phenotype of *oft1* mutant lines. These results demonstrated that these conserved catalytic residues are essential to AtOFT1's function as well, and the uncomplemented seed sets of these lines could not be explained by a lack of construct expression or incorrect subcellular localization. These result not only illustrated that AtOFT1 shares a more intimate sequence relationship than previously determined, but strongly suggested that its catalytic mechanism may be protein O-fucosylation.

Investigating the catalytic identity of AtOFT1 proved challenging as endogenous and recombinant expression was consistently retained in the membrane fraction of all expression platforms tested as well as in *Arabidopsis thaliana* and was not produced by the cell-free expression kit tested. Although, successful solubilization out of seedling overexpressing *AtOFT1-GFP* was achieved with the Profoldin Membrane Protein Detergent Kit. However, purification issues were faced using anti-GFP magnetic beads to isolate solubilized AtOFT1-GFP, as the protein would only elute off of the AC medium under denaturing conditions. In the future, this problem should be easily circumventable by creating an overexpression construct with a different affinity purification epitope

translationally fused to *AtOFT1* and introgressing it into *Arabidopsis thaliana* to facilitate non-denaturing AC elution conditions and finally allowing for the catalytic activity of AtOFT1 to be evaluated.

During our struggles with recombinant expression of AtOFT1 in a soluble form, we postulated that at least some of the *Arabidopsis thaliana* putative POFT family members could be expressed. Indeed, out of 5 family members tested, 3 expressed in a soluble form in *E. coli* (AtESMD1, AtMSR1, and AtFRB1). These results also indicated that these family members could be isolated by AC to complete homogeneity at yields that were substantially sufficient for further examination of the protein's catalytic requirements. Our investigatory efforts in this vein were initially focused on characterizing AtMSR1 due to its demonstrated robust expression in our preliminary expression evaluation. Subjecting recombinantly expressed and isolated AtMSR1 to 7 different possible sugar-nucleotide donor substrates illustrated that this protein only utilizes GDP-fucose and none of the other sugar-nucleotides examined. This result is in line with the sugar-nucleotide donor substrate of metazoan POFT1s (Lira-Navarette *et al.,* 2011). DSF preoptimized with recombinantly expressed MBP demonstrated that AtMSR1 is a metal independent enzyme, as the protein became less stable in the presence of $MnCl_2$. Again, this result was in agreement with the characteristics of metazoan POFT1s (Lira-Navarette *et al.,* 2011), and further highlighted the catalytic similarities between AtMSR1 and metazoan POFT1s. Moreover, the same sugar-nucleotide donor substrate analysis was conducted on recombinantly expressed and isolated AtFRB1, and equal to AtMSR1, AtFRB1 only utilizes GDP-fucose as its preferred sugar-nucleotide donor substrate out of the sugar-nucleotides tested. These results added substance to our

hypothesis that the *Arabidopsis thaliana* putative POFT family are protein O-fucosyltransferases as they share a conserved catalytic domain with metazoan POFT1s as well as known key catalytic characteristics of these enzymes.

Fascinatingly, while composing this dissertation new biochemical evidence was illuminated, indicating all 39 genes belonging to the putative POFT family do not encode POFTs, as was first postulated by Hansen *et al.,* 2012. AtFRB1 and AtRRT4 were recently expressed in HEK293 cells, and catalytic analysis clearly demonstrated that these family members are rhamnosyltransferases that specifically participate in the elongation of the backbone of RG-I (personal communication with Debra Mohnen at the Complex Carbohydrate Research Center, University of Georgia). These genes formed a distinct group in our phylogenetic analysis of the putative POFT family that is composed of 8 other family members, including *AtRRT1, AtRRT2,* and *AtRRT3* (Figure 3.25). Moreover, the 39 genes belonging to the putative POFT family mostly cluster into four subgroups in our analysis, with *AtOFT1* forming the smallest gene grouping with 3 other family members. The preliminary evidence that AtFRB1 utilizes GDP-fucose, albeit at almost half the efficiency as AtMSR1, suggests that this enzyme may also have the ability to utilize more than one sugar-nucleotide substrate. In the future, expanding the repertoire of sugar-nucleotide substrates used to assess these family members, specifically UDP-rhamnose, should aid in providing a more accurate identification of these family members as well as further provide valuable insights into the putative POFT family subgroupings. Additionally, investigating non-protein acceptor substrates for these family members, specifically cell wall polysaccharides, would be wise as both AtRRT4 and AtFRB1 specifically transfer rhamnose onto the nascent end of galacturonic residues

and the expansion in general expansion of glycosyltransferases in land plants has been rationally proposed to be due to their polysaccharide-rich cell walls (Hansen *et al.,* 2012). Assessing non-protein substrates of this family, such as cell wall polysaccharides, can be achieved by catalytic analysis in glycan arrays, in which Strasser *et al.*, 2021 suggests different approaches to generating these on-chip assays.

Implementation of the fucose-specific AAL lectin allowed for the global Arabidopsis thaliana O-fucosylated proteome to be visualized. Isolation of these O-fucosylated proteins from Col-0 seedlings using AAL-agarose AC medium demonstrated that many O-linked glycans containing fucose are present in the Arabidopsis proteome. Identification of these proteins by mass spectrometry should allow for potential protein targets of the *Arabidopsis thaliana* putative POFT family to be identified by comparing the fucosylation protein profiles of mutant and wildtype lines. Furthermore, use of this AC medium should provide fundamental insight into the requirements of this type of post-translational modification on a target protein as well as the specific function this modification imparts on the target protein. Such an experiment to date has not been performed. Therefore, this data would greatly enhance our overall understanding of protein O-fucosylation, as little is currently known about this this type of modification in plant systems.

III. A putative model for the *oft1* mutant phenotype

We initially characterized a novel family member, *AtOFT1*, as a necessary enzyme in PTs that facilitates efficient PT penetration through the stigma-style interface and demonstrated these lines exhibit increased biomass. Although, the underlying pathway(s) associated with these phenotypes are currently outstanding, we postulate three

broad possibilities that could explain *oft1's* mutant phenotypes (Figure 4.1). First, we propose that *oft1* may lack the ability to perceive or utilize style provided molecular cues, as *oft1* PTs are retained largely retained in these tissues. Additionally, in *SIV* fertilization experiments, *oft1* pollen tubes exhibit a growth rate that is slower than Col-0 following emergence from the style, indicating the signaling cues that naturally induce rapid growth in these tissues was not perceived. Although investigations into the hypothesis with *oft1* have yet to be evaluated, exogenous application of GABA at low concentrations as well as tobacco stylar extract to *in vitro* germinated PTs has been used to identify PT mutants defective in perceiving these essential stylar molecules (Muschietti *et al,.* 1998; Wengier *et al.,* 2003).

Second, we postulate *oft1* may lack the cell wall composition necessary to sustain the rapid and targeted growth through the closed pistil tissues. Although, the seed mucilage and cell walls of *oft1* mutant pollen tubes have not been examined, the monosaccharide composition of mutant stems showed increased xylose content in the secondary cell walls, indicating that there is an abnormality in *oft1's* cell wall polysaccharide composition. Interestingly, exogenous application of xyloglucan oligosaccharides (XGO), or breakdown products of XyG, to tobacco BY2 cells or whole plants accelerated cell elongation and division, increased primary root growth, and stimulated pathogen defense responses, indicating that XGOs function in signaling, stress responses, cell division and transcriptional control as well as enhance expression of cell wall metabolism-related genes (González-Pérez *et al.,* 2014). Therefore, it is conceivable that an increase in xylose content may be eliciting a global response that could be contributing to the observed increase in root length, hypocotyl elongation, seed mucilage,

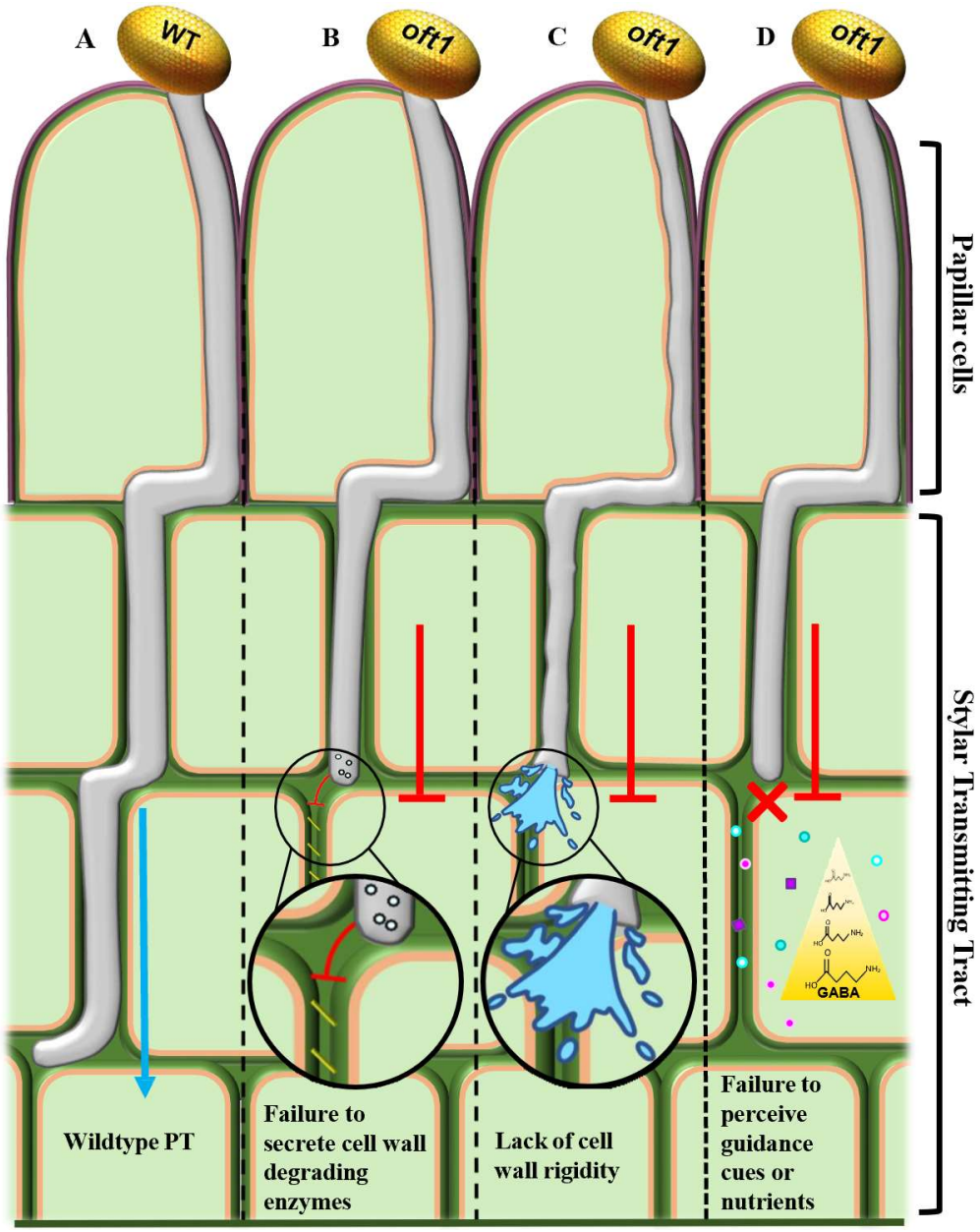

Figure 4.1: Illustration of proposed mechanisms for *oft1*$^{-/-}$ mutant pollen tube penetration defect. A, Col-0 (WT) pollen tube (PT) rapidly traversing the transmitting tract towards the ovary, while *oft1*$^{-/-}$ mutant PTs (A-C) exhibit slower penetration through these tissues, which most often results in arrested growth in the stigma and style. B, *oft1*$^{-/-}$ PT may not secrete or activate female tissue cell wall degrading enzymes, making passage through these tissues arduous. C, *oft1*$^{-/-}$ PTs may lack a cell wall rigidifying component that aids in penetrating though the female tissue layers during fertilization. D, *oft1*$^{-/-}$ PTs may lacks a functional receptor that is necessary for these mutant PTs to respond to positional guidance cues within the stylar transmitting tract (TT) or to metabolize the nutrients supplied by the female.

and seed and rosette diameter of *oft1* mutants. Furthermore, increased XyG in *oft1* PTs could be limiting cell expansion by too rigidly associating with cellulose microfibrils that are present at the apex and shanks of the elongating PT (Chebli *et al.,* 2012). Use of cell wall polysaccharide-specific fluorescent antibodies to probe the composition of *in vitro* germinated *oft1* mutant pollen tubes and seed mucilage compositions may be an effective tool to quickly evaluate this hypothesis.

Lastly, we postulate that *oft1* mutant PTs lack the ability to effectively secrete cell wall degrading enzymes. This hypothesis only accounts for the PT penetration defect exhibited by these mutants but may be a result of a disrupted cell wall polysaccharide composition, as described in the second theory. During double fertilization, the PT secretes a wide range of diverse proteins and peptides, and the PT secretome is specifically enriched in cell wall degrading enzymes, which not only suggests that these enzymes are required to maintain an elastic, rapidly growing pollen tube but additionally implies that the maternal tissues must also be loosened to accommodate the rate of PT elongation (Flores-Tornero *et al.,* 2021). Therefore, it is possible that *oft1* mutant PTs cannot effectively penetrate the stigma and style and continue to fail at efficient fertilization even in the absence of the stigma-style interface due to the pistil tissues being too rigid to traverse. Furthermore, increased Xyl in the secondary cell wall and XyG in primary cell walls have been demonstrated to prevent cell wall remodeling enzymes from accessing polysaccharides in these tissue layers (Selig *et al.,* 2009; Gille and Pauly, 2012). Therefore, increased XyG in the pollen tube could be preventing PT secretory vesicle cargo from reaching the extracellular space. XyG as well as vesicles targeted for exocytosis are derived from the Golgi-*trans* Golgi network, as this organelle mediates

both the biosynthesis of most cell wall polysaccharides and the sorting and packaging of exocytic vesicles (Champanoni and Blatt, 2006; Chebli *et al.,* 2012; Jai *et al.,* 2018; Oikawa *et al.,* 2013). AtOFT1 is also localized to the *trans*-Golgi-apparatus (Smith *et al.,* 2018a; Smith *et al.,* 2018b). Thus, investigating the endomembrane dynamics of *oft1* in *in vitro* germinated PTs by live cell imaging using plasma membrane-specific dyes, such as FM4-64 in conjunction with polysaccharide-specific fluorescent antibodies could quickly shed light on both the endomembrane trafficking dynamics in these mutants as well as the distribution of polysaccharides.

IV. Future directions

In this chapter, some key experiments to further our understanding of the *Arabidopsis thaliana* putative POFT family have been proposed. A continuation of suggested experimentation and recommendations for alternative investigatory approaches are outlined here.

a. Identifying the gene disrupted in *soft1* EMS lines

We initially postulated that the disrupted gene in *soft1* EMS lines was another member of the Arabidopsis putative POFT family due to the list of candidates containing another family member. Additionally, reports from other family members demonstrated that the single *AtFRB1 (AT5G01100)* mutants (*frb1)* exhibited cell wall alterations that resulted in a severe cell and organ dissociation phenotypes that could be completely suppressed by loss-of-function in another Arabidopsis putative POFT family member, *AtESMD1 (AT2G01480; esmd1)* (Neumetzler *et al.,* 2012; Verger *et al.,* 2016; Kohorn *et al.,* 2021). Furthermore, this team demonstrated that the same severe cell dissociation

phenotype was observed in the exonic *qua1* single mutant associated with a putative galacturnosyltransferase, *QUASIMODO1* (*AtGAUT8; AT3G25140*) and its similar cell wall detachment defects could also be effectively suppressed by loss-of-function in *AtESMD1* (Verger *et al.,* 2016; Kohorn *et al.,*2021). Although, our initial theory that the Arabidopsis POFT family member *At1g11990* was the gene disrupted in *soft1* lines was incorrect, as demonstrated by the double *At1g11990/oft1* homozygous T-DNA knockout lines did not restore silique length or seed set, a potentially more logical target in light of correctly identifying the *soft2* gene candidate is *GALACTURNOSYLTRANSFERASE (GATL3;At1g13250).* A Leucine11→Phe mutation was observed in *soft1* EMS lines, which is natively predicted to encodes a 5X Leu repeat domain that facilitates its anchoring and interactions in the Golgi. Further interesting, is its tissue specific expression pattern that is highly abundant in all floral organs, and is specifically high in the style, which is also the location of the pistil that *oft1* mutant pollen tubes have a problem traversing and further supports the formative suppression model (Kong *et al,.* 2013). The other candidate is, is a member of the exostosin family, *At1g21480,* which contains a Val416→Ile in its predicted signal anchoring sequence (72% predicted by SignalP-5.0 server), and mutant lines in a homolog of this gene display a fertilization defect at ambient humidity (30-40%) that result in a reduction in seed set and silique length, which can interestingly be rescued under high humidity conditions (Lao *et al,.* 2003). Furthermore, this protein resides in the Golgi-apparatus, and mutant lines suggest they function in some process underlying pectin biosynthesis (Lao *et al,.* 2003). Creating double *oft1/galt3* and *oft1/At1g21480* mutant T-DNA lines would provide insight into a potential interactions in the Golgi between AtOFT1 and either or potentially both of these

proteins. Lastly, the loss of function phenotype of *oft1/qui1* double mutant lines has also been of upmost interest, as *QUA1* seems to play an intimate role in the putative POFT family in Arabidopsis.

Although the mechanism of how the Arabidopsis putative POFT family and the GAUT family interact to impart co-regulatory functions remains unknown, a potential theory may be gleaned by looking at the mechanism of protein O-fucosylation by AtSPY. O-fucosylation of AtRG1 by SPY leads to inactivation of this master growth regulatory protein, while O-GlcNAcylation at the same amino acid residues by SECRET AGENT (AtSEC, At3g04240) activates AtRG1, allowing for expression of its downstream genes (Zantella *et al.,* 2017). Thus, the regulation of AtRGA1 is facilitated by competitive glycosylation by either SPY or SEC. Considering the case of the Arabidopsis putative POFT and GAUT families, a similar competitive glycosylation model may be at play for other transcriptional regulators yet to be identified. and may further explain the variety of phenotypes displayed by *oft1* mutants. For example, AtOFT1 and AtGAUT14 potentially competitively glycosylate the same residues within a transcription factor or both proper O-fucosylation and galacturonsylation of the regulatory protein may be required to mediate the genetic pathways controlled by the glycosylated protein. In *oft1* mutants, this dysregulation of the acceptor substrate may lead to constitutive activation or repression of the genetic pathway. Furthermore, the lack of a full seed set in *oft1/gaut14* double mutants could be the result of AtGAUT13 continuing to retain activity in these lines and to a degree facilitating galacturonsylation of the regulatory element and acting to some degree redundantly with AtGAUT14, which may be the cause of the incomplete suppression observed in the *oft1/gaut14* lines. Performing coimmunoprecipitation and

mass spectrometry with membrane microsomes prepared from *oft1-2$^{-/-}$;UBQ10::OFT1-GFP* 10-day-old light grown transgenic seedlings may be useful for determining potential protein substrates of AtOFT1, and further may elucidate if AtOFT1 directly interacts with AtGAUT14.

b. Suggestions for evaluating the identity of the other POFTs

All but two members of the *Arabidopsis thaliana* putative POFT family have been experimentally determined to localize to the Golgi-apparatus membrane (Smith *et al.,* 2018a; Smith *et al.,* 2018b; Nikolovski *et al.,* 2012; Takenaka *et al.,* 2018; Stonebloom *et al.,* 2016; Verger *et al.,* 2016). Furthermore, this study attempted expression of 6 members of this family (AtOFT1, AtMSR1, AtFRB1, AtESMD1, AtEDA30, and At1g04910), which experimentally demonstrated their strong membrane-association, as only 50% were successfully expressible in a soluble form at high enough yields to allow for downstream analyses even with extensive engineering to remove their predicted transmembrane domain as well as increase solubility by translational fusion to MBP. Additionally, the experimentally observed lifetimes of isolated AtMSR1Δ28 and AtFRB1Δ144 exhibited a rapid decrease in stability following isolation and are not amenable to flash freezing and storage at -80ºC, which poses extreme difficulties in downstream functional analyses. Taken together, these results indicate an improved method of protein expression and isolation of these proteins should be considered.

Not surprisingly, our general knowledge pertaining to the structure and function of membrane proteins across all organisms has been dramatically hindered due to experimental obstacles surrounding their expression, homogenous isolation, and functional stability (Dörr *et al.,* 2016; Errasti-Murugarren *et al.,* 2021; Hardy *et al.,*

2018). Moreover, membrane proteins represent 25-30% of the human genome yet only 2% of the known structures are membrane proteins, and in a recent search of all protein structures deposited in the Protein Data Bank (PDB, RCSB.org), less than 2.5% of all proteins across all species were membrane proteins (Pollock *et al.,* 2018; Errasti-Murugarren *et al.,* 2021; Hardy *et al.,* 2018; Sligar and Denisov, 2021). Nonetheless, experimental advancements, such as the use of novel detergents to solubilize these proteins out of membranes, expression systems, isolation techniques, and compounds that increase stability, have progressed our knowledge of these proteins (Errasti-Murugarren *et al.,* 2021). Herein, I summarize an alternative strategy for approaching expression of other members of the Arabidopsis putative POFT family, as the catalytic identities of all members of this predicted family should be investigated.

As described above, the limited success with expression of these plant proteins has been extremely difficult. Of the proteins that were expressible, extensive modification was required to allow for 3 family members to be expressed and exhibit extreme instability. Furthermore, only one proprietary detergent was successful at solubilizing AtOFT1 out of seedling membranes. In light of these challenges, a rational solution to further evaluating these proteins may be to embrace their endogenous membrane integration, instead of continuing to experimentally struggle to increase their abundance in the soluble protein fraction of expression hosts or further assess non-denaturing detergents for their ability to solubilize these proteins out of membranes. Of considerable interest are styrene-maleic acid copolymers (SMAs), which are detergent-free amphipathic polymers of maleic anhydride and styrene that can be directly applied to cells or membrane protein extracts to spontaneously form water soluble nanodiscs that

are ~10nm in size called styrene-maleic acid lipid particles (SMALPs) (Dörr *et al.,* 2016; Pollock *et al.,* 2018; Hardy *et al.,* 2018; Errasti-Murugarren *et al.,* 2021). Unlike nanodisc technology, which utilizes a membrane protein scaffold and requires either cell-free translation or detergent solubilization of your membrane protein of interest (MPOI) prior to nanodisc integration, the SMA itself acts to lasso and partition the lipid bilayer directly from the endogenous host membranes, resulting in a SMALP population consists of the native host lipid bilayer with and without the MPOI and other membrane proteins (Sligar and Denisov, 2021; Hardy *et al.,* 2018; Dörr *et al.,* 2016; Pollock *et al.,* 2018). Isolating the SMALPs containing the MPOI is facilitated through regular affinity chromatography and retention of the native hydrophobic lipid bilayer has been shown to stabilize the MPOI, which further maintains its structure and function (Bada Juarez *et al.,* 2019; Fiori *et al.,* 2020). Other advantages of SMAs over traditional nanodiscs besides being more-cost and time effective, include preservation of the native protein-protein interactions allowing for multi-protein complex determination as well as protein-lipid interactions, as the MPOI's native lipid bilayer may be essential to its structure and function, which is further attractive for cryo-EM studies (Errasti-Murugarren *et al.,* 2021; Fiori *et al.,* 2020; Dörr *et al.,* 2016).

SMAs are commercially available and their use in plant systems have been successful for determining the structure of SLOW ANION CHANNEL 1 (SLAC1) and mapping the critical phosphorylation sites for channel activation, investigating chloroplast thylakoid multiprotein complexes to study the structure-function dynamics of photosystems I and II related to thylakoid heterogeneity, characterizing the Arabidopsis SALT OVERLAY SENSITIVE 1 (SOS1) Na^+/H^+ antiporter, and determining the

metabolon multi-enzyme complex that catalyzes the cyanogenic glucoside, dhurrin, during insect attack in Sorghum, among others (Dörr *et al.,* 2016; Deng *et al.,* 2021; Kototych *et al.,* 2019; Kototych *et al.,* 2021; Bell *et al.,* 2015; Dutta *et al.,* 2020; Laursen *et al.,* 2016). Thus, implementation of this system in Arabidopsis could not only allow for these putative POFTs to be expressed without removal of their hypothesized N-terminal membrane domain, which could disrupt their endogenous function, but would further allow for precise catalytic evaluation due to them maintaining their native hydrophobic environment, lead to structure determination, and elucidate protein-protein interactions or multiprotein complex formation. Moreover, implementation of this system would allow for soluble fusion proteins, such as MBP to be proteolytically cleaved form the POFT following AC, further eliminating variables surrounding modification to the native protein structure-function relationship. Alternatively, recombinant production in an alternative eukaryotic recombinant expression system, such as tobacco or yeast, could expedite the process of catalytic identification and structure determination, as this would eliminate the need for generation of individual Arabidopsis transgenic expression lines.

V. Perspectives and key consideration

Could disrupted ROS signaling explain the *oft1* mutant phenotypes?

Although three general theories that could account for the *oft1* mutant phenotype have been proposed, I will offer one additional consideration due to the fact that to my knowledge no reports exist of an *Arabidopsis thaliana* mutant that exhibits 1) completely normal PT growth under *in vitro* conditions, yet 2) *in vivo,* PTs cannot penetrate the stigma-style interface, and additionally 3) displays increased vegetative tissue biomass. Due to these mixtures of mutant traits being so novel, one could only reconcile that

AtOFT1 must either function to regulate a diverse array of pathways, or the underlying pathway that *AtOFT1* participates in is a multifaceted signaling cascade that is present in multiple tissue types and functions in a tissue-specific manner. Leaning towards the latter explanation, an alternative hypothesis is that *oft1* mutant lines may be disruption in reactive oxygen species (ROS) signaling.

ROS, including $O_2^{\bullet -}$, H_2O_2, $OH^{\bullet}$, and O_2^{-}, functions as diverse tissue-specific intracellular and extracellular communication molecules that are involved in plant sexual reproduction, stress response, and plant development (Zhang *et al.,* 2020). Interestingly, a recent report demonstrated loss-of-function in the Arabidopsis putative POFT family member *AtESMD1* suppresses ROS accumulation and *FADlox* gene expression in Wall Associated Kinase (WAK) *WAK2cTAP* hyperactive dominant transgenic lines (*esmd1-1*$^{-/-}$*/WAK2cTAP*) and partially restored the dwarfed phenotype induced by single *WAK2cTAP* expression lines, illustrating AtESMD1 regulates these two mechanisms of stress-induced signal transduction in a WAK-independent manner (Kohorn *et al.,* 2021). In plants, ROS can be produced by amine oxidases, such as copper-containing amine oxidases (CuAO) and polyamine oxidases (PAO), peroxidase, quinone reductases, and NADPH oxidases (NOX (Kärkönen and Kuchitsu, 2015; Haung *et al.,* 2019)). Of the ROS-producing NADPH oxidases, RESPIRATORY BURST OXIDASE HOMOLOGS (RBOH) proteins reduce O_2 present in plant tissues to the superoxide anion $O_2^{\bullet -}$, which can then be further metabolized into H_2O_2 through an enzyme dependent or independent manner. RBOH enzymes are heavily regulated by protein kinases and the H_2O_2 they produce is considered an important redox molecule due to relative stability compared to other ROS, which allows for this RBOH-produced ROS to facilitate rapid and reversible oxidation of

target proteins. Additionally, H_2O_2 can easily traverse the plasma membrane (PM) into the cell wall via PM-localized aquaporins (Chapman *et al.,* 2019; Haung *et al.,* 2019). In Arabidopsis, the RBOH family is composed of 10 gene members (*RBOHA-J*) and show highly spatiotemporal-tissue specific ROS production that functions specifically in cell growth, division, and differentiation, cell wall formation, root hair and PT growth, stomatal closure, senescence, programmed cell death, and responses to abiotic and biotic stress (Chapman *et al.,* 2019; Haung *et al.,* 2019; Kärkönen and Kuchitsu, 2015; Zhang *et al.,* 2020). The connection to phytohormone signaling pathways, including auxin, abscisic acid (ABA), and brassinosteroid (BR) further extends the functional network of complex biological processes RBOH-generated ROS species can regulate (Chapman *et al.,* 2019, Haung *et al.,* 2019).

In primary roots, RBOH*A-D* and *F* are the main ROS mediators that establish its defined architecture and governs distinct zones of cell division and elongation (Huang *et al.,* 2019). For example, the double mutant lines *rbohd1*/*rbohf1* systematically showed *AtRBOHD* and *AtRBOHF* functionally regulate ABA-induced inhibition of primary root elongation by ROS production, which activates root PM Ca^{2+} permeable channels, leading to increased cytosolic $Ca^{2+}$and inhibition of root growth and demonstrated ROS inhibits auxin signaling (Jaio *et al.,* 2013; Lv *et al.,* 2018). Interestingly, overexpression of *AtOXR2* (*At2g05590*), a member of the oxidation resistant protein family, exhibited increased ROS, ABA signaling, and ascorbate, which led to increased primary root length, larger rosettes, and increased stem biomass, exhibiting the versatility and tightly coordinated interplay that is involved in maintaining ROS homeostasis and its impacts on plant morphology (Colombatti *et al.,* 2019). Additionally, in contrast to light grown

hypocotyls, the increased length of etiolated hypocotyls length in *oft1* mutant seedlings reflects increased cell expansion, and ROS species directly participate and mediate this process (Gendreau *et al.,* 1997; Kärkönen and Kuchitsu, 2015; Schmidt *et al.,* 2016).

Finally, ROS species found in both male and female reproductive tissues play fundamental roles in the process double fertilization, including pollen hydration and germination, PT growth in the pistil, and PT reception by the ovule as well as facilitate downstream response pathways (Zhang *et al.,* 2020; Kaya *et al.,* 2014; Chapman *et al.,* 2019; Sankaranarayanan *et al.,* 2020). *AtRBOH* and *AtRBOHJ* are partially redundant ROS-producing enzymes critical for proper PT polarized tip growth, as the double *rbohH/rbohJ* mutant fails to effectively sustain ROS at the apical PT tip as well as in localized regions of the PT PM, resulting in PTs failing to penetrate the stigma-style interface, leading to a reduced silique length and seed set (Kaya *et al.,* 2014; Boisson-Dernier *et al.,* 2009). Interestingly, the receptor-like kinases (RLKs) ANXUR1/2 (ANX1 and ANX2) double mutant lines (*anx1/anx2*) are phenotypically similar to both the *oft1* and *rbohH/rbohJ* double mutant PT behaviors *in vivo* (Smith *et al.,* 2018a; Smith *et al.,* 2018b; Kaya *et al.,* 2014; Boisson-Dernier *et al.,* 2009). Furthermore, overexpression of *ANX1* alone led to unstable PTs due to continued exocytosis of cell wall material to the PT PM that was uncoupled to the PT elongation rate, resulting in PT growth arrest in the style, but when *ANX1* was overexpressed in the *rbohH/rbohJ* double mutant background, the PT cell wall defects were abolished (Boisson-Dernier *et al.,* 2009). Recently, Arabidopsis pollen tube integrity during growth in the style was reported to be facilitated by a multiprotein complex localized to the apical PT PM, which functions upstream of RBOHH/J and includes ANX1/2, Buddha's Paper Seal 1/2 (BUPS1/2), and LORELEI-

like-GPI anchored proteins 2/3 (LLG2/3). The complex is activated in the style by its cognate ligand, rapid alkylation factor 4/19 (RALF4/19) to produce ROS and maintain Ca^{2+} dynamics necessary for PT growth (Zhang *et al.,* 2020).

Taken together, disruption to ROS signaling could account for the phenotypes displayed by *oft1* mutants through a diverse array of postulations that are specific to each cell tissue type. For example, do upstream activation targets of ROS signaling or the proteins that regulate them require O-fucosylation that are lacking in *oft1* lines, resulting in the increased vegetative characteristics as well as PT defects of this mutant? Another hypothesis is that the vegetative characteristics may be due to infertility, while the reproductive characteristics of *oft1* PTs may be a result of an extracellular protein lacking an essential O-fucosylation modification resulting in the PT not being recognized by the pistil? This theory is conceivable due to the observation that *oft1* PTs defects are only apparent when in contact with the pistil tissues. Of note, protein O-fucosylation plays an important role in plant immunity, and the only confirmed Arabidopsis protein O-fucosyltransferase reported to date, *AtSPINDLY,* is compromised in apoplastic and stomatal defense mechanisms in loss-of-function lines (Zhang *et al.,* 2019; Bi *et al.,* 2021). Furthermore, even though the scope of known O-glycosylated proteins in plant systems is limited to hydroxyproline-rich glycoproteins (HRGPs), secreted hormone peptides, and DELLA proteins, a case for their dysfunction as a result of a lacking O-glycan can be made for each of the phenotypes *oft1* exhibits, as these enzymes play integral roles in almost every facet of plant physiology (Strasser *et al.,* 2021). Thus, investigating the ROS patterns in different tissues of *oft1* mutant lines would be beneficial to deciphering the pathways AtOFT1 functions in and can be achieved by cell-

permeable fluorescent ROS-specific probes or transgenic expression of redox and ROS-response proteins, such as roGFP and HyPer (Fichman *et al.,* 2019).

References

Bada Juarez, J. F., Harper, A. J., Judge, P. J., Tonge, S. R., & Watts, A. (2019). From polymer chemistry to structural biology: The development of SMA and related amphipathic polymers for membrane protein extraction and solubilisation. *Chemistry and Physics of Lipids*, *221*(Journal Article), 167–175. https://doi.org/10.1016/j.chemphyslip.2019.03.008

Balanzà, V., Martínez-Fernández, I., Sato, S., Yanofsky, M. F., & Ferrándiz, C. (2021). Inflorescence Meristem Fate Is Dependent on Seed Development and FRUITFULL in Arabidopsis thaliana. *Frontiers in Plant Science*, *10*(Journal Article), 1622–1622. https://doi.org/10.3389/fpls.2019.01622

Bell, A. J., Frankel, L. K., & Bricker, T. M. (2015). High Yield Non-detergent Isolation of Photosystem I-Light-harvesting Chlorophyll II Membranes from Spinach Thylakoids: Implications for the organization of the PS I antennae in higher plants. *Journal of Biological Chemistry*, *290*(30), 18429–18437. https://doi.org/10.1074/jbc.M115.663872

Bi, Y., Deng, Z., Ni, W., Shrestha, R., Savage, D., Hartwig, T., Patil, S., Hong, S. H., Zhang, Z., Oses-Prieto, J. A., Li, K. H., Quail, P. H., Burlingame, A. L., Xu, S.-L., & Wang, Z.-Y. (2021). Arabidopsis ACINUS is O-glycosylated and regulates transcription and alternative splicing of regulators of reproductive transitions. *Nature Communications*, *12*(1), 945–945. https://doi.org/10.1038/s41467-021-20929-7

Boavida, L. C., Shuai, B., Yu, H.-J., Pagnussat, G. C., Sundaresan, V., & McCormick, S. (2009). A Collection of Ds Insertional Mutants Associated With Defects in Male Gametophyte Development and Function in Arabidopsis thaliana. *Genetics (Austin)*, *181*(4), 1369–1385. https://doi.org/10.1534/genetics.108.090852

Boisson-Dernier, A., Roy, S., Kritsas, K., Grobei, M. A., Jaciubek, M., Schroeder, J. I., & Grossniklaus, U. (2009). Disruption of the pollen-expressed FERONIA homologs ANXUR1 and ANXUR2 triggers pollen tube discharge. *Development (Cambridge)*, *136*(19), 3279–3288. https://doi.org/10.1242/dev.040071

Bum, Y., & Cosgrove, D. J. (2012). Changes in Cell Wall Biomechanical Properties in the Xyloglucan-Deficient xxt1/xxt2 Mutant of Arabidopsis. *Plant Physiology (Bethesda)*, *158*(1), 465–475. https://doi.org/10.1104/pp.111.189779

Campanoni, P., & Blatt, M. R. (2006). Membrane trafficking and polar growth in root hairs and pollen tubes. *Journal of Experimental Botany*, *58*(1), 65–74. https://doi.org/10.1093/jxb/erl059

Cascallares, M., Setzes, N., Marchetti, F., López, G. A., Distéfano, A. M., Cainzos, M., Zabaleta, E., & Pagnussat, G. C. (2020). A Complex Journey: Cell Wall Remodeling, Interactions, and Integrity During Pollen Tube Growth. *Frontiers in Plant Science*, *11*(Journal Article), 599247–599247. https://doi.org/10.3389/fpls.2020.599247

Chapman, J. M., Muhlemann, J. K., Gayomba, S. R., & Muday, G. K. (2019). RBOH-Dependent ROS Synthesis and ROS Scavenging by Plant Specialized Metabolites To Modulate Plant Development and Stress Responses. *Chemical Research in Toxicology*, *32*(3), 370–396. https://doi.org/10.1021/acs.chemrestox.9b00028

Chebli, Y., Kaneda, M., Zerzour, R., & Geitmann, A. (2012). The Cell Wall of the Arabidopsis Pollen Tube—Spatial Distribution, Recycling, and Network Formation of Polysaccharides1[C][W][OA]. *Plant Physiology (Bethesda)*, *160*(4), 1940–1955. https://doi.org/10.1104/pp.112.199729

Chou, Y.-H., Pogorelko, G., Young, Z. T., & Zabotina, O. A. (2015). Protein-protein interactions among xyloglucan-synthesizing enzymes and formation of Golgi-localized multiprotein complexes. *Plant and Cell Physiology*, *56*(2), 255–267. https://doi.org/10.1093/pcp/pcu161

Colombatti, F., Mencia, R., Garcia, L., Mansilla, N., Alemano, S., Andrade, A. M., Gonzalez, D. H., & Welchen, E. (2019). The mitochondrial oxidation resistance protein AtOXR2 increases plant biomass and tolerance to oxidative stress. *Journal of Experimental Botany*, *70*(12), 3177–3195. https://doi.org/10.1093/jxb/erz147

Crawford, B. C. W., Ditta, G., & Yanofsky, M. F. (2007). The NTT Gene Is Required for Transmitting-Tract Development in Carpels of Arabidopsis thaliana. *Current Biology*, *17*(13), 1101–1108. https://doi.org/10.1016/j.cub.2007.05.079

Deng, Y.-N., Kashtoh, H., Wang, Q., Zhen, G.-X., Li, Q.-Y., Tang, L.-H., Gao, H.-L., Zhang, C.-R., Qin, L., Su, M., Li, F., Huang, X.-H., Wang, Y.-C., Xie, Q., Clarke, O. B., Hendrickson, W. A., & Chen,

Y.-H. (2021). Structure and activity of SLAC1 channels for stomatal signaling in leaves. *Proceedings of the National Academy of Sciences - PNAS*, *118*(18), 1. https://doi.org/10.1073/pnas.2015151118

Dörr, J. M., Scheidelaar, S., Koorengevel, M. C., Dominguez Pardo, J., Schäfer, M., van Walree, C. A., & Killian, J. A. (2016). The styrene-maleic acid copolymer: : A versatile tool in membrane research. *European Biophysics Journal*, *45*(1), 3–21. https://doi.org/10.1007/s00249-015-1093-y

Dutta, D., Esmaili, M., Overduin, M., & Fliegel, L. (2020). Expression and detergent free purification and reconstitution of the plant plasma membrane Na+/H+ antiporter SOS1 overexpressed in Pichia pastoris. *Biochimica et Biophysica Acta. Biomembranes*, *1862*(3), 183111–183111. https://doi.org/10.1016/j.bbamem.2019.183111

Elleman, C. J., Franklin-Tong, V., & Dickinson, H. G. (1992). Pollination in Species with Dry Stigmas: The Nature of the Early Stigmatic Response and the Pathway Taken by Pollen Tubes. *The New Phytologist*, *121*(3), 413–424. https://doi.org/10.1111/j.1469-8137.1992.tb02941.x

Errasti-Murugarren, E., Bartoccioni, P., & Palacín, M. (2021). Membrane Protein Stabilization Strategies for Structural and Functional Studies. *Membranes (Basel)*, *11*(2), 155. https://doi.org/10.3390/membranes11020155

Fernando, W. G. D. (2012). Plants: An International Scientific Open Access Journal to Publish All Facets of Plants, Their Functions and Interactions with the Environment and Other Living Organisms. *Plants*, *1*(1), 1–5. https://doi.org/10.3390/plants1010001

Fichman, Y., Miller, G., & Mittler, R. (2019). Whole-Plant Live Imaging of Reactive Oxygen Species. *Molecular Plant*, *12*(9), 1203–1210. https://doi.org/10.1016/j.molp.2019.06.003

Fiori, M. C., Zheng, W., Kamilar, E., Simiyu, G., Altenberg, G. A., & Liang, H. (2020). Extraction and reconstitution of membrane proteins into lipid nanodiscs encased by zwitterionic styrene-maleic amide copolymers. *Scientific Reports*, *10*(1), 9940. https://doi.org/10.1038/s41598-020-66852-7

Flores-Tornero, M., Wang, L., Potěšil, D., Hafidh, S., Vogler, F., Zdráhal, Z., Honys, D., Sprunck, S., & Dresselhaus, T. (2021). Comparative analyses of angiosperm secretomes identify apoplastic pollen tube functions and novel secreted peptides. *Plant Reproduction*, *34*(1), 47–60. https://doi.org/10.1007/s00497-020-00399-5

Gendreau, E. (Institut N. de la R. A., Versailles, France.)., Traas, J., Desnos, T., Grandjean, O., Caboche, M., & Hofte, H. (1997). Cellular basis of hypocotyl growth in Arabidopsis thaliana. *Plant Physiology (Bethesda)*, *114*(1), 295–305. https://doi.org/10.1104/pp.114.1.295

Gille, S., & Pauly, M. (2012). O-Acetylation of Plant Cell Wall Polysaccharides. *Frontiers in Plant Science*, *3*(Journal Article), 12–12. https://doi.org/10.3389/fpls.2012.00012

González-Pérez, L., Perrotta, L., Acosta, A., Orellana, E., Spadafora, N., Bruno, L., Bitonti, B. M., Albani, D., Cabrera, J. C., Francis, D., & Rogers, H. J. (2014). In tobacco BY-2 cells xyloglucan oligosaccharides alter the expression of genes involved in cell wall metabolism, signalling, stress responses, cell division and transcriptional control. *Molecular Biology Reports*, *41*(10), 6803–6816. https://doi.org/10.1007/s11033-014-3566-y

Guo, H., Mockler, T., Duong, H., & Lin, C. (2001). SUB1, an Arabidopsis Ca2+-binding protein involved in cryptochrome and phytochrome coaction. *Science (American Association for the Advancement of Science)*, *291*(5503), 487–490. https://doi.org/10.1126/science.291.5503.487

Hansen, S. F., Harholt, J., Oikawa, A., Scheller, H. V., & Joint Bioenergy Institute (JBEI). (2012). Plant Glycosyltransferases Beyond CAZy: A Perspective on DUF Families. *Frontiers in Plant Science*, *3*(Journal Article), 59–59. https://doi.org/10.3389/fpls.2012.00059

Hao, L., Liu, J., Zhong, S., Gu, H., & Qu, L.-J. (2016). AtVPS41-mediated endocytic pathway is essential for pollen tube–stigma interaction in Arabidopsis. *Proceedings of the National Academy of Sciences - PNAS*, *113*(22), 6307–6312. https://doi.org/10.1073/pnas.1602757113

Hardy, D., Desuzinges Mandon, E., Rothnie, A. J., & Jawhari, A. (2018). The yin and yang of solubilization and stabilization for wild-type and full-length membrane protein. *Methods (San Diego, Calif.)*, *147*(Journal Article), 118–125. https://doi.org/10.1016/j.ymeth.2018.02.017

Huang, H., Ullah, F., Zhou, D.-X., Yi, M., & Zhao, Y. (2019). Mechanisms of ROS Regulation of Plant Development and Stress Responses. *Frontiers in Plant Science*, *10*(Journal Article), 800–800. https://doi.org/10.3389/fpls.2019.00800

Hummel, M. (2008). Biomass recalcitrance; deconstructing the plant cell wall for bioenergy. *SciTech Book News*, *32*(4). https://doi-org.unr.idm.oclc.org/10.1002/9781444305418.ch5

Jander, G., Baerson, S. R., Hudak, J. A., Gonzalez, K. A., Gruys, K. J., & Last, R. L. (2003). Ethylmethanesulfonate Saturation Mutagenesis in Arabidopsis to Determine Frequency of Herbicide Resistance. *Plant Physiology (Bethesda)*, *131*(1), 139–146. https://doi.org/10.1104/pp.102.010397

Jia, P.-F., Xue, Y., Li, H.-J., & Yang, W.-C. (2018). Golgi-localized LOT regulates trans-Golgi network biogenesis and pollen tube growth. *Proceedings of the National Academy of Sciences - PNAS*, *115*(48), 12307–12312. https://doi.org/10.1073/pnas.1809206115

Jiang, L., Yang, S.-L., Xie, L.-F., Puah, C. S., Zhang, X.-Q., Yang, W.-C., Sundaresan, V., & Ye, D. (2005). VANGUARD1 Encodes a Pectin Methylesterase That Enhances Pollen Tube Growth in the Arabidopsis Style and Transmitting Tract. *The Plant Cell*, *17*(2), 584–596. https://doi.org/10.1105/tpc.104.027631

Jiao, Y., Sun, L., Song, Y., Wang, L., Liu, L., Zhang, L., Liu, B., Li, N., Miao, C., & Hao, F. (2013). AtrbohD and AtrbohF positively regulate abscisic acid-inhibited primary root growth by affecting Ca2+signalling and auxin response of roots in Arabidopsis. *Journal of Experimental Botany*, *64*(14), 4183–4192. https://doi.org/10.1093/jxb/ert228

Johnson, M. A., & Preuss, D. (2002). Plotting a Course: Multiple Signals Guide Pollen Tubes to Their Targets. *Developmental Cell*, *2*(3), 273–281. https://doi.org/10.1016/S1534-5807(02)00130-2

Kärkönen, A., & Kuchitsu, K. (2015). Reactive oxygen species in cell wall metabolism and development in plants. *Phytochemistry (Oxford)*, *112*(Journal Article), 22–32. https://doi.org/10.1016/j.phytochem.2014.09.016

Kaya, H., Nakajima, R., Iwano, M., Kanaoka, M. M., Kimura, S., Takeda, S., Kawarazaki, T., Senzaki, E., Hamamura, Y., Higashiyama, T., Takayama, S., Abe, M., & Kuchitsu, K. (2014). Ca^{2+}-Activated Reactive Oxygen Species Production by Arabidopsis RbohH and RbohJ Is Essential for Proper Pollen Tube Tip Growth. *The Plant Cell*, *26*(3), 1069–1080. https://doi.org/10.1105/tpc.113.120642

Kim, S.-J., Chandrasekar, B., Rea, A. C., Danhof, L., Zemelis-Durfee, S., Thrower, N., Shepard, Z. S., Pauly, M., Brandizzi, F., Keegstra, K., & Michigan State Univ., E. L., MI (United States). MSU-DOE Plant Research Laboratory. (2020). The synthesis of xyloglucan, an abundant plant cell wall polysaccharide, requires CSLC function. *Proceedings of the National Academy of Sciences - PNAS*, *117*(33), 20316–20324. https://doi.org/10.1073/pnas.2007245117

Kohorn, B. D., Greed, B. E., Mouille, G., Verger, S., & Kohorn, S. L. (2021). Effects of Arabidopsis wall associated kinase mutations on ESMERALDA1 and elicitor induced ROS. *PloS One*, *16*(5), e0251922–e0251922. https://doi.org/10.1371/journal.pone.0251922

Kong, Y., Zhou, G., Abdeen, A. A., Schafhauser, J., Richardson, B., Atmodjo, M. A., Jung, J., Wicker, L., Mohnen, D., Western, T., & Hahn, M. G. (2013). GALACTURONOSYLTRANSFERASE-LIKE5 Is Involved in the Production of Arabidopsis Seed Coat Mucilage. *Plant Physiology*, *163*(3), 1203–1217. https://doi.org/10.1104/pp.113.227041

Korotych, O. I., Nguyen, T. T., Reagan, B. C., Burch-Smith, T. M., & Bruce, B. D. (2021). Poly(styrene-co-maleic acid)-mediated isolation of supramolecular membrane protein complexes from plant thylakoids. *Biochimica et Biophysica Acta. Bioenergetics*, *1862*(3), 148347–148347. https://doi.org/10.1016/j.bbabio.2020.148347

Korotych, O., Mondal, J., Gattás-Asfura, K. M., Hendricks, J., & Bruce, B. D. (2019). Evaluation of commercially available styrene-co-maleic acid polymers for the extraction of membrane proteins from spinach chloroplast thylakoids. *European Polymer Journal*, *114*(Journal Article), 485–500. https://doi.org/10.1016/j.eurpolymj.2018.10.035

Kurasawa, K. (Tohoku Univ., Sendai (Japan)), Matsui, A., Yokoyama, R., Kuriyama, T., Yoshizumi, T., Matsui, M., Suwabe, K., Watanabe, M., & Nishitani, K. (2009). The AtXTH28 gene, a xyloglucan endotransglucosylase/hydrolase, is involved in automatic self-pollination in arabidopsis thaliana. *Plant and Cell Physiology*, *50*(2), 413–422. https://doi.org/10.1093/pcp/pcp003

Lao, N. T., Long, D., Kiang, S., Coupland, G., Shoue, D. A., Carpita, N. C., & Kavanagh, T. A. (2003). Mutation of a family 8 glycosyltransferase gene alters cell wall carbohydrate composition and causes a humidity-sensitive semi-sterile dwarf phenotype in Arabidopsis. *Plant Molecular Biology*, *53*(5), 687–701. https://doi.org/10.1023/B:PLAN.0000019074.60542.6c

Laursen, T., Borch, J., Knudsen, C., Bavishi, K., Torta, F., Martens, H. J., Silvestro, D., Hatzakis, N. S., Wenk, M. R., Dafforn, T. R., Olsen, C. E., Motawia, M. S., Hamberger, B., Møller, B. L., & Bassard, J.-E. (2016). Characterization of a dynamic metabolon producing the defense compound dhurrin in

sorghum. *Science (American Association for the Advancement of Science)*, *354*(6314), 890–893. https://doi.org/10.1126/science.aag2347

Levitin, B., Richter, D., Markovich, I., & Zik, M. (2008). Arabinogalactan proteins 6 and 11 are required for stamen and pollen function in Arabidopsis. *The Plant Journal : For Cell and Molecular Biology*, *56*(3), 351–363. https://doi.org/10.1111/j.1365-313X.2008.03607.x

Li, Z., Han, K., Pak, J. E., Satkunarajah, M., Zhou, D., & Rini, J. M. (2017). Recognition of EGF-like domains by the Notch-modifying O-fucosyltransferase POFUT1. *Nature Chemical Biology*, *13*(7), 757–763. https://doi.org/10.1038/nchembio.2381

Lira-Navarrete, E., Valero-González, J., Villanueva, R., Martínez-Júlvez, M., Tejero, T., Merino, P., Panjikar, S., & Hurtado-Guerrero, R. (2011). Structural insights into the mechanism of protein O-fucosylation. *PloS One*, *6*(9), e25365–e25365. https://doi.org/10.1371/journal.pone.0025365

Liu, X., Salokas, K., Tamene, F., Jiu, Y., Weldatsadik, R. G., Öhman, T., & Varjosalo, M. (2018). An AP-MS- and BioID-compatible MAC-tag enables comprehensive mapping of protein interactions and subcellular localizations. *Nature Communications*, *9*(1), 1188–1188. https://doi.org/10.1038/s41467-018-03523-2

Lv, B., Tian, H., Zhang, F., Liu, J., Lu, S., Bai, M., Li, C., & Ding, Z. (2018). Brassinosteroids regulate root growth by controlling reactive oxygen species homeostasis and dual effect on ethylene synthesis in Arabidopsis. *PLoS Genetics*, *14*(1), e1007144–e1007144. https://doi.org/10.1371/journal.pgen.1007144

McKay, M. J., Afrose, F., Koeppe, R. E., & Greathouse, D. V. (2018). Helix formation and stability in membranes. *Biochimica et Biophysica Acta. Biomembranes*, *1860*(10), 2108–2117. https://doi.org/10.1016/j.bbamem.2018.02.010

McMillan, B. J., Zimmerman, B., Egan, E. D., Lofgren, M., Xu, X., Hesser, A., Blacklow, S. C., & Argonne National Lab. (ANL), A., IL (United States). Advanced Photon Source (APS). (2017). Structure of human POFUT1, its requirement in ligand-independent oncogenic Notch signaling, and functional effects of Dowling-Degos mutations. *Glycobiology (Oxford)*, *27*(8), 777–786. https://doi.org/10.1093/glycob/cwx020

Michard, E., Lima, P. T., Borges, F., Silva, A. C., Portes, M. T., Carvalho, J. E., Gilliham, M., Liu, L.-H., Obermeyer, G., & Feijo, J. A. (2011). Glutamate Receptor—Like Genes Form Ca^{2+} Channels in Pollen Tubes and Are Regulated by Pistil D-Serine. *Science (American Association for the Advancement of Science)*, *332*(6028), 434–437. https://doi.org/10.1126/science.1201101

Mollet, J.-C., Leroux, C., Dardelle, F., & Lehner, A. (2013). Cell Wall Composition, Biosynthesis and Remodeling during Pollen Tube Growth. *Plants (Basel)*, *2*(1), 107–147. https://doi.org/10.3390/plants2010107

Muschietti, J., Eyal, Y., & McCormick, S. (1998). Pollen Tube Localization Implies a Role in Pollen-Pistil Interactions for the Tomato Receptor-Like Protein Kinases LePRK1 and LePRK2. *The Plant Cell*, *10*(3), 319–330. https://doi.org/10.1105/tpc.10.3.319

Mutanwad, K. V., Zangl, I., & Lucyshyn, D. (2020). The Arabidopsis O-fucosyltransferase SPINDLY regulates root hair patterning independently of gibberellin signaling. *Development (Cambridge)*, *147*(19). https://doi.org/10.1242/dev.192039

Neumetzler, L., Humphrey, T., Lumba, S., Snyder, S., Yeats, T. H., Usadel, B., Vasilevski, A., Patel, J., Rose, J. K. C., Persson, S., & Bonetta, D. (2012). The FRIABLE1 gene product affects cell adhesion in Arabidopsis. *PloS One*, *7*(8), e42914–e42914. https://doi.org/10.1371/journal.pone.0042914

Nikolovski, N., Rubtsov, D., Segura, M. P., Miles, G. P., Stevens, T. J., Dunkley, T. P. J., Munro, S., Lilley, K. S., & Dupree, P. (2012). Putative Glycosyltransferases and Other Plant Golgi Apparatus Proteins Are Revealed by LOPIT Proteomics. *Plant Physiology (Bethesda)*, *160*(2), 1037–1051. https://doi.org/10.1104/pp.112.204263

Oikawa, A., Lund, C. H., Sakuragi, Y., Scheller, H. V., & Joint Bioenergy Institute (JBEI). (2013). Golgi-localized enzyme complexes for plant cell wall biosynthesis. *Trends in Plant Science*, *18*(1), 49–58. https://doi.org/10.1016/j.tplants.2012.07.002

Pagnussat, G. C., Yu, H.-J., Ngo, Q. A., Rajani, S., Mayalagu, S., Johnson, C. S., Capron, A., Xie, L.-F., Ye, D., & Sundaresan, V. (2005). Genetic and molecular identification of genes required for female gametophyte development and function in Arabidopsis. *Development (Cambridge)*, *132*(3), 603–614. https://doi.org/10.1242/dev.01595

Palanivelu, R., Brass, L., Edlund, A. F., & Preuss, D. (2003). Pollen Tube Growth and Guidance Is Regulated by POP2, an Arabidopsis Gene that Controls GABA Levels. *Cell*, *114*(1), 47–59. https://doi.org/10.1016/S0092-8674(03)00479-3

Palanivelu, R., & Tsukamoto, T. (2011). Pathfinding in angiosperm reproduction: Pollen tube guidance by pistils ensures successful double fertilization. *Wiley Interdisciplinary Reviews. Developmental Biology*, *1*(1), 96.

Pollock, N. L., Lee, S. C., Patel, J. H., Gulamhussein, A. A., & Rothnie, A. J. (2018). Structure and function of membrane proteins encapsulated in a polymer-bound lipid bilayer. *Biochimica et Biophysica Acta. Biomembranes*, *1860*(4), 809–817. https://doi.org/10.1016/j.bbamem.2017.08.012

Qu, L.-J., Li, L., Lan, Z., & Dresselhaus, T. (2015). Peptide signalling during the pollen tube journey and double fertilization. *Journal of Experimental Botany*, *66*(17), 5139–5150. https://doi.org/10.1093/jxb/erv275

Ralet, M.-C., Crépeau, M.-J., Vigouroux, J., Tran, J., Berger, A., Sallé, C., Granier, F., Botran, L., & North, H. M. (2016). Xylans Provide the Structural Driving Force for Mucilage Adhesion to the Arabidopsis Seed Coat. *Plant Physiology (Bethesda)*, *171*(1), 165–178. https://doi.org/10.1104/pp.16.00211

Sankaranarayanan, S., Ju, Y., & Kessler, S. A. (2020). Reactive Oxygen Species as Mediators of Gametophyte Development and Double Fertilization in Flowering Plants. *Frontiers in Plant Science*, *11*(Journal Article), 1199–1199. https://doi.org/10.3389/fpls.2020.01199

Schmidt, R., Kunkowska, A. B., & Schippers, J. H. M. (2016). Role of Reactive Oxygen Species during Cell Expansion in Leaves. *Plant Physiology (Bethesda)*, *172*(4), 2098–2106. https://doi.org/10.1104/pp.16.00426

Sears, R. M., May, D. G., & Roux, K. J. (2019). BioID as a Tool for Protein-Proximity Labeling in Living Cells. *Methods in Molecular Biology (Clifton, N.J.)*, *2012*(Journal Article), 299.

Selig, M. J., Adney, W. S., Himmel, M. E., & Decker, S. R. (2009). The impact of cell wall acetylation on corn stover hydrolysis by cellulolytic and xylanolytic enzymes. *Cellulose (London)*, *16*(4), 711–722. https://doi.org/10.1007/s10570-009-9322-0

Singh, S., & Mittal, A. (2016). Transmembrane Domain Lengths Serve as Signatures of Organismal Complexity and Viral Transport Mechanisms. *Scientific Reports*, *6*(1), 22352–22352. https://doi.org/10.1038/srep22352

Sligar, S. G., & Denisov, I. G. (2021). Nanodiscs: A toolkit for membrane protein science. *Protein Science*, *30*(2), 297–315. https://doi.org/10.1002/pro.3994

Smith, D. K., Harper, J. F., & Wallace, I. S. (2018b). A potential role for protein O-fucosylation during pollen-pistil interactions. *Plant Signaling & Behavior*, *13*(5), e1467687–e1467687. https://doi.org/10.1080/15592324.2018.1467687

Smith, D. K., Jones, D. M., Lau, J. B. R., Cruz, E. R., Brown, E., Harper, J. F., & Wallace, I. S. (2018a). A Putative Protein O -Fucosyltransferase Facilitates Pollen Tube Penetration through the Stigma—Style Interface. *Plant Physiology (Bethesda)*, *176*(4), 2804–2818. https://doi.org/10.1104/pp.17.01577

Somoza, S. C., Sede, A. R., Boccardo, N. A., & Muschietti, J. P. (2021). Keeping up with the RALFs: How these small peptides control pollen–pistil interactions in Arabidopsis. *The New Phytologist*, *229*(1), 14–18. https://doi.org/10.1111/nph.16817

Sprunck, S. (2020). Twice the fun, double the trouble: Gamete interactions in flowering plants. *Current Opinion in Plant Biology*, *53*(Journal Article), 106–116. https://doi.org/10.1016/j.pbi.2019.11.003

Stonebloom, S., Ebert, B., Xiong, G., Pattathil, S., Birdseye, D., Lao, J., Pauly, M., Hahn, M. G., Heazlewood, J. L., Scheller, H. V., & Lawrence Berkeley National Lab. (LBNL), B., CA (United States). (2016). A DUF-246 family glycosyltransferase-like gene affects male fertility and the biosynthesis of pectic arabinogalactans. *BMC Plant Biology*, *16*(84), 90–90. https://doi.org/10.1186/s12870-016-0780-x

Strasser, R., Seifert, G., Doblin, M. S., Johnson, K. L., Ruprecht, C., Pfrengle, F., Bacic, A., & Estevez, J. M. (2021). Cracking the "Sugar Code": A Snapshot of N - and O -Glycosylation Pathways and Functions in Plants Cells. *Frontiers in Plant Science*, *12*(Journal Article), 640919–640919. https://doi.org/10.3389/fpls.2021.640919

Sugimoto, H., Kondo, S., Tanaka, T., Imamura, C., Muramoto, N., Hattori, E., Ogawa, K., Mitsukawa, N., & Ohto, C. (2014). Overexpression of a novel Arabidopsis PP2C isoform, AtPP2CF1, enhances plant

biomass production by increasing inflorescence stem growth. *Journal of Experimental Botany*, *65*(18), 5385–5400. https://doi.org/10.1093/jxb/eru297

Takenaka, Y., Kato, K., Ogawa-Ohnishi, M., Tsuruhama, K., Kajiura, H., Yagyu, K., Takeda, A., Takeda, Y., Kunieda, T., Hara-Nishimura, I., Kuroha, T., Nishitani, K., Matsubayashi, Y., & Ishimizu, T. (2018). Pectin RG-I rhamnosyltransferases represent a novel plant-specific glycosyltransferase family. *Nature Plants*, *4*(9), 669–676. https://doi.org/10.1038/s41477-018-0217-7

Tol, N. van, Rolloos, M., Pinas, J. E., Henkel, C. V., Augustijn, D., Hooykaas, P. J. J., & van der Zaal, B. J. (2017). Enhancement of Arabidopsis growth characteristics using genome interrogation with artificial transcription factors. *PloS One*, *12*(3), e0174236–e0174236. https://doi.org/10.1371/journal.pone.0174236

Verger, S., Chabout, S., Gineau, E., & Mouille, G. (2016). Cell adhesion in plants is under the control of putative O-fucosyltransferases. *Development (Cambridge)*, *143*(14), 2536–2540. https://doi.org/10.1242/dev.132308

Voiniciuc, C., Gunl, M., Schmidt, M. H.-W., & Usadel, B. (2015). Highly Branched Xylan Made by IRREGULAR XYLEM14 and MUCILAGE-RELATED21 Links Mucilage to Arabidopsis Seeds. *Plant Physiology (Bethesda)*, *169*(4), 2481–2495. https://doi.org/10.1104/pp.15.01441

Wang, L., Wang, W., Wang, Y.-Q., Liu, Y.-Y., Wang, J.-X., Zhang, X.-Q., Ye, D., & Chen, L.-Q. (2013). Arabidopsis Galacturonosyltransferase (GAUT) 13 and GAUT14 Have Redundant Functions in Pollen Tube Growth. *Molecular Plant*, *6*(4), 1131–1148. https://doi.org/10.1093/mp/sst084

Wang, Y., Mortimer, J. C., Davis, J., Dupree, P., Keegstra, K., & Great Lakes Bioenergy Research Center (GLBRC). (2013). Identification of an additional protein involved in mannan biosynthesis. *The Plant Journal : For Cell and Molecular Biology*, *73*(1), 105–117. https://doi.org/10.1111/tpj.12019

Waterhouse, A., Bertoni, M., Bienert, S., Studer, G., Tauriello, G., Gumienny, R., Heer, F. T., de Beer, T. A. P., Rempfer, C., Bordoli, L., Lepore, R., & Schwede, T. (2018). SWISS-MODEL: homology modelling of protein structures and complexes. *Nucleic Acids Research*, *46*(W1), W296–W303. https://doi.org/10.1093/nar/gky427

Wengier, D., Valsecchi, I., Cabanas, M. L., Tang, W., McCormick, S., & Muschietti, J. (2003). The Receptor Kinases LePRK1 and LePRK2 Associate in Pollen and When Expressed in Yeast, but Dissociate in the Presence of Style Extract. *Proceedings of the National Academy of Sciences - PNAS*, *100*(11), 6860–6865. https://doi.org/10.1073/pnas.0631728100

Won, S.-K., Lee, Y.-J., Lee, H.-Y., Heo, Y.-K., Cho, M., & Cho, H.-T. (2009). Cis-Element- and Transcriptome-Based Screening of Root Hair-Specific Genes and Their Functional Characterization in Arabidopsis. *Plant Physiology (Bethesda)*, *150*(3), 1459–1473. https://doi.org/10.1104/pp.109.140905

Yang, C., & Lü, X. (2021). Chapter 5—Composition of plant biomass and its impact on pretreatment. In X. Lü (Ed.), *Advances in 2nd Generation of Bioethanol Production* (pp. 71–85). Woodhead Publishing. https://doi.org/10.1016/B978-0-12-818862-0.00002-9

Young, R. E., McFarlane, H. E., Hahn, M. G., Western, T. L., Haughn, G. W., & Samuels, A. L. (2008). Analysis of the Golgi Apparatus in Arabidopsis Seed Coat Cells during Polarized Secretion of Pectin-Rich Mucilage. *The Plant Cell*, *20*(6), 1623–1638. https://doi.org/10.1105/tpc.108.058842

Zentella, R., Sui, N., Barnhill, B., Hsieh, W.-P., Hu, J., Shabanowitz, J., Boyce, M., Olszewski, N. E., Zhou, P., Hunt, D. F., Sun, T.-P., & Duke Univ., D., NC (United States). (2017). The Arabidopsis O-fucosyltransferase SPINDLY activates nuclear growth repressor DELLA. *Nature Chemical Biology*, *13*(5), 479–485. https://doi.org/10.1038/nchembio.2320

Zhang, L., Paasch, B. C., Chen, J., Day, B., & He, S. Y. (2019). An important role of l-fucose biosynthesis and protein fucosylation genes in Arabidopsis immunity. *The New Phytologist*, *222*(2), 981–994. https://doi.org/10.1111/nph.15639

Zhang, M. J., Zhang, X. S., & Gao, X.-Q. (2020). ROS in the Male-Female Interactions During Pollination: Function and Regulation. *Frontiers in Plant Science*, *11*(Journal Article), 177–177. https://doi.org/10.3389/fpls.2020.00177

Zheng, Y.-Y., Lin, X.-J., Liang, H.-M., Wang, F.-F., & Chen, L.-Y. (2018). The Long Journey of Pollen Tube in the Pistil. *International Journal of Molecular Sciences*, *19*(11), 3529. https://doi.org/10.3390/ijms19113529

Zhong, R., Cui, D., & Ye, Z. (2019). Secondary cell wall biosynthesis. *The New Phytologist*, *221*(4), 1703–1723. https://doi.org/10.1111/nph.15537

Zwiewka, M., Nodzyński, T., Robert, S., Vanneste, S., & Friml, J. (2015). Osmotic Stress Modulates the Balance between Exocytosis and Clathrin-Mediated Endocytosis in Arabidopsis thaliana. *Molecular Plant*, *8*(8), 1175–1187. https://doi.org/10.1016/j.molp.2015.03.007